Shoreline response to multi-scale oceanic forcing from video imagery

Donatus Bapentire Angnuureng

université de BORDEAUX

THÈSE PRÉSENTÉE

POUR OBTENIR LE GRADE DE

DOCTEUR DE

L'UNIVERSITÉ DE BORDEAUX

ÉCOLE DOCTORALE

SPÉCIALITÉ

Physique de l'environnement

Par Donatus Bapentire Angnuureng

Shoreline response to multi-scale oceanic forcing from video imagery

Sous la direction de : Nadia Senechal
(co-directeur : Rafael Almar)
(co-directeur : Bruno Castelle)
(co-directeur :Kwasi Appeaning Addo)

Soutenue le 06/07/2016

Membres du jury :

M. HALL Nicholas	Professor	Université de Toulouse	Président
M. ANTHONY Edward	Professor	CEREGE, Aix-Provence	Rapporteur
M. OUILLON Sylvain	Professor	IRD-LEGOS	Rapporteur
M.RANASINGHE Roshanka	Professor	UNESCO-IHE, Pays-Bas	Rapporteur

Titre : Réponse de shoreline à forçage océanique multi-échelle à partir d'images vidéo

Résumé :

Le but de cette étude était de développer une méthodologie pour évaluer la résilience des littoraux aux évènements de tempêtes, à des échelles de temps différentes pour une plage située à une latitude moyenne (Biscarrosse, France). Un site pilote des tropiques, la plage de Jamestown (Ghana), non soumis aux tempêtes, a également été analysé. 6 ans (2007-2012) de données sur la position du trait de côte, obtenues quotidiennement par imagerie vidéo, ainsi que les prévisions hydrodynamiques (ECMWF EraInterim) ont été analysées. Le climat de vagues est dominé par les tempêtes (Hs> 5% de seuil de dépassement) et leurs fluctuations saisonnières; 75% des tempêtes se produisent en hiver, et plus de 60 tempêtes ont été identifiées au cours de la période d'étude. Une régression multiple, montre qu'alors que les intensités des tempêtes actuelle et précédente ont un rôle majeur sur l'impact de la tempête, la marée et les barres sableuses jouent un rôle majeur sur la récupération de plage. La position moyenne du trait de côte calculée sur la période de récupération post-tempête montre que la plage de Biscarrosse se reconstruit rapidement (9 jours) après un évènement isolé et que les séries de tempêtes (clusters) ont un effet cumulatif diminué. Les résultats indiquent que le récurrence individuelle des tempêtes est clé. Si l'intervalle entre deux tempêtes est faible par rapport à la période de récupération, la plage devient plus résistante aux tempêtes suivantes; par conséquent, la première tempête d'une série a un impact plus important que les suivantes. Le trait de côte répond, par ordre décroissant, aux évènements saisonniers, à la fréquence des tempête et aux d'échelle annuelle. La méthode EOF montre de bonnes capacité à séparer la dynamique « uniforme » et « non-uniforme » du littoral et décrit différentes variabilités temporelles: les échelles saisonnières et à court terme dominent, respectivement, la première EOF (2D) et le second mode (3D). Le littoral de Jamestown a été étudié comme base d'un projet pilote entre 2013-2014. Les fluctuations du niveau de l'eau jouent un rôle prédominant sur l'évolution de la position du trait de côte. Les vagues et les estimations des marées obtenues par l'exploitation d'images vidéo sont corrélées avec les données de prévisions. Cette étude pionnière montre que cette technique peut être généralisée à toute l'Afrique de l'Ouest en tenant compte des multiples diversités et de la variabilité du climat régional, à travers un réseau d'observations.

Mots clés :

Littoral, tempêtes, récupération de plage, marées, sableuses

Title :Shoreline response to multi-scale oceanic forcing from video imagery

Abstract :

The aim of this study was to develop a methodology to statistically assess the shoreline resilience to storms at different time scales for a storm-dominated mid-latitude beach (Biscarrosse, France). On a pilot base, storm-free tropical Jamestown beach (Ghana) was also analysed. 6-years (2007-2012) of continuous video-derived shoreline data and hindcasted hydrodynamics were analysed. Wave climate is dominated by storms (*Hs*>5% exceedance limit) and their seasonal fluctuations; 75% of storms occur in winter with more than 60 identified storms during the study period. A multiple regression on 36 storms shows that whereas current and previous storm intensity have predominant role on current storm impact, tide and sandbar play a major role on the post-storm recovery. An ensemble average on post-storm recovery period shows that Biscarrosse beach recovers rapidly (9 days) to individual storms, and sequences of storms (clusters) have a weak cumulative effect. The results point out that individual storm recurrence frequency is key. If the interval between two storms is low compared to the recovery period, the beach becomes more resilient to the next storms; and the first storm in clusters has larger impact than following ones. Shoreline responds in decreasing order at seasonal, storm frequency and annual timescales at Biscarrosse. The EOF method shows good skills in separating uniform and non-uniform shoreline dynamics, showing their different temporal variability: seasonal and short-term scales dominate first EOF (2D) and second (3D) modes, respectively.

The shoreline at Jamestown was studied on pilot base from 2013-2014. Water level channges play a major role on shoreline changes. Waves estimates from video are in good agreement with hindcasts. This study shows the potential of the technique, to be replicated elsewhere in West Africa with all its diversity and regional climate variability through a coastal observation network.

Keywords :

Shoreline, storms, beach recovery, tides, sandbars

Unité de recherche

[EPOC, B18, UMR CNRS 5805 EPOC - OASU
Université de Bordeaux
Site de Talence - Allée Geoffroy Saint-Hilaire
CS 50023
33615 PESSAC CEDEX
FRANCE]

Dedication

To my parents (Tampog Kpinizuma and Yaw Yelbieyi Guo)

Aknowledgement

The international research stays gave me the opportunity to work with two leading laboratories in terms of coastal hydrodynamics to extreme storms and shoreline evolution as a whole. The experiences that I went through during my stays in LEGOS, Toulouse and EPOC, Bordeaux have built me not only intellectually but also personally. I am extremely grateful for having had the opportunity to meet such talented scientists and to share their expertise with me.

Many thanks to ARTS ('Allocations de Rercherche pour une Thèse au Sud') organisation for their immense financial support and design to strengthen research capacities in developing countries. I would also like to thank the French Embassy in Ghana for their support as ARTS. I thank also the facilitators of the Physical Oceanography and Application program in Benin; Dr. Bernard Bourles, Prof. Nick Hall and Dr. Yves du Penhoat.

I thank Dr. Nadia Senechal, my advisor, for her tireless roles as a mentor and advisor both in the field and through writing papers, administrative works and helping to advance this thesis. I would like to thank Dr. Rafael Almar co-supervisor, for first of all the creation of this thesis. His exuberance for the study and relentless passion to approach every scientific inquiry with the utmost enthusiasm influenced me to always do my best, and then try even harder to exceed my limits. Dr. Almar's patience and hope he had in me guided me this far and this thesis would not be success without him. He has taught, challenged, and encouraged me in an apprenticeship beyond my highest expectations. I would also to like to thank Dr. Bruno Castelle, a co-supervisor, for his active and constant response to all my requests. Dr. Castelle kept me on my toes in consistence with the saying that '*spare the rod spoil the child'*. I would like to thank Dr. Kwasi Appeaning Addo, co-supervisor, for being one of the most important and influential people in my academic, educational, and personal advancements. Over the last few years, Dr. Appeaning Addo has not only been an advisor and mentor, but also as an encouraging father. I also thank Dr. Vincent Marieu for his guidance in retrieving the video data and writing of my research.

My sincere gratitude also goes to Professor Domwini Dabire Kuupole (Vice Chancellor), Dr. Denis Aheto, Dr. Anani K. Fenin of University of Cape Coast and Mr. A. K. Armah of University of Ghana for their support and helps in getting me to this level. I would also like to thank the many graduate and undergraduate students who would have helped in one way or the other with field data acquisition during this study. And lastly, my deepest gratitude to the family and friends who have given me so much love, encouragement, and support during the last three years of my thesis endeavors. Many new things are in the future and I look forward to working with all of you again.

TABLE OF CONTENTS

Glossary

Variable name	Phyical Significance	units
	Constant	
g	Gravitational acceleration	9.81 ms^{-2}
ρ	Density of water	1.0 kg m^{-3}
	Forcing parameters	
C	Phase speed	ms^{-1}
Cg	Group speed	ms^{-1}
d_{min}	Lowest offshore water level	m
D	Storm duration	hr or days
Dir	Wave direction	° or rad
f	Camera focal length	m
h_b	Water depth at breaking	m
Hs	Significant wave height	m
Hs_{max}	Maximum storm height	m
Hb	Wave breaker height	m
$H_{b[lm]}$	Breaker height (video)	m
I	Storm intensity	m^2hr
I_i	Previous storm intensity	m^2hr
L	Offshore wavelength	m
P	Wave power	j/m^2
R	runup	m
RTR	Relative tide range	
$R\text{-}SLR$	Relative sea levl rise	
SLA	Sea level anomaly	m
T_p	Peak wave period	s
$T_{p(lm)}$	Peak wave period (video)	s
TR	Tide range	m
ζ	Horizontal setup	m

γ	wave breaking parameter	
	Morphodynamic parameters	
S	horizontal swash	m
T_r	Post-storm impact	m
w_s	sediment fall velocity	m/s
X	Cross-shore coordinate	m
Y	Alongshore coordinate	m
$\Delta\langle X_{s,i}\rangle$	Storm impact	m
$\sigma(X_s)$, 3D, $\Delta(X)$	Alongshore non-uniformity	m
$\langle \boldsymbol{X_s} \rangle$, 2D, $\langle \boldsymbol{X} \rangle$	Alonshore averaged shoreline position	m
$\langle \boldsymbol{X_b} \rangle$	Alonshore averaged sandbar position	m
ϕ	Beach memory	days

CHAPTER ONE

Introduction

".....It ain't what you don't know

that gets you into trouble.

It's what you know for sure that just ain't so"

Mark Twain

1 Introduction

1.1 Motivation

1.2 Scientific challenge

1.3 Organization of Dissertation

1.1 Motivation

The coastal zone is increasingly attractive given the evolution of modern socio-economic activities resulting in dense human settlements. Fertile coastal lowlands, abundant marine resources, water transportation, intrinsic values, amongst others motivate this coastal habitation. According to Small and Nicholls [2003], 23% of the worldwide population (1.2 billion people) lived within 100 km of the coastline in 1990, increasing up to 41% in 2003 [Martinez et al., 2007]. In addition, the United Nations (UN) Atlas of the Oceans [2010] stated that about 44% of the world population lives within 150 km of the coastline (e.g. Figure 1.1), and the rate of population growth is accelerating rapidly. Within the next 25 years, the coastal population is likely to further increase by approximately 25%, or by 18 million people, with most of the growth occurring in the already crowded states [Scavia, 2002]. An implication is that it may drive important economic development for coastal nations [Finkl, 1996]. For instance, in Hawaii it is estimated that over 60% of all jobs are related to tourism, which is driven by the appeal of sandy beaches [Fletcher et al., 1997; Genz et al., 2007]. Other coastal economies include commercial and subsistence fisheries, ports and industrial facilities that rely on shipping to coastal waters.

The increasing human pressure in the coastal zone, on the other hand, disturbs the natural equilibrium state and exposes the people to risk. Over the past century, the direct impact of human activities on the coastal zone has been more significant [Anthony et al., 2014] than impacts that can be attributed to climate change [Scavia et al., 2002; Lotze et al., 2006]. The major direct impacts include drainage of coastal wetlands, deforestation and reclamation, and discharge of sewage, fertilisers and contaminants into coastal waters. The situation whereby coastal lands are reclaimed for development (Figure 1.1), coastal sand is mined for construction purposes, vegetations are harvested for fuel, urbanisation of the coastal zone, damming, deep water harbours and dikes [Gilbert and Vellinga,1990; Meade and Moody, 2010], amongst others, makes coastal areas under unprecedented threat. This leads to increased erosion and flooding as a consequence of reduced sediment input, resulting in land and property loss among others. Financial losses brought about by beach erosion, submersion and storm damage are approaching economically and politically insupportable levels leading to changes in the paradigm: doing nothing costs more than finding adaptive strategies [IPCC AR5, 2013]. The importance of the coastal system therefore calls for better perception of its evolution.

Beach erosion is a difficult hazard to gauge for the stackholders because of the wide range of temporal scales and causes involved. For instance, it is hard to differentiate between the changes at seasonal or interranual scales, or those induced by the paroxysmal events (10^1 to 10^2 of meters), from long-term beach erosion due to sea level rise (centimeters to meters per year). In a sense, the general

public does not recognize the ubiquitous nature of beach erosion; they believe that the problem exists at only a few, well-publicized erosional hot spots. To further compound the problem, there is a paucity of quantitative shoreline change data. This can make researchers to assign, in other words generalise, e.g. a rate-of-change to an entire state [Galgano and Douglas, 2000], due to lack of information at other sections of their coasts. Recent research reports that global sea level may rise at unprecedented rate during the twenty-first century [0.3-0.4 mm/yr ± 0.8 m over 21th century, see Leuliette et al. 2004; Beckley et al. 2007; Ranasinghe et al., 2013; Cazenave et al., 2014], which in turn will likely drive increased erosion rates [Cooper and Pilkey, 2004; Stive et al., 2004, Ranasinghe and Stive, 2009; Ranasinghe et al., 2012]. Sea level rise exceeding one meter in some areas within the 21st century will increase the frequency and severity of storm impact [Gilbert and Vellinga,1990; Brooks, 2013]. For instance, increased mean sea level will result in a dramatic decrease of the return period of submersion events.

Ensuring the safety of growing coastal communities in the future requires more effective land use management policies based on accurate data, and a better understanding of coastal dynamics is therefore pressing [Galgano, 2008]. It is necessary to develop methodologies and to better quantify the causes of erosion to refine current and future public policy. One of the key challenges that engineers currently face is the lack of complete understanding on how our coastlines will potentially adapt to changing wave conditions and over what timescale this adaptation might occur.

1.2 Scientific challenges

Beach change covers a wide range of temporal and spatial scales. Stive et al. [2002] summarized studies around the world showing that different time scales (Table 1.1) can be identified, from hours to millennia. For instance, wave ripples with wavelengths of tens of centimeters, which can form or change within minutes [Becker et al., 2007]; and individual storm events that can alter the nearshore in hours, flattening the beach profile and causing offshore sandbar migration [e.g. Shepard, 1950]; seasonal (middle term) variations of the beach profile [Komar, 1998] with spatial scales of several km and time scales in the order of several years [Verhagen, 1989] or inter-annual changes in the submerged sandbar morphology like the so-called Net Offshore Migration including cyclic offshore migration of up 15years [Ruessink and Kroon, 1994]. Since the study of the nearshore is concerned with a wide range of scales, this must always be first assessed when approaching a certain problem at the coastal system.

An ideal measurement campaign requires some previous knowledge of the scales in order to define the spatial and temporal resolution of the survey and its duration. At a certain scale of interest, the effect of the lower scales will be described as boundary conditions and the effect of higher scales will be considered as noise. For instance, Stive et al. [2002] reviewed that beach variability at short and medium

time scales are the most relevant to coastal management, though underestimating the influence of longer-term effects as reported more and more in recent studies [among others; Yates et al., 2009; Pianca and Holman, 2015; Castelle et al., 2015].

Figure 1.1. Beach system, showing the use of coastal environments [credit: google images].

Overall, the shoreline is the interface between the water and beach [Komar, 1998]. It is commonly adopted as an indicator of both short and long-term coastline changes [Moore, 2000; Aarninkhof et al., 2003; Boak and Turner, 2005; Farris and List, 2007] and is central in defining coastal hazard. The shoreline presents temporal fluctuations at time scales of years, seasons down to single events [Yates et al., 2009, Davidson et al., 2009; Splinter et al., 2014; Castelle et al., 2014]. The presence of multiple time scales, with often predominantly percepted dramatic short-term storm event impacts might shelter longer, slow but key, persistent storms versus persistent impact or seasonal-to-interranual fluctuations of wave conditions. Although post-storm recovery is important, it is still poorly known. Scarce information currently exists on this transitional period as the beach comes back to its position prior to a storm event. This means storm recurrence frequency can influence the impact of storms and play on transient or longer term persistent impact.

Table 1.1. Spatio-temporal shoreline variability modified after Stive et al. [2002]

Time scale	Spatial scale	Scale description	Forcing factors	Morphological factors
Centuries to millennia	>100 km	Very long term	Relative sea-level changes and long-term climate changes	Sediment availability and differential bottom changes
Decades to centuries	10-100 km	Long term	Relative sea level changes, sand waves and extreme events	Coastal inlet cycles and littoral prism
Years to decades	1-5 km	Middle term	Wave climate variations, storms /extreme events	Surf zone bar cycles
Hours to years	0 - 1 km	Short term	Wave, tide, surge conditions and seasonal climate variations	Beach profile and sandbar dynamics

In spite of decades of research [e.g. Dolan and Davis, 1992; Sallenger, 2000; Coco et al., 2014; Karunarathna et al., 2014; Senechal et al., 2015], the immediate response of a beach system to storm event is still difficult to predict. This is because only wave contribution is generally considered to be the cause of shoreline changes. The modulation by sandbar and tide are often disregarded. Sandbars (Figure 1.2) are elongated shoals at wave-dominated coastlines commonly located parallel to the shoreline. The white bands offshore (Figure 1.2) indicate wave breaking on shallow bathymetry due to the presence of sandbars (outer and inner). The interface between the land and the water at mean sea level is digitised to mark the shoreline while the centers of the white bands are digitised alongshore (horizontally) and used as the sandbar location (Figure 1.2). Sandbars may result in less energy available to cause shoreline change (sheltering effect) and thus making the dynamics of the sandbar key to nearshore changes [van Enckevort and Ruessink, 2003, Vousdoukas et al., 2012]. Davis and Hayes [1984] indicated that beach morphology is not simply dependent on the absolute wave or tide, but also on the interaction between the two. While the importance of waves has been well documented, the influence of tides though recognised [Wright et al., 1984; Wright et al, 1987; Masselink and Short, 1993], is subtler and less understood. As a consequence, understanding and predicting shoreline change at barred beaches in mixed wave and tide environments remains a challenge due to the complex interactions between waves, tide [Davis, 1985; Masselink and Short, 1993] and sandbars [Banno and Kuriyama, 2012] as well as to previous conditions [Yates et al., 2009; Davidson et al., 2013], which usually are not directly accounted for.

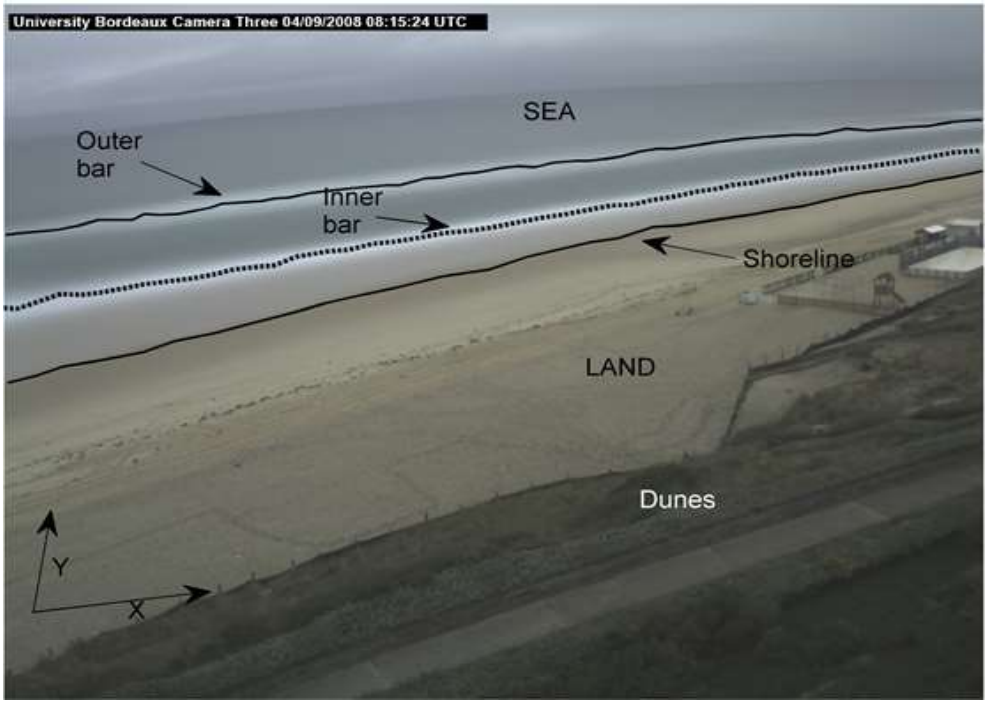

Figure 1.2. A 10-min time exposure video image on September 4, 2008 from the camEra video system, Biscarrosse.

Different approaches have been used to investigate shoreline evolution. They include ground truth surveys of cross-shore profiles [Miller and Dean, 2007] using GPS [e.g., Morton et al., 1993; Ruggiero et al., 1999; Yates et al., 2009] or using airborne LIDAR systems [Sallenger et al., 1999; Stockdon et al., 2002]. These approaches cannot be performed dayly on the long term. Such surveys are typically performed monthly, which does not allow capturing short-term storm-driven changes. The most significant changes that typically occur during and immediately after storms can therefore be missed. In addition, conventional methods are restricted by storm surge and wave-induced setup and runup and usually cannot extend much beyond the low-tide waterline. In recent decades, shore-based video cameras have become increasingly popular for monitoring beach changes. This is because it can be used to build a database of frequent (~hourly), long-term (~years) and spatially-extensive observations of beach behaviour [Holland et al., 1997, Holman and Stanley, 2007; Holman and Haller, 2013]. Video systems perform satisfactorily under diverse conditions such as storms and fair weather, and capture information along the entire beach (~kilometers) including the geometry of the submerged morphology such as sandbars [Lippmann and Holman, 1989]. This disruptive method has promoted a better understanding of the hydro- and morphodynamics [Holman and Stanley, 2007; Holman and Haller, 2013]. It has also provided operational and real time observations [Coco et al., 2005; Pearre and Puleo, 2009] as well as

data to feed and validate numerical [Smith et al., 2007; van Dongeren et al., 2007; Davidson et al., 2013] and conceptual models [e.g. Turki et al., 2013]

This thesis is part of ARTS ('Allocations de Rercherche pour une Thèse au Sud') programmes, designed to strengthen research capacities in developing countries. Its purpose is to prepare young researchers to integrate the higher education and research systems of a developing country once they have finished their PhDs. In this work, the shoreline response at different scales to current and previous wave conditions is seen as an important concern for coastal users. This is compounded by the lack of adequate knowledge in the shoreline recovery, and the modulation of the shoreline variation by tides and sand bars. This work will contribute to increase our understanding of shoreline variability and its primary driver including frequency of storms and seasonal evolution, modulation of the storm impact and recovery by tide and sandbar, will help coastal managers appreciate shoreline evolution and better incorporate the impact of storms into Shoreline Management Plans (SMPs).

The main aim of this study is to develop a methodology to statistically assess shoreline resilience to storm events at different time scales for Atlantic conditions applied to storm-dominated mid-latitude (Biscarrosse, France) and storm-free tropical (Accra, Ghana) beaches.

In order to achieve this, 3 objectives have been defined.

i) Quantify shoreline resilience to storms and sequences of storms, under the modulation of tide and sandbar at Biscarrosse, SW France.

ii) Assess the two-dimensional (2D) and three-dimensional (3D) shoreline behaviour at multiple scales at Biscarrosse, SW France.

iii) Test a pioneering study on the influence of waves and tide on shoreline change at the microtidal Jamestown beach, Accra- Ghana.

1.3 Organization of Dissertation

The document is divided into 6 chapters and two annexes:

Chapter 2: Processes of coastal hydro- and morphodynamics. Previous studies on multi-scale coastal wave climate and morphodynamics are reviewed. Other forcings such as tide and sandbars are described.

Chapter 3: Study area, data and methods. Study areas, the intermediate meso-macrotidal Biscarrosse and microtidal James town beaches, are presented, though Biscarrosse is the principal site of this dissertation.

Chapter 4: Statistical approach of coastal response to storms. The impact of storms is investigated, together with the modulation of tides and cross-shore sandbar locations on storm impact and recovery rates, using a multi-linear regression analysis.

Chapter 5: Two and three-dimension shoreline changes at short and seasonal scales. Cross-shore migration and alongshore deformation of shoreline are quantified through an empirical orthogonal analysis and combined with equilibrium shoreline modelling.

Chapter 6: Jamestown beach evolution under video surveillance. The potential for the extraction of waves, water level, and shoreline evolution is explored at the pilot site of Jamestown in Ghana over a 6-month period. Estimates are compared with hindcast data and main drivers of shoreline changes are identified

Chapter 7: Concluding remarks, discussion and perspectives

Bibliography: Presents a list of the references cited in this work.

Annex: Contains a list of the different scientific contributions that resulted in the completion of this thesis and other extra researches.

2 **Hydro-morphodynamic coastal processes**

...It is astonishing and incredible to us, but not to Nature;

for she performs with utmost ease and simplicity

things which are even infinitely puzzling to our minds...

Galileo

2.1 Wave dynamics in the nearshore: refraction, diffraction and breaking

2.2 Beach system

2.2.1 Bar-berm beach dynamics

2.2.2 Wave-induced short term morphodynamics

2.2.3 Tides and their control on nearshore processes

2.3. Shoreline dynamics

2.3.1 Shoreline definition: a review

2.3.3 Sandbar to shoreline coupling

2.4. Transient and persistent effect of storms

2.4.1 Wave climate and storminess: regional to beach scale

2.4.1.1 Wave climate

2.4.1.2 Storms

2.4.2 Storms impact

2.4.3 Post-storm Recovery

2.5 Shoreline acquisition and prediction

2.5.1 Different *conventional* shoreline measurement techniques

2.5.2 Video monitoring: context and background

2.5.2.a Video monitoring of the nearshore: 25 years of developments and use

2.5.2.b Shoreline and sandbar from video

2.5.3 Predicting shoreline evolution using models

2.1 Wave dynamics in the nearshore: refraction, diffraction and breaking

Waves in deep water are sinusoidal in form. Ideal wind waves in sinusoidal motion are typically characterized by a point of maximum elevation, i.e. the wave crest, and a point of minimum elevation, the trough [Davidson-Arnott, 2010]. The dynamics of waves from deep water to the nearshore (defined here as the region where waves are significantly affected by the bottom) is crucial to estimate inshore wave characteristics. In the nearshore, waves undergo changes due to shoaling, diffraction, refraction and depth-induced breaking and can move sediment and affect the seabed morphology, particularly during storms [Weaver and Slinn, 2010].

Waves bend towards shallow water along the beach due to refraction; a process in which the wave crests tend to parallel (Figure 2.1a) the depth contours and waves breaking parallel to the shoreline. Obliquely-incident breaking waves generate longshore currents that cause alongshore sediment transport. Diffraction (Figure 2.1b) occurs for large along-crest wave energy gradients. Wave diffraction is important in ports, harbours or around offshore islands.

The nearshore can be categorised into 3 distinct zones [Short, 1986] namely wave shoaling seaward of the breaker point, a surf zone of breaking waves and a swash zone of final wave dissipation on the upper beach (Figure 2.2a). The nature and extent of each of these zones ultimately determine the beach changes. The width of the shoaling, surf and swash zones, are functions of sediment size and wave height [Dean and Dalrymple, 2002]. Nearshore wave breaking, which is a widely known activity [Dean and Dalrymple, 2002; Svendsen, 2006; Davidson-Arnott, 2010] is also responsible for energy dissipation and sediment movement. Generally, waves break as they reach a limiting steepness of wave height to depth ratio $\gamma = h_b/L$, [Svendsen, 2006; Davidson-Arnott, 2010].

Figure 2.1 a) Wave refraction causes wave fronts to parallel the shape of the coastline as they approach shore and encounter ground (courtesy of google images) b) wave diffraction around a exposed feature; waves bend after passing an obstacle

These breaking waves exist in different forms namely spilling, plunging, surging and collapsing breakers [Iribaren, 1949; Battjes, 1974; Wang et al., 2002] which have been estimated based on the non-dimensional surf zone similarity parameter ξ_b [Battjes, 1974].

$$\xi_b = \tan\beta \left(\frac{H_b}{L}\right)^{-0.5} \qquad (2.1)$$

where β is beach slope, h_b is depth at breaking, L is deep water wavelength and H_b is the breaker height.

Though the breaker type is difficult to generalise on a non-uniform bathymetry, on alongshore-uniform beaches, breaker type is classified as surging/collapsing ($\xi_b > 3.3$), plunging ($0.5 < \xi_b < 3.3$) and spilling ($\xi_b < 0.5$) [Iribaren, 1949; Galvin, 1968; Battjes, 1974]. Plunging waves are characterized by an arched shape with a convex back and a concave front (seen on Figure 2.2a).

After breaking, the wave energy is dissipated over a variable cross-shore distance, a process that causes turbulence in the breaker zone. Besides, a surf bore is created as the top of the wave forms an air bubble between the crest and the plunging top. The kind of breaking, however, depends on the bottom topography. On barred beaches it is seen that after the first breaking the energy dissipation becomes zero as the water depth behind the bar increases and it is kept as zero until the next breaking occurs [Wanatabe, 1988]. An important factor in the breaking process is also in the wave height and the water level that

determine the position of breaking. Shoaling occurs when the progressive wave encouter the seabed. If the water level is too high and the waves are not encoutering the seabed, shoaling will not occur and the waves do not break. At steep beaches, plunging or surging wave breaking occurs on the upper beach, while gently sloping beaches produce a spilling breaking over wide distances to dissipate wave energy [Galvin, 1968; Svendsen, 2006; Davidson-Arnott, 2010].

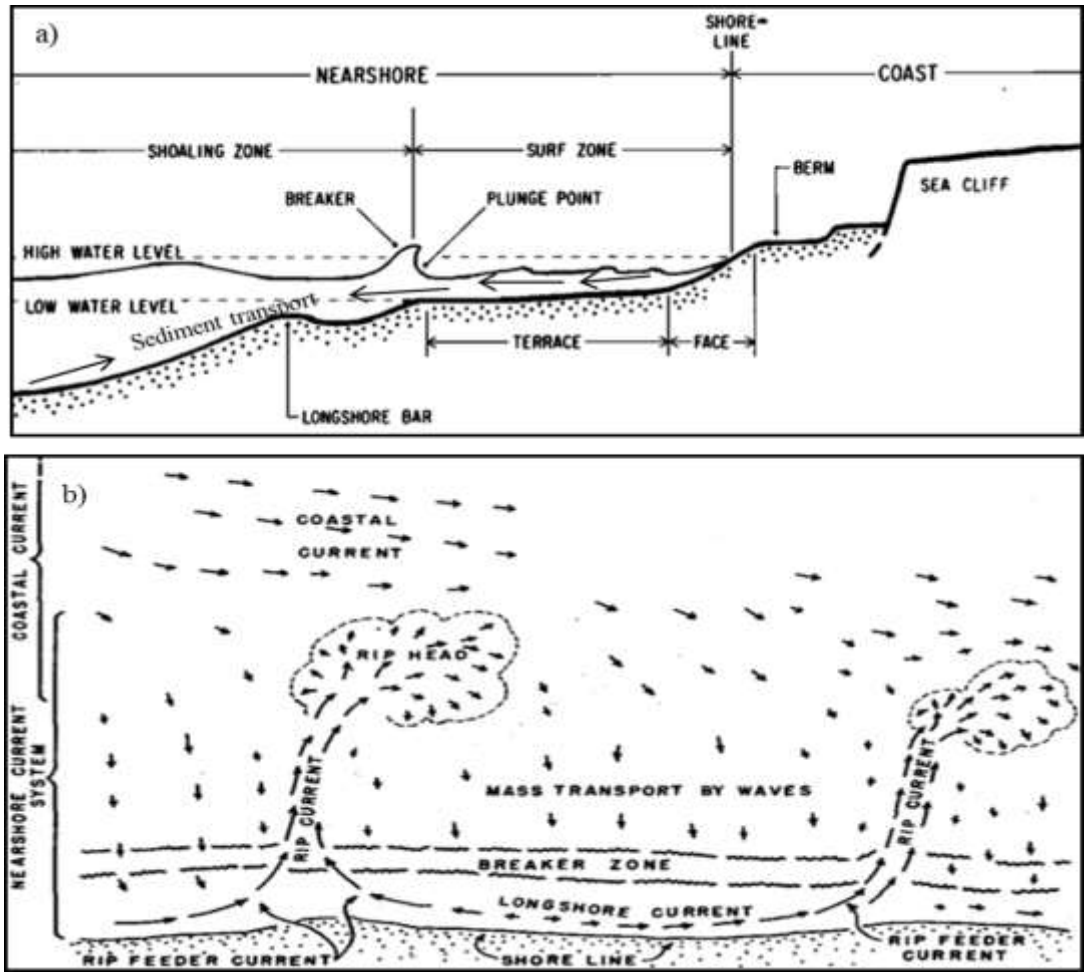

Figure 2. 2 a) schematic typical beach profile, terminology and zonation b) Schematic diagram of surface flow in coastal and nearshore current systems. Length of arrows indicates their relative magnitudes [Source: Shepard and Inman, 1951].

When water run up on anyone standing on a beach, they often feel the water tugging the sand away from under their feet, due to a force called undertow. This undertow is a wave-induced current, generated to compensate for the shoreward mass flux of the waves. Near the bed, it interacts with wave motion to dictate the amount of sediment put in suspension, after wave breaking. In the water column, it moves sediment offshore, counteracting the suspended flux due to waves. Hence, this current is crucial in

determining the amount and direction of sediment movement in nearshore regions [Guannel and Ozkan-Haller, 2014]. The breaking of waves in the nearshore results in changes of the wave-induced momentum that drive nearshore currents and pressure gradients [Maa et al., 2001]. Hence understanding these flows is a prerequisite to predicting morphological change. Besides, the mean breaking-wave driven nearshore circulation has a complex three-dimensional structure even on relatively simple bathymetry.

Breaking waves may generate strong offshore flows often call rip currents (Figure 2.2b) when waves push water up the beach face. If there is an area where the water can flow back out into the ocean more easily, such as a break in the sand bar, then a rip current can form. These are strong, offshore-directed currents known to pull the water (or sediments) at all water depths through the surf zone and dissipates offshore of the breaking waves. These are also essential currents for nearshore management.

In general, observed breaking induced currents contain substantial fluctuations [Raubenhimer, 2004] at infragravity periods (about 1 minute) that appear to result from a combination of gravity and vorticity (e.g. shear) waves, but the generation mechanisms and overall significance of these low frequency motions are largely unconsidered. One possible reason for this is lack of nearshore wave conditions. For example, on most study sites breaking waves are used [e.g. Maa et al., 2001; Guza and Feddersen, 2012; Splinter et al., 2014a] though breaking waves are usually obtained from mathematical relations [e.g. Larson et al., 2010] through some sporadic means.

2.2 Beach system

2.2.1 Bar-berm beach dynamics

One approach to the quantification of beach morphology has been the identification of sets of morphologic states. Investigations have long showed that beaches experience distinct seasonal onshore/offshore transport of sand [Shepard, 1950; Shepard and Inman, 1951]. A simple but well-known example of such parameterisation is the summer-winter (or bar-berm) model [e.g. Shepard, 1950], based on observations that the shape of many beaches tends to change from unbarred to barred profiles (Figure 2.3). The beach is considered only in a one-dimensional structure of erosion or accretion; the basic beach profiles attainable are the swell profile formed when the waves are of low steepness and the barred profile or storm profile formed when the waves are of high steepness. Variation of forcing conditions results in uniform sediment movement onshore/offshore. It is assumed that the exchange of material between the bar and the berm takes place under conservation, that is, no material is lost offshore. The volume eroded from the berm is assumed stored in one offshore bar (or, representative morphological volume) that will reach a certain equilibrium bar volume if the wave conditions are steady and the grain size does not vary.

If the bar volume at any given time is smaller than the equilibrium volume, then the sandbar volume will grow, and vice versa. From Figure 2.3, we see that growth in bar volume causes the corresponding decrease in berm volume (and shoreline retreat), and decay in bar volume causes increase in berm volume (and shoreline advance). Alongshore-averaged (or two-dimensional 2D) cross-shore sandbar dynamics can thus be considered as morphologic adjustment to the hydrodynamic forcing [Aagaard et al., 1998], and more precisely the convergence of sediment transport at the breakpoint.

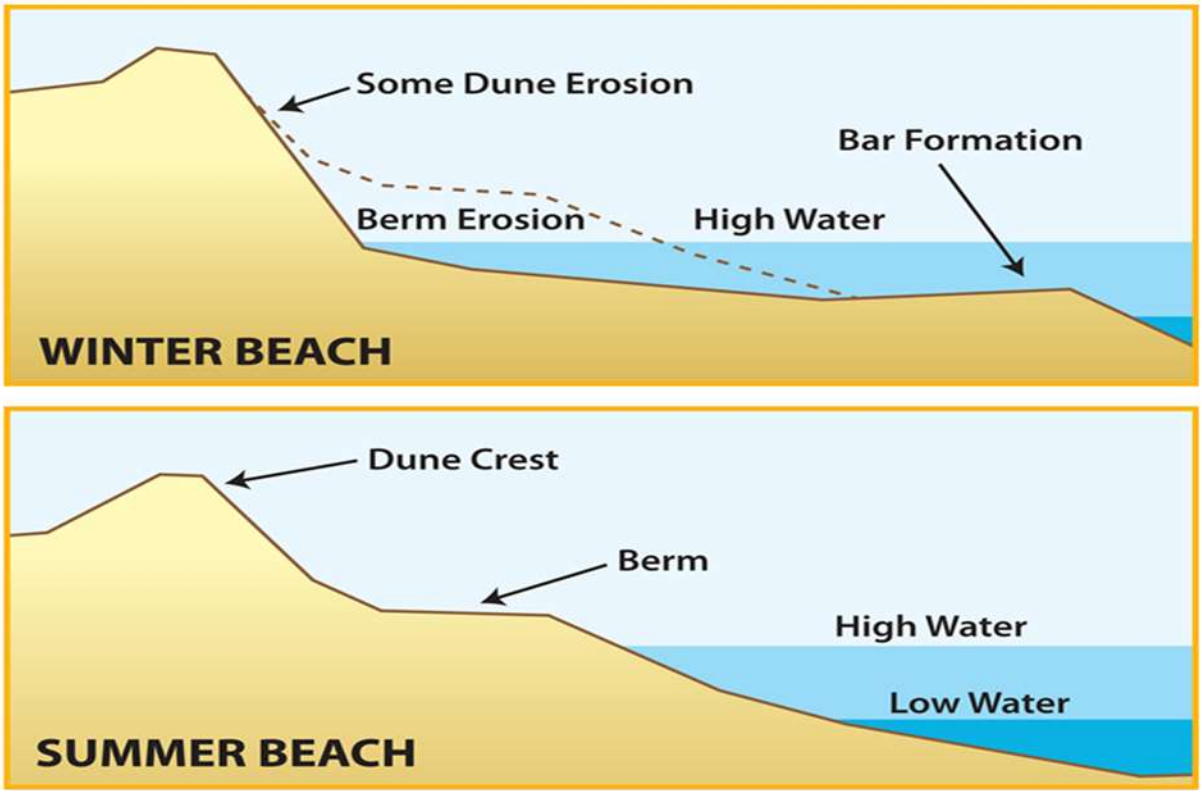

Figure 2.3. Seasonal transformation from a summer beach (lower plot) to a winter beach (upper plot), accessed on 26/01/2016 on Google search.

Longshore bars are common features at wave-exposed beaches, and have influence on the foreshores [Takeda and Sunamura, 1992]. They also constitute the dominant mode of bed variability in the submerged nearshore area. While annual cycles are observed at most coastlines, with offshore migration during energetic winter months, significant changes also occur on a much shorter time scale, especially in response to storms. It has long been known that during storms or energetic conditions, sandbar moves seaward (through undertow current) and moves landward during low energetic conditions [Birkemeier, 1984; Gallagher et al., 1998; Hoefel and Elgar, 2003] as shown in Figure 2.4. Additionally, seasonal trends in sandbar location can often be observed, whereby a sandbar is located more seaward

after autumn and winter months with high waves than after the low-wave spring and summer months. It has also long been established that sandbar strongly controls the wave breaking location [Lippmann and Holman, 1989; Plant and Holman, 1998; Ruessink et al., 2007] and, hence, cross-shore sediment transport patterns; this may reinforce or suppress further bathymetric modifications [Plant et al., 2001] through a feedback on hydro-morphodynamics. For instance, wave-breaking across an outer bar affects the hydrodynamics and hence the evolution of an inner bar. Sediment transport will be affected by the incidence of obliquely breaking waves (they lead to longshore transport) and the kind of sandbars that occur.

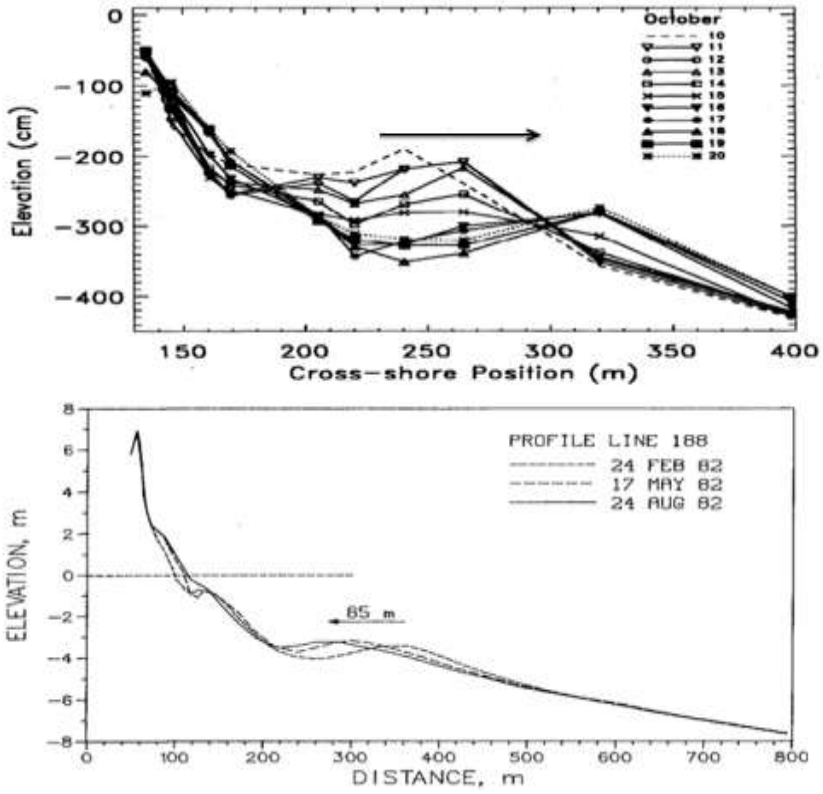

Figure 2.4. Sandbar migration during storms and non-storm period. Upper panel: rapid offshore movement of sandbar resulting from ten stormy days [Gallagher et al., 1998]. Lower: slow onshore migration of the outer bar during a six month period of low wave conditions [Birkemeier, 1984].

Lippmann and Holman [1990] identified that the most frequently observed sandbar morphologies are the longshore-periodic (rhythmic) bars where linear bars occur under highest wave conditions, though unstable (mean residence time = 2 days). The study found out that shore-attached rhythmic bars were the most stable (mean residence time of 11 days) and generally form 5-16 days following peak wave events. Non-rhythmic, three-dimensional bars are very transient (mean residence time = 3 days), making the

beach changes more complex than the usual 2D-structure. Given that transitions to higher states occur under rising wave energy among the possible higher beach states, this suggests that up-state, erosional transitions (based on offshore bar migration) are better described by an equilibrium model where response is better correlated with incident wave energy than with preceding morphological state. Therefore, further understanding is required especially in regions where tide range and wave conditions are very comparable.

2.2.2 Wave-induced short term morphodynamics

Numerous attempts [Wright and Short, 1984;Hansen and Barnard, 2010; Splinter et al., 2014b] have been made to relate short term (daily or weekly) fluctuations in the wave field with beach changes. Notably, Wright and Short [1984] developed an empirical predictive model to relate beach states to the dimensionless Dean parameter, Ω. In order to understand the complexity of the beach due to variation in forcing and morphology, they used Ω [Goulay, 1968] given in Eq. 2.2 to classify three distinctive beach types based on the wave breaking height H_b, period T, and sediment characteristics (the sediment fall velocity w_s):

$$\Omega = \frac{H_b}{W_s T} \qquad (2.2)$$

Wright and Short [1984] showed that the three distinctive beach states are related to Ω with Ω>6, 1< Ω<6 and Ω < 1 for dissipative, intermediate and reflective beaches, respectively. In this classification, these three beach states are subdivided into six commonly occurring beach states: dissipative, longshore bar trough (LBT), rhythmic bar and beach (RBB), transverse bar and rip (TBR), low-tide terrace (LTT), and reflective. Following this beach classification by Wright and Short [1984], a beach cannot be resumed to a pure cross-shore profile evolution but present irregularities in the longshore due to variation in forcing (Figure 2.5).

As indicated earlier, the cross-shore beach dynamics can be of an alongshore uniform (or two-dimensional, 2D) character and reflect overall on/offshore shoreline migration depending on the energy incident on the beach. Variation of the beach cross-shore position, for example the isolevel position, is a clear and easily-understood indicator of beach accretion and erosion, with seaward and landward migration, respectively. From Wright and Short [1984], beaches are mostly 2D for very energetic conditions or 3D for intermediate conditions. In the 2D state, the beach varies minimally or not all alongshore (Figure 2.5a). By the Wright and Short model, a beach can therefore have 2D patterns if it is in the dissipative or reflective state. In times when larger amount of energy due to forcing occurs, erosional sequences [Short, 1999] could cause the beach state to jump to the dissipative state within hours

[Lippmann and Holman, 1990; Van Enckevort and Ruessink, 2003; Ranasinghe et al., 2004]. In the dissipative state (Figure 2.5a), it is believed that there would be the removal of berm feature yielding a 2D profile and the development of bar type profiles. Simply, beach cusps are non-existent or minimal while the beach now shows no alongshore variations. In the dissipative state, the beach is gentle and is characterized by wide surf zone. On the other hand, during the reflective state (Figure 2.5f) when wave conditions are weak, the beach becomes steep with berms prograding seaward to give a wider beach and narrow surf zone leaving the beach in 2D form. The trends and prediction of 2D positions are therefore tricky because the beach state can only be identified by its modal state [Wright and Short, 1984]; in other words the present beach state is determined by the recent history of both the wave field and the beach morphology.

During an accretionary (downstate) sequence with decreasing energy, the 2D dynamics turn into 3D as the beach advances through several intermediate states, from high energy dissipative members towards the reflective state over a number of days to weeks [Lippmann and Holman, 1990; Van Enckevort et al., 2004] and become 2D again. In the intermediate state of moderate to high energy, the longshore beach component is alongshore non-uniform (or three-dimensional, 3D) and mostly corresponds to changes in the non-uniformities in the shoreline. 3D shoreline development are associated with periodic developments such as cusps [Coco and Murray, 2007] or forced pattern from sandbar irregularities (Figure 2.5b to e) that form during the intermediate states according to the Wright and Short classification. With characteristic rip circulation, dynamic bar forms, abundant surf zone and beach sediment and moderate waves, they can undergo rapid changes as wave height fluctuates causing rapid reversals in onshore-offshore and alongshore sediment transport [Wright and Short, 1984].

Increasing in energy and irregularity, the intermediate states are identified as LTT, TBR, RBB, and LBT (Figure 2.5b to Figure 2.5e). Wright and Short [1984] show that the intermediate beaches exhibit complex morphologies with increasing three dimensionality due to structures such as the bar-trough topography or bathymetry, formed during the mechanism of an up or downstate. As explained earlier, sandbar dynamics may therefore be significant for the nearshore complexity as sandbar moves about beneath the water, altering the movement of waves and water depth. Recently, Stokes et al. [2015] additionally showed that a tidally-modulated wave power term may influence the rate of morphological change, like the 3D dynamics. Besides, given this likely interaction between 2D sandbar and shoreline, it is possible to hypothesise that sandbar positions can affect 3D shoreline variations and the larger nearshore dynamics.

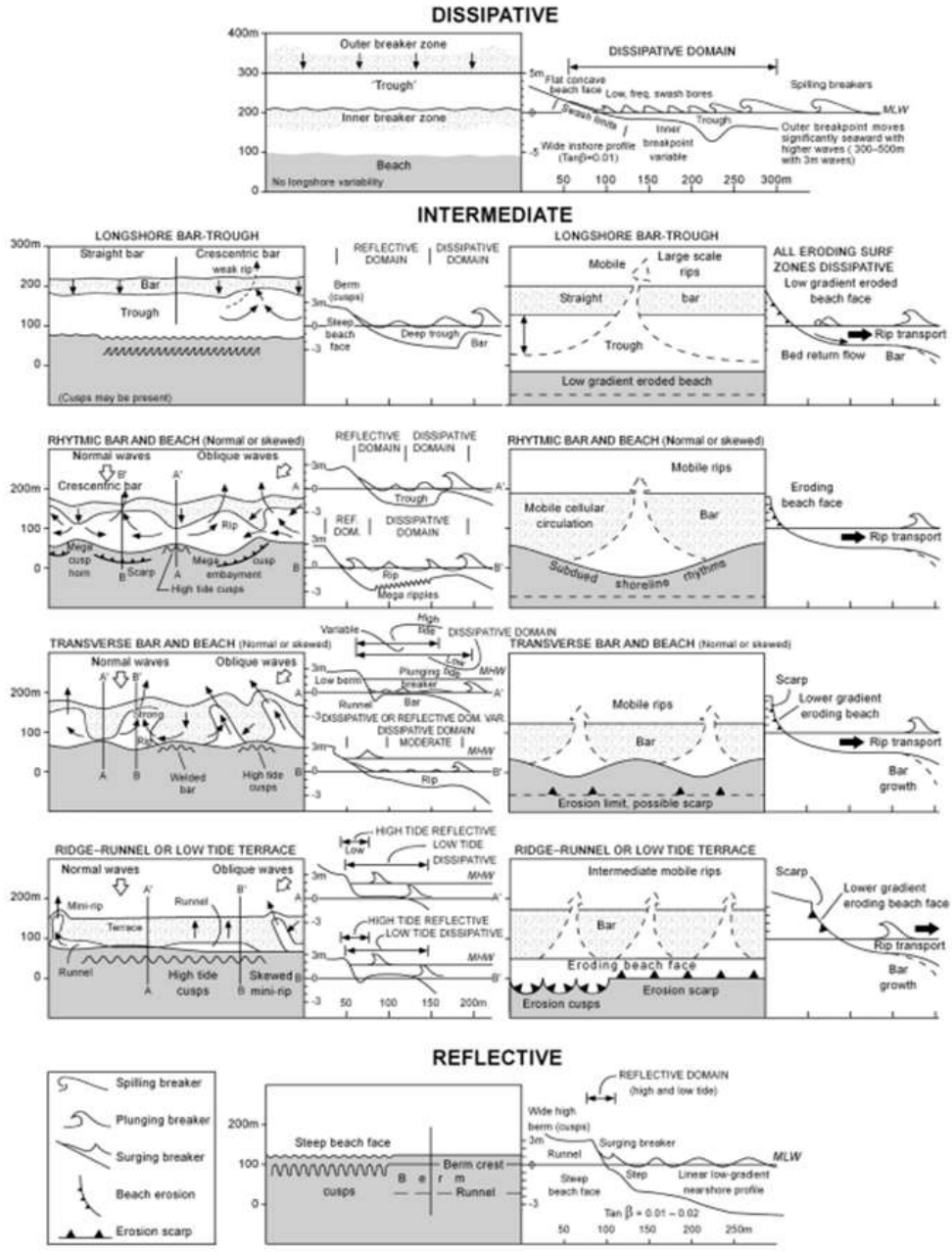

Figure 2.5. Plan and profile configurations of the six major beach states [Wright and Short, 1984; Short, 2006] based on the dimensioless Dean parameter $\Omega = H_b/w_sT$. From (a) to (f), we have decreasing energy and Ω, respectively for dissipative, LBT, RBB, TBR, LTT and reflective states.

2.2.3 Tides and their control on nearshore processes

Astronomical tides drive substantial modulation of wave action on beach dynamics and subsequent beach types (Figure 2.6). Beaches are classified as microtidal (<2 m), or meso-tidal (2-4 m) or macro-tidal (> 6 m) based on the tide properties [Davies, 1964; Masselink and Short, 1993; Short, 1996].

Micro-tidal beach systems are assumed to be wave dominated, with a low tide range that has a minor to negligible role in determining beach morphology. Tide is therefore largely ignored in assessing general beach morphodynamics. At microtidal beaches, the swash, surf and shoaling zones are therefore assumed to be stationary [Short, 1996]. In contrast, tide range is important on macro-tidal beaches as it could result in the formation of multiple sandbars and changes in swash processes. When waves suspend sediment in the narrow surf zone, inducing pulse-like high sediment concentration in shallow water, the suspended sediment can be advected by the tidal current causing erosion [Shi et al., 2013). Davidson and Turner [2009] found that increasing the tidal range diminishes the bar amplitude and spread it out across the profile. The impact on shoreline erosion is thus lessened by increasing the tidal range *TR*, as the impact is distributed over a broader region of the profile.

Generally, small tidal range is expected to increase surf zone and swash processes and thus to result in rather short response times to time-varying incident wave conditions, whereas a large meso- to macro-tidal range favours shoaling-wave processes and, hence, increases the response time. The significance of tidal oscillations for the beach morphodynamics can be quantified by the ratio of tidal range to wave height [Masselink and Short, 1993; Short, 1996; Masselink et al., 2006]. For values of the relative tide range (RTR, Eq. 2.3) exceeding 5-10, morphodynamic effects of tidal translation is significant [Masselink and Short, 1993].

$$RTR = \frac{TR}{H_b} \qquad (2.3)$$

From equation 2.2 and equation 2.3, the RTR can be linked to the dimensionless fall velocity, Ω that Wright and Short [1984] took to describe the beach states:

$$\Omega = \frac{TR}{RTR(W_S\, T)} \qquad (2.4)$$

This formulation suggests that increasing *RTR* values result in low Ω and reflective beaches, while decreasing values may result in more dissipative beaches. Landward of the breaker zone, single bar beaches are dominated by surf and swash zone processes. This is not always so especially on two or multiple barred beaches [Masselink and Short, 1993; Short, 1996]. As tide range increases the impact of both the swash and surf zone processes decreases. The *RTR* values do define tide-dominance when the values are large and wave-dominance when *RTR* values are small. For each tidal cycle, the maximum H_b can be considered representative of the breaker condition; even during energetic waves and large tides. Masselink and Short [1993] as well as Short [1996] reviewed that when Ω>1 or *RTR* < 5 the formation of sandbars is prevalent, whereas when Ω<1, there is formation of berm under dominant onshore transport (Figure 2.6).

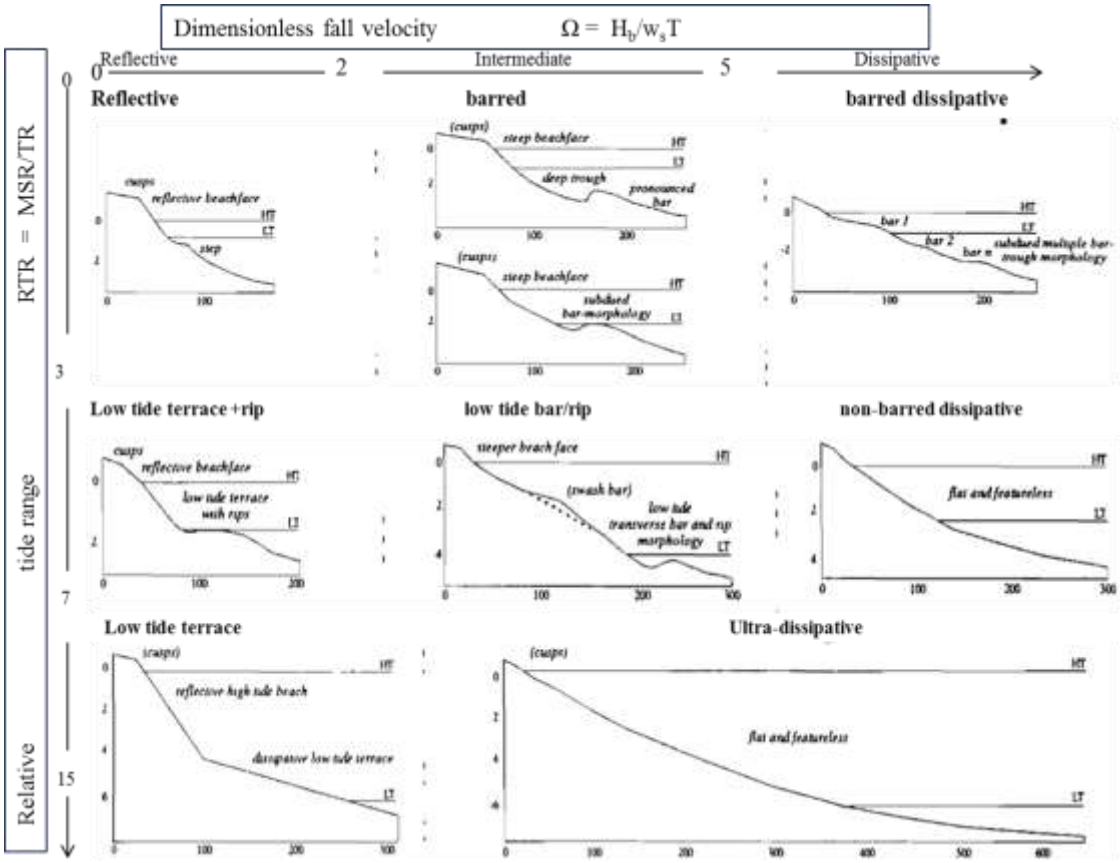

Figure 2.6. Conceptual beach model [Masselink and Short, 1993]. The Beach state is a function of the relative tide range ($RTR = TR/H_b$). HT and LT refer to mean high tide and mean low tide levels, respectively.

In addition, the formation of an intertidal bar around the mid-tide position during low-wave conditions and neap tides can be triggered by a reduction in *TR* but not the rise in H_b. For example, a new forcing parameter, Hydrodynamic Forcing Index (*HFI*), has been proposed that allows representing the cumulative effect of wave and tide forcing [Almar et al., 2010]. The *HFI* index is defined as the ratio of offshore significant wave height *Hs* to the (averaged over a tidal cycle) lowest offshore water level d_{min} experienced over a tidal cycle above the lowest astronomical tide (LAT):

$$HFI = \frac{Hs}{d_{min}} \qquad (2.5)$$

This *HFI* parameter is somewhat more suited to storm impact than the *RTR* at the time scale of storms as *HFI* is high during a storm, which is not necessarily the case for *RTR*.

2.3 Shoreline dynamics

2.3.1 Shoreline definition: a review

The shoreline has been broadly investigated and defined [e.g. Crowell et al., 1991; Moore et al., 2000; Stockdon et al., 2002]. Shoreline is commonly identified with indicators (proxies) based on geographical, morphological or hydrodynamical considerations [e.g. List and Farris, 1999; Zhang et al., 2002; Stockdon et al., 2002]. The shoreline can be defined at the location of the waterline identified by a change in colour or gray tone caused by differences in water content around it or a line of seaweed and debris. For some, shoreline is the seaward edge of the vegetation. Boak and Turner [2005] reviewed these proxies (Figure 2.7) into visually discernible coastal features (e.g. high water lines, HWL) and specific tidal datum (the intersection of the coastal profile with a specific vertical elevation, e.g. mean high water, MHW line).

The HWL, which delineates the landward extent high tide watermark, is commonly chosen as the shoreline. However, a vast number of studies [Crowell et al., 1991; Moore et al., 2000; Stockdon et al., 2002] indicate difficulties in interpreting HWL from aerial photographs. In addition, on a low-sloping beach the horizontal offset of the shoreline indicator HWL due to wave, tide, or wind effects can be on the order of several tens of meters [Thieler and Danforth, 1994].

On the other hand, tide-coordinated or datum-based shorelines based on tidal elevation generally consist of the position of a specified elevation contour. Figure 2.7 (lower section) shows an example of the shoreline definitions based on tidal datums [Plant and Holman, 1997; Madsen and Plant, 2001; Aarninkhof et al., 2003; Kingston, 2003; Moore et al., 2006] commonly used with digital detection techniques (e.g. video images). The shoreline is defined at the interface between the beach and the sea only at the selected tide (elevation contour). Despite this, unlike microtidal beaches, on meso- to macrotidal barred beaches it is not straightforward to select the elevation that best represents the overall beach response. In line with this, Castelle et al. [2014] recently found out that the intersection of the coastal profile with the MHW level is an effective shoreline proxy for meso- to macrotidal, high-energy, multiple-barred beaches. Due to its location on the upper beach, the inner-bar and berm dynamics have little influence on the shoreline estimation. Such selection is also motivated by previous findings at Ocean Beach where changes in the MHW and MSL shoreline proxies are well correlated ($R = 0.9$ for most of the beaches) to volumetric change [Hansen and Barnard, 2009; List and Farris, 2007].

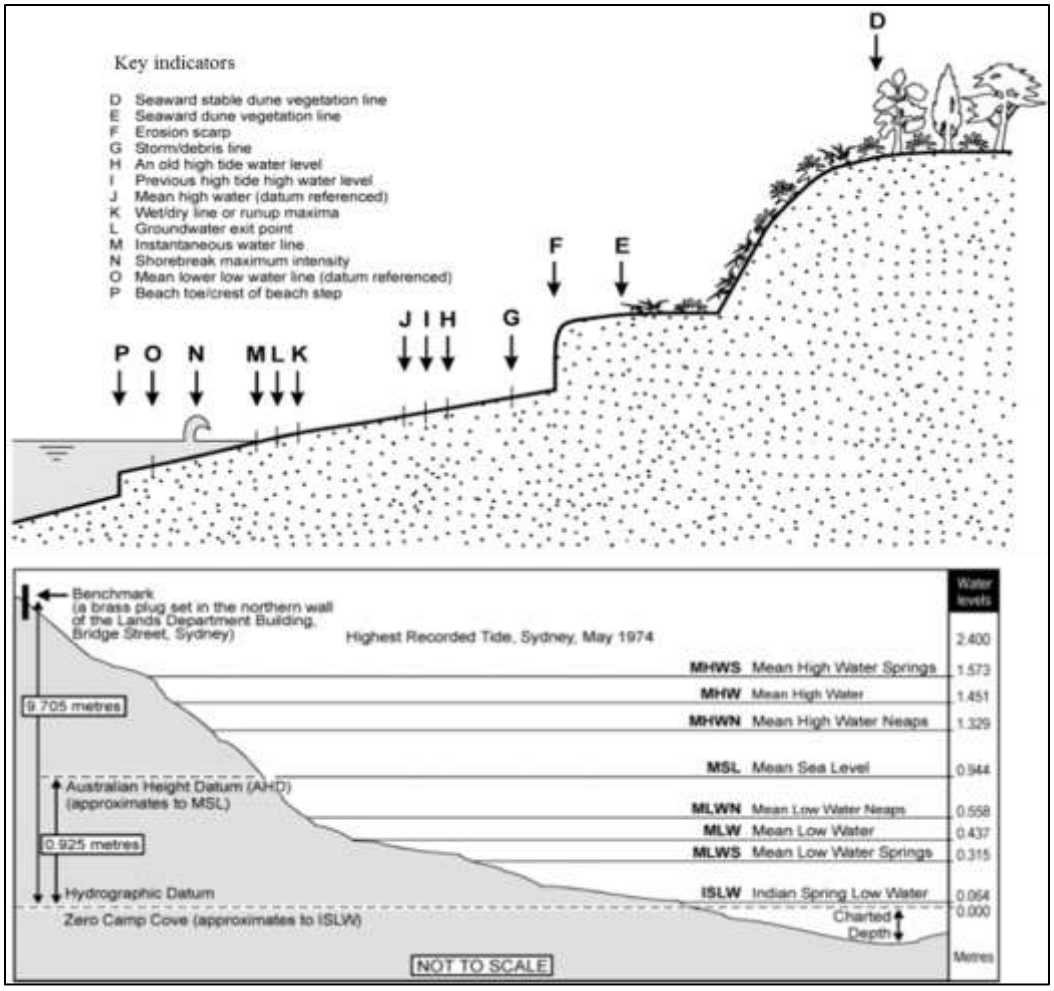

Figure 2.7. Shoreline indicators based on specific tidal datums (upper plot). On the lower plot are tidal datums used along the New South Wales coastline, Australia [adapted from Boak and Turner, 2005] as proxy for shoreline.

2.3.2 Sandbar and shoreline coupling

Sandbars reduce the amount of wave energy reaching the shoreline by limiting the wave height through breaking. The coupling between sandbar and the shoreline may be linked to the distance between the sandbar and the shoreline [e.g. Sonu, 1973; Wright and Short, 1984; Van de Lageweg et al., 2013]. Sonu [1973] observed an out-of-phase relationship of inner bar and shoreline patterns, i.e. an inner bar bay facing a seaward bulge in the shoreline. An in-phase relationship can also sometimes be observed with an inner bar horn facing a seaward bulge in the shoreline [Castelle et al., 2010; Price and Ruessink, 2011]. The relationship between inner- and outer bar patterns is reminiscent of the more commonly observed relationship between inner bar patterns and shoreline rhythms [e.g. Wright and Short, 1984; Coco et al., 2005; Thornton et al., 2007]. In a related study, Davidson and Turner [2009] identified that

when the bar is lower in amplitude and located closer to the shoreline, it lessens shoreline erosion. Several processes and physical parameters have been hypothesised to affect the sandbar-shoreline coupling. Birkemeier [1984] showed that the beach profile configuration is modified by the location and horizontal movements of the sandbar crest. That large change to the profile in terms of volume movements always resulted in significant sandbar movement.

One parameter that links this sandbar and the morphology is the beach steepness (slope) parameter, γ (defined as h_b/L in section 2.1); it dictates where the wave breaks on the beach. Recent works [e.g. Davidson and Turner, 2009] have shown that increasing γ can move the bar progressively shoreward, while decreasing γ causes a seaward translation. However, Davidson and Turner [2009] found that on average, varying γ has negligible impact on the shoreline evolution. From Davidson and Turner [2009] review, it is deduced that although the shoreline and sandbar sections of the profile could be coupled in the sense that erosion of sediment from the shoreface is deposited on the sandbar, it is still insufficient to substantiate that enhanced dissipation over a developed sandbar might reduce energy levels at the shoreline relative to erosion. Interestingly, no increase in sandbar width was seen to impact the shoreline evolution. In essence, this indicates not all sandbar characteristics affect the shoreline. Another parameter, the sandbar crest depth variability, though important [Coco et al., 2005; Ruessink et al., 2007] maybe less useful as an indicator of sandbar activity on the shoreline, since large sandbar movements occur with little or no change in crest depth. However, Pruszak et al. [2011] revealed that the location of the inner sandbar and the shoreline can exhibit a reasonably high correlation showing their onshore/offshore movements are very consistent even if in the outer sandbar region the location of the outer bars subsystem is much less correlated with the shoreline position. Finally, the angle of wave incidence has been suggested to affect the phase of coupling of shoreline and sandbar since larger angle of incidence drive strong longshore currents, while longshore currents destroy sandbar variability [Price and Ruessink, 2013].

There seems to be some debate as to how and what is associated to sandbar to shoreline coupling. Although the variability of bars and their links to environmental factors has been the objective of many analyses, the direct interactions between sandbar and the shoreline still seem to be insufficiently identified. The relation between the sandbar and the shoreline could be more complex due to the presence multiple sandbars, as there can be interaction between the inner bar and outer bar [e.g. Castelle et al., 2010; Price and Ruessink, 2013]. At present, previous models and methods have not explained the quantitative content of the sandbar in relation to shoreline change in comparison to other parameters such as the waves and tides and antecedent conditions. The link between shoreline and sandbar location is sketchy as we found in the literature. For instance the relative contribution of the sandbar location to

shoreline changes during storms in isolation and during recovery has not been clearly observed in the literature. Questions like how the sandbar to shoreline distance will influence beach recovery magnitudes and recovery duration can be used to establish a relation between the location of sandbar and the shoreline.

2.4. Transient and persistent effect of storms

2.4.1 Wave climate and storminess: regional to beach scale

2.4.1.a Wave climate

Waves are the main driver of nearshore hydro-morphodynamics and are generated by wind either locally or from distant location. The height and period of the waves depend on the speed and duration of the generating winds and the fetch. The types of waves that break on a beach and their seasonal variance are known as the wave climate. Several findings suggest that along wave-dominated coastlines, the impact of regionally-varying wave climates will have a more significant impact in the coming decades and cannot be ignored in forecasting future shoreline variability [Brunel and Sabatier, 2009; Ranasinghe et al., 2012; Ruggiero, 2013]. In light of this, offshore and coastal wave climate evolution is particularly important for human activities at high energetic regions (e.g. Bay of Biscay and the French Atlantic coast). To achieve this, the storminess (intensity and recurrence of storms) [Masselink and van Heteren, 2014] and wave seasonality are key.

In the last half-century, the variation in wave climate has been analysed along the North Atlantic. Wang and Swail [2001] detected an upward trend in seasonal extremes of *Hs* from 1958-1997, where higher rates occur in winter. Dodet et al. [2010] investigated the variability in the North-East Atlantic Ocean (25°W-0°W and 30°N–60°N), with hindcast (1953–2009) waves. They detected strong seasonal and inter-annual fluctuations of wave climate, with winters characterized by large and long-period waves of mean direction spreading from south-west to north-west, and summers characterized by smaller and shorter-period waves originating from northern directions. From northern (55°N) to southern (35°N) latitudes, the significant wave height (*Hs*) decreases by roughly 40%, the mean wave direction rotates clockwise by about 25% while the peak period (*Tp*) only grows by 5%. Linear trend analysis between these years showed spatially variable long-term trends, with a significant increase of *Hs* (up to 0.02 m/yr) and a counterclockwise shift of direction (up to -0.1° per year) at the northern latitude, contrasting with a fairly constant trend for *Hs* and a clockwise shift of direction (up to +0.15° yr) at southern latitudes, while in the long-term trends of *Tp* are less significant. This variation in the trend of wave parameters is very significant especially when wave effect dominates the beach processes.

Using dynamical and statistical methods [Charles et al., 2012; Laugel et al., 2014], projected wave heights, periods and directions have been analysed at regional scale along the coast of the Bay of Biscay. Clockwise shift of winter swell directions is linked to the intensification and the northeastward shift of strong wind core in the North Atlantic Ocean. As offshore changes in the wave height and the wave period as well as the clockwise shift in the wave direction continue toward the coast, it would impact the coastal dynamics by reducing longshore wave energy. Similarly, the large scale spatial variability of sea states at the French Atlantic coast was assessed by Butel et al. [2002] using wave rider time series at Biscarosse (in 26 m depth). 3D histogram distributions (Figure 2.8) of significant wave heights, periods and directions indicate that a wide range of wave directions and age can be measured at Biscarosse, mainly due to atmospheric forcing.

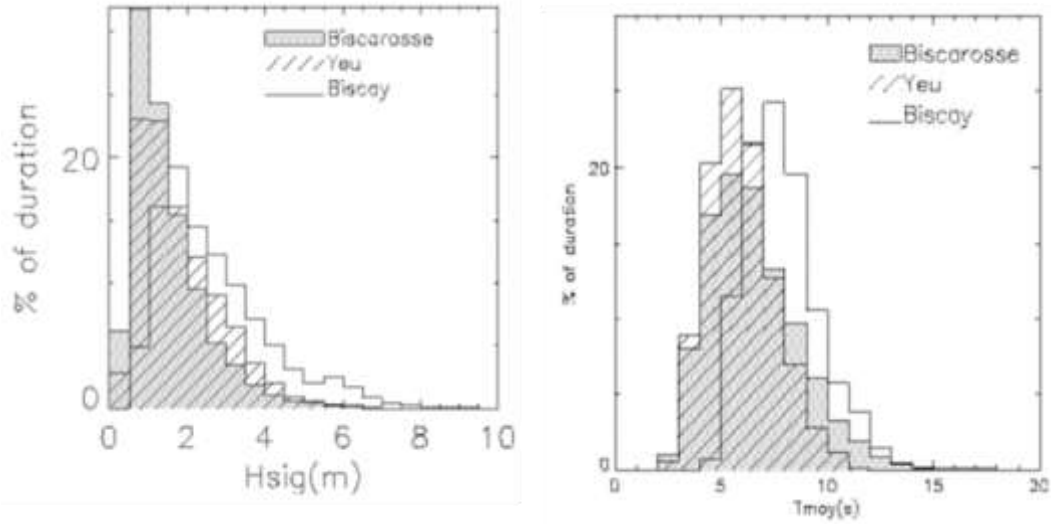

Figure 2.8. Left: 1-D histograms of significant wave height (Hs) and, Right: mean period (Tp). Gray shade is for Biscarosse, dashed surface is for Yeu, and white with thick lines is for Biscay after Butel et al. [2002].

It is shown that Biscarosse beach, a characteristic of most of the beaches encountered in the SW France is exposed to long and energetic waves originating mainly from the W-NW. During fall and winter seasons (typically November to March) the mean significant wave height and mean period are high while during spring and summer (typically April to October) the mean significant wave height is low [Butel et al., 2002]. Woolf et al. [2002] established a relationship between wave height anomalies and large scale atmospheric pressure patterns over the Northeast Atlantic on the basis of satellite altimetry. More precisely they attributed part of the variability to the North Atlantic Oscillation (NAO) and secondarily to the East Atlantic Pattern (EA). In most cases, North Atlantic Oscillation (NAO) and other climatic indices

of the Atlantic Ocean have been mainly linked with temperature, precipitation and large scale circulation patterns over Europe which has been found to drive the trend of wave parameters and consequently an effect on storms. For example, Dodet et al. [2010] found strong positive and negative Pearson correlation between the *Hs* and NAO for the northern and southern sections of northeast Atlantic, respectively. Even though, several findings have found low [in summer e.g. Bauer, 2001] or no [with local conditions e.g. Dupuis et al., 2006] relation between NAO and *Hs* over several times, it stresses the importance of atmospheric pressure gradient, and that comparisons between other wave parameters and NAO index could be relevant.

2.4.1.b Storms

Storms definition exist in different topics. In meteorology, a storm is defined relative to the wind intensity that is characterised by a low pressure center, spiral rain bands and strong winds [Geng and Sugi, 2003]. While storms are generally well-defined from a meteorological perspective, it is not so in coastal erosion studies [Lee et al., 1998; Ferreira, 2005; Callaghan et al., 2008; Vousdoukas et al., 2012; Coco et al., 2014]. More common storm definition are based on their intensity: hurricane (when a storm's maximum sustained winds reach 74 mph) Katrina, Camille and Andrew in the tropical or subtropical waters [Blake et al., 2011]. In coastal science, some studies propose a classification based on duration [e.g. Saffir, 1977] or wave characteristics [e.g. Dolan and Davis, 1992] with the Saffir-Simpson Scale. Based on the wave characteristics, the impact of larger wave conditions could therefore be site specific, depending on the resilience of each beach which accounts for the complications in coastal storm definition (Table 2.1). Studies such as Dolan and Davis [1992] and Mendoza et al. [2011] use storm energy to define storm intensity. These classifications consider the magnitudes and duration of the storms, statistically called hierarchical agglomerative techniques due to some step-by-step similarity measure, which do not necessarily relate directly to the damage they cause. Storms have been variously defined as dramatic changes in wave conditions or distinct events during which waves exceed a certain height for a certain amount of time.

For example, Callaghan et al. [2008] chose a threshold of 3 m for analysis of the wave climate off Australia to define storms. Ferreira [2005], on the Portuguese west coast, used 6 m (Table 2.1) to insure that they only considered storms that were responsible for significant beach erosion. To remove subjectivity, the storm threshold maybe determined using probability distribution of the wave height (Figure 2.9); for example, the 99.5% exceedance level [Luceno et al., 2006] or the 95% exceedance level [Splinter et al., 2014a) or the impact on the beach (erosion or inundation). In case of continuous stormy conditions, if they occur within a short interval, they are considered as one, taking an empirically arbitrary

value: 3 days interval is considered in Luceno et al. [2006], 6 hours in Li et al. [2014], amongst others. Table 2.1 shows a literature review of storm definitions.

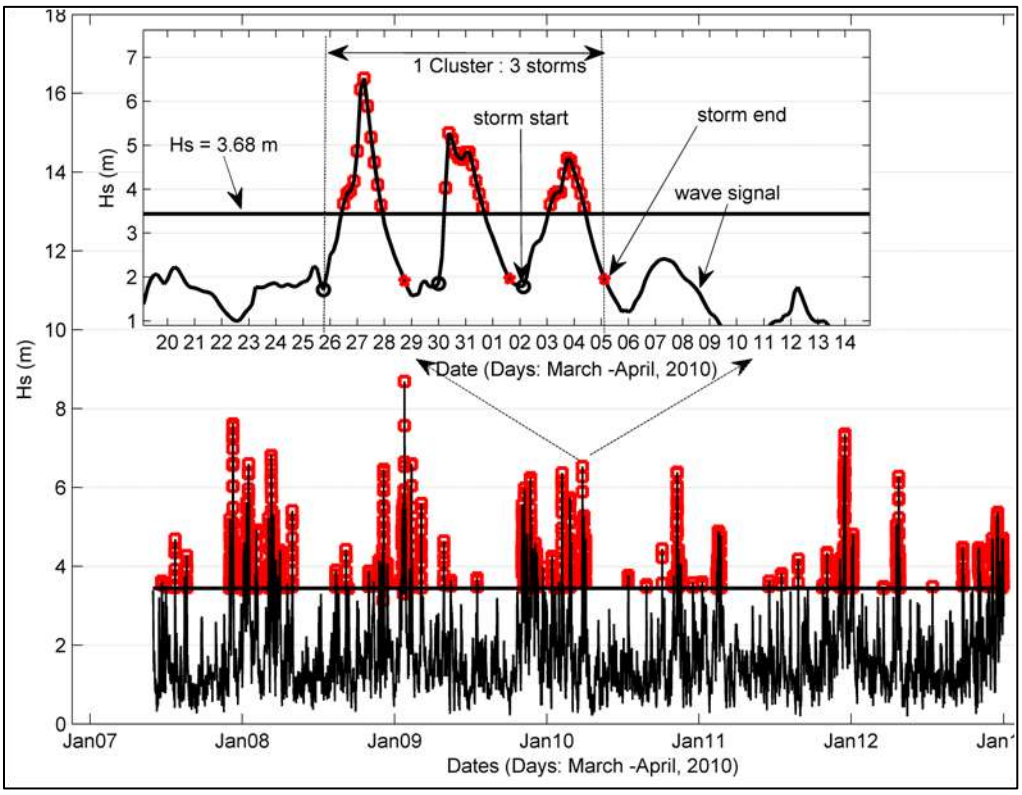

Figure 2.9. Time-series of 3-hourly wave height along the SW coast of France from April, 2007 to December, 2012.The subplot in the upper part of this Figure shows three exceedances (marked as storms) but considered as single cluster if the time span was less than 9 days. The threshold is set at the 95 % probability distribution of all the wave conditions.

As for individual storms, the definition of storm clusters is unclear in coastal research. Sequence of storms (or clusters) generally follow the 'morphological' definition when storm recurrence interval is shorter than the time needed by the beach to recover to individual storms [e.g. Morton et al., 1995]. As indicated on Figure 2.9 (inset), a cluster could be defined based only on the storm occurrence time interval and *Hs*. This definition is still widely used in coastal erosion studies [e.g. Loureiro et al., 2012; Karunarathna et al., 2014; Senechal et al., 2015]. Classifying storms in clusters still remains a challenge in the coastal domain. This is in line with Birkemeier et al. [1999] that design storm conditions may need to be recomputed based on the frequency of storm sequences, as opposed to individual wave or storm conditions.

What is lacking in the literature is the detail description of the clusters; maximum, minimum and average duration and how the cluster relates to the nearshore morphology. There is no global clustering principle (though not done here), and most of the literature given in Table 2.1 have actually not shown the criteria for defining the clusters. In most cases, however, speculative recovery duration is used. In chapter IV, this study has outlined a simple methodology that links this morphology and storm clusters, through the post-storm beach behaviour.

2.4.2 Storm impact

Storm-dominated coast erode largely during winter compared to summer. Investigations on storm impact include non-cumulative storm analyses [e.g. Ruggiero et al., 1999; Frazer et al., 2009; Coco et al., 2014; Splinter et al., 2014a] where individual storms are independent events in which frequent storms or storm sequences do not have a persistent influence on longer term shoreline change, but individual major storms of varied magnitudes at large return periods; and grouped (clustered) storm analyses [e.g. Ferreira 2005; Karunarathna et al., 2014] where storm sequences enhance shoreline erosion. The latter result has further been evidenced recently by equilibrium-based semi-empirical shoreline models [e.g. Yates et al., 2009; Davidson et al., 2013; Castelle et al., 2014] with storms rapidly eroding a beach due to a large disequilibrium between the high-energy storm and the previous beach state, as the beach progressively reaches a new equilibrium under prolonged constant waves. The fact that individual or sequence of storms at several sites follow different response durations makes storm characterization still uncertain [e.g. Davis and Dolan, 1992; Mendoza et al., 2011; Splinter et al., 2014a; Senechal et al., 2015]. The debate on which is the most severe; individual storm or a cluster of the storms, further complicates the definition of storms.

During storm, as wave heights increase to storm level, beach berms and sometimes the dunes erode in response, lowering the beach slope as sand is pulled offshore from the upper portions of the beach [Coco et al., 2014] and deposited in protective offshore sandbars. The beach profile becomes flat and gentle as more sediment is spread resulting in a more concave beach shape [Wright and Short, 1984]. Individual storm impact on shoreline has been accessed commonly through the correlation of the storm energy and the shoreline change. In an example, Ferreira [2005] used the convolution morphological model developed by Kriebel and Dean [1993], to analyse the consequences of these storms. This model consists of simple analytical solutions to predict the time-dependent beach profile response to severe coastal storms. The model tries to answer the need for simple methods of analysing beach erosion or accretion due to variable wave and water-level conditions. An important assumption in the model is that beaches subjected to steady-state erosion forcing conditions respond toward a stable or equilibrium form in consistence with the equilibrium models [e.g. Yates et al., 2009; Davidson et al., 2013].

Table 2.1. Selection of storms and storm clusters at several sites. Minimum hours describe how long time is required for a wave to last and be considered a storm after exceeding the selected threshold. Maximum time of cluster gives the time between storms beyond which two or more storms are considered desolate. 'None' in the table means the authors did not define the criteria.

Site	**Storm Hs threshold**	**Min. duration**	**Defining reason**	**Cluster definition**	**Reference**
France SW	4 m	12	98% exceedance	14 days	Senechal et al 2015
Australia	3 m	1	None	9 days	Karutharathna et al 2014
Narrabeen	2 m	None	95% exceedance	1-2 months	Splinter et al 2014
Portugal	6 m	None	Erosion	2-3 weeks	Ferreira 2005
Catalonia	2 m	6	Erosion	72 hr	Mendoza et al 2011
Australia	3 m	1	None	None	Callaghan et al 2008
Carolina	4 m	None	Erosion	39 days	Lee et al 1998
Atlantic	1.5 m	None	Erosion	Varies	Dolan and Davis 1992

To mention, the effects of not only astronomical tide but also atmospherical tides have been addressed in the Storm Impact Scale model proposed by Sallenger [2000]. This is often used to predict storm impacts on beach and dune systems [e.g. Stockdon et al., 2007; Masselink and van Heteren, 2014]. Amongst the active factors that affect beach profile changes include tides, however, most model investigations neglect the effects of tides, winds and rainfall [Gourlay, 2011] and reproduce only the action of waves upon various beach materials. Storm surge, defined as the water level associated with inverse barometer, might have a substantial influence under low-pressure systems and seasonal variations [Weaver and Slinn, 2004;Walton and Dean, 2009;Melet et al., 2016]. As it is still unclear what the dominant process in shoreline dynamics is associated to, tides could improve model perfomances.

2.4.3 Post-storm recovery

Storm events represent a major factor controlling short to middle term morphological evolutions of many sandy shorelines. In the event of changing storm regimes associated with climate change [e.g. see Zhang et al., 2002] it is important to understand the potential effects of storms on beaches and dunes and how they recover after these high-energy events. A number of studies have assessed the impact of storms on beaches and dunes and on their post-storm morphological adjustment, but most of them were conducted along microtidal (see Table 2.2) and storm-dominated coastlines [Morton et al., 1994, 1995, Zhang et al., 2002]. Though some authors analysed the morphological response of beaches and dunes to

storms on macrotidal coasts [Cooper et al 2004; Maspataud et al., 2009] very few investigated post-storm recovery in large tidal range coastal environments, thus our understanding of the post-storm beach changes is still limited.

Remarkably, the time scale of shoreline response maybe rapid not only during the erosional period of high storm waves but also during the recovery period when wave heights are relatively lower and slow recovery is expected. This recovery period is highly site-specific [Morton et al., 1994] and yet not clearly addressed in the literature. Shoreline recovery from storms depends on the severity of the prior event(s) and on how far the sediment has been transported offshore. Recovery of beaches after either storm or large hazard has been observed to take several durations. On the east coast of South Africa, Corbella and Stretch [2012] observed an average beach recovery period of 2 years based on observations at three-month interval, similar to Phang-nga after the 2004 Indian Ocean tsunami [Choowong, et al., 2009]. This data is sparse such that the recovery of significant events occurring in less than three months could be missed. The response of the beach system during recovery has also been highlighted by equilibrium models [Yates et al., 2009; Davidson et al., 2013; Splinter et al., 2014b]. Equilibrium models [e.g. Yates et al., 2009; Davidson et al., 2013] show that storm impact depends on the previous conditions of the waves or the beach state. However, the definition of clusters based on beach recovery [Ferreira, 2005] time supposes that beach recovery occurs even if this might not be the case [Ruessink et al., 2007].

Table 2.2. Sample shoreline recovery studies that indicate the duration of recovery for each site, the frequency (temporal resolution) of data collection, tidal range (TR), diagnostic and data length (size)

Site	Duration	Data frequency	TR	Diagnostic	Data size	Reference
South Africa	2 yrs	3 months	Micro	Profile positon	37 yrs	Corbella and Stretch 2012
Palm & Duck	5 days	1 day	Micro	Beach state	2&4 yrs	Ranasinghe et al 2012
Narrabeen	27 days	1 hour	Micro	Beach state	6 yrs	Davidson et al 2013
North Sea	never	1 month	Macro	Profile position	4 months	Maspataud et al 2009

This is more particular when wave conditions follow the energetic events and do not allow onshore sediment transport (e.g. because of wave incidence angle or waves not being energetic enough). The methods used to estimate the recovery (diagnostics) are different and there is the need for an objective inter-site comparison of the recovery times using a single diagnostic.

The recovery process is clearly still not understood from the previous researches. For instance, literature does not define how tides relate or contribute to time variation of beach recovery or how the location of sandbar affects the shoreline during recovery.

2.5 Shoreline acquisition and prediction

2.5.1 Different conventional shoreline measurement techniques

Several data sources such as historical land-based photographs, coastal maps and charts, aerial images, beach surveys, multispectral or hyperspectral images, light detection and ranging (LIDAR) digital elevation model (DEM) data, and microwave sensors can be used to extract the shoreline locations. There are two types of shorelines that people are mostly interested in extracting; the instantaneous and tide-coordinated shoreline. The former is usually done at the moment the data source is acquired (e.g. with orthophotos, aerial photographs or satellite images) while the latter is done at some selected tide level [Li et al., 2002]. Description of these shoreline detection techniques can be found in Boak and Turner [2005] and in section 2.3 of this study, thus, only a few of the common data sources that are widely used for shoreline studies are briefly described in this section.

Aerial photographs have been used extensively to determine shoreline positions and erosion rates. On aerial images, several different features on the beach and backshore have been used as proxy lines [Boak and Turner, 2005], including the bluff or dune line, the seaward vegetation line, and the high water line. The latter is usually defined as the wetted line where there is a marked contrast between the wet and dry sand. Various investigators [Dolan et al., 1978; Leatherman, 1983; Fisher and Overton, 1994; Boak and Turner, 2005] have described formalized methods for using this line to monitor shoreline change. Aerial images typically have broad spatial coverage but their temporal coverage is limited by the acquisition time. In addition, the images can be distorted with radial or projective distortions caused by the change in the pitch, yaw, or roll of the acquisition sensor field of view during the flight time. They must be undistorted before utilizing them in a shoreline extraction process [Moore, 2000; Boak and Turner, 2005].

Another shoreline measurement technique is done by the use of differential GPS (geographical positioning systems) surveys. GPS depend on the constellation of 3 or more satellites to provide accurate (~cm) location of objects. With two GPS; one stationary receiver at a reference and the other receiver moved along the shoreline proxy of interest (e.g. HWL, LWL, transects), the beach in the intertidal region can be mapped. Pajak and Leatherman [2002] concluded that the GPS method was more accurate than aerial photography to identify specific shoreline features of interest.

Another method to measure shoreline is through LIDAR (LIght Detection And Ranging). LIDAR applications have also been widely used. Since the current study does not involve aerial or lidar data, only brief explanations are given. Airborne LIDAR has the ability to cover hundreds of kilometers of coast in a relatively short period [Stockdon et al., 2002]; LIDAR is based on the measurement of the time it takes a laser beam, from leaving the instrument, to return after reflection. Knowledge of the speed of light allows a distance to be calculated and the use of differential GPS specifies an exact location. Tidal datum-based shorelines such as MHW can then be found by fitting a function to cross-shore profiles of LIDAR data [Stockdon et al., 2002]. This data source is generally limited in its temporal and spatial availability because of cost. The main advantage of LIDAR data is that it can cover large areas very quickly. The detection of LIDAR points in water areas can also be difficult, because a laser scanner does not have reflectance of the water, particularly when they are standing waters, though some reflectance of the water is possible when there are some waves or some objects above the water surface.

Each of these methods share basically similar techniques which include the identification of the wet sand line, the tracing and recording of this line, and the measurement of change, either relative to an earlier shoreline position, or relative to a reference line offshore. The implementation of these techniques has shown significant success in the coastal research albeit their challenges. They give direct measurement of beach changes; however, historical records can be non-existent, they can be expensive and unable to use during harsh weather conditions.

2.5.2 Video monitoring: Context and background

Field measurements (Figure 2.10) have provided a great deal of information on the nearshore beach system [e.g. Sonu, 1973; Wright and Short, 1984; Plant et al., 1998; Aarninkhof et al., 2003; Poate et al., 2013]. Amongst the different measurement types, shore-based video monitoring constitutes one of the fastest growing techniques and has become a widely recognised technique the world around. The main advantages of the video observations are that they can be made frequently (several times per day), over long time periods (decades), and they span large distances alongshore (O (km)). The primary disadvantage of video observation methods is that, in most cases, they do not give a direct estimate and need a complex pre- and post-processing of images. Another setback of most video stations is that, they do not operate in the night, so cameras are only operational during daylight hours. However, in situations where analysis is done with the interest to use one image per day, this setback is not important.

2.5.2.a Video monitoring of the nearshore: 25 years of developments and use

Following the Argus video camera system [Holman et al.,1993; Holman and Stanley, 2007] developed initially by the Coastal Imaging Laboratory, several video systems (e.g. camEra, Sirena, Horus, KOSTA) can now be found around the world. A video monitoring system typically consists of several cameras (typically one to nine), to cover the area of interest in the field of view, and allowing a coverage of several kilometers. Cameras are usually mounted on an elevated position (typically >15 m above MSL) along the coast and connected to an ordinary PC on site, which in turn transfer data through internet to distant server. In a situation where none of these exists, data is manually downloaded with an external hard drive. Data acquisition is continuous (varies down to 2 Hz sampling frequency) during daylight hours and operate through all weather conditions. This is the difference between video system and traditional or conventional measurement techniques.

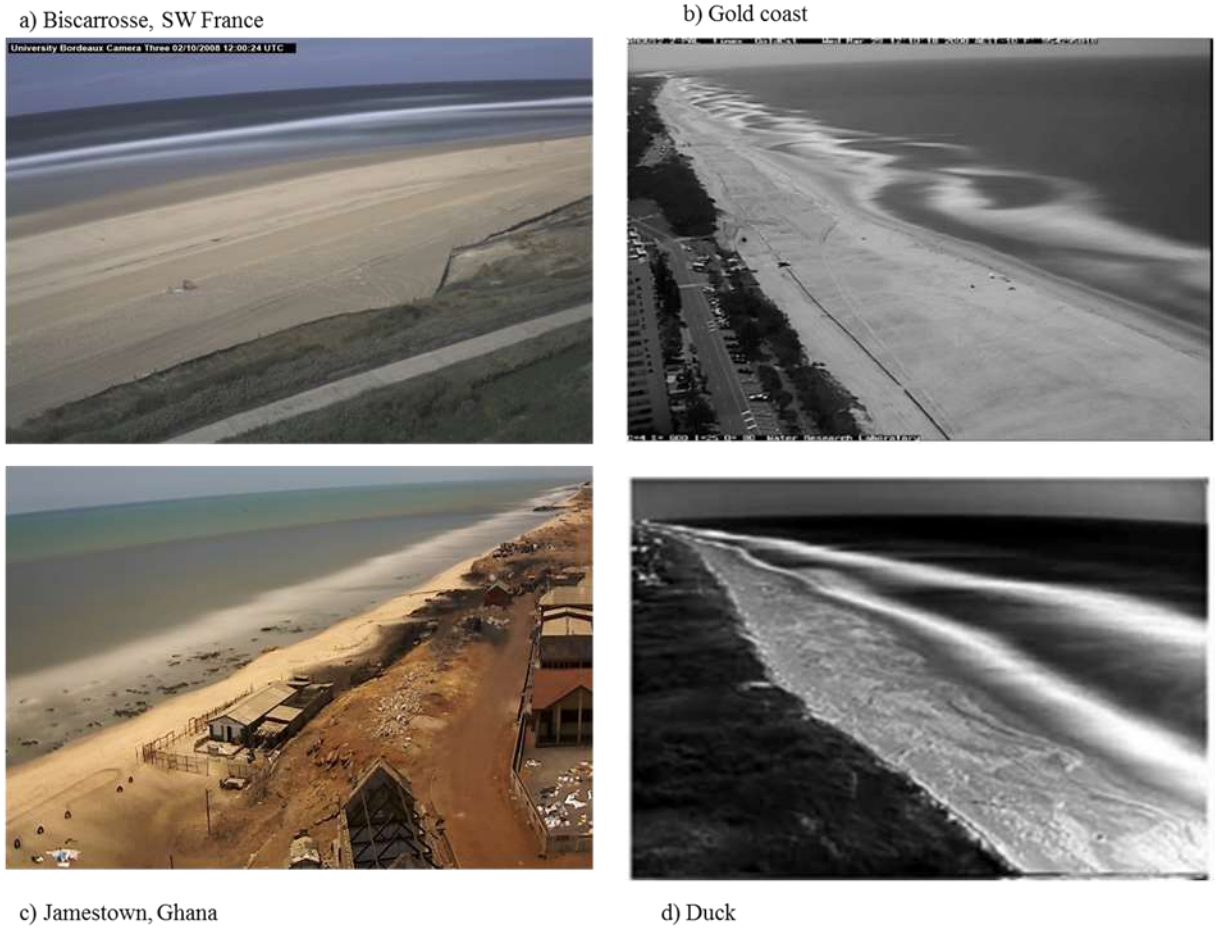

Figure 2.10. Different time exposure images from around the world (a) Biscarrosse (b) Gold Coast [Plant et al., 2007] (c) Jamestown, Ghana (d) Duck [Plant et al., 1999]. Plot (a) shows a wide summer beach

with signals of multiple bars (white bands) (b) shows irregular sandbars (white bands) c) shows narrow beach with rocks closely outside the intertidal zone while d) shows shore-parallel sandbars.

Since the process of data collection is fully automated, the marginal operating costs are virtually zero. Each standard collection usually consists of three types of images (see Argus image types and conventions) as indicated in Figure 2.11 are acquired every 10 min to hours typically, depending on the research focus; 1) A snapshot image for quality control, 2) Time exposure images (often called timex) commonly used for shoreline and sandbar studies as they average-out high-frequency fluctuations due to incident wave modulations and give a statistically stable image of the wave breaking pattern [Lippmann and Holman, 1989] and shoreline transition. 3) Timestack images consist in pixel transect, generally cross-shore, that are used to describe waves characteristics.

2.5.2.b Shoreline and sandbar from video

Video system observations have been applied to the extraction of several nearshore morphological and wave parameters. Using timex video images, several studies [e.g. Lippmann and Holman, 1989; Van Enckevort et al., 2003;Ruessink et al., 2007; Almar et al., 2010] analysed the scales and morphology of sandbars based on the dissipation over the crests of the bar, given that the pixel intensity is proportional to the local wave energy dissipation (breaking).

Similarly, video system data has been used to extract shoreline location. Swash motions at the shoreline may generate foam and produce a distinct shore-parallel band of high light intensity in time exposure images. Plant and Holman [1997] named the bright band the shoreline intensity maximum (SLIM) in their study done along Duck, North Carolina. The SLIM was nearly always visible and was generally an excellent proxy for the actual shoreline. The coordinates of the shoreline can then be mapped and tidal elevations assigned in order to provide bathymetric data [Madsen and Plant, 2001]. Another technique to extract shorelines from video is the pixel intensity clustering PIC [Aarninkhof, 2003].

The red-green-blue color sharp transition between the dry (red dominated) and water (blue or green dominated) pixels is identified as the shoreline. This approach was developed because the SLIM method failed to work on more dissipative beaches. Other methods include the artificial neural network ANN [Kingston, 2003] and even datum dependent semi-automatic methods [Senechal et al., 2015]. For more detailed discussion, a comprehensive review of shoreline detection from video is given by Plant et al. [2007]. The shoreline-detection methods mentioned above are sensitive to waves and lighting conditions. For instance, the SLIM method by Plant and Holman [1997] and augmented SLIM [Pianca et al., 2015] is sensitive to variations in water levels which can scale the effects of both setup and run-up,

and fog can reduce the color signal strength [Aarninkhof et al., 2003]. Despite these, the results of shoreline measured from video have been comparable to that of topographic surveys [Holman and Haller, 2013]. Plant et al. [2007] and Almar et al. [2012] present results for validation and discussion of the video method performances.

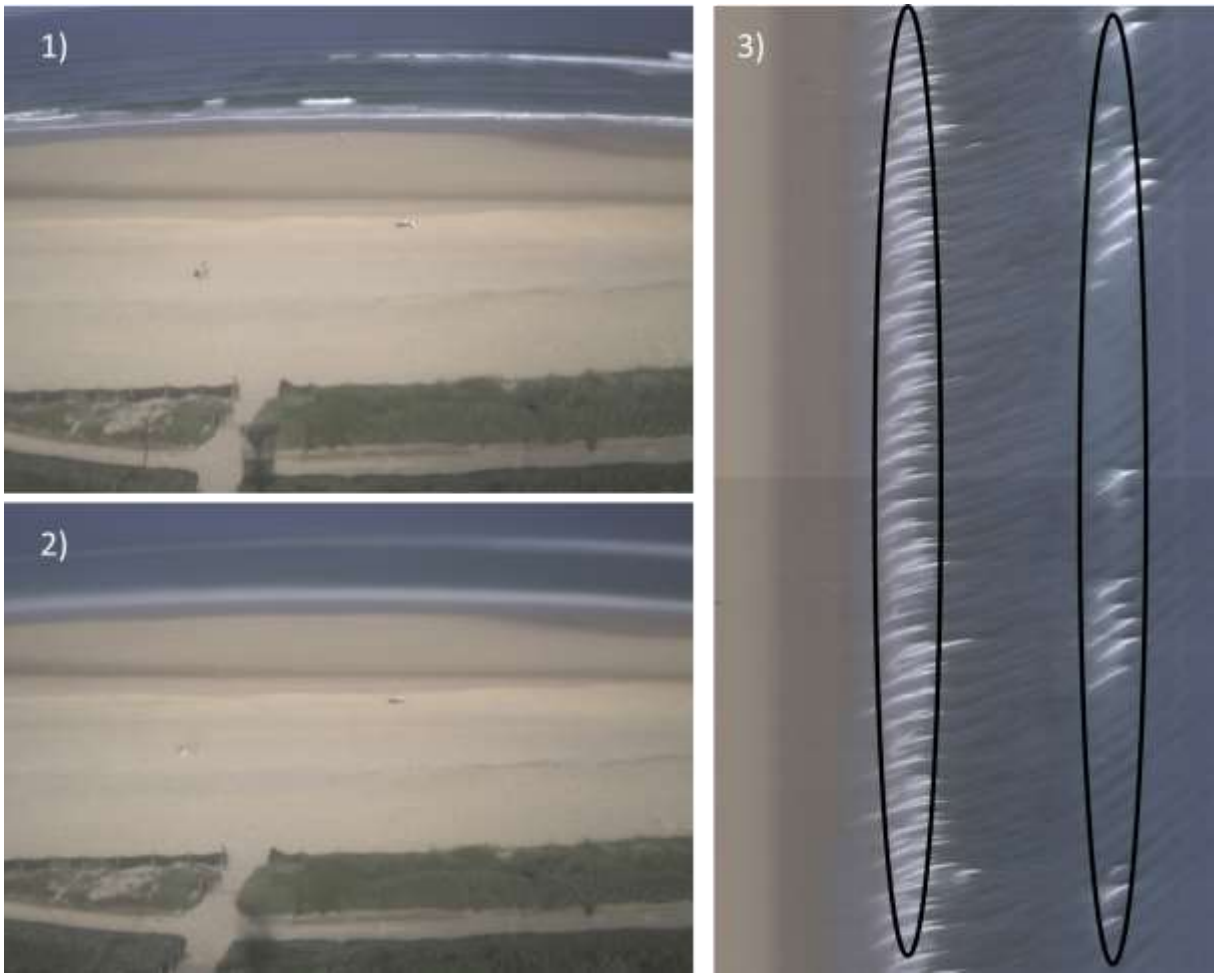

Figure 2.11. Example of each image type on the 01/06/2009 at Biscarrosse; 1) A snapshot image for quality control, 2) Time exposure images (often called timex). 3) Timestack image, a pixel transect, cross-shore used to describe waves properties. In 3), also shows two breaking locations cycled, reminiscent of a double barred beach.

2.5.3. Predicting shoreline evolution using models

Coastal managers, scientists and engineers have long sought a robust and practical methodology for the estimation of shoreline change, over time-scales spanning several years to decades. There are existing models [e.g. Cowell et al., 2003; Karunarathna et al., 2009; Horrillo-Caraballo, 2010], which are

currently close to satisfying these requirements and include a considerable level of empiricism and may be termed data-driven models. Probably the most widely used is the GENESIS model [Hanson and Kraus, 1989] which is applicable where alongshore gradients in sediment transport dominate. Recently there have been several advances in the field of long-term but relatively high-resolution (weeks to months) shoreline prediction due to predominantly cross-shore sediment transport processes. These studies [e.g. Davidson and Turner 2009; Davidson et al., 2013; Yates et al., 2009] have found out that a practical approach to hindcasting (and potentially forecasting) of multi-year shoreline variability may be developed from a combined consideration of the evolving disequilibrium state of a beach through time, and the rapidly-varying forcing caused by prevailing wave conditions. These core ideas build upon earlier disequilibrium concepts introduced by several authors including the work of Wright et al. [1985], Plant et al. [1999] and Miller and Dean [2004], where the evolution of beach-state, sand bars and shorelines were examined, respectively. Davidson and Turner [2009] developed a behavioural template model which hindcasted beach profile evolution including beach flattening, shoreline recession and the development of breakpoint sandbars during episodes of erosion. Not only can these models predict the on-offshore location, but the alongshore irregularities development as found by Stokes et al. [2015]. However, the influence of tide and sandbar, that are supposed to be important for the short-term response of the shoreline to storm and recovery rate are to be implemented in such models that take only into account for waves.

CHAPTER THREE

Study area, data and methods

……No law of nature however general has been

established all at once,

its recognition has always been preceded by

many presentiments….

Dmitri Mendeleev

CHAPTER 3: STUDY AREA, DATA AND METHODS

3.1 Description of study sites

3.1.1 Environmental settings of Biscarrosse beach

3.1.2 Hydrodynamics of Biscarrosse beach

3.1.3 Morphology of Biscarrosse beach

3.1.4 Introduction to Jamestown beach

3.2 Hydrodynamic data at Biscarrosse

3.2.1 Wave data

3.2.2 Waterline elevation data

3.3 Morphological data at Biscarrosse

3.3.1 Pre-processing, georeferencing and rectification

3.3.2 Processing of images: merging images

3.3.3 Shoreline and sandbar detection

3.4 Error Analysis

3.4.1 Inaccuracy in the shoreline location

3.4.2 Inaccuracy in the sandbar location

3.1 Description of study sites

Two sites were selected in this study: the meso-to macro-tidal Biscarrosse beach and the micro-tidal Jamestown beach. The main site is Biscarrosse while Jamestown is studied on pilot base. Biscarrosse beach is the main site because we have long duration of data at that site. Biscarrosse beach is located in high energetic wave dominated section along the North Atlantic while Jamestown beach is a low energy beach in the Gulf of Guinea region.

3.1.1 Environmental settings of Biscarrosse beach

Biscarrosse beach is located in the southern part of the French Atlantic coast (Figure 3.1), an unconsolidated, low lying coast, bordered by high aeolian dunes [Pedreros et al., 1996; Michel and Howa, 1997]. This 250 km long N-S oriented coast is only interrupted by the 5-km wide Arcachon lagoon inlet, in which several extensive sand banks have developed as part of a well developed tidal delta. Biscarrosse beach is located about 15 km south of the tidal inlet and can be considered distant from the zone of influence of the tidal delta, at short time scale. It is also noted that this beach is not fully a natural system as there have been upperbeach nourishments when necessary. Biscarosse beach, by its characteristics, serves as one of the prototypes of the beaches in the SW France (Figure 3.1), particularly within the framework of DYNALIT (DYNamique du LITtoral et du trait de côte) service of national observatory (SNO).

3.1.2 Biscarrosse beach: wave and tide forcing

Biscarrosse beach is oriented to the North at an angle of 8.5°. The beach is exposed to long and energetic waves originating mainly from the W-NW direction. This study area is part of the North-East Atlantic Ocean (25°W–0°W and 30°N–60° N), investigated by Dodet et al. [2010] using a 57-year hindcast data, obtained with a spectral wave model forced with reanalysis wind fields at different water depths. The hindcast analysis revealed firstly strong seasonal fluctuations of wave climate, with winters characterized by large and long-period waves of mean direction spreading from south-west to north-west, and summers characterized by smaller and shorter-period waves originating from northern directions. Using similar data, Charles et al. [2012] observed additionally several trends for recent periods. Notably, an increase of summer significant wave height, a southerly shift of autumn extreme wave direction, and a northerly shift of spring extreme wave direction. They found that wave fields can also exhibit high interannual variability, with a normalized standard deviation of seasonal wave height greater than 15% in winter time. The interannual variability of the wave climate at this area is reported to relate to the North Atlantic Oscillation Index [Butel et al., 2002; Dodet et al., 2010] where NAO influences the occurrence

and tracks of storms. The wave climate is energetic with an annual mean significant wave height of 1.4 m and an associated period of 6.5 s. During fall and winter seasons (typically September to March) the mean significant wave height is around 1.6 m with a mean period of 7.3 s, while during spring and summer (typically April to August) the mean significant wave height is about 1.1 m with a shorter wave period (6 s). Butel et al. [2002] investigated large scale spatial variability of sea states at Biscarrosse from 1980 – 2000 in a 26 m water depth as part of their study to give a complete wave classification on the Aquitanian coast. While there can be large variation, they indicated that maximum wave height during winter storms can sometimes reach 10 m.

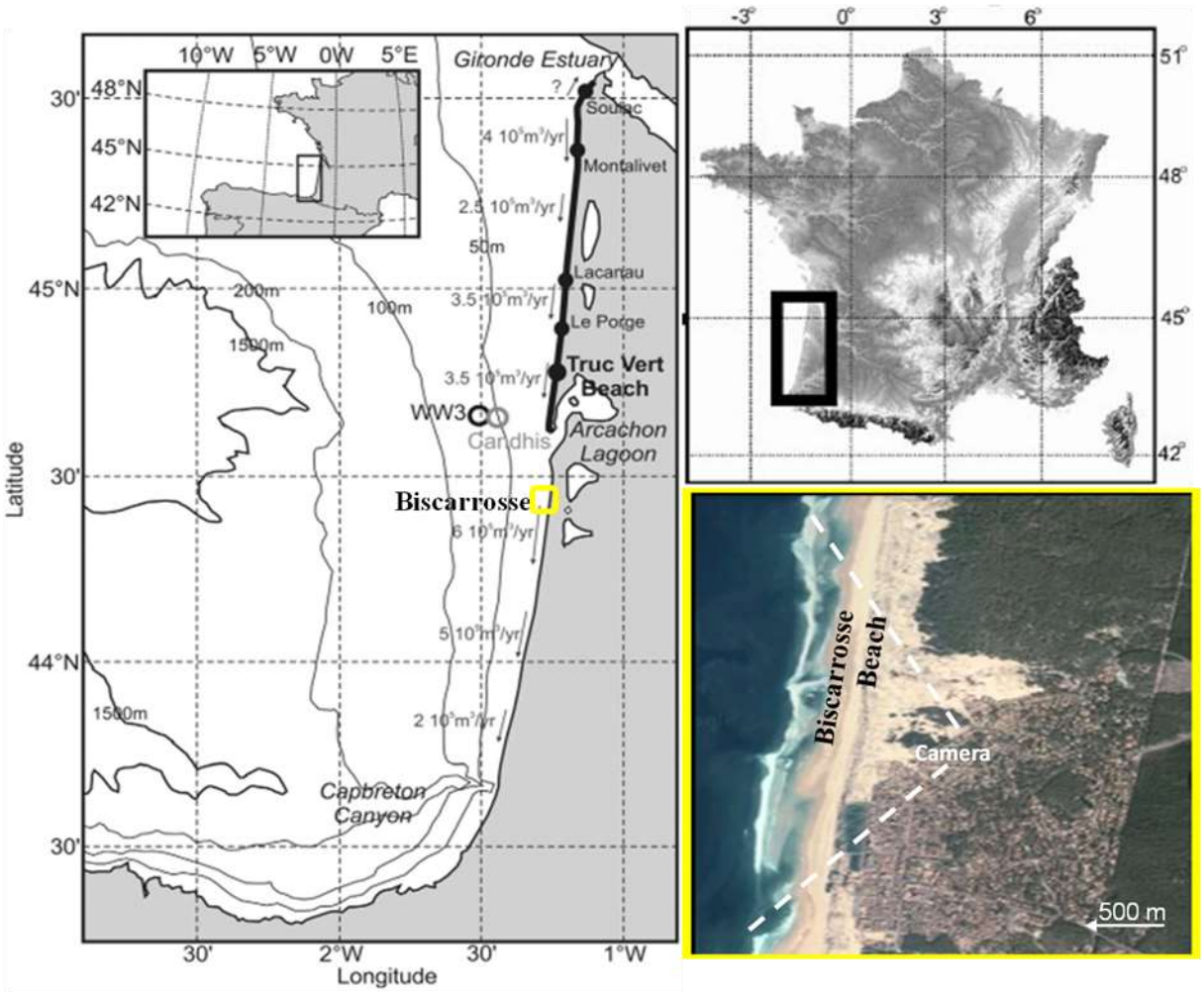

Figure 3.1. Location of the study site, Biscarrosse beach (SW France), showing the WW3 grid node (triangle) located at -1°30' W, 44°30' N and CANDHIS buoy (triangle) at 1°26.8'W, 44°39.15' N and the video station. The quatitative longshore drifts are shown at the various sites along the entire French Atlantic coast [courtesy: Castelle et al., 2015].

At this site, tide is semidiurnal with meso–to-macrotidal amplitude and an average value of 2.9 m which increases up to 5 m during spring tides. The tide is the main component of the water level for the water line variation, aside the effect due to breaking waves, the wind and inverse barometer (atmospheric pressure). These results are significant at Biscarrosse, and must be stimulated further for clear understanding in line with shoreline changes.

3.1.3 Morphology of Biscarrosse beach

Biscarrosse beach currently faces an erosion of about 2 m/yr [Eurosion, 2004] while the Aquitanian coast (SW France) is subject to an overall shoreline erosion of 1 to 3 m/year [Idier et al., 2013]. Driven by oblique waves, the longshore drift is mainly southward and has been estimated roughly around 600,000 m^3/m/yr [Figure 3.1, Abadie et al., 2006; Castelle et al., 2015]. The beach generally consists of a double bar system comprising intertidal and subtidal sandbars [Almar et al., 2009].

Following Wright and Short [1984] classification, Peron and Senechal [2011] found that the most typical beach states observed for Biscarrosse fall in the category of Low Tide Terrace, LTT, and Transverse Bar and Rip (TBR). The intertidal bar commonly exhibits complex three dimensional (3D) morphology with a mean wavelength of about 400 m [Lafon et al., 2002; Castelle et al., 2007; Almar et al., 2010] that can sustain energetic events [Ba and Senechal, 2013; Peron and Senechal 2011; Senechal et al., 2015]. Figure 3.2 represents the general bathymetry of Biscarrosse (Figure 3.2a) which shows the presence of inner sandbar between 200 and 400 m (Figure 3.2b) and the outer sandbar around 700 m from the shoreline, measured during the Biscarrosse field experiment in June, 2007 [Bruneau et al., 2009]. Figure 3.2b shows the beach is gentle, with an average observed slope of 0.03. Both sandbars migrate southward as a result of the southerly longshore drift [De Melo et al., 2002; Lafon et al., 2004; Castelle et al., 2015]. Using three years of video observations, Senechal et al., [2015] also discussed the possibility that the presence of the subtidal bar explained the persistence of TBR states (mean residence time of about 24 days reaching maximum at 103 days), even during high energetic conditions as reported by Almar et al., [2010]. Senechal et al. [2015] showed that the range of variation of the inner sandbar positions (120 m) at Biscarrosse is two and half times larger than the range of variation of the shoreline position and that rapid erosion can be observed, even under moderate conditions.

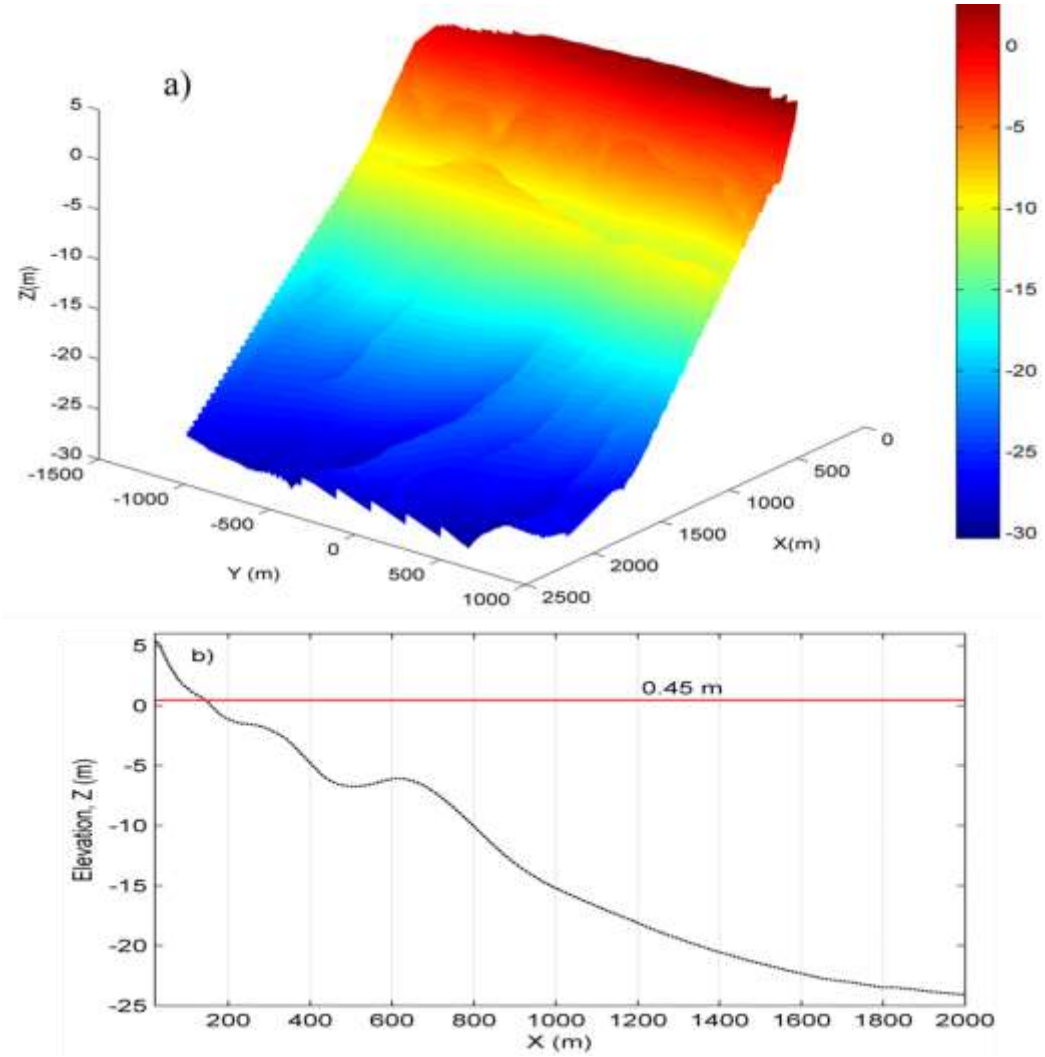

Figure 3.2. a) Biscarrosse beach bathymetry in June, 2007 and (b) the averaged profile. The two sandbars, intertidal and subtidal (outer) sandbars, are visible on the profile. The horizontal line indicates the tide level used to define shoreline (0.45 m above MSL).

3.1.4 Introduction to Jamestown beach

Jamestown is located in Accra (detail is shown in chapter 6), capital of Ghana, which has a 550 km long coastline. The general Ghana coastline consists of mixed rocky and sandy beaches. The coast is sandy in the western part and rocky in the east [Anthony et al., 2016]; however, the section under focus is sandy. Tidal regime is microtidal, and wave conditions are moderate [mean wave height of 1.4 m and 11 s period, Appeaning Addo et al.,2008; Angnuureng et al., 2013]. Shoreline erosion along the Ghana coastline is on the rise with a current erosion rate of 2 m/yr [Wiafe et al., 2013]; though it can reach 17 m/yr at some hotspots [see Angnuureng et al., 2013]. The motivation for choosing this site includes

amongst others, erosion with events of overtopping and breaching of the dune inducing important inundations [Folorunsho et al., 1995]. The site is also a major fishing community, important economically, but draws the attention to the impact of activities from the fisher folks.

3.2 Hydrodynamic Data at Biscarrosse

3.2.1 Wave data

In this study, the wave data are retrieved from Wavewatch III [WW3; Tolman, 1991] model, forced by wind (NOAA) with a 3 h resolution over a 5-year period from 2007 to 2013. The WW3 model considers the effect of the tides and surges on forced wind waves. Data are extracted at the grid point (1°30'W, 44°30'N, Figure 3.1) facing the beach in about 70-m water depth. In-situ measurements are also collected over the same period, though intermittently, with the CANDHIS (Centre d'Archivage National de Données de Houle In Situ) directional wave buoy, moored in 54-m depth (1° 26.8′ W, 44° 39.15′ N; Figure 3.1). The model significant wave height Hs_{WW3} are corrected via a linear regression with the buoy data $Hs_{Candhis}$ [Castelle et al., 2014] and showed in Figure 3.3a and Figure 3.3b. In Figure 3.3b, the solid and dashed black lines indicate mean shoreline orientation and shore-normal incidence, respectively. The dashed grey lines indicate ground swell shadowing regions to the North and to the South. The link is given by $Hs_{Candhis} = 0.9052 Hs_{WW3} - 0.01526$. The overall directional wave climate used in our study is given in Figure 3.3b and Figure 3.3c, showing wind seas at a wide range of directions and high-energy swells from the W–NW sector. The angle represents the direction wave comes from and the color represents the magnitude of the significant wave height indicated in the legend. Each sector is 10° wide. Modal *Hs* (1.12 m) is below average (1.69 m) which suggests a skewed distribution with few large wave events. On the other hand, T_p varies between 2.5 s and 21.2 s with average and modal values as 10.2 and 10.8 s respectively.

Wave data present numerous storm events, with the major events identified to cause dramatic beach changes. To develop a storm classification, three main steps are done in this study: (1) storm definition and identification, (2) selection of the parameter to characterize the storms according to a given criterion, and (3) quantification of the impact. In Chapter four we illustrate how the storms are defined for this study. The storm energy are commonly used to assess the impact of the storm on morphology, because one of the main objectives of the classification is to provide an idea on the potential hazards induced by the storms and the classification variable should reflect their intensity. Apart from the Saffir-Simpson scale [Simpson, 1971; Saffir, 1979] that is mostly used for hurricanes, the state-of-the-art storm classification is the Intensity Scale [Dolan and Davis, 1992]. The storm intensity *I* is obtained basically with the product of maximum or mean Hs-squared (energy *E*) and the duration *N* of the storm (see

literature and Chapter four). Uncertainties due to this simple method include over or underestimation of the storm intensity.

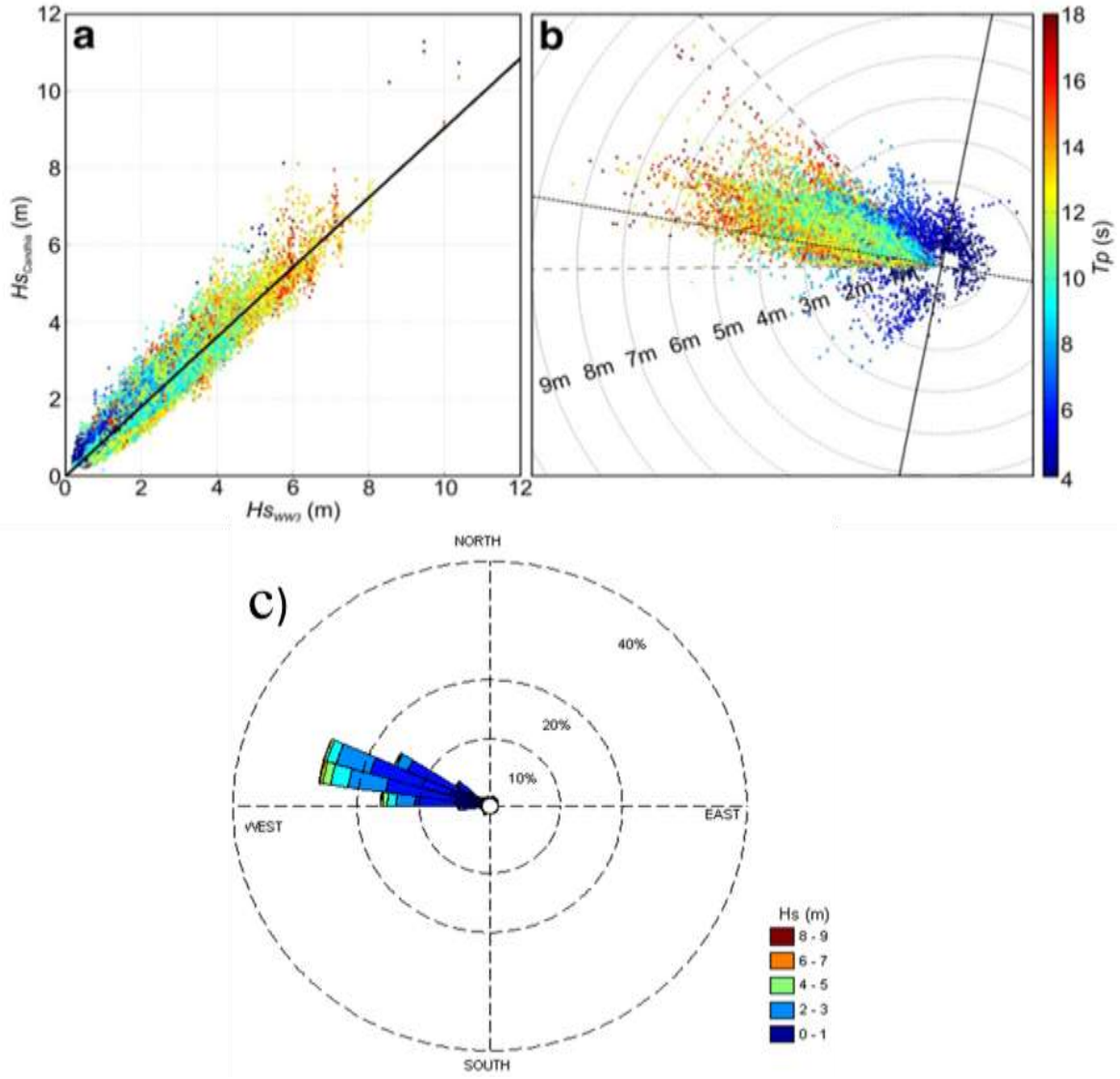

Figure 3.3. a) Correcting wave data with measured significant wave height at the Candhis buoy $Hs_{Candhis}$ versus 3-hour modelled significant wave height $Hs_{WW3.}$ The solid black line indicates the relation between the two data sets b) Resulting distribution of entire wave data set [after Castelle et al., 2014]. Colorbar indicates peak wave period in seconds c) Wave rose diagram based on data from WW3.

Recently, other researches [e.g. Mendoza et al., 2011; and Splinter et al., 2014] have found it more appropriate to use timeseries of waves within the storm.

$$I=\sum E = \int_0^N \frac{1}{8}\,\rho g H_{rms}^2 \Delta t \qquad (3.1)$$

Assuming a Rayleigh distribution of waves, H_{rms} can be substituted by $Hs/\sqrt{2}$ [Dean and Dalrymple, 1991] and Eq. (3.1) becomes:

$$I = \int_0^N \frac{1}{16}\,\rho g H_s^2 \Delta t \qquad (3.2)$$

Similarly, assuming the waves travel in a group with speed C_g, wave power is defined as $P = EC_g$ and for deep-water the integrated wave power can be written as:

$$\sum P = \int_0^N \frac{1}{64\pi}\,\rho g^2 H_s^2 T_P \Delta t \qquad (3.3)$$

And assuming the storm starts at *t1* and ends at *t2* while all other variables are constant, *E* can be written as in Mendoza et al. [2011]:

$$E = \int_{t1}^{t2} H_s^2\,\Delta t \qquad (3.4)$$

where ρ is the density of sea water, g is acceleration due to gravity. The latter equation has been used throughout this study. It is simple yet gives similar results as the first three equations.

3.2.2 Waterline elevation data

The water level (combination of astronomical tide, atmospherical tide and wave setup) affects the wave transformation along the surf zone and can modify the breaking and swash locations. In particular, high-wave energy events generally coincide with high water levels (atmospherical low depth/or storm surge with high tide) which affect the upper part of the beach [i.e. dry beach, dunes, among others, Splinter et al., 2014] and coastal structures (i.e. seawalls, dune revetments). Astronmical tide data can be acquired through several means; models and in situ with tide gauges. For this study, there is no tide gauge at Biscarrosse, therefore tides (Figure 3.4) were retrieved with WXtide model [Flater, 2010] at closest tide gauge at Arcachon, which is 15 km distant. Figure 3.4a is a representation of all tide data used in this study. Daily amplitudes range between 1.1 and 5.13 m during neap and spring tide, respectively. On Figure 3.4b, the corresponding image times for each camera were overlaid. For example, Figure 3.4b shows Camera 5, C5 did not function for the last two days, indicated by an empty solid line. Other cameras are marked which shows the presence of images.

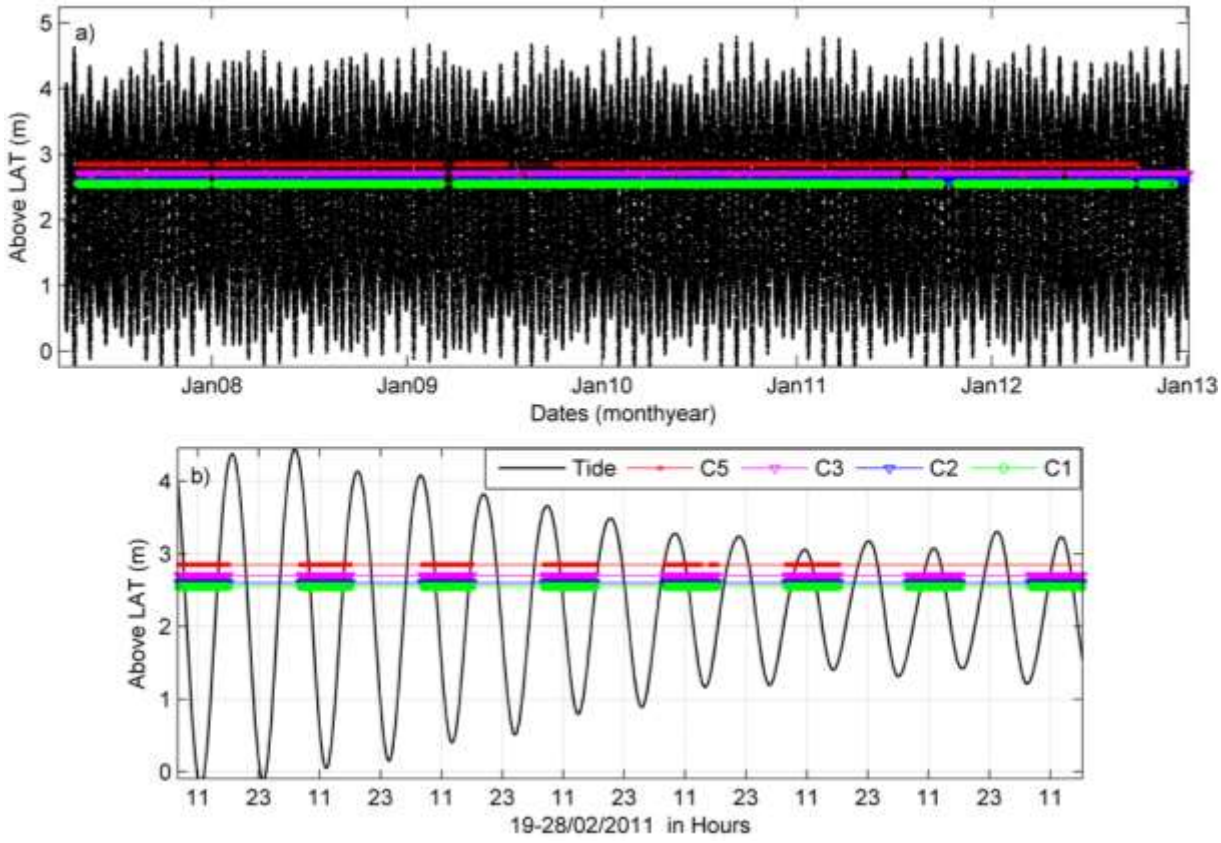

Figure 3.4 Schematic for tide and times when images were selected based on 2.7 m tide elevation above lowest astronomical tides (LAT). Time series of cameras one to five (C1, C2, C3, C5) were overlaid.

3.3 Morphological data at Biscarrosse

A shore-based video system was installed at Biscarrosse beach (Landes, France) in April 2007 by EPOC laboratory (CNRS/University of Bordeaux) in collaboration with the New Zealand National Institute of Water and Atmosphere (NIWA). Initially, the video station had five high resolution color cameras (3.5 MPix) fixed atop the fore dune at 26 m above the mean sea level (MSL), but only four cameras have been in good state and used throughout this study. The system provides three types of images every 15 minutes: instant snapshot to check the image quality, cross-shore time stacks (time series of radial pixel intensity) to compute high frequency wave characteristics and 10-min time exposure (or timex) images, that are used for detecting the position of sandbars and shoreline. Images that were of bad quality (due to fog, blurred, etc) were removed and times during which camera did not operate were excepted. The beach area covered by each of the four video cameras extends 2-km in the longshore and 1 km across shore which ensures covering alongshore structures non-uniformities such as rhythmic shapes,

resolved at both shoreline and sandbar locations. Thus the main data to be used to analyse the morphological changes is obtained from the video system.

In this study, shoreline is defined based on tidal datum which has already been discussed in the literature [Quartel et al., 2008; Davidson et al., 2010]. Here, the shoreline is taken as the contour at the lowest high tide 2.7 m ± 0.1 m above Lowest Astronomical Tide to be consistent with previous studies [e.g. Senechal et al., 2015]. This datum contour was found to be best correlated to the supratidal beach volume and is thus considered as a suitable proxy [Ba and Senechal, 2013). The other reason for the choice of this contour is because it gives at least, a shoreline per day that maximises the number of data points, in line with our need for covering shoreline evolution from daily to seasonal scales. Based on the chosen tidal elevation to pick the shoreline, shoreline data covers 50% (1,038 days in 1,966 days) of the studied period.

On the other hand, the sandbar is identified from the timex images. The video system technique allows the visualization and subsequent quantification of nearshore morphology based on the patterns of incident wave breaking [Lippmann and Holman, 1989]. The premise of the technique is that more waves break over the shallows of the bar than surrounding areas. The sharp contrast between breaking and nonbreaking regions is imaged photographically. All sandbar images used here are taken at 1.7 m above LAT. At higher LATs may be waves do not break on the sandbar. Sandbar data covers only 20% of the studied duration, because an additional condition was used to ensure wave breaking is uniquely on the sandbar. Images are discarded when $Hs > 2.5$ m because breaking might occur continuously from the bar to the shore under such energetic conditions [e.g. Van de Lageweg et al., 2013].

3.3.1 Pre-processing, georeferencing and rectification of images

The intrinsic camera calibration can be done in the laboratory before the field deployment: Radial (distortions along radial lines from the center of an image) and tangential lens distortion are the largest source of errors and typically the only type of distortions accounted for in video image processing. Detail description of how to estimate distortion is found in the literature [Holman et al., 1993; Holland et al., 1997; Almar et al., 2009). The photogrametric transformation between three dimensional (3-D) world and two dimensional 2-D image coordinates is called rectification, or geo-referencing [Lippmann and Holman, 1989; Holland et al., 1997]. The geometry and labeling conventions used in the rectification process are shown in Figure 3.5. Image coordinates will be denoted with small letters (x,y), and ground coordinates will be denoted with capital letters (X,Y). The optic center of the camera is located at point (X_0, Y_0, Z_0), a distance Z above the ground plane. The relation between the 3D world Cartesian coordinates and the 2D image point is defined by the optical center, f, and the camera orientation (Eq. 3.7-

Eq. 3.8). The orientation is defined by the three angles; φ (azimuth), τ (tilt), and σ (roll). Using the parameters defined in Figure 3.6 and the information above, the coordinate transformation between image and world coordinates are driven in terms of the following collinearity equations under the condition that the camera center, the image point, and the object point all lie on a straight line [Holland et al., 1997]:

$$X = (Z - Z_0)\, Q + X_0 \qquad (3.5)$$

$$Y = (Z - Z_0)\, P + Y_0 \qquad (3.6)$$

where

$$Q = \frac{m_{11}x + m_{21}y - m_{31}f}{m_{12}x + m_{22}y - m_{33}f} \qquad (3.7)$$

$$P = \frac{m_{12}x + m_{22}y - m_{32}f}{m_{13}x + m_{23}y - m_{33}f} \qquad (3.8)$$

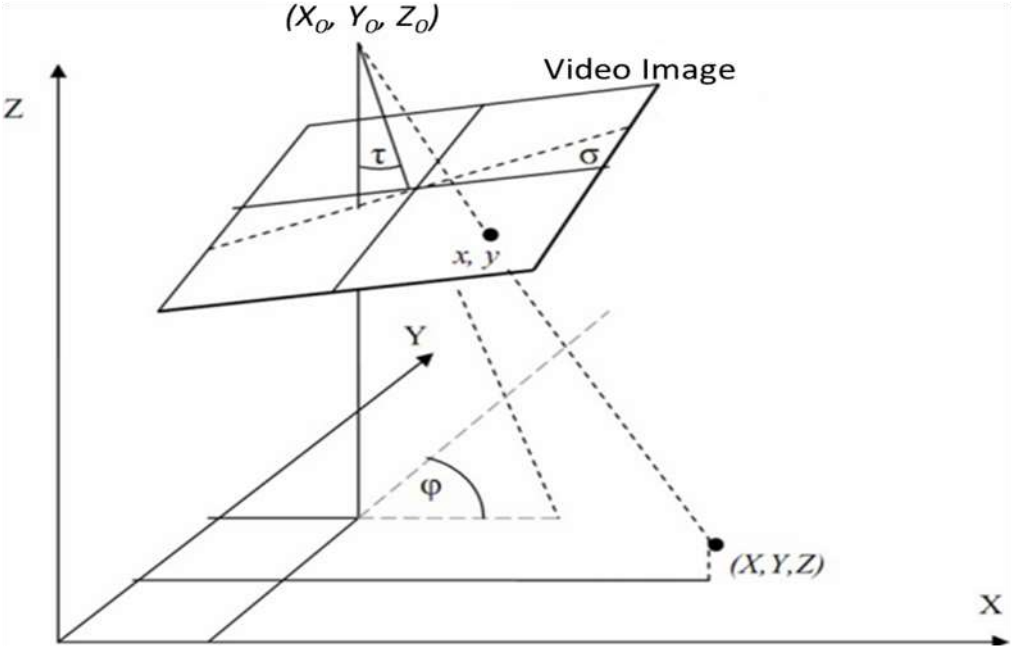

Figure 3.5. Basic geometry of video imagery of beach scenes. The camera, at location (X_0, Y_0, Z_0), is mounted at a height of Z above the origin, tilted at an angle of τ with respect to the vertical, and is rotated through an azimuthal angle of φ with respect to the positive y-axis. Ground control points are seen on the screen at image coordinates that define the angle σ.

The notations m_{ij} are orthogonal rotation matrices or direction cosines and can be derived in terms of three successive rotations about the angles φ (azimuth), τ (tilt) and σ (roll). Finally, to transform the 2-D (x, y) to 3-D cannot be estimated because the system of equations is underdetermined (two equations with three unknowns). This is solved by projecting the image on a planar horizontal field [Lippmann and Holman, 1989; Almar, 2009] by keeping z at a fixed water level.

$$m=\begin{bmatrix}\cos(\varphi) & \sin(\varphi) & 0\\ \sin(\varphi) & \cos(\varphi) & 0\\ 0 & 0 & 1\end{bmatrix}\begin{bmatrix}1 & 0 & 0\\ 0 & \cos(\tau) & -\sin(\tau)\\ 0 & \sin(\tau) & \cos(\tau)\end{bmatrix}\begin{bmatrix}-\cos(\sigma) & -\sin(\sigma) & 0\\ -\sin(\sigma) & \cos(\sigma) & 0\\ 0 & 0 & 1\end{bmatrix} \quad (3.9)$$

3.3.2 Processing of images: Biscarrosse video and merging images

Figure 3.6a shows that camera viewfields overlap. These overlaps are removed and images are geo-referenced and merge to a single plan view (Figure 3.6b). The merging was purposefully done to give a wide alongshore coverage after the rectification.

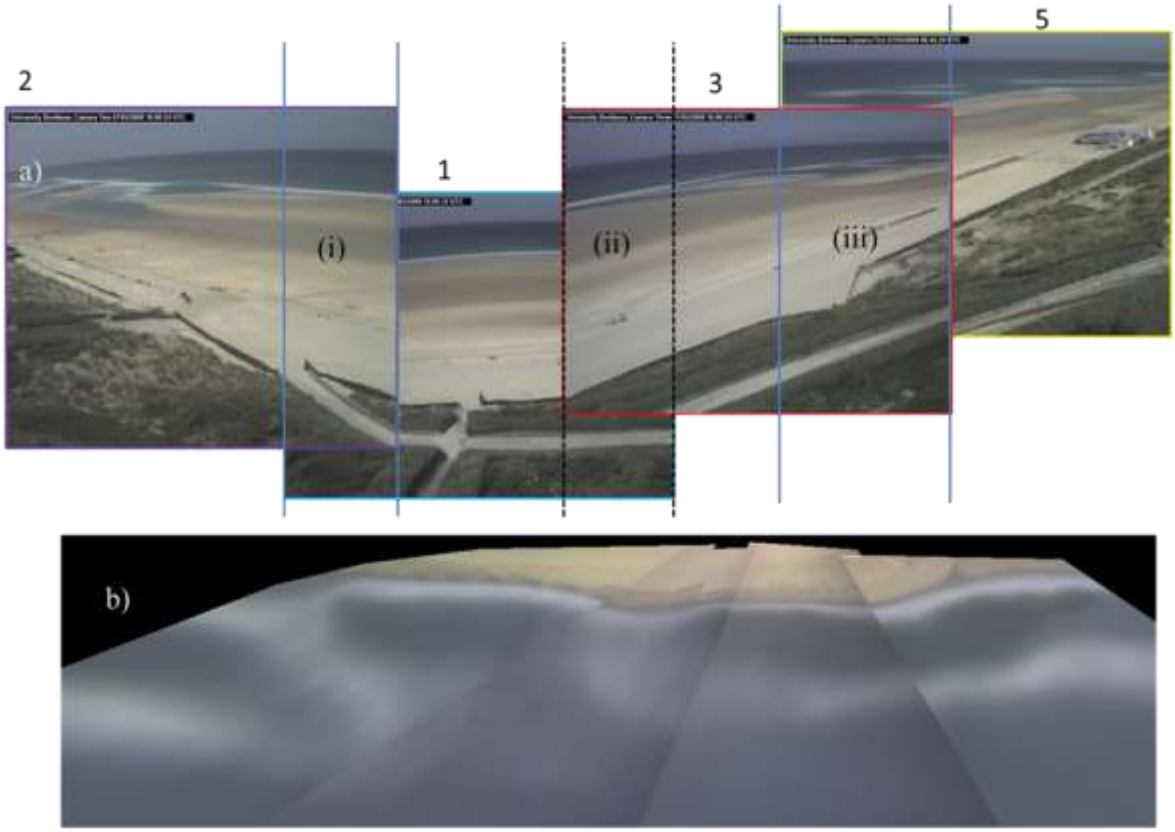

Figure 3.6. Merging of images: a) Oblique timex images for cameras (2, 1, 3, and 5) that show overlaps (i, ii, iii); b) rectified merged image using the various timex images.

3.3.3 Shoreline and sandbar delineation

Using timex images, the shoreline is manually delineated at the interface between the water and land on merged images (Figure 3.7) while the sandbar crest location is manually delineated from the pixel intensity maximum corresponding to the maximum of time-averaged incident wave breaking [Lippmann and Holman, 1989]. This is indicated by the white bands on the image (see Figure 3.7).

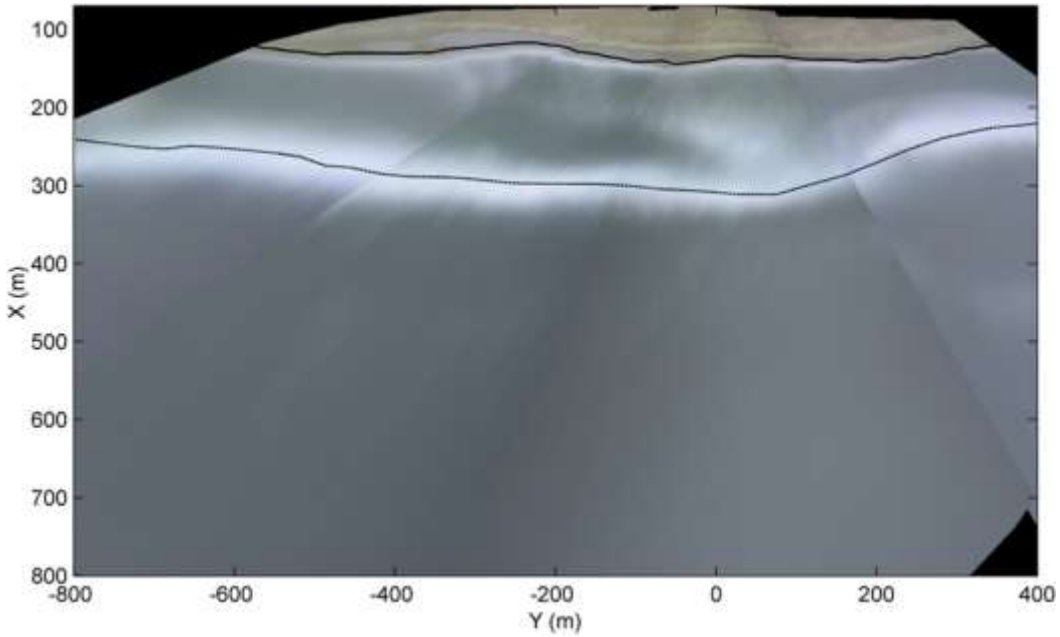

Figure 3.7. This shows manual digitisation of shoreline (thick solid line) and inner sandbar location (dotted line) from an oblique timex image. The camera location is traced to 0 m value alongshore (Y).

Following Plant et al. [1999], a time stack of the alongshore-averaged intensities was done to visually check the quality of shoreline and sandbar detection (Figure 3.8), from 2007 to 2012.This also shows the trend and seasonality in the data set.

3.4. Error analysis

3.4.1 Inaccuracy in the shoreline location

The sources of error or uncertainty of the observed shoreline in this study originate from:

1) The rectification of images from pixels to real world coordinates. This error includes that of pixel footprint (resolution) from oblique view and the accuracy of rectification from ground control points (the reference coordinates). Generally, the resolution of rectified images (in metric units) obtained is a function of the height, *h* of the camera and the distance of interested beach features from the camera:

$$\text{Resolution} = \frac{\chi}{\sqrt{r^2+h^2}} \qquad (3.10)$$

where $r_s = \sqrt{(x - x_o)^2 + (y - y_o)^2}$, is the distance from the camera location to the object on the image, (x_o,y_o) is the image center while (x,y) is the object location on image. When χ=1, the resolution estimated is only in the lateral direction, while for longitudinal resolution, $\chi = h/r_s$.

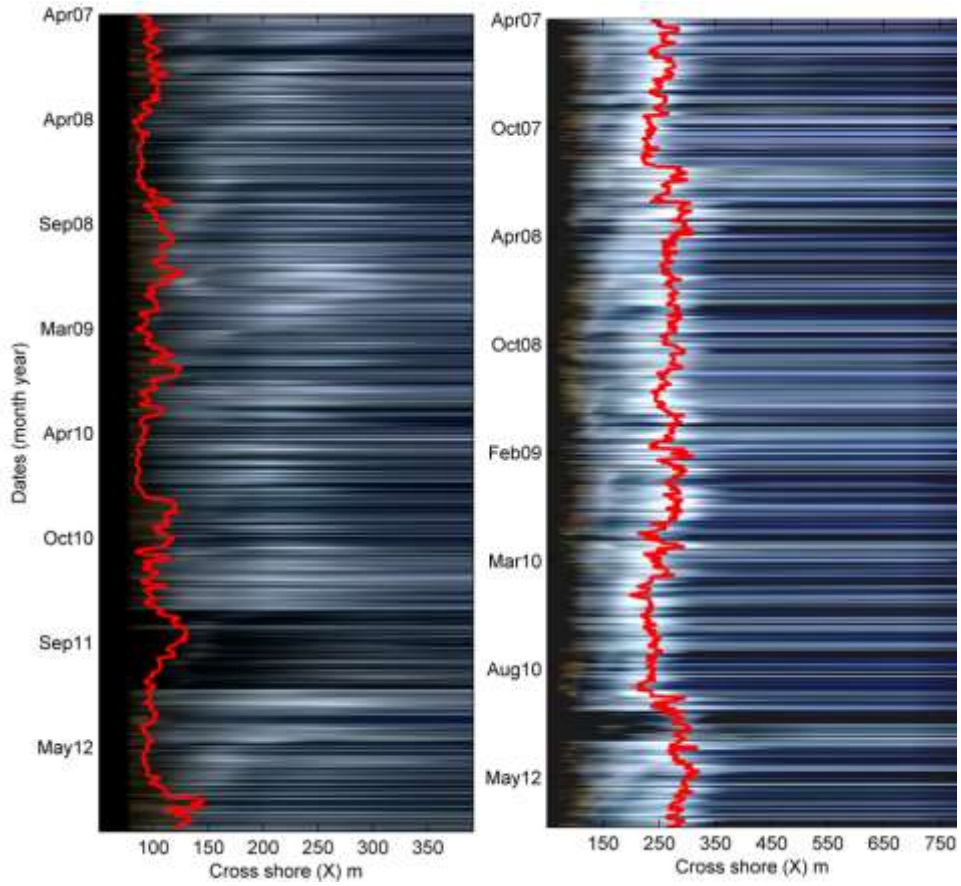

Figure 3.8. a) Shoreline evolution for all data sets b) sandbar evolution for all data set

For the usual camera configuration looking down the beach with an oblique angle, the spatial resolution footprint is

$Lx \sim r_s \Delta\sigma$ (lateral resolution) (3.11)

$Ly \sim r_s \Delta\sigma / \cos(\tau + \sigma)$ (longitudinal resolution) (3.12)

For example, a typical wide-angle view (roll) of σ = 30 °, range of 100 m and camera tilt of 75°, the pixel footprint is about Lx = 0.1 m and Ly = 0.39 m, good for the run-up application (Holman et al.,1991).

At Biscarrosse, the resolution of images is estimated separately in cross shore and alongshore directions. Figure 3.9a represents the location of the GCPs (ground control points) on a timex image. The digitized

shoreline positions range from 80 m to 160 m. Figure 3.9b suggests that in front of the camera, shoreline cross-shore resolution (foot print) is less than 0.5 m and worsen to 1.5 m at the edge (lowest tide time or widest beach time), which reaches 4 m in the alongshore (Figure 3.9c).

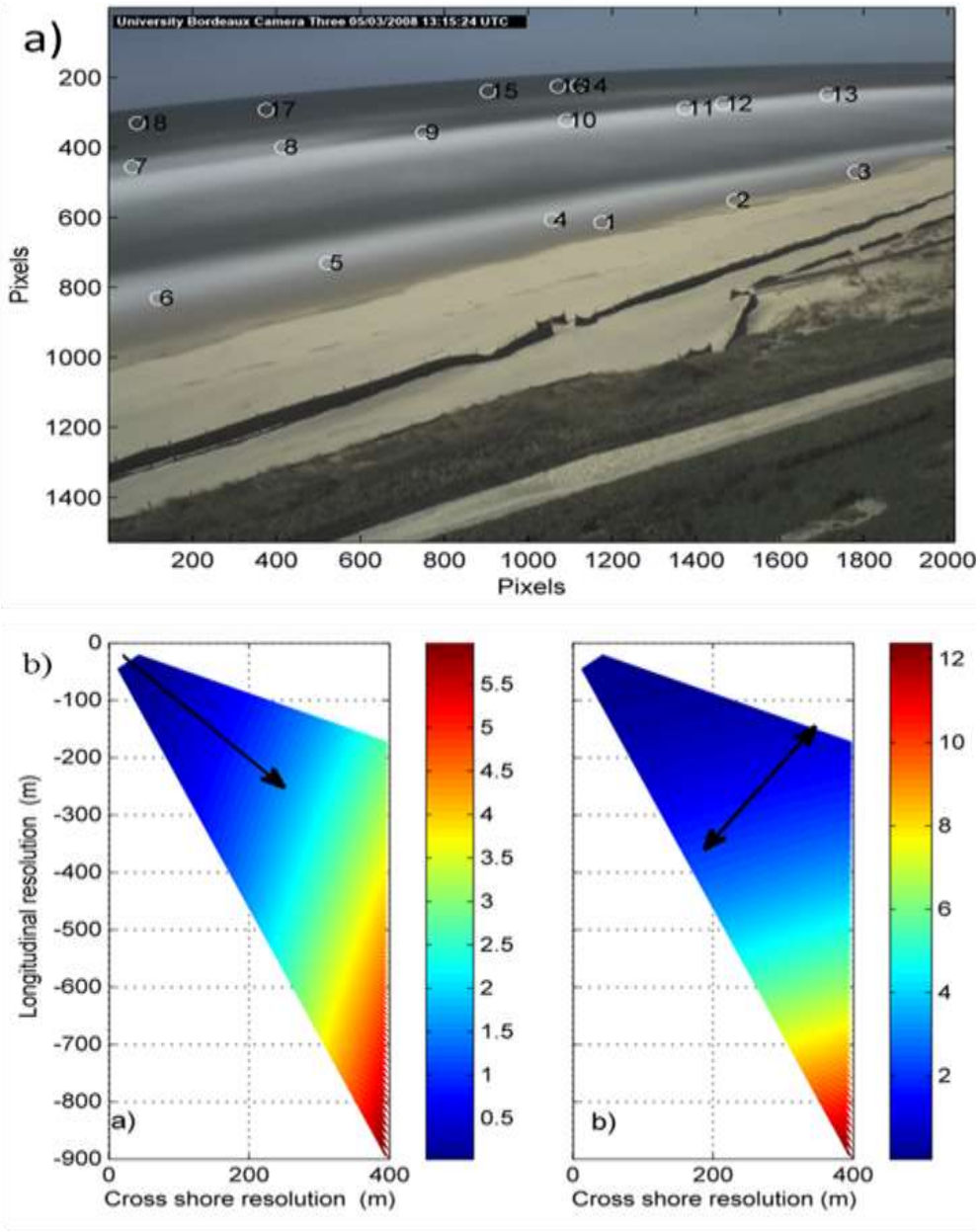

Figure 3.9. Image resolutions showing pixel foot print (m/pixels) per meter in color bar. In (b) is the foot print in front of the camera moving offshore (following the arrow) and in (c) is the footprint perpendicular (by arrow) or alongshore to the camera view direction

On the other hand, Figure 3.10 shows an example of the rectification of an image using 18 GCPs and equations 3.5 - 3.6. The errors incurred at each point can be estimated by comparing differences between the measured GCPs and the estimated GCPs (see Eq. 3.5 and Eq. 3.6) of objects located on the image. It must be pointed out that the error due to the rectification also depends on several factors that were taken into account; the water level elevation and wave induced set up and the camera height stated above. There is very strong correlation between the measured and estimated GCPs ($r > 0.98$) in both cross shore and alongshore directions. Figure 3.10c shows the measued GCPs and the estimated GCPs in the rectification.

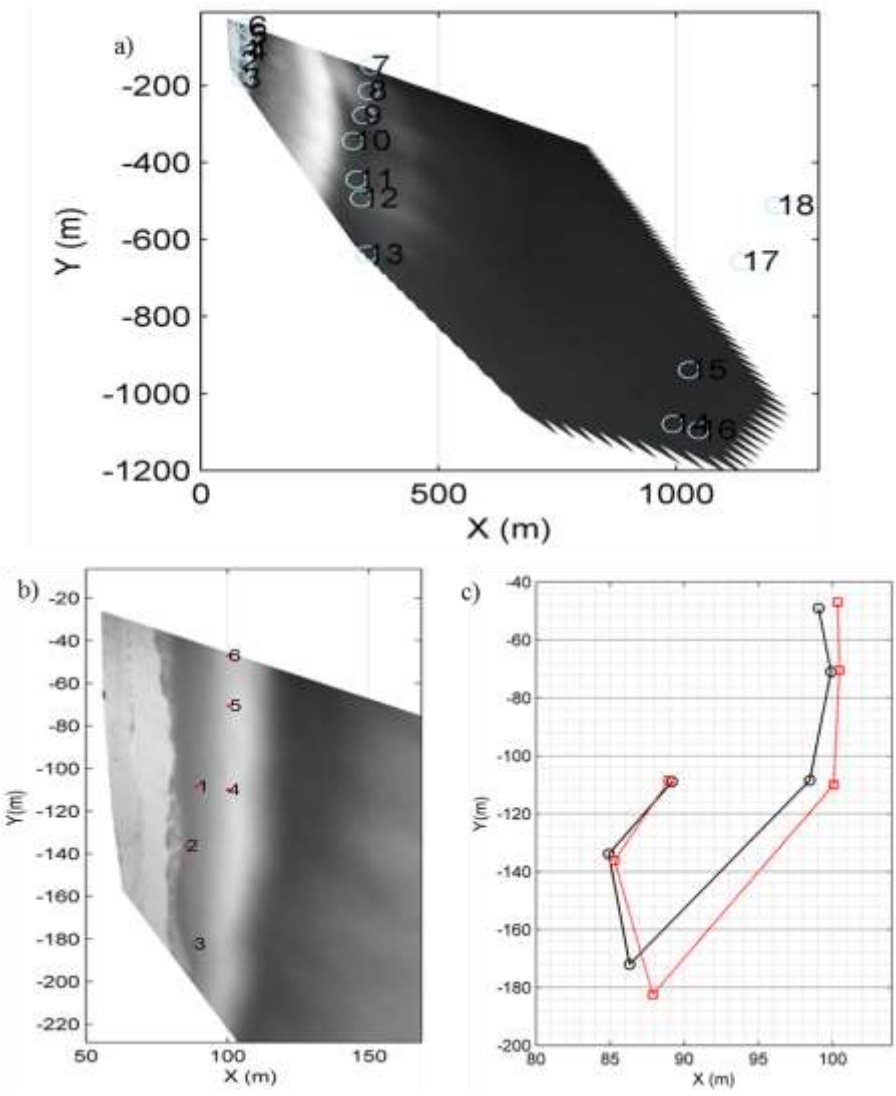

Figure 3.10. (a) Rectified image that shows the location of ground control points (circles and numbers) used for rectifying images with focus on the shoreline (b); c) differences between estimated GCPs (circle line) and measured GCPs (square line). Cross shore is in X(m) and alongshore is in Y(m).

Despite this, the mean absolute error obtained when rectifying pixel image can be large. At the far distant cross shore alongshore location (~86, 180), rectificatin is poor with about 10 m and 2 m resolutions, respectively, while close to the camera (the first point), resolutions are 0.4 and 0.2 m. For this study, mean error due to the rectification at the cross shore shoreline is 1.1 m.

2) Elevation contour level. Selecting a single water level is particularly important as it can minimize significant errors. Castelle et al. [2014] observed that if water levels of 0.4 and 1.5 m above MSL are selected, RMSE values of 10 m and 7.5 m are attainable, respectively, when measured values are compared to estimated values. In this study, the average water level (tidal elevation used) selected was 2.7 m. But we added also images that were very close to this elevation, at range of ± 0.1 m giving the tidal values at 2.7 m ± 0.1 m. The errors due to the selected water level were estimated by the ratio of the water level variation ± 0.1 m to the beach slope (0.03). In Figure 3.11, it is shown that the shoreline at MSL is improved by about 1 m when water level of Z = 0.4 m above MSL is considered. By this technique, each image or shorline had a known error associated to it. On average, a horizontal error due to tidal variation of 0.30 m was achieved due to this water level changes, though at sometime it reaches 5 m as indicated by the distribution on Figure 3.12a.

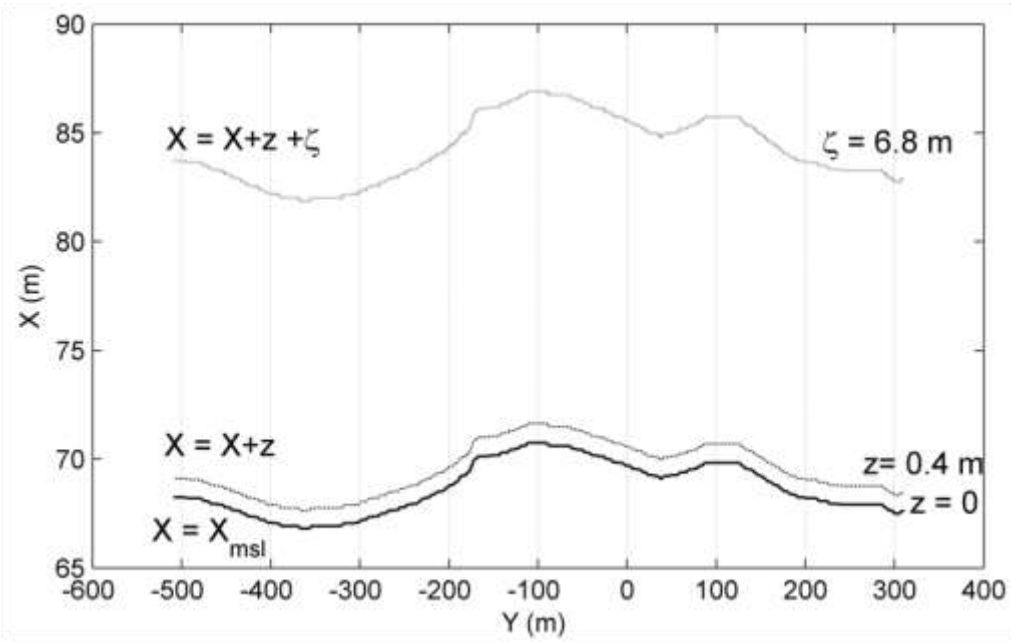

Figure 3.11. Schematic shoreline location (X) due to the effect of water level and setup.

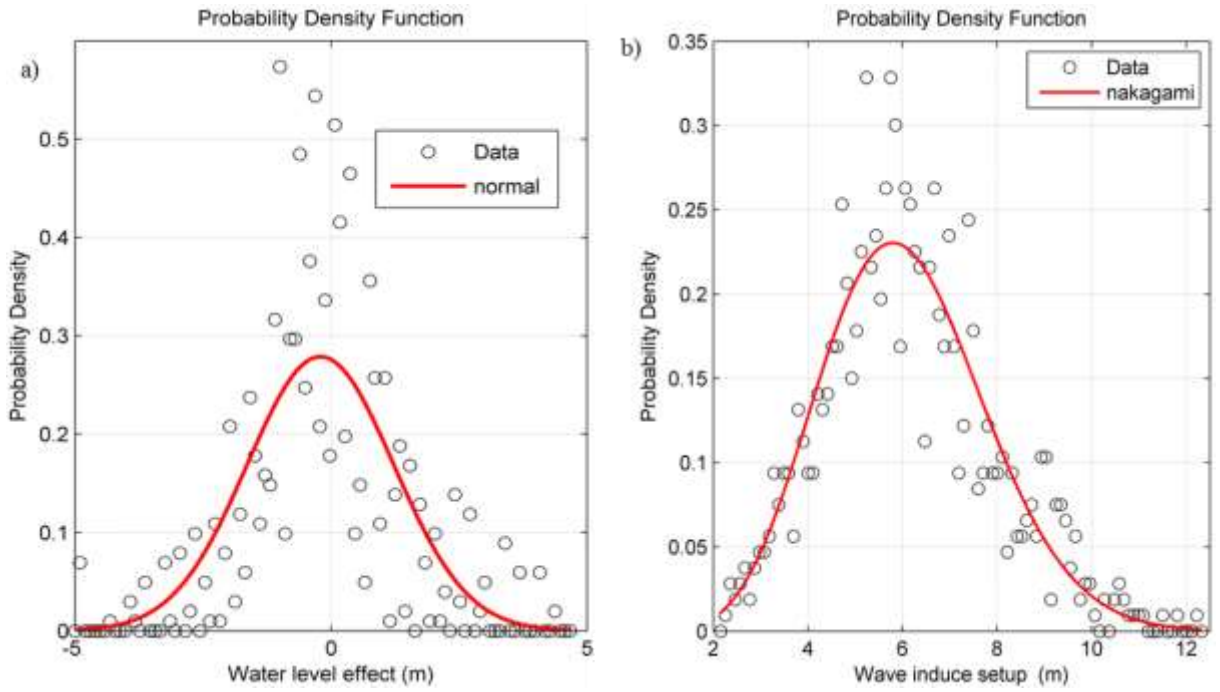

Figure 3.12 a) Normal distribution of the water level effect b) Nakagami distribution of wave induce setup on the changes of the measured shoreline

3) Wave setup (ζ), swash and runup (R). The setup can be defined as the local elevation in the mean water level on the foreshore, caused by the reduction in wave height through the surf-zone [Bowen et al., 1968; Goulay, 1992]. It can be proportional to the wave height at breaking. The swash consists of an onshore uprush and an offshore accelerating downrush while the wave run-up is the maximum level the waves reach on the beach relative to the still water level. Wave run-up is therefore the sum of the wave set-up and the wave swash (Figure 3.13). Quantifying the magnitude of runup is critical to accurately estimate shoreline location. Using empirical correction model, Plant et al. [2007] reported that local estimates of setup and swash amplitudes reduced shoreline elevation errors by about 50%. Wave setup can cause an increase in water level elevations on the order of 20–50% of the offshore breaking wave height [see Dean and Walton, 2009] and can be a significant portion of the overall storm surge. In this study, the setup term has been computed using the formulation from Stockdon et al. [2006].

There are several parameterizations of the runup, R and the setup but the most current and widely used was obtained by Stockdon et al. [2006]:

$R = <\zeta> + S/2$ *(3.13)*

$< \zeta > = 0.35\beta\sqrt{HsL_o}$ (β being upper beach slope) (3.14)

Hs and L_o are the offshore wave height and length, respectively, *S* is the swash. The most important part of the shoreline here is the cross shore location. The cross-shore setup (error), ζ_z, was estimated on the cross-shore position [see Senechal et al., 2015] when the beach slope is eliminated as in eq. 3.10:

$$\zeta_z = 0.35\sqrt{HsL} \qquad (3.15)$$

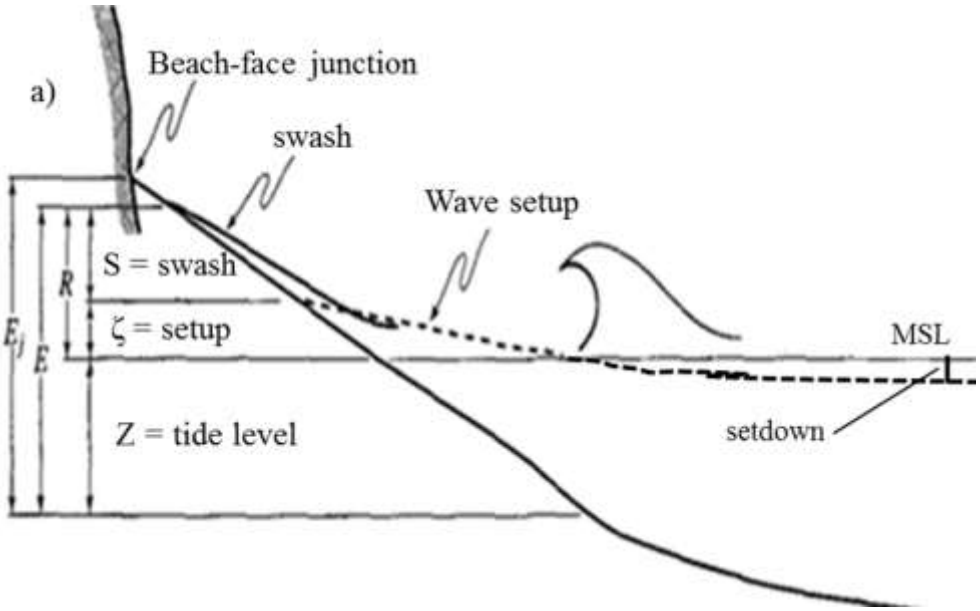

Figure 3.13. a) The quantitative assessment of wave setup, η in shoreline positions (modified from Ruggierro et al., 1996).

However, this is just an estimation because submerged bathymetry (e.g. presence of sandbar) and tide might be of substatial importace in the estimation of waterline level. Figure 3.12b shows the distribution of the wave induced setup that was estimated. Setup error for this study ranges from 2 to 12 m; however, average value obtained here is 6 m.

Other sources of error include the atmospheric pressure and wind effects. The overall uncertainty on the shoreline location is about 8.6 m, due to tide (0.3 m), setup (6 m), rectification (2 m) and digitisation (0.3 m). Only one analyst digitized the shorelines for all images to minimize different interpretations from multiple analysts.

3.4.2 Inaccuracy in the sandbar location

On the other hand, the inner sandbar positions range from 200 m to 350 m, the pixel footprint (metric resolution) at sandbar location ranges from 2 m to 10 m (Figure 3.9b and c). The error due to rectification is about 5 m in the sandbar area between 200 and 400 m cross shore, discussed in (1) of *section 3.4.1.* For

the errors associated to sandbar detection, the location of maximum intensity (reminiscent of sandbars) in a video image is known to deviate from the in-situ sandbar position, depending on the water level and wave height [Van Enckevort and Ruessink, 2001; Alexander and Holman, 2004]. Waves break further seaward (shoreward) of the sandbar crest with increasing (decreasing) wave height and decreasing (increasing) water level. A change in wave height or water level between subsequent image observations causes a change in location of maximum wave breaking in the images not associated with real sandbar migration. According to Lippmann and Holman [1989, 1990], error in identifying the maximum wave dissipation, in which the estimated bar crest positions are weighted offshore from the true bar crest location is less than 5-10% of the cross shore distance to the crest. Implementing this for this study, the average uncertainty to identify the true crest location is 10 m. Sandbar location in this thesis is approximated with an uncertainty of 16 m after combining all sources of errors including water level, wave effect, digitisation and rectification.

CHAPTER FOUR

Statistical approach of coastal response to storms

.....Life is like riding a bicycle.

To keep your balance,

You must keep moving.....

Albert Einstein

Chapter 4. Statistical approach of coastal response to storms

4.1 Introduction

4.2. ARTICLE: Shoreline resilience to individual and sequence of storms at a meso-macrotidal barred beach (in revision, *Geomorphology*)

4.2.1. Introduction

4.2.2. Methods

4.2.2a Field site

4.2.2b Video data

4.2.2c Storms

4.2.3. Results

4.2.3a Characteristics of individual storms and morphological impact

4.2.3b Modulation of storm impact and recovery by previous events, tides and sandbar

4.2.3c Storm sequences

4.2.4. Discussion

4.2.4a. Role of waves and tide on storm impact

4.2.4b. Importance of the frequency of recurrence of storms for shoreline resilience

4.2.4c. Uncertainties on video-derived data

4.2.5. Conclusions

4.1 Introduction

As previously introduced in Chapters 2 and 3, the fluctuation of shoreline position in a variety of time scales introduces many difficulties when reconstructing shoreline trends [Crowell et al., 1993; Short, 1999]. This variability in shoreline position may be the response to a single factor or a combination of several factors. Principal causes of coastal erosion or accretion have been individual large storm events [Anfuso et al., 2007; Zhang et al., 2002], seasonal variability in wave energy [Masselink and Pattiaratchi, 2001], multiyear to decadal-scale variations in storminess and coastal morphodynamics [Stive et al., 2002]. The analysis at medium to long term scales may be influenced by large short term events (e.g. storm or tide), yet, the importance of short term events always overshadows long term events if the duration of study is not long enough. To estimate the mean rate of shoreline changes that happen annually alongshore, the predictions must deal with both the erosive storm response, as well as the accretionary post-storm recovery, and not only with individual storms, but also sequences of storms and multi-annual trends , tides and climatic events. It is important to know that the short term littoral evolution is necessary for a proper management of coastal erosion.

In this chapter, first a methodology is presented to extract storms and then estimate the contribution of their impact on shoreline evolution during and after storms through statistical multiple regressions. Secondly, the role of storm return frequency and recovery duration are estimated and, the effect of sandbar location and tidal shoreline modulations are evaluated. Finally, discussion and perspectives are made relating statistical outcome to equilibrium based results.

4.2. ARTICLE: Shoreline resilience to individual and sequence of storms at a meso-macrotidal barred beach (under revision, *Geomorphology*).

DONATUS BAPENTIRE ANGNUURENG*[1, 2, 3], RAFAEL ALMAR[2], NADIA SENECHAL[1], BRUNO CASTELLE[1], KWASI APPEANING ADDO [3], VINCENT MARIEU[1], ROSHANKA RANASINGHE[4, 5, 6]

1. *UMR EPOC, University of Bordeaux/CNRS, Bordeaux, France.*
2. *UMR LEGOS, University of Toulouse/CNRS/IRD/CNES, Toulouse, France.*
3. *MAFS/Remote Sensing Laboratory, University of Ghana, Accra, Ghana.*
4. *UNESCO-IHE, Delft, The Netherlands*
5. *Harbour, Coastal and Offshore engineering, Deltares, Delft, The Netherlands*
6. *University of Twente, Enschede, The Netherlands*

Abstract

This paper investigates the impact of individual and sequence of storms on the macrotidal barred Biscarrosse beach in SW France, using 6-years of daily video observations. Based on 36 individual storms and 13 storm clusters, our results show that shoreline retreat is governed by the first storms in clusters, while the impact of subsequent events is less pronounced. Storm cluster impact on shoreline is not cumulative with the total retreat being less than the sum of individual storms contributions. The average post-storm beach recovery duration at this site is 9 days, which increases with tidal range and is modulated by the presence of the sandbar. Our results reveal that not only is the energy of storms important but also their frequency of recurrence, which underlines existing interactions between short storm events and longer-term sequences and seasonal evolution.

Keywords: storm clusters, beach erosion, beach recovery, sandbar, extreme events impact, open beach, short-term morphodynamics

*** Corresponding author:** +33 758 510 201 (D. B. Angnuureng)

***E-mail*:** *angnuureng@yahoo.com*

4.2.1. Introduction

Sustainable management of coastal resources requires a thorough understanding of the processes that drive changes in the shoreline location. The shoreline is a highly dynamic interface between land and ocean and is thus affected by various forcings operating at different spatio-temporal scales. Shoreline evolution is to a large extent governed by meteorological and oceanic conditions: waves, tides, currents and atmospheric conditions (wind, inverse barometer). It is generally assumed that wave breaking is the main driver of coastal evolution but its role is strongly modulated by other factors. For example, on the lower part of the beach, a storm may have more erosive impact at low tide than at high tide. Although many studies have focused on either simple or complex paradigms of shoreline evolution from Wright and Short [1984] beach classification, to more complex cross-shore equilibrium models [Yates et al., 2009] and a mix of cross-and longshore-based models [Morton et al., 1993; Hansen and Barnard, 2010], the response to perpetually changing forcing conditions is still somewhat unclear [Ranasinghe et al., 2012; Pianca et al., 2015]. The fact that beaches eventually recover to their pre-storm state means that the response does not only depend on the storm conditions but also on other factors such as sea level and long-term trend [Zhang et al., 2002], the previous beach state [Wright et al., 1985; Grasso et al., 2009; Yates et al., 2009] and/or previous wave conditions [Davidson et al., 2013; Splinter et al., 2014b].

Given that individual storms can result in dramatic shoreline changes, some studies treat storms as outliers [Zhang et al., 2002]. Storms are considered independent from long-term evolution and described separately because of rapid post-storm recovery. They suggest that a storm may induce undulations independently to any long term trend. Zhang et al. [2002] support the assertion of Douglas and Crowell [2000] that the most practical option is to remove such events from any long-term evolution consideration, though they may contribute significant information to the long-term signal at any given time. In contrast, Fenster et al. [2001] observed that individual storms do not need to be excluded from a long-term analysis of shoreline changes while Genz et al. [2007] observed that identifying storm contributions improves the prediction of the long term shoreline but concluded that this needed to be further investigated. The short term storm-induced shoreline change ranges from rapid erosion to slower post-storm recovery and is influenced by storm characteristics [e.g. energy and duration, individual versus storm clusters; see among others, Ciavola et al., 2007; Yates et al., 2009; Karunarathna et al., 2014; Coco et al., 2014; Senechal et al., 2015].

Investigations on storm impact mainly follow two approaches; non-cumulative analyses [e.g. Ruggiero et al., 1999; Frazer et al., 2009; Coco et al., 2014; Splinter et al., 2014a] which take individual storms as independent events and show that frequent storms or storm sequences do not have a persistent influence on longer term shoreline evolution which is influenced only by major individual storms with large return periods (e.g. 1 in 100 year); and cumulative storm analyses [e.g. Ferreira, 2005; Karunarathna et al., 2014] which show that storm sequences enhance shoreline erosion. The latter result has been further evidenced recently by equilibrium-based semi-empirical shoreline models [e.g. Yates et al., 2009; Davidson et al., 2013; Castelle et al., 2014] with storms rapidly eroding a beach due to the large disequilibrium between the high-energy storm and the previous beach state, as the beach tries to reach a new equilibrium under prolonged high energy waves. This discrepancy in conclusions means that individual or storm sequences at different sites generate different responses making storm response characterization still rather uncertain [e.g. Dolan and Davis, 1992; Mendoza et al., 2011; Splinter et al., 2014a; Senechal et al., 2015].

Shoreline recovery from storms depends on the severity of the event(s) and on how far the sediment has been transported offshore [Corbella and Stretch, 2012]. With high frequency (daily) video data, post-storm recovery durations of 5 to 10 days have been reported by Ranasinghe et al. [2012] for the microtidal Palm, Australia and Duck, USA beaches, respectively. The recovery duration is yet to be investigated at high energy meso-to macrotidal beaches with such long term high frequency data though it has been postulated to be rapid [Senechal et al., 2015]. Based on few storms, Ba and Senechal [2013] observed at the apex of the storm weak retreat of the shoreline, while the recovery period is very short as the shoreline was back to its initial position only 2 days after the apex of the storm. Beach recovery from

storms is therefore still poorly understood and the study of issues relating to the shoreline response to storm recurrence or frequency are uncommon in the literature.

Although it is widely accepted that the rate of shoreline change due to cross-shore sediment transport is mostly affected by the incident wave energy [e.g. Wright et al., 1987; Stockdon et al., 2002; Callaghan et al., 2008; Yates et al., 2009], the influence of tidal range and sandbar location cannot be overlooked. It has been observed that storm events, while capable of causing large short-term changes in the shoreline, do not singularly account for the overall observed change [Hansen and Barnard, 2010), and wave impact could be negligible with respect to the magnitude of the seasonal signal and the effect of the inter-annual signals [Pianca et al., 2015]. In macrotidal environments, tides are regarded as a primary factor in the control of the hydrodynamic and sedimentary processes of intertidal flats [Davis et al., 1972; Davis, 1985; Masselink and Short, 1993; Dissanayake et al., 2012]. The tidal range and its translation rate, determine the action of the waves upon the beach. There is field evidence for the tidal modulation (attenuation) of incident wave power by the tide [Davidson et al., 2008; Guedes et al., 2011] which eventually affects the shoreline. Zhang et al. [2002] observed that the combination of large waves with high water levels during five continuous high tides caused the largest recorded dune (upper beach) erosion from Long Island, New York, to Cape Hatteras. This suggests that the effect of tides actually depends on the part of beach (upper, intertidal or lower) being investigated. Banno and Kuriyama [2012] reported that although offshore wave energy fluxes affect the shoreline, the maximum and minimum tides also play key roles. Rosen [1977] observed that a decreasing tidal range results in long-term (~80 years) shoreline erosion on the microtidal Virginia Chesapeake Bay. Studies on microtidal beaches have shed further light onto the impact of tides on the shoreline [e.g. Shi et al., 2013; Wright et al., 1987]. However, the effect of tides on storm erosion at macrotidal sandy shorelines is relatively poorly investigated.

Changes in sandbar location due to varying wave conditions have been widely documented [e.g. Wright and Short, 1984; Wright et al., 1985; Lippmann and Holman, 1990; Gallagher et al., 1998; Castelle et al., 2007a] where cross-shore sandbar locations appear correlated with the changing wave conditions and tides [Guedes et al., 2011]. Sandbars are observed to migrate toward an equilibrium location which is dependent on waves [Plant et al., 1999]. Bar decay can result in its inability to offer protection during consequent less intense storms leading to massive and unexpected coastal erosion [Castelle et al., 2007b; Walstra et al., 2012]. Alongshore variation in depth and cross-shore location of sandbars work as a forcing template for the inshore wave field that result in localized beach and dune erosion during storms [Thornton et al., 2007; Castelle et al., 2015]. At barred beaches with large tidal ranges, it is observed [e.g. Almar et al., 2010; Ba and Senechal, 2013] that both the sandbar and the tide modulate onshore wave breaking intensity and control morphological changes [Coco et al., 2005; Stokes et al., 2015]. Although shoreline and sandbar changes have been studied rather extensively [e.g.

Lippmann and Holman, 1990; Plant et al., 1999; Hansen and Barnard, 2010; van de Lageweg et al., 2013], they have been studied mostly separately and the direct interactions between them are weakly identified, especially in meso- to macrotidal environments. The combined effect of tides and sandbar on short-term shoreline evolution is uncertain, particularly for storm impact and beach recovery duration.

In order to address the above mentioned knowledge gaps, six years (2007-2012) of daily video observations at Biscarrosse, a barred meso-to-macrotidal beach, are analyzed. In Section 4.2.2 the study site and video methods used are described. Section 4.2.3 presents the results on the shoreline response to storms at time scales from days to years, with an emphasis on the influence of storm recurrence and the modulation played by tidal range and sandbar. The role of tide on shoreline response to storms and the importance of the frequency of recurrence of storms on shoreline resilience are discussed in Section 4.2.4.

4.2.1 Methods

4.2.2a. Field site

Biscarrosse beach, located in the SW France (Figure 4.1), is exposed to long and energetic waves originating mainly from the W-NW. The mean annual offshore significant wave height *Hs* is 1.4 m with an associated peak period T_p of 6.5 s. Waves show a seasonal variability [Butel et al., 2002]: during fall and winter seasons (November to March) mean *Hs* is 1.6 m with a T_p of 7.3 s, while during spring and summer (April to October) mean *Hs* is 1.1 m with a shorter T_p (6 s) [Butel et al., 2002]. The tidal range has an average value of 2.9 m which increases up to 5 m during spring tide. The average beach slope is about 0.03 while sediment at the site consists of fine to medium quartz sand with median-grain sizes ranging from 0.2 to 0.4 mm [Lafon et al., 2002].

Biscarrosse is an open double-barred beach; the outer bar often exhibits crescentic patterns, while the inner-bar in the intertidal domain commonly exhibits a transverse bar and rip (TBR) morphology with a mean wavelength of about 400 m [Lafon et al., 2002; Castelle et al., 2007; Almar et al., 2010]. Based on three years of daily video images, Peron and Senechal [2011] also indicate that both up-state and down-state transitions were dependent on the previous beach state and that no ‘direct jump’ from the reflective state to the dissipative beach state was observed. They also discussed the possibility that the presence of the subtidal bar probably explained the persistence of TBR states (mean residence time of about 24 days reaching maximum at 103 days), even during high energetic conditions as reported in other similar environments [Almar et al., 2010]. Using three years of video observations, Senechal et al. [2015] showed that the range of variation of the inner sandbar location (120 m) at Biscarrosse is two and half times larger than the range of variation of the shoreline and that rapid erosion of the shoreline can be observed under moderate conditions.

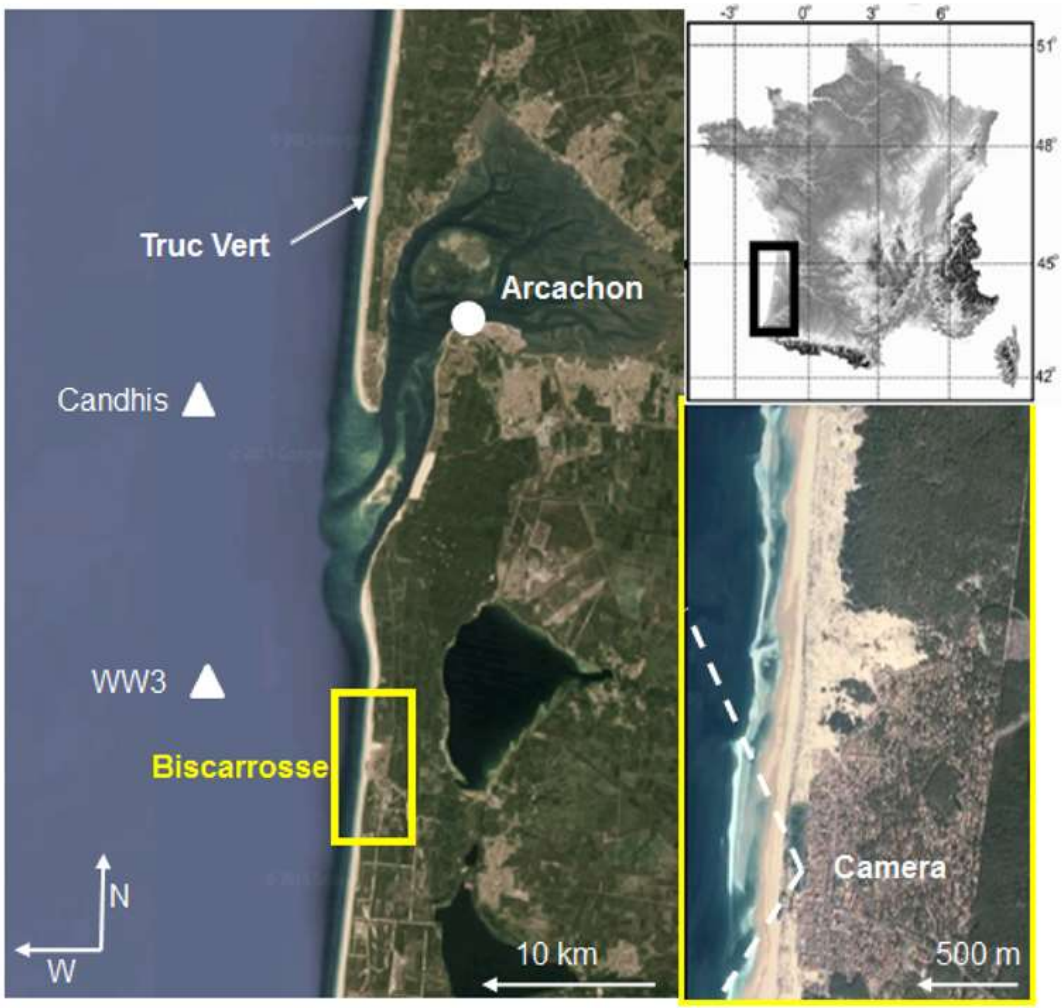

Figure 4.1. Location of the study site, Biscarrosse beach (SW France), showing the WW3 grid node (triangle) located at -1°30' W, 44°30' N and Candhis buoy (triangle) at 1°26.8'W, 44°39.15' N and the video station.

4.2.2b. Video data

A shore-based video system [e.g. Lippmann and Holman, 1989, 1990; Holman et al., 1993; Plant and Holman, 1997] was installed at Biscarrosse beach in April, 2007 by EPOC laboratory (CNRS/University of Bordeaux) in collaboration with the New Zealand National Institute of Water and Atmosphere (NIWA) [see Almar et al., 2009; Senechal et al., 2015]. The video station contains five color cameras fixed atop the fore dune at 26 m above the mean sea level (MSL), though only four camera images (Figure 4.2a-d) were in good state during the present study observation period. The system provides three types of images every 15 minutes: snapshot, cross-shore time stacks and 10-min time exposure (or timex) images. A region covering beach area of 1200 m longshore and 400 m cross shore is

selected (Figures 4.2e and 4.2f). Images are merged and rectified on a 1 m x 1 m grid using conventional photogrammetric methods [Holland et al., 1997]. The transformation between oblique image and real-world coordinates was achieved using 18 control points surveyed with a differential GPS (DGPS, centimetric accuracy). The origin (X=0, Y=0) of the local coordinate system is the camera location oriented along the beach cross-shore (X) and alongshore (Y) directions. Vertical Z=0 origin is Mean Sea Level (MLS). The mean pixel resolution at the shoreline location is about 0.1 m and 0.2 m in the alongshore and cross-shore direction, respectively, which worsens to 1-3 m at the viewfield edges.

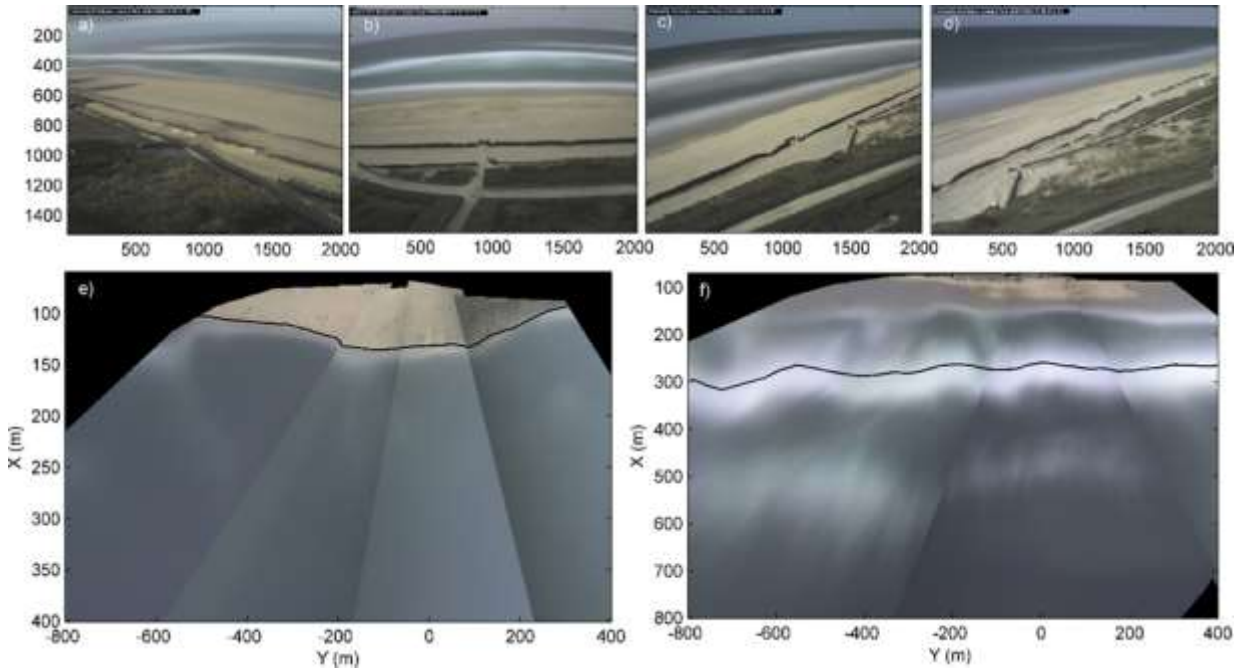

Figure 4.2. Illustration of cameras view fields from (a-d) oblique 10-min averaged images with manual delineation of e) shoreline (29 Sept. 2008) and f) inner-sandbar crest (15 June, 2007) on rectified, merged images.

Commonly used proxies for shoreline position are either based on visual assessment (e.g. the high water line) or datum-based proxies [see Boak and Turner, 2005; Moore et al., 2006]. Datum-based shorelines generally consist of the cross-shore position of a specified elevation contour, such as mean high water (MHW), the method chosen in this study. Shorelines derived from video have become increasingly common [Plant and Holman, 1997; Aarninkhof et al., 2003; Plant et al., 2007; Smit et al., 2007]. Different categories of images have been used to delineate shoreline with first methods based on gray images [Plant and Holman, 1997; Madsen and Plant, 2001] being the popular SLIM method, a typical approach where an intensity peak is used as a proxy for the location of the shoreline, and suitable for reflective beaches [Plant et al., 2007], followed by color (or both color and gray), a more sophisticated method [Turner et al.,

2001; Aarninkhof et al., 2003; Almar et al., 2012] based on color segmentation, applicable to detecting the shoreline at both reflective and dissipative beaches. In this study, errors have been minimized with the manual delineation of the shoreline (Figure 4.2e) to ensure quality dataset. The days when images had bad quality (e.g. sun glint, fog) were discarded. At meso- to macrotidal barred beaches, it is difficult to select the elevation that best represents the overall intertidal complex morphology, as observed by Castelle et al. [2014]. Following this and to minimize their influence of the complex intertidal zone, shoreline location was defined here for elevations at 0.45 m ± 0.1 m above MSL (Figure 4.2) which corresponds to the lowest high tide level, commonly used through video imagery to get daily shoreline data at meso-macrotidal beaches [e.g. Birrien et al., 2013; Senechal et al., 2015]. Due to the absence of a tide gauge at Biscarrosse, tide used here was extracted from tidal harmonics [WXtide software, Flater, 2010] with reference to the closest point at Arcachon (1°10 W, 44°40 N, Figure 4.1), about 30 km from Biscarrosse, after correction of the phase-lag. Overall, the video-derived shoreline dataset covers 1036 days in 6 years, which is 54.2% of the study period.

Timex images (Figure 4.2f) are used to average-out high-frequency intensity fluctuations due to individual waves and give a statistically stable pattern of the breaking [Lippmann and Holman, 1989; van Enckevort and Ruessink, 2001]. The high-intensity bands associated with breaking (see Figure 2f) are commonly used as a proxy for bar crest location [Lippmann and Holman, 1989; Pape and Ruessink, 2008; Almar et al., 2010; Guedes et al., 2011]. There is always a substantial error O (1-10 m) when locating the cross-shore position of the bar crests [van Enckevort and Ruessink, 2001]. This is mostly due to the translation of the breaking zone resulting from the changes in wave characteristics and tidal level [Lippmann and Holman, 1989; van Enckevort and Ruessink, 2001]. In order to reduce the differences between the detected and actual bar crest location, and to be consistent with previous methodologies [e.g. van de Lageweg et al., 2013; Senechal et al., 2015] images for which *Hs*> 2.5 m were discarded, also because breaking might occur continuously from the outer bar to the shore under such energetic conditions. Inner bar extraction was done at constant water level of 0.55 ± 0.1 m below MSL. The detection resulted in 411 daily alongshore-averaged cross-shore sandbar positions $<X_b>$ or lines which is 20% of the entire period.

4.2.2c. Storms

Wave data have been retrieved from Wavewatch III model [Tolman, 1991] at the grid point facing the beach (1°30'W, 44°30'N, Figure 4.1) in about 70-m water depth, at a 3-hour interval over the study period (2007-2012). The significant wave height, *Hs* was further corrected via linear regression with a

directional wave buoy (1°26.8'W, 44°39.15'N) moored in 50-m water depth, following Castelle et al. [2014].

A pre-selection of extreme data needs to be done before proceeding to the analysis. In statistics an 'extreme event' is defined as a sample (i.e. sea state) that is deviated significantly from the mean of its distribution function. In engineering studies, the most common parameter that is used to define whether a process is extreme or not is the wave height (*Hs*). In the extreme value theory, two methods are described to select the extreme values: (1) annual maxima method and (2) peaks over threshold method [Dorschet al., 2008]. The main drawback of the 'Annual Maxima method' is that it only allows the selection of one value per year or event, that largely reduces the data series. In the present case the peaks over threshold method (POT) is used. The POT method assumes that once we have placed a threshold, all the items over this level are peaks and significant. Unfortunately, it has always been difficult to define a correct *Hs* threshold value that describes an energetic sea state due to site specific properties. An *Hs* value that is only exceeded by the 8-10% of the time is a commonly agreed criterion among scientists [e.g. Dorschet al., 2008; Rangel-Buitrago and Anfuso, 2011]. In the present work, only values with a probability of occurrence less than 5% are considered as storms which correspond to *Hs* of 3.68 m, also in line with Splinter et al. [2014a] and Castelle et al. [2015]. A single storm is thus defined as a continuous period of *Hs* exceeding this threshold (Figure 4.3) and lasting at least one tidal cycle (12 hours), following Senechal et al. [2015] approach. Storm intensity *I* (m^2hr) is defined in several studies [e.g. Dolan and Davies, 1992; Karunarathna et al., 2014; Senechal et al., 2015] as the product of the maximum *Hs* by the storm duration in line with annual maxima method. Here *I* follows the definition by Mendoza et al. [2011] and POT method, and is computed as the integration of time-varying *Hs* over storm duration:

$$I = \int_{t_1}^{t_2} H_s(t)^2 dt \qquad (1)$$

where the duration *D* is the time between the beginning t_1 and the end t_2 of the storm (Figure 4.3b). Initiation of a storm *t1* was defined as the time when the three hourly-averaged *Hs* exceeded the 0.75 quantile (1.9 m) to be consistent with Masselink et al. [2014]; the end of the storm *t2* was the time when the three hourly-averaged *Hs* returned below 1.9 m.

Storm impact $\Delta\langle X_{s,i}\rangle$ is estimated as shoreline migration from the beginning to the end of each storm, equivalent to the end point rate method [Genz et al., 2007]. The shoreline migration from the beginning to the first maximum recovery value after each storm was assumed as the post-storm recovery T_r . Following Ranasinghe et al. [2012] where the post-storm beach recovery duration was estimated based on the beach states, their post-storm recovery duration is the time for the nearshore morphology to

evolve from a post-storm state (e.g. Dissipative/LBT) to its modal state (i.e. the most frequently occurring beach state e.g. RBB or TBR).

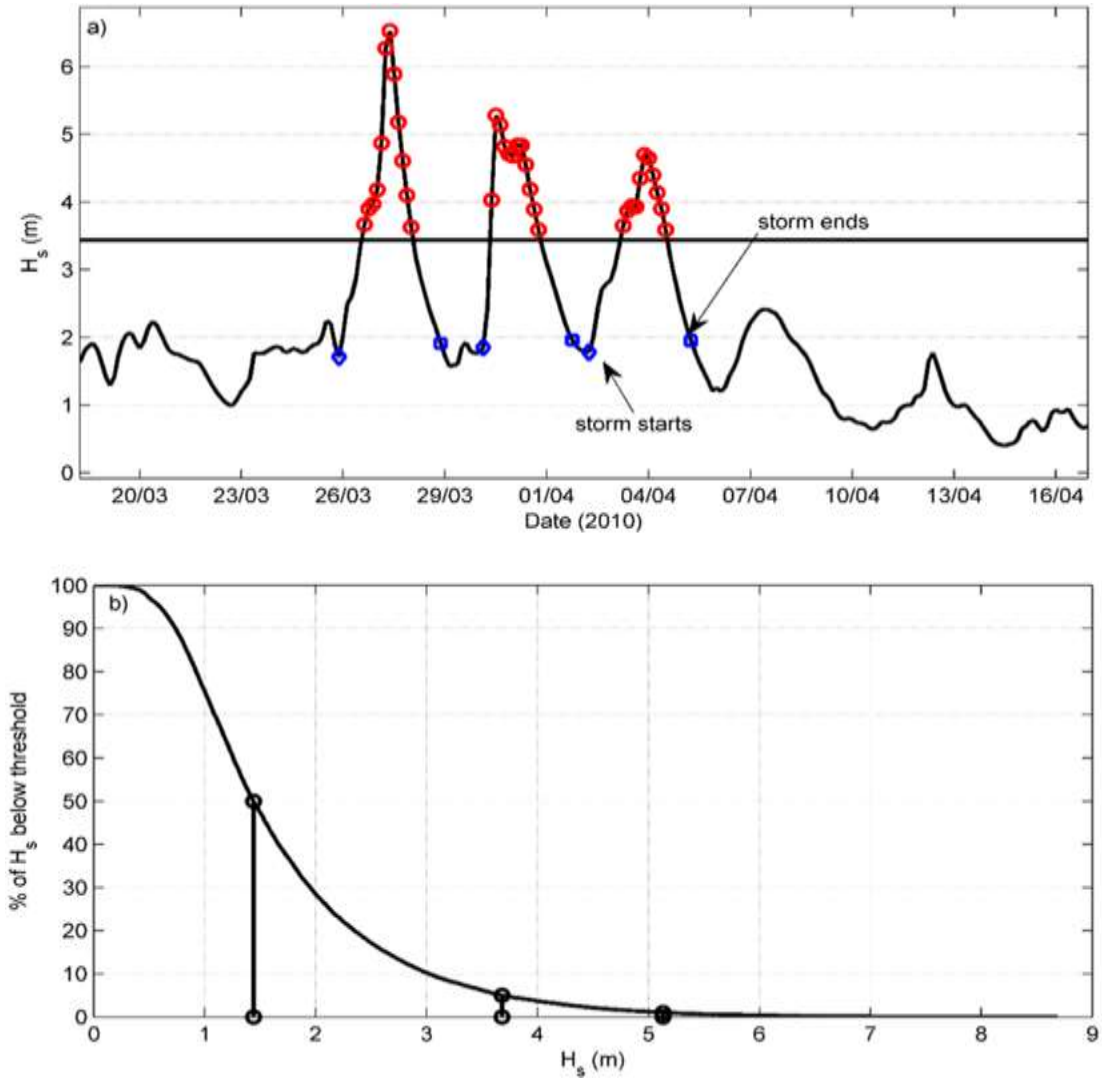

Figure 4.3. Illustration of the method to pick a) storm characteristics, beginning and end of *Hs* above the threshold (*Hs*=3.8 m, 95% exceedance level, shown as horizontal line) and in b) the exceedance level where the 50, 95 and 99% levels are shown. Definition of storm events are site-specific [Masselink et al., 2014], and the *Hs* thresholds used here were selected because they produced clearly identifiable storm events.

The time taken to reach the first maximum recovery values after each storm was accepted as the recovery duration in this study but this could not be related to the beach states. The recovery duration refers to the post-storm period of continuous accretion towards its equilibrium pre-storm state (T_r). Thus,

to obtain the over all recovery duration in the six years, the time taken by the daily average post-storm evolution to reach the maximum recovery value was found.

A multiple linear regression is used to investigate the role of 5 forcing parameters on $\Delta\langle X_{s,i}\rangle$ and T_r: the current storm energy I_i, previous storm, time interval between storms, tide range *TR* and sandbar-to-shoreline distance. The current storm is defined here as the last storm while the previous storm precedes the current storm.

The previous storm influence is defined as the ratio of previous storm impact to the time interval (in days).

$$Y = co + \sum_{1}^{n} C_k Z_k + \varepsilon \qquad (2)$$

where *Y* the response variable, *Z* is the predictor or causative mechanism variable, *n* is the number of events (36 here), c_o and C_k are the non-standardized regression coefficients and ε is the residual term. Forcing terms are considered independent. The use of a linear regression for possible non-linear relationships between the various parameters is to identify the predominant parameters.

The relative contribution *P(Z)* of each forcing parameter is estimated from the ratio of individual variance to the total:

$$P(Z) = 100\sqrt{\frac{S_k}{S_Y}}\ (k = 1, 2, \ldots 5) \qquad (3)$$

where S_k is the variance of C_kZ_k and S_Y is the sum of variances of *Y* components and *k* the number of dependent parameters.

4.2.3. Results

Figure 4.4a shows that wave regime has large seasonal variations, rather low and high energetic in summer and winter, respectively, with *Hs* ranging from less than 1 m to 9 m. Figure 4.4c shows that the alongshore-averaged shoreline location $\langle X_s\rangle$ also follows a seasonal cycle with most onshore (85 m) and offshore (150 m) position in winter and summer, respectively. In Figure 4.4d, the alongshore-averaged sandbar location $\langle X_b\rangle$ shows a large variability (range of 110 m), varying between 212 m to 322 m with outermost location in winter and a less marked seasonal cycle. On average, the sandbar-to-shoreline distance $\langle X_b\rangle$-$\langle X_s\rangle$ is 162 m but can be larger (227 m) or shorter (102 m) during large (winter) and weak (summer) wave conditions, respectively.

4.2.3a. Characteristics of individual storms and morphological impact

60 storms were identified over the study period (Figure 4.5), though only 36 were further accounted for in our analyses due to gaps in video data. The mean peak storm wave height was 4.9 m (s.d. = 1.04 m) with the mean wave height throughout the storms duration being 4.5 m (s.d. = 0.8 m). The mean storm wave periods throughout all the storms was 12.15 s (s.d. = 2.16 s), and the mean storm duration was 33 hr (s.d. = 32 hr). 2011 recorded the lowest number of these extreme storms with 9 storms and most of them did not cause erosion and any substantial shoreline change (+ 3 m) for instance. The overall average interval between storms is 27 days (Table 4.1) with 60% recurring within 10 days, though this occurrence is observed to be predominantly seasonal: sparse in summer and frequent in winter (Figure 4.5).

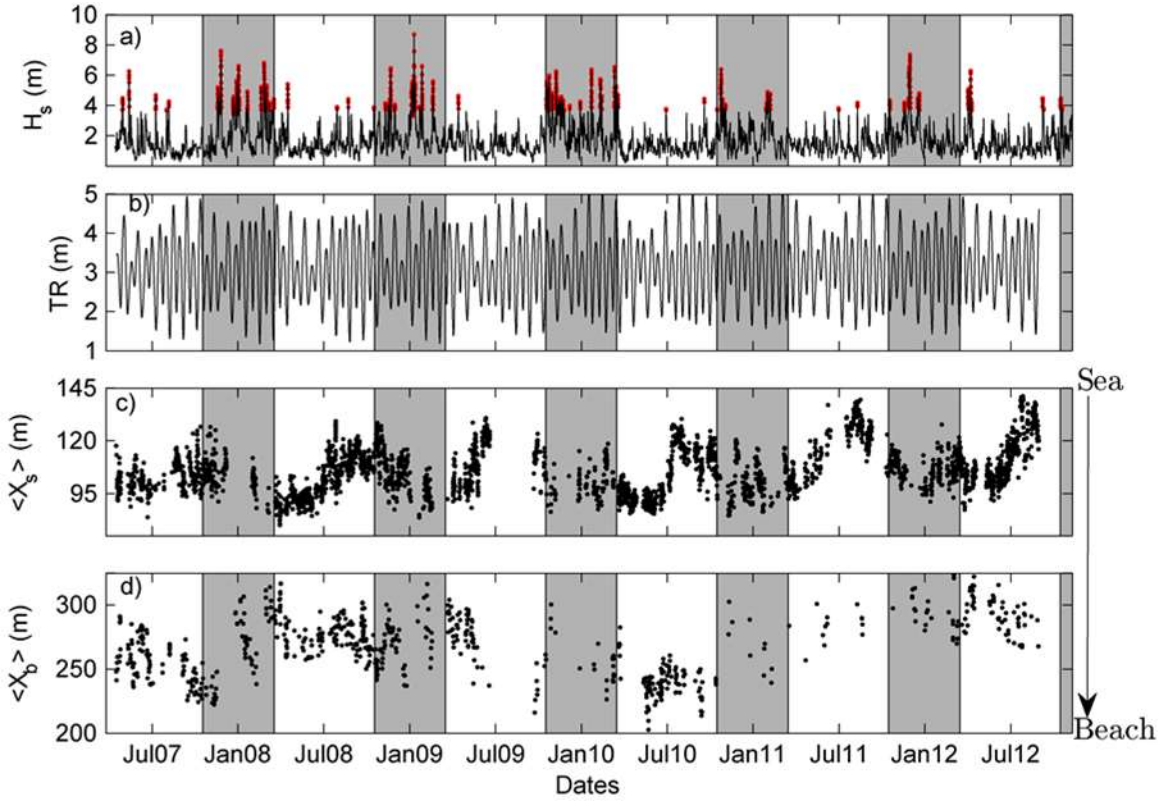

Figure 4.4. Time series of a) significant wave height *Hs* with storm periods (*Hs* >3.68 m are marked in red), b) tidal range *TR* c) alongshore-averaged shoreline location $<X_s>$ and d) alongshore-averaged sandbar location $<X_b>$. For c) and d) distance is from the camera. Winter periods (November to March) are indicated in grey.

Seasonal analysis in Figure 4.6 indicates that storms are more frequent in winter months, while occurring almost throughout the year. In summer months, only a few and short storms (<6 hr) are observed and not met the requirement of a complete tidal cycle (see Section 4.2.2.c). It is also seen in Figure 4.6 that standard deviation of storm energy is large in winter, which can explain the variability observed in shoreline response. The largest number of storms and most extremes (*Hs* > 5 m, defined as the 99% percentile, Table 4.1) are observed in 2008 (24%), 2009 (20%) and 2010 (19%), which induced cumulated large erosion particularly in 2009 (Table 4.1). Individual storms result in a wide range of shoreline impacts (Table 4.1), from large erosion (-21 m) to even accretion (+14 m). The immediate cause of this is unknown, but sediment input from dune erosion constitutes a possible effect of the upper beach accretion [van Gent et al., 2008]. The mean storm impact on shoreline throughout all the storms is an erosion of 8.7 m (s.d. = 8.9 m).

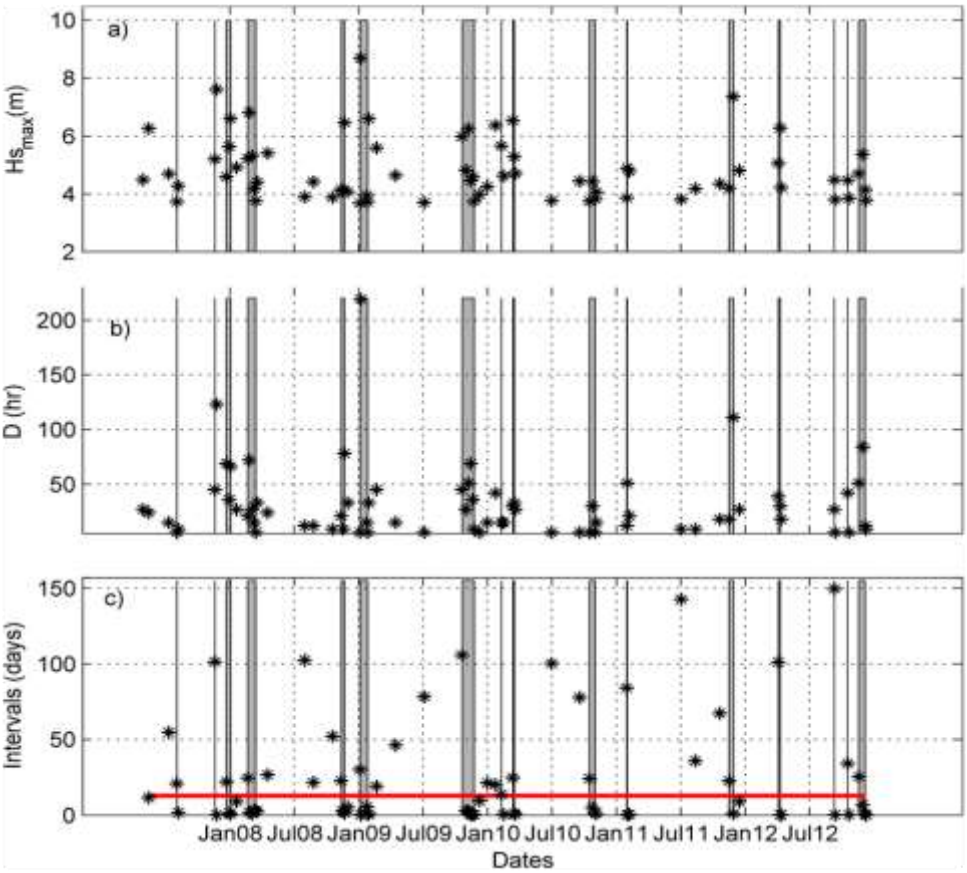

Figure 4.5. Temporal evolution of the characteristics of storms a) *Hs* b) storm duration (hours) *D* and c) storm recurrence interval or return time (in days). Clusters of storms (or group of storms) are shaded. In c) the red horizontal indicates the threshold of 60% storms with approximately 10-day return period.

Table 4.1. Average storm characteristics from 2007-2012 of maximum *Hs* (m), percentage (%) of extreme storms (*Hs* > 5.0 m, 99% threshold), storm impact $\Delta\langle X_{s,i}\rangle$ (m), storm duration (in days) and yearly average return period of storms (interval in days)

	Storm number	**Hs_{max} (m)**	**Hs_{max}>5m (%)**	**$\Delta\langle X_{s,i}\rangle$ (m)**	**Duration (days)**	**Interval (days)**
2007	7	4.7	11.1	-6.4	2.7	38.0
2008	18	5.0	25.9	-8.0	3.4	16.0
2009	15	5.0	25.9	-12.4	4.0	20.0
2010	13	4.7	22.2	-6.5	2.5	23.2
2011	9	4.8	3.7	3.0	2.7	39.5
2012	11	4.5	11.1	-10.3	4.5	29.8
mean	12	4.8	1.0	-7.0	3.3	27.0

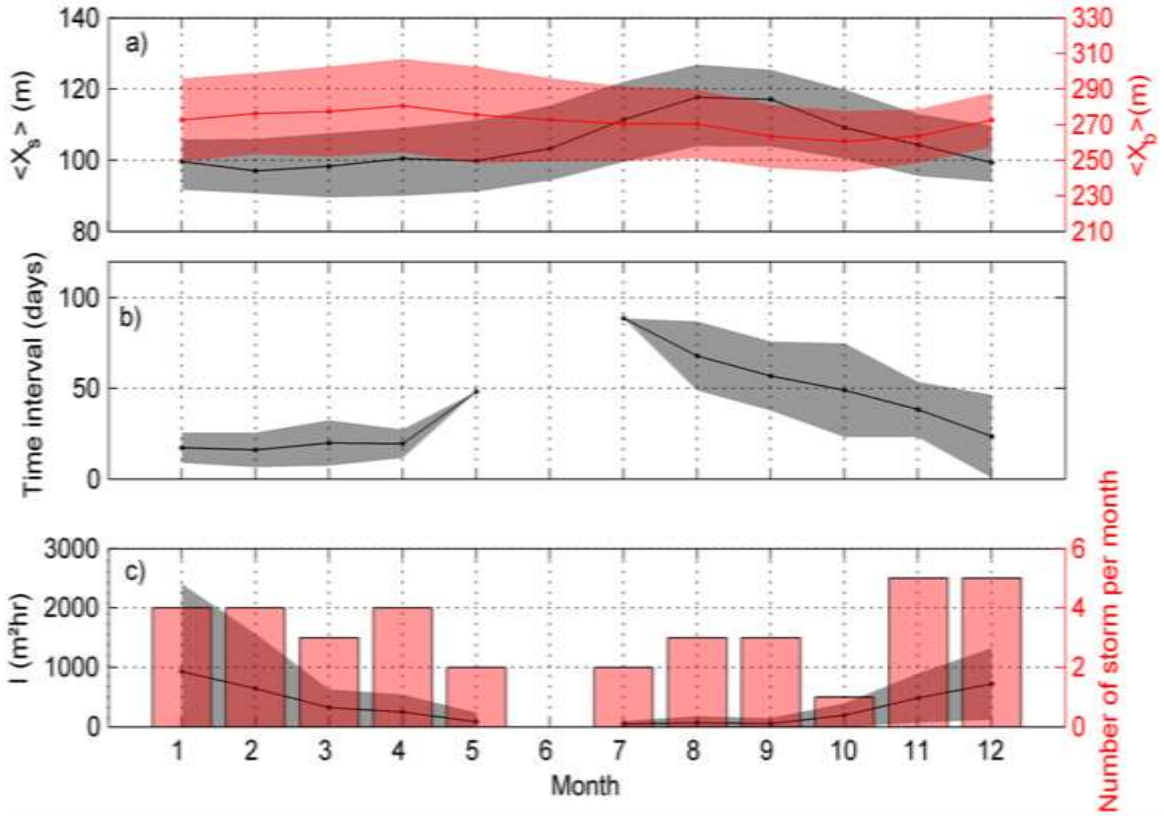

Figure 4.6. Monthly-averaged characteristics of a) shoreline $\langle X_s\rangle$ and sandbar locations $\langle X_b\rangle$ b) recurrence interval between storms and *c)* average storm energy *I* (m^2hr) and number of storms per month. Shaded areas around lines indicate the monthly standard deviation.

4.2.3b. Modulation of storm impact and recovery by previous events, tides and sandbar

Storm impact on shoreline is often quantified separately from the influence of sandbar and tide, despite some recent attempts [e.g. Senechal et al., 2015; Stokes et al., 2015].

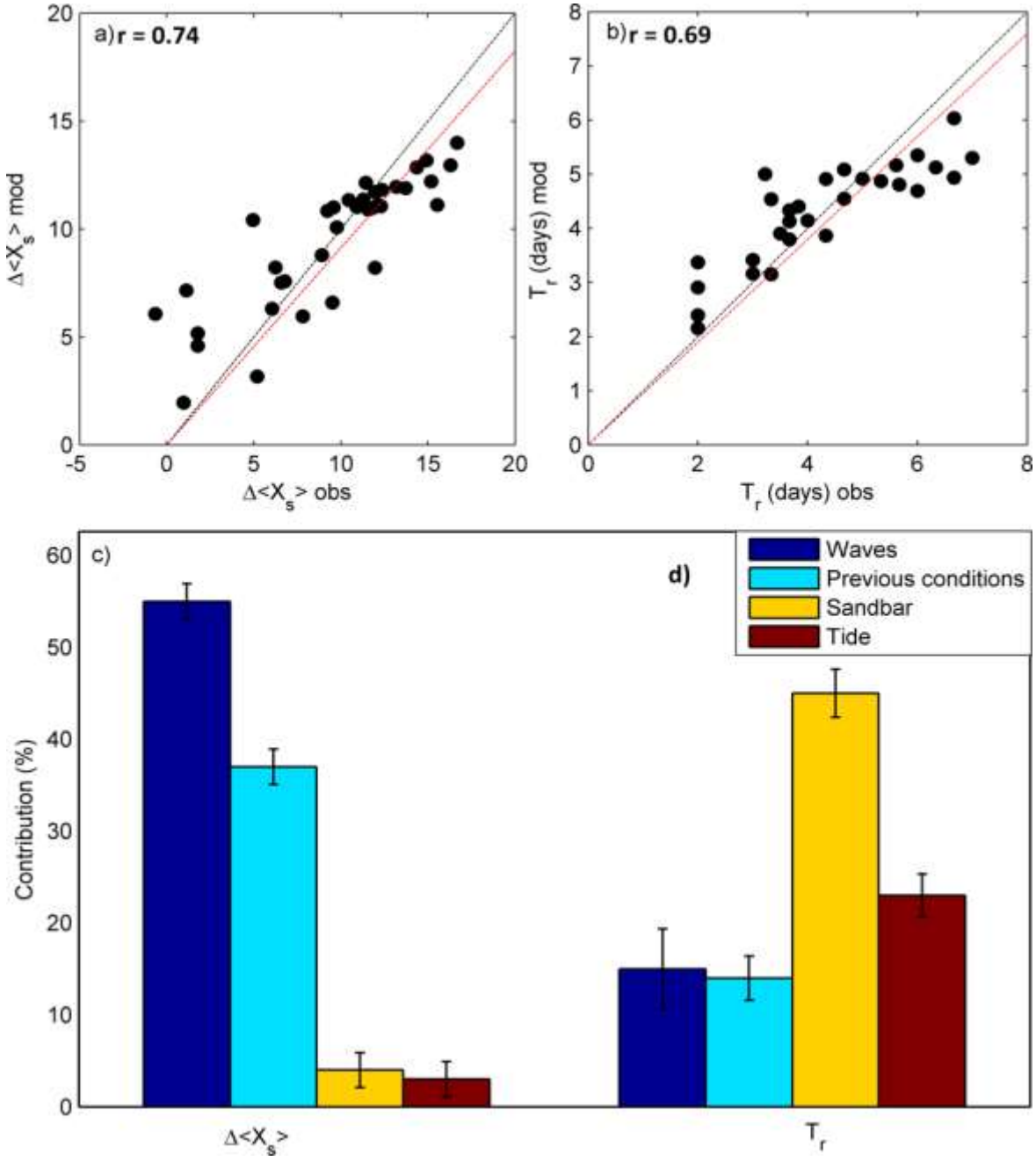

Figure 4.7. Multiple linear regression analyze for $\Delta<X_{s,\,i}>$ (left) and T_r (right). Scatter plots in upper panels a) and b) stand for the comparison between observed variables and reconstructed. Lower panel c) and d) describe the percentage of reconstructed signal explained by each component. Errorbars show the 95% confidence levels. Overall correlation coefficients *r* are indicate on the upper panels.

Here, the relative contribution of the current and previous storms, tide and sandbar, are investigated together through a multiple linear regression (described in Section 4.2.2.c). Overall, Figure 4.7a-b show that a good agreement is found between reconstructed and observed $\Delta\langle X_{s,\,i}\rangle$ and T_r with regression coefficients equal to 0.74 and 0.69 (both significant at 95% level), respectively. Considering the level of noise of the variables, these results suggest a robust physical relationship. Figure 4.7c shows that storm impact depends predominantly (55%) on current storm energy. It is a common outcome that wave conditions dominate the shoreline response during storms [e.g. Yates et al., 2009; Davidson et al., 2013; Castelle et al., 2015], with large intensities (i.e. *D* and/or *Hs*) resulting in large impacts on shoreline, but here we show that previous conditions have a substantial role (37%) while modulation by tide and sandbar plays only a minor role (9% for tide and sandbar altogether).

By contrast, during recovery (Figure 4.7d), these results almost reverse; while current and previous wave conditions have a secondary importance (15% and 13%, respectively), tide and sandbar contributions rise to 45 and 23%, respectively. This shows clearly the difference of behavior of the beach during energetic wave-dominated periods and fair weather complex recovery conditions.

4.2.3c. Storm sequences

Figure 4.8 shows an ensemble-averaged analysis of the evolution of sandbar and shoreline location during the post-storm recovery period. Note that the error of each alongshore digitised shoreline is approximately 9 m estimated for the individual image. To reduce this error data was alongshore averaged and used throughout this study in the analysis.

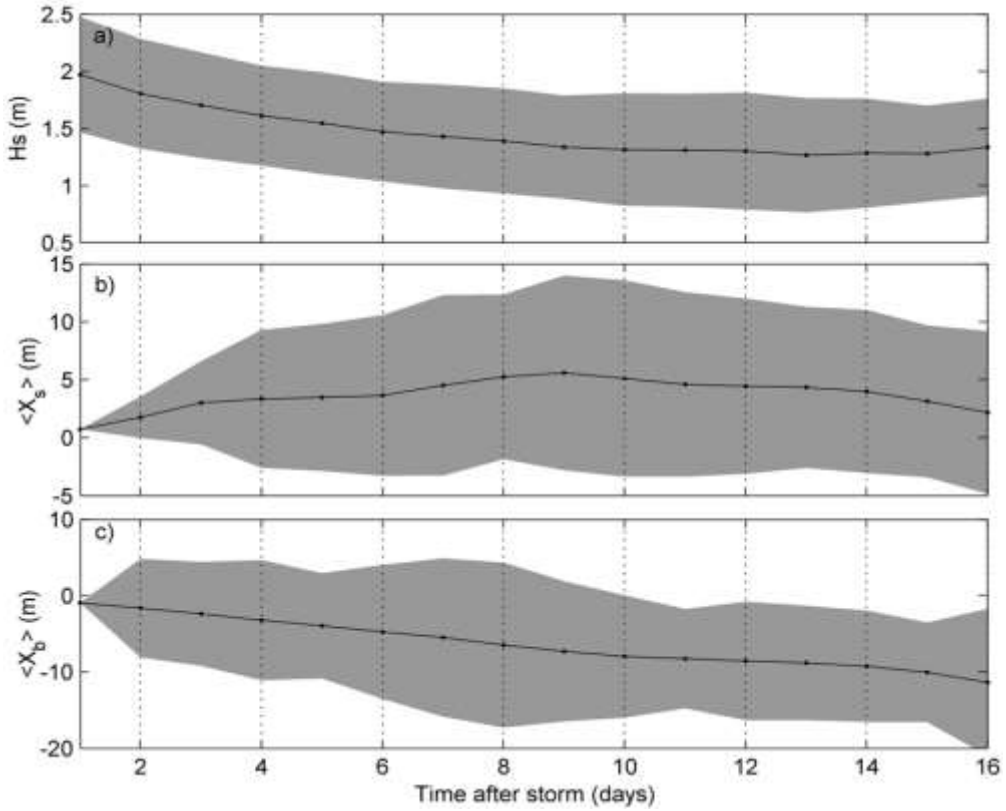

Figure 4.8. Ensemble-averaged evolution during post-storm recovery period for a) *Hs*, b) shoreline location $<X_s>$ and c) sandbar location $<X_b>$ from their location at the end of the storm.

Note that even further averaging was done on the shoreline location over daily post-storm period to understand the post-storm recovery, diminishing this error. Figure 4.8b shows that while waves are decreasing, the shoreline continuously migrates offshore (3.7 m/day) before it reaches stabilization after 9 days on average, which can be used as an estimate for the post-storm recovery duration T_r at Biscarrosse [following Ranasinghe et al., 2012)]. This post-storm recovery duration is different from the time interval between storms; whereas the interval between storms could comprise both accretion and erosion, T_r is purely continuours accretion. Interestingly, while the shoreline is observed to stabilize in 9 days, the sandbar continuously migrates onshore under persisting moderate wave conditions, indicating a longer recovery but also a post-storm onshore migration that is likely to end up with the bar welding to the upper beach under persistent calm conditions, in line with downstate beach transition schemes [Ranasinghe et al., 2004; Pape and Ruessink, 2008; Almar et al., 2010].

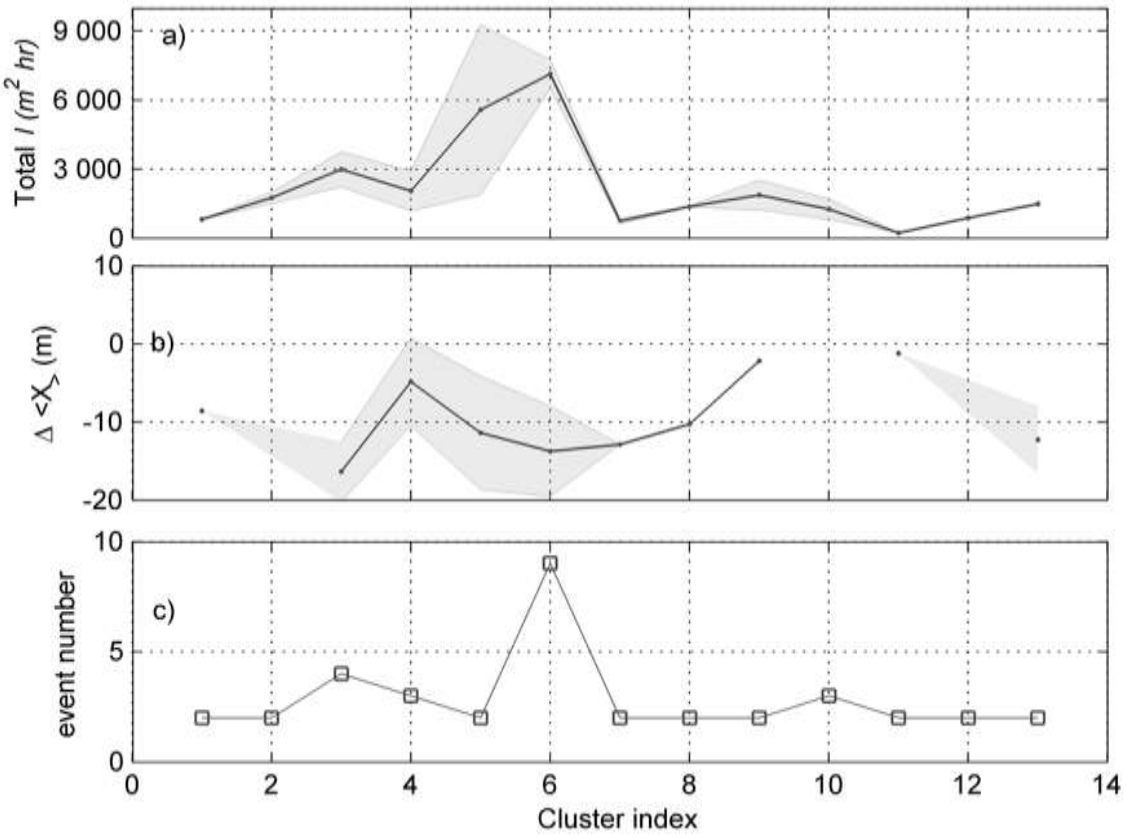

Figure 4.9. Schematic of a) storm clusters total energy, b) average impact and c) the number of storm events in each cluster

Based on this recovery duration, storm clusters are defined as a group of storms in which storms recur within less than 10 days. 13 clusters are identified within the 6-year period with at least one per year. The overall impact of clusters on shoreline location ranges from no substantial change to 16 m of recession (Figure 4.9). The cluster with the largest number (Ns) of storms observed in Nov-Dec 2009 with a total energy of 7133 m^2hr (Figure 4.9) resulted in 14 m erosion. However, a smaller cluster of 2 events with sum energy of 5573 m^2hr resulted in 11 m shoreline retreat, as this cluster includes the longest storm lasting 12 days.

Figure 4.10a shows the impact of ranked storms $\Delta\langle X_{s,i}\rangle$ from one to five in the clusters. Note that the storm numbering here only depends on the occurrence sequence of the individual storms in the cluster, which means the first storm is not necessarily the most energetic. It appears clearly that storm impact within a cluster decreases with storm rank. The influence of previous storms and the importance of recurrence is discussed in the next section.

4.2.3d. Uncertainties on video-derived data

Maybe more than other survey techniques (e.g. DGPS, LIDAR) used in coastal science, video measurements are subject to large uncertainties [Stanley and Holman, 2007]. In particular, the shoreline-detection methods are sensitive to waves and lighting conditions. For instance, the SLIM method by Plant and Holman [1997] is sensitive to variations in water levels which can scale the effects of both setup and run-up, and fog can reduce the color signal strength [Aarninkhof et al., 2003]. However, the results of shoreline measured from video have been comparable to that of topographic surveys [Holman and Haller, 2013] and the cause of differences has been extensively discussed in previous works [e.g. Aarninkhof et al., 2003; Plant et al., 2007; Almar et al., 2012]. In addition to the error related to image rectification estimated here at 1 m, an error of 0.5 m is added for shoreline identification equal to the pixel footprint. Due to the lack of information on the actual surf zone bathymetry, the main horizontal uncertainty, the wave-induced setup was estimated at $0.35\beta\sqrt{HsL}$, with β the upper beach slope and L the offshore wave length, following Stockdon et al. [2006]. Aarninkhof et al. [2003] reported that such simplification introduces minor deviations in the wave-induced setup at the shoreline. The associated error on shoreline location is about 6 m considering the average beach slope (0.03), but ranges between 2 and 12 m. At complex submerged morphology beaches such as Biscarrosse, alongshore variations of wave-induced setup can be found [e.g. Apotsos et al., 2008; Bruneau et al., 2009]. In our study, this bias is substantially reduced because shoreline location is estimated out of stormy periods. Given the restraints listed above we estimate that the overall uncertainty on video-derived shoreline location is about 9 m.

The reason for choosing low tide to pick the sandbar location relates to the fact that waves barely break over the inner bar at high tides for intermediate to fair energetic conditions. Several studies have shown that surveyed sandbar crests and those extracted from timex video images are in good agreement [R^2 ~ 0.8; Lippmann and Holman, 1989; Plant and Holman, 1998]. The accuracy also depends on the rectification error of 1-2 m and due to manual digitization and the pixel footprint of 2 m, tide- and wave-induced artificial shift [van Enckevort and Ruessink, 2001; Pape and Ruessink, 2008; Almar et al., 2010] of 5-10 m. An aliasing rising from inner bar longest irregularities wavelengths, not necessarily covered by video viewfield, can arise and impact on alongshore averaged location [Almar et al., 2010]. On the whole, an accuracy limit of 15 m on the inner bar location can be considered as reasonable in our study, consistent to what was found at Truc Vert beach, 30-km distant [Almar et al., 2010].

4.2.4. Discussion

4.2.4a. Role of waves and tide on storm impact

Results in Section 4.2.3b show that the influence of tide and sandbar during storms on the shoreline is weak, or even not substantial (8% in total, with correlation coefficient <0.1, not significant for tide and 0.2, significant at 95% level for sandbar), in comparison with storm intensity and previous storm. Though it has been observed elsewhere [e.g. Rosen, 1977; Davidson and Turner, 2009] that spring tides might enhance storm impact of the upper beach, it is hard to conclude with our dataset. It is noted that the shoreline proxy used in this study could have an impact on the contribution of the tides during storms. Similarly, the sandbar has only a limited influence on storm impact; the closer the sandbar is to the shoreline and the more the inner sandbar will be coupled to the shoreline and plays its sheltering effect, for example, by limiting incoming wave height [Masselink et al., 2006; Almar et al., 2010; Senechal et al., 2015] by the breaking over the shallow crest. Given that this is a double bar beach, a coupling between the inner and outer sandbars could influence the effect of the innerbar on the shoreline. During post-storm period, Figure 4.7d shows that both tide and sandbar location affect substantially the recovery duration. The relative tidal range (*RTR= TR /Hs*) decreases and wave action becomes strongly controlled by tidal level and sandbar location, or most probably a combination of both. Under such moderate wave conditions, large tidal range will result in reducing the occurrence of surf-zone processes at the upper beach and thus increase recovery duration. It will also change the breaking intensity and occurrence over the bar which can have a direct consequence on the fine threshold between erosion/accretion and no change as observed by Almar et al. [2010]. Stokes et al. [2015] observed that at seasonal scale, the inclusion of tide (through a modulation of incoming wave energy) improves the prediction of shoreline change, and it is expected that it is even truer at short event time scales, in particular the post-storm relaxing time.

4.2.4b. Importance of the frequency of recurrence of storms for shoreline resilience

Our results point out the significance of the so called beach memory effect [e.g. Turki et al., 2012; Reeve et al., 2014] where shoreline response to events depends on the antecedent conditions [e.g. see Splinter et al., 2014a]. Noteworthy, in Section 4.2.3b the correlation coefficient between preceding storm influence and storm impact is negative (-0.35, significant at the 95% level), which means that the larger and closer is the previous storm, the weaker is erosion. If storm recurrence is long enough, individual storm impacts become independent as the beach has time to recover and reach its pre-storm equilibrium. If the interval is sufficiently short such as for storms in sequences in Section 4.2.3c, only the previous storm appears to have a destabilizing effect on the beach while the subsequent conditions decreasingly

impact the beach. This is consistent with Dissanayake et al. [2015] who found that the largest erosion was always observed for the first storm, because the beach has an insufficient time to recover before the successive storms. In sequences, the weaker impact of higher ranked storms is thought to be associated with the fact that the beach is evolving toward an energetic equilibrium state, this at the time-scale of a sequence of a few storms. Some studies [e.g. Lee et al., 1998; Ferreira, 2005] show that the damages due to several moderate storms can be comparable or even greater than a single storm of higher magnitude.

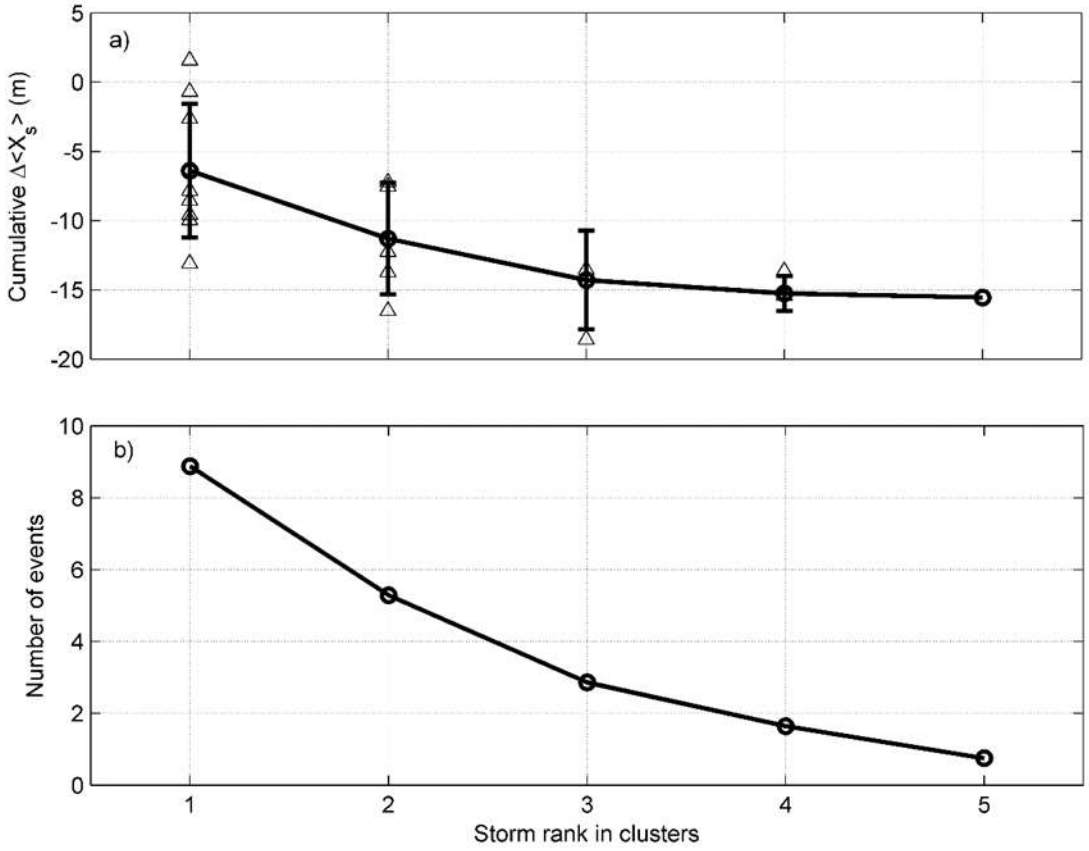

Figure 4.10. Cluster of storms. a) Cumulative storm impact and b) number of storms taken into account as a function of their rank in the cluster. Circles and triangles in a) stand for average and individual values, respectively. In a) offshore direction is traced by more positive values.

Our observations are in line with Coco et al. [2014] and Splinter et al. [2014a] who demonstrated that a sequence of storms does not necessarily result in cumulative erosion, though sequences of frequent event can affect slightly the resilience capacities [Dissanayake et al., 2015]. These results support the idea of a link between event time scale and seasonal evolution, and that the frequency of recurrence of storms and its change over time (e.g. seasonal, interannual, climate change) are of primary importance in assessing beach equilibrium and evolution.

4.2.5. Conclusions

Six years of video-derived shoreline and sandbar locations were collected at the meso- to macrotidal barred beach of Biscarrosse, SW France. Over 60 individual storms (~15 storms per year) were identified using 5% exceedance for *Hs* (*Hs*>3.68 m) as the storm threshold. The average storm recurrence is 27 days with 60% of the storms recurring within 10 days. This large recurrence shows a strong seasonality in storm occurrence, also reflected in the shoreline and sandbar locations.

Storm impact is predominantly influenced by the current storm (55%) but previous events also play a significant role (37%), while modulating parameters such as the sandbar-to-shoreline distance and tides play only a secondary role (8%). Antecedent stormy conditions were also observed to reduce current storm impact, likely explained by the adjustment of the beach to a more energetic state.

With moderate wave energy during post-storm recovery, the influence of the tidal range and the sandbar increases (23 and 45%, respectively), with recovery duration increasing for larger tidal range and larger distance between the sandbar and the shoreline. These results argue in favor of integrating sandbar and tide effects in shoreline equilibrium models as proposed by Stokes et al. [2015], especially the way in which they influence the complex beach recovery process, which could substantially improve model performance at longer time scales.

An ensemble average of storm recovery conditions shows that the beach recovers within 9 days, and therefore a storm cluster was defined as a group of storms in which the time interval between successive storms is less than 10 days. Within the 13 such identified storm clusters, the first storms resulted in the highest erosion. This is in agreement with equilibrium-based approaches where storms are less and less effective in eroding the beach as the beach progressively reaches a new equilibrium with the prevailing wave conditions. These results clearly suggest the existence of interactions between scales and illustrate the key role of the temporal evolution of not only the storm intensity but also their frequency of recurrence when considering in beach resilience.

CHAPTER FIVE

Two- and three-dimension shoreline changes at short and seasonal scales.

".....If the facts don't fit

the theory, change

the facts....."

ALBERT EINSTEIN

Chapter 5: Two and three dimension shoreline changes at short and seasonal scales.

5.1 Introduction

5.2 (Article): Two and three-dimensional shoreline behaviour at a meso-macrotidal barred beach

5.2.1 Introduction

5.2.2 Data and methods

5.2.2.a Study area

5.2.2.b Offshore hydrodynamic forcing

5.2.2.c Video derived shoreline and sandbar

5.2.2.d Data processing

5.2.3 Results

5.2.3.a Shoreline changes at daily and seasonal scales

5.2.3.b Separating 2D and 3D dynamics through EOF

5.2.3.c Testing the effect of tides and sandbar

5.2.4 Discussion

5.2.5 Conclusion

5.3. Equilibrium shoreline dynamics

5.3.1. Data requirements to further improve equilibrium-based shoreline models on meso-macrotidal beaches

5.3.2. Modulation of shoreline response time by tide range and sandbar locations

5.3 Sensitivity of the beach memory to tide P_T and crest depth at sandbar location P_b

5.3.4 Conclusion

5.1 Introduction

Although it is recognised that as a result of climate change, ongoing investment and population growth in the coastal zone, the risks posed by short- to medium-term storm patterns, long-term climatic variability and sea-level rise on shoreline change are hypothesized to increase drastically, shoreline evolution has often been analysed on the seasonal or long-term scales because field data collection at the event scale or higher frequency is difficult. It is anxious that to mitigate the impact of future climate change, one first requires accurate predictions of shoreline evolution from the timescales of hours (storm) to years/decades, including seasonal cycles. Indeed, deciphering the respective contribution of the different forcings (e.g. wave characteristics, tide, offshore morphology) to shoreline change is paramount to the design and implementation of integrated coastal zone management strategies.

In this chapter, we describe 2D and 3D shoreline change at Biscarrosse beach. In addition, we assess statistical and empirical equilibrium models to hindcast shoreline change. In particular, we include the role of tide and sandbar in the equilibrium shoreline model, which was previously driven by wave energy only. Finally, the limitations of the Biscarrosse dataset and recommendations for applying this type of equilibrium model are discussed.

5.2. (ARTICLE): TWO AND THREE-DIMENSIONAL SHORELINE BEHAVIOUR AT A MESO-MACROTIDAL BARRED BEACH (*in preparation*)

DONATUS BAPENTIRE ANGNUURENG*[1], RAFAEL ALMAR[2], NADIA SENECHAL[1], BRUNO CASTELLE[1], KWASI APPEANING ADDO[3], VINCENT MARIEU[1], ROSHANKA RANASINGHE[4, 5, 6]

1. *EPOC (University of Bordeaux/CNRS), Bordeaux, France.*
2. *LEGOS (University of Toulouse/CNRS/IRD/CNES), Toulouse, France.*
3. *MAFS/Remote Sensing Laboratory, University of Ghana, P. O. Box LG 99, Accra, Ghana.*
4. *UNESCO-IHE, Delft, The Netherlands.*
5. *Harbour, Coastal and Offshore engineering, Deltares, Delft, The Netherlands.*
6. *Research School of Earth Sciences, The Australian National University, Canberra, Australia.*

Abstract

The present work investigates cross-shore shoreline migration as well as its alongshore variability (deformation) on timescales of days to years using 6 years of time-averaged images. At the meso-to macro-tidal barred beach of Biscarrosse, the data show that shoreline variability is dominated (52%) by seasonal frequency (summer/winter modulation of waves). Our findings show the importance of short-term events with 28% of shoreline variability. Whereas previously observed seasonal evolution is dominated by wave climate modulation, we found that short-term storm-driven evolution is influenced by tidal range and surf-zone sandbar characteristics. This is even more the case for the alongshore deformation of the shoreline which is dominated by short-term evolution. An EOF analysis reveals that the first mode of shoreline change is associated with cross-shore migration and explains 58% of the shoreline variability. The second mode that was associated to deformation including data noise explains 42% of shoreline variability. Correlation analysis was used to further evaluate the linear relationship between each of 2D/3D shoreline variability and the spatio-temporal eigenfunctions, associated with individual modes.

Keywords: video imagery, shoreline change, event scale, seasonal evolution, sandbar, tide, Biscarrosse beach, Aquitaine Coast, EOF

5.2.1 Introduction

Understanding and further predicting shoreline evolution is of primary interest for coastal scientists and engineers [Ranasinghe and Stive, 2009]. Sandy beach morphodynamics is mostly controlled by geological (e.g. headland, sediment size) and hydrodynamic (e.g. waves, tide) settings [Stive et al., 2002]. Shoreline position can be defined through a wide range of proxies [see Boak and Turner, 2005], with shoreline dynamics being sensitive to the proxy used [Harley et al., 2011; Castelle et al., 2014]. For example, the upper dry beach is more impacted by extreme events than the lower beach which dynamics is generally smoother and influenced by intertidal features such as sandbars. Shoreline changes include variations in both the cross-shore (migration) and alongshore (including deformation) directions. It has been known for a long time that shoreline tends to slowly migrate seaward for low- to moderate-energy waves, including post-storm conditions, while shoreline migrates shoreward rapidly during severe storms [Yates et al., 2009; Splinter et al., 2014a]. These accretive and erosive sequences are generally associated with an increase in surf-zone sandbar three-dimensionality that is sometimes mirrored at the shoreline [Wright and Short, 1984].

From observation and modelling efforts, several studies [e.g. Yates et al., 2009; Hansen and Barnard, 2010; Splinter et al., 2013; Splinter et al., 2014b] showed that intermediate beaches respond

predominantly at seasonal timescales rather than to individual events, with the seasonal modulation of waves being the primary driver. In the meantime, over the past two decades video imagery [e.g. Argus, Holland et al., 1997; Holman and Haller, 2013] has been successful in monitoring continuously (daily) the long-term shoreline [e.g. Plant et al., 2007; Pianca et al., 2015] and sandbar [e.g. Lipmann and Holman, 1989; Van Enckevort, 2003] behaviour. One disadvantage of video system is that the data is remotely sensed, which therefore involves errors that are essentially controlled by the camera station set-up (e.g. resolution, height, implementation rectification method). Nonetheless, video monitoring provide insight into short- to long-term beach change, which can potentially be used to drive mathematical and numerical models to further predict shoreline positions. Video monitoring is therefore used herein to address shoreline change on the timescales from days (storms) to years.

Historically, 2D behaviour has been quantified by statistical methods including spectral and empirical orthogonal function (EOF) methods [see Rihouey and Maron, 2003; Miller and Dean, 2007a, 2007b; Stokes et al., 2013; Lemke et al., 2014]. The EOF method has commonly been used to describe shoreline spatio-temporal variability, especially on embayed or pocket beaches and constrained environments [e.g. close to breakwaters, Fairley et al., 2009; and river mouths, Pradjoko et al., 2010; Blossier et al., 2015] and in the vicinity of groins [Lemke et al., 2014]. Intermediate open sandy beaches often exhibit natural alongshore variability owing to the presence of rip channels. EOF modes have been used regularly to identify cross-shore profile variability but much less frequently to assess longshore variability. The relation that these EOF modes have with cross-shore averaged shoreline locations (2D) and their deviations (3D) has not been studied in detail. Although EOF eigenfunctions are purely mathematical in nature they can unravel physical interpretations [Winant et al., 1975; Winant and Aubrey, 1976]. Stokes et al. [2013] analysed morphodynamic changes through EOF and showed that the second most dominant mode of EOF involves the development of a periodic low-tide rip channel accompanied by a steepening of the beach and an increase in 3D structure. The authors also indicated that 40% of the beach variability was discarded as noise with respect to the EOF analysis.

At barred beaches in meso-macrotidal environments; shoreline response is driven by the combined effect of sandbar and tide modulation of incoming wave energy [Masselink and Short, 1993]. In addition, 3D shoreline behaviour is sometimes linked to that of the offshore sandbar(s). When rip currents flow through the bay sections of crescentic sandbar it could locally erode the beach [Sonu, 1968; Van de Lageweg et al. 2013]. In large tidal-range environments, tide has been shown to influence the development of 3D features in the shoreline [Stokes et al., 2015], which is further addressed here.

The present paper aims at improving our understanding of shoreline change at the double barred meso-macrotidal beach of Biscarrosse. First 2D/3D shoreline data are described through EOF modes and the influence of tide and sandbar on shoreline evolution on short timescales (days) is further addressed.

5.2.2. Data and methods

5.2.2.a Study area

Biscarrosse beach is located in SW France (Figure 5.1), and is exposed to long and energetic waves originating mainly from the W-NW (yearly-averaged significant wave height, *Hs* = 1.4 m and the mean peak wave period T_p= 6.5 s). Waves reaching the Aquitanian coast are generated by W-E tracking subpolar deep low pressure systems over the North Atlantic Ocean. They are therefore, strongly seasonally modulated [Butel et al., 2002], with longer and more energetic waves in winter (November - March) and less energetic waves in summer (April – October). This meso-macro tide is semidiurnal with highest astronomical and mean neap tidal ranges of 5 m and 2.9 m, respectively.

Figure 5.1b represents the general bathymetry of Biscarrosse (Figure 5.1a) which shows the presence of inner sandbar between 200 and 400 m (Figure 5.1b) and the outer sandbar around 700 m from the shoreline, measured during the Biscarrosse field experiment in June, 2007 [Bruneau et al., 2009]. Biscarrosse is therefore an open double-barred beach; the outer bar often exhibits crescentic patterns, while the inner-bar in the intertidal domain commonly exhibits a transverse bar and rip (TBR) morphology with a mean wavelength of about 400 m [Lafon et al., 2002; Castelle et al., 2007b; Almar et al., 2010]. Peron and Senechal [2011] also indicate that both up-state and down-state transitions were dependent on the previous beach state and that no ‘direct jump’ from the reflective state to the dissipative beach state was observed. The average beach slope is about 0.03 while sediment at the site consists of fine to medium quartz sand with median-grain sizes ranging from 0.2 to 0.4 mm [Lafon et al., 2002].

5.2.2.b Offshore hydrodynamic forcing

The wave data are obtained from the Wavewatch III model [Tolman, 1991] over the 2007-2012 period in about 70-m depth every 3 hours at the grid point -1°30’ W, 44°30’ N facing the beach (location of the WW3 grid point is shown in Figure 5.1). Wave height was corrected via a linear regression fit with in situ data from a directional wave buoy (1°26.8’W, 44°39.15’ N, Figure 5.1) moored at 54-m water depth [Castelle et al., 2014].

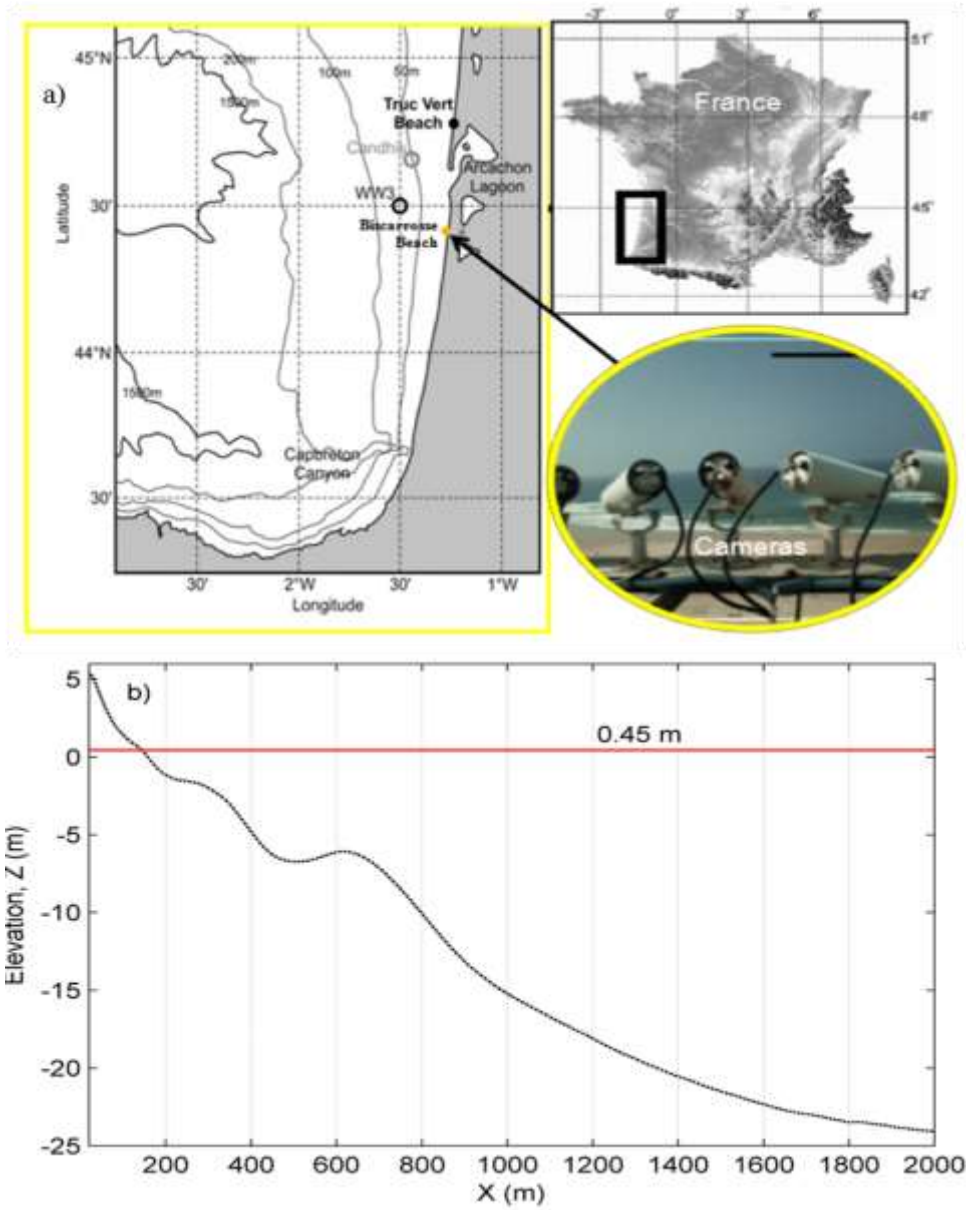

Figure 5.1. (a) Location of Biscarrosse beach (SW France), with WW3 buoy located at -1°30' W, 44°30' N and Candhis buoy (at 1°26.8'W, 44°39.15' N) and video station (yellow dot on the beach). (b) Alongshore-averaged beach profile of Biscarrosse beach measured in June, 2007. The horizontal line is the selected water level for shoreline proxy (2.7 m above the lowest astronomical tide, i.e. 0.45 m above mean sea level).

5.2.2.c Video-derived shoreline and sandbar

A shore-based video system was installed at Biscarrosse beach in April, 2007 by Environments and Paleoenvironments Oceanic and Continental (EPOC) laboratory in collaboration with the New Zealand National Institute of Water and Atmosphere (NIWA). The video station comprises five colour cameras

fixed atop the fore dune at 26 m above mean sea level (MSL), but only four cameras worked over the study period (Figure 5.2 a-d). The system provides three types of images every 15 min: instant, cross-shore time stacks and 10-min time exposure images which are here used for shoreline detection. The images are merged (Figure 5.2e and f) and rectified on a 1 m x 1 m local grid using a direct linear transformation. The local grid origin is the camera location and the coordinate system is oriented in the cross-shore and alongshore directions. In the shoreline area, in front of the video cameras, pixel resolution is about 0.1 m and 0.2 m in the alongshore and cross-shore direction, respectively, and worsens to about 1 m and 3 m at the alongshore ends of the view field. Shoreline extraction from the video is now a common practice in coastal engineering and research studies [e.g. Ranasinghe et al., 2004; Aarninkhof et al., 2003; Smit et al., 2007]. Shoreline position is here defined as the intersection of the beach profile with a given tidal datum. In this study, the chosen datum is 0.45 m ±0.1 m above mean sea level, corresponding to the lowest high tide level to be consistent with Senechal et al. [2015]. This datum was chosen to insure the collection of daily shoreline data.

In addition to the error margins related to image rectification, estimated close to 2 m, an error margin of approximately 0.3 m is added for shoreline digitization. Shoreline delineation is performed visually by a human operator to ensure quality dataset. The wave-induced set-up is an additional factor influencing the short-term (at the scale of a storm) nearshore water level that could result in a significant error. The assessment of this impact was made by the use of a simple setup formula ($0.35\beta\sqrt{HsL}$, β being upper beach slope) following Stockdon et al. [2006] and Senechal et al. (2015). The error in wave-setup induced cross-shore shift of the shoreline ranges from 2 m to 12 m, with an average estimated to 6 m. This uncertainty increases when longshore variations of setup are large owing to large waves breaking across alongshore variable offshore sandbar(s). In addition, the horizontal error due to tide elevation estimation obtained ranges from 0 to 5 m with an average of 0.3 m. In total, accounting for error on manually detected shoreline location from video images is about ±9 m. Secondly we estimated the error that could result from digitising sandbar location. Basically, the crest location of maximum wave dissipation is influenced by the water level, degree of wave breaking, digitisation and rectification. An average error of ±16 m was obtained. Shoreline (X_s, in Figure 5.2f) and sandbar (X_b, Figure 5.2e) manual delineation procedure and shoreline uncertainties are extensively described in Angnuureng et al., in revision with Geomorphology.

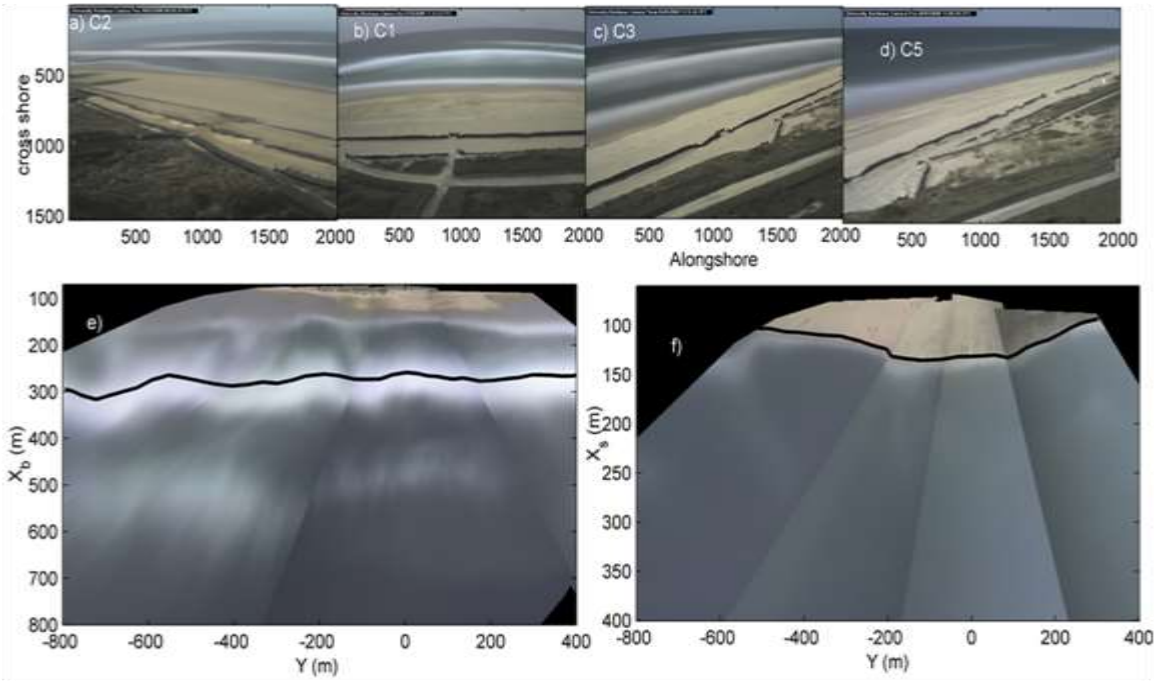

Figure 5.2. Illustration of camera arrangements on field (a-d) and merged 10-min averaged image with manual delineation of e) inner-sandbar crest (15 June, 2007) and f) shoreline (29 Sept. 2008) as black solid lines.

5.2.2.d Data processing

The alongshore-averaged cross-shore shoreline location (2D, $<X_s>$) is estimated by averaging the shoreline positions (X_s) alongshore. The shoreline alongshore non-uniformity (3D, $\sigma(X_s)$) that accounts for the development of irregularities such as cuspate patterns is estimated through the alongshore standard deviation of the shoreline $\sigma(X_s)$. The spatial extent of all shorelines is 600 m in the alongshore and 150 m in the cross-shore direction. The 6-year long time series of shoreline position ensures a relevant assessment of shoreline dynamics. The shoreline time series is separated into three different temporal scales; the event (daily, 1 day- a month), seasonal (monthly, 1- 3 months) and interannual (yearly, 12 months and above) scales. For example, daily data are built by removing the neighbouring 30-day point average to daily values. To determine the dominant scales affecting beach variability, the relative contribution $C_j(X)$ of these components to the total shoreline variability is computed as the ratio, in percentage, of the shoreline variance at each scale to the total variance (S_Y) Eq. (5.1):

$$C_j(X) = 100 * \sqrt{\frac{S_j}{S_Y}} \qquad (j=1, 2, 3) \qquad (5.1)$$

where S_j is the variance (square of the standard deviation) of daily, seasonal or interannual shoreline data and S_Y is the sum of these variances.

In this paper, EOF analysis is implemented to obtain the uniform and non-uniform components of daily shoreline data. The EOF analysis is then applied to decompose the spatio-temporal dataset into spatial eigenfunctions $e_k(x)$, corresponding eigenvalues and associated temporal coefficients $c_k(t)$ following Miller and Dean [2007a] and Lemke et al. [2014] as given by Eq. (5.2).

$$y(x,t)= \sum_{k=1}^{n} a_k e_k(x) c_k(t) \qquad (5.2)$$

where $y(x, t)$ is the shoreline spatio-temporal matrix and $n = 1036$ is the number of shoreline observations; $e_k(x)$ and $c_k(t)$ are the spatial and temporal eigenfunctions, respectively. $a_k = \sqrt{\lambda_k n_x n_t}$ with λ_k the eigenvalue associated with the k^{th} eigenfunction. In the presence of sampling variability an ambiguity exists whenever EOFs are not well separated. The degree of separation required for uniqueness of the EOF modes depends upon the effective number of the degrees of freedom in the input data, N*, which is equivalent to the number of independent data points in the input time series. To determine the number of EOFs to use, North et al. [1982] gave a rule of thumb relating the error in eigenvalues to the intervals between them. Larger intervals mean lower errors between EOFs. Indeed, if the sampling error, $\Delta\lambda = \lambda\left(\frac{2}{N*}\right)^{1/2}$ is equal or greater than the spacing between neighbouring eigenvalues, then the errors of the associated EOFs are comparable. Determining N* is difficult because the number of degrees of freedom in geophysical time series is difficult to estimate reliably, but space averaging can increase the effective number of independent samples and the sampling error [Leith, 1973]. N* was defined as N* = $Y\left(\frac{1-r_{auto}{}^2}{1+r^2{}_{auto}}\right)$, which depends on the spatial length, Y and r_{auto}, the commulative spatial autocorrelation divided by n (1036). Th sampling error limits the number of EOFs that can be considered significant for reconstruction of the input data. Based on these criteria, a normalized eigenvalue spectrum (not shown) of shoreline position revealed that only two modes can be considered (i.e. one significant and rest indistinguishable) to the contribution of the shoreline variability.

In contrast to Stokes et al. [2013] who use EOF to disentangle and quantify the dominant modes of change occurring at monthly to seasonal time scales, therefore discarding the degenerate EOFs as noise, this study assumes that these higher or degenerate EOFs may contribute to short term longshore variability. We already admitted the data noisiness in the shoreline retrieval which should be applied in the results.

5.2.3. Results

Figure 5.3 shows that waves and morphological parameters follow large seasonal variations as previously reported by Castelle et al., [2014] from bimonthly beach surveys. To eliminate any shoreline data outliers, standard z-score approach was used. This approach is used to check also how noisy the digitized data is. From the first to the last year, Figure 5.3 shows that maximum summer shoreline position gradually advances seaward (at an average rate of 1.497 m/yr from August 2007 to August 2012) suggesting an overall slow accretion over the study period. This is in line with observation in Castelle et al. [2014] at Truc Vert beach (80 km distant) who show a 4-yr accretion trend between 2010 and 2012. The contribution of short, seasonal and interannual scales of shoreline evolution to the total 2D (3D) variability were estimated at 28 (32), 52(49) and 20(19), respectively (see method section).

5.2.3.a Shoreline changes at daily and seasonal scales

Before daily shoreline change estimation, specious (outliers) data identified through z-score were eliminated. At the daily scale, the average absolute 2D shoreline migration rate is 2.03 m/day (Table 5.1), with a maximum erosion of 11.86 m/day (24-September-2010) while maximum daily accretion observed is 15.8 m/day (23-June-2007). In the former case, all wave height conditions for this day (averaged *Hs* = 2.12 m) were above the study data average (~1.7 m), though there were incidence (shoreline orientation of about 8.5° N) of short period waves (average T_p = 7.4 s; ø = 288°). In the latter case of accretion, wave conditions were moderate but wave periods remained low (*Hs* = 2.05 m; T_p = 8.2 s) with a much wider wave incidence angle (ø= 291.6°).

The extent of 3D features also varies at an average rate of 1 m/day, and the maximum value is observed in summer with about 5 m/day (on 1st Sept. 2012). This maximum change in daily 3D shoreline is associated to the wave conditions. 3D changes maybe linked to 'potentially erosive' wave conditions [Senechal et al., 2015] because one month prior to 1/09/2012 data shows *Hs* were comparable, however, two weeks prior to 1/09/2012, wave height average from 16-30 August, 2012 was 1.47 m which then decreased rapidly to 1.13 m on 1/09/2012 with all wave conditions becoming weaker.

The results in Table 5.1 suggest that daily shoreline variations may be weak in winter periods when the beach is close to an alongshore-uniform dissipative state. In general, the link between daily *Hs* and daily shoreline position is found to be weak, (r ~ 0.35 at zero lag, significant at the 95% level) for both 2D and 3D components. Wave direction shows the lowest link (r~0) with 3D development just as T_p seems to have no influence (r ~ 0.1, significant at the 95% level) with 2D. These results underline that daily shoreline evolution is complex and influenced by other drivers such as tide and the presence of the

sandbar, as previously observed in Angnuureng et al., in revision with Geomorphology. It is interesting to notice that 2D and 3D changes are weakly linked (r~0.20) at daily scale, which suggests they can be treated separately. Nonetheless, it is important to acknowledge that the shoreline dataset is noisy and, accordingly, that shoreline change on short timescales is to some extent distorted.

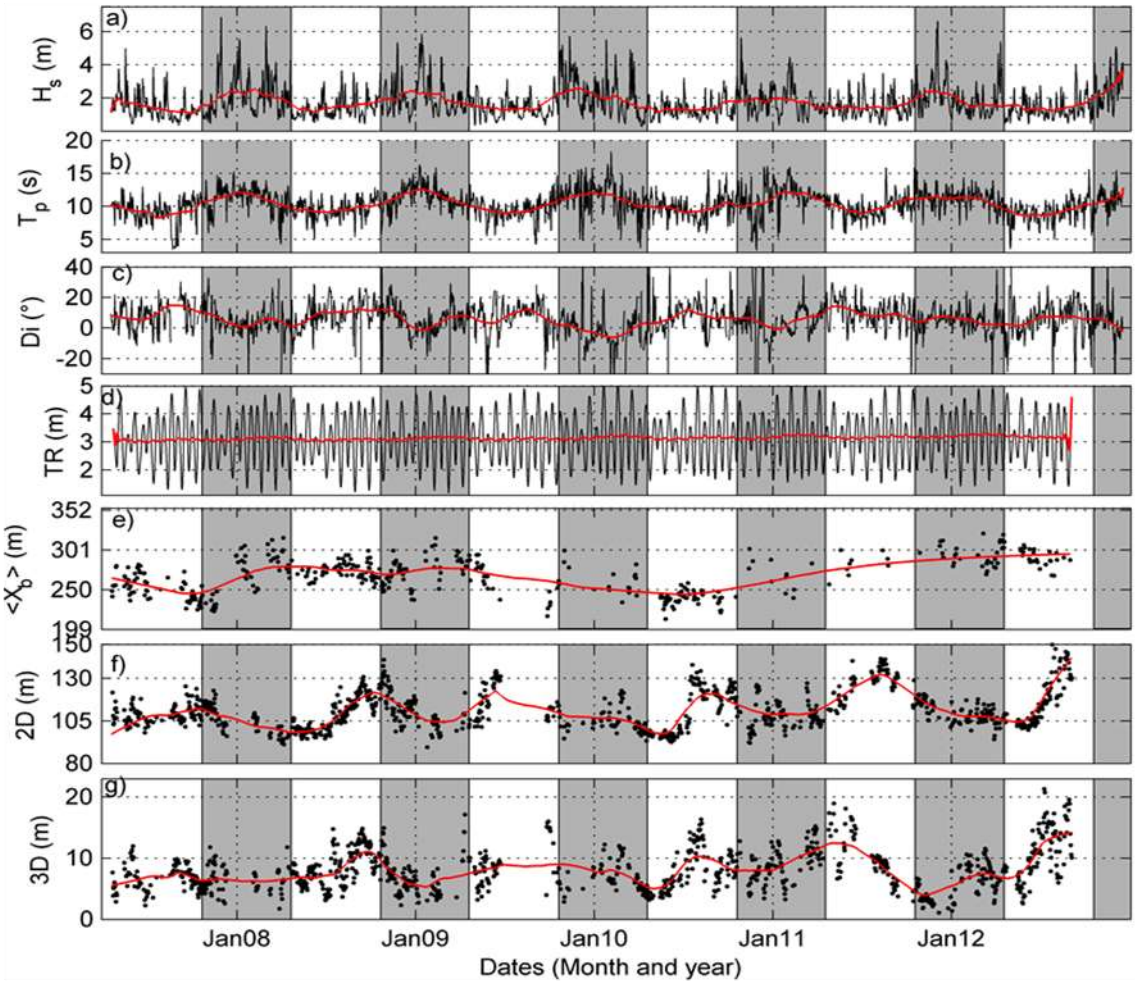

Figure 5.3. Daily wave and video time series from April, 2007 to Dec., 2012; a) *Hs*, b) T_p, c) *Dir* normal to the beach, d) 3D or σ<*X*> (in black dots) e) Tide range *TR*, f) <*X*> or 2D in dots. Seasonal signals are shown by solid thick red lines on all the subplots.

Shoreline average seasonal 2D variations (Figure 5.3, Table 5.1) can show large amplitude with a wide beach in summer and fall months (+10 m from average location of 105.5 m) while the narrowest beach is observed in spring and winter (-7 m from the average, *see* Table 5.1). This is associated with a typical large accretion during the spring months (+7 m/month) and a moderate erosion (-4 m/month) during the fall months. On the other hand, the 3D values are the largest (9 m) in spring and summer months in

consistence with Senechal et al. (2015). At the seasonal scale, the influence of *Hs* on 2D and 3D changes is moderate (r~ 0.3), Table 5.2.

Table 5.1. Alongshore uniform, 2D *(<X>)* and alongshore non-uniform, 3D (*σ(X))* shoreline statistics at the daily and monthly scales relative to the mean shoreline location (105.5 m) averaged for DJF: winter, MAM: spring, JJA: summer, and SON: fall.

Daily scale	*2D* (m)	Absolute *Δ (2D)* (m/day)	*3D* (m)	Absolute *Δ(3D)* (m/day)
Winter (Dec.- Feb)	-7	1.8	6.5	0.0
Spring (Mar. – May)	-10	2.3	8.6	1.0
Summer (Jun. – Aug.)	+6	2.6	9.6	1.5
Fall (Sep. – Nov.)	+11	2.8	8.3	1.0
Monthly scale	*2D* (m)	Absolute *Δ(2D)* (m/month)	*3D* (m)	Absolute *Δ(3D)* (m/month)
Winter (Dec. - Feb.)	-11	6.0	6.0	3.0
Spring (Mar. – May)	-7	13.0	8.6	5.0
Summer (Jun. – Aug.)	+4	11.0	9.6	4.6
Fall (Sep. – Nov.)	+10	10.0	8.0	3.0

Table 5.2. Correlation *r* at zero lags between wave parameters and 2D/3D data averaged over daily and monthly values, for daily and seasonal periods as indicated.

	Daily correlations		**Seasonal correlations**	
	2D	3D	2D	3D
Hs (m)	-0.28	-0.35	-0.27	-0.32
Tp (s)	-0.07	-0.10	-0.35	-0.25
Dir (/°)	-0.13	-0.08	0.06	0.21

5.2.3.b Separating 2D and 3D dynamics through EOF

On most of the images, the shoreline was available between -300 m and 300 m in the alongshore direction. Thus, to limit data discrepancies the EOF was implemented on this section only. The first 4 EOF components explain over 91% of the total shoreline variability distributed as 58.3, 15.6, 11.3 and 6

% respectively. Based on the method described in Section 5.2.2, the degrees of freedom N^* is 9 while the spacing between neighbouring eigenvalues $\Delta\lambda$ is found to be larger than the difference between eigenvalues of the second and higher EOFs. This means only one distinct eigenvalue (i.e. the first) is significant while the others are indistinguishable and must be treated as one in contrast to Stoke et al. [2013] where higher modes were discarded. Thus only the first and combined EOF modes are analysed below. The coefficients of cross-correlation between the first and second temporal EOF functions and the 2D and 3D time series that were estimated are given in Table 5.3.

Table 5.3. Daily correlation between reconstructed shorelines of the first and second EOF functions with $<X_s>$ and $\sigma(X_s)$. ΔX_y and δX_y are the cross-shore averaged and deviations at each alonghshore position, while $<X_s>$ and $\sigma(X_s)$ are the alongshore averaged cross shore data. $e_k(x)$ and $c_k(t)$ are the spatial and the temporal EOF functions, respectively.

Spatial	ΔX_y	δX_y
$e_1(x)$	0.69	0.80
$e_2(x)$	-0.16	-0.32
Temporal	$\boldsymbol{<X_s>}$	$\sigma(X_s)$
$c_1(t)$	0.85	0.44
$c_2(t)$	-0.32	-0.30

The strongest correlation (r~0.85) is obtained between the first temporal mode $c_1(t)$ and 2D data which is not the case for $c_2(t)$ (r~ -0.3) and 2D, that is preferentially linked to $\sigma(X_s)$ data. Intuitively, due to the prevailing link between $c_2(t)$ and temporal $\sigma(X_s)$ contribution of temporal mode 2, poor correlation is observed between $c_2(t)$ and the alongshore-averaged shoreline (2D). In table 5.3, the second EOF function shows opposite signs in the spatial eigenfunctions, indicating a deformation of the shoreline: extrema identify areas of maximum variability, while nodal points indicate stability [see also Miller and Dean, 2007a]. On Figure 5.4, the temporal and spatial modes as well as the 2D/3D shorelines are compared. Generally, $e_2(x)$ shows fluctuations at length L~300 m, nodes and antinodes, between negative and positive values (Figure 5.4d) standing for beach stability and deformations; the $e_2(x)$ spatial mode is around zero which is not the case in $e_1(x)$, Figure 5.4b confirms the close link between the second EOF mode and the dynamics of the $\sigma(X_s)$ data. In Figure 5.4b of $e_1(x)$, there is no node or antinode, which indicates an overall migration of the shoreline at all locations, similarly with ΔX_y spatial pattern, representing an overall alongshore-uniform migration (i.e. same sign at all longhsore locations).

In Figure 5.4a, it can be seen that the $c_1(t)$ and $<X_s>$ timeseries have a predominant seasonal evolution. In contrast, the second temporal function, $c_2(t)$ and $\sigma(X_s)$ timeseries (Figure 5.4c) are more affected by events, which can be attributed to non-uniformities development/destruction and longshore migration of these features. Even though Figure 5.4c shows no scale of $c_2(t)$ variability, variation in its associated $\sigma(X_s)$ is averagely longer than the first temporal function. The temporal variability of mode one is dominated by the presence of a 4 to 6 month oscillation, while in mode two both long (> a year) and short (<3 months) signals are evident.

At this study area, the inner bar in the intertidal domain commonly exhibits a TBR morphology with a mean alongshore averaged wavelength of about 300-400 m [Lafon et al., 2002], with up- and down-state sequences assicated with changes of the alongshore deformation of the shoreline. Changes at -50 < Y < 100 in Figure 5.4b suggest the influence of rip channels, however, this goes against the fact that rip channels migrate downdrift with no prefered spatial occurrence over the years.

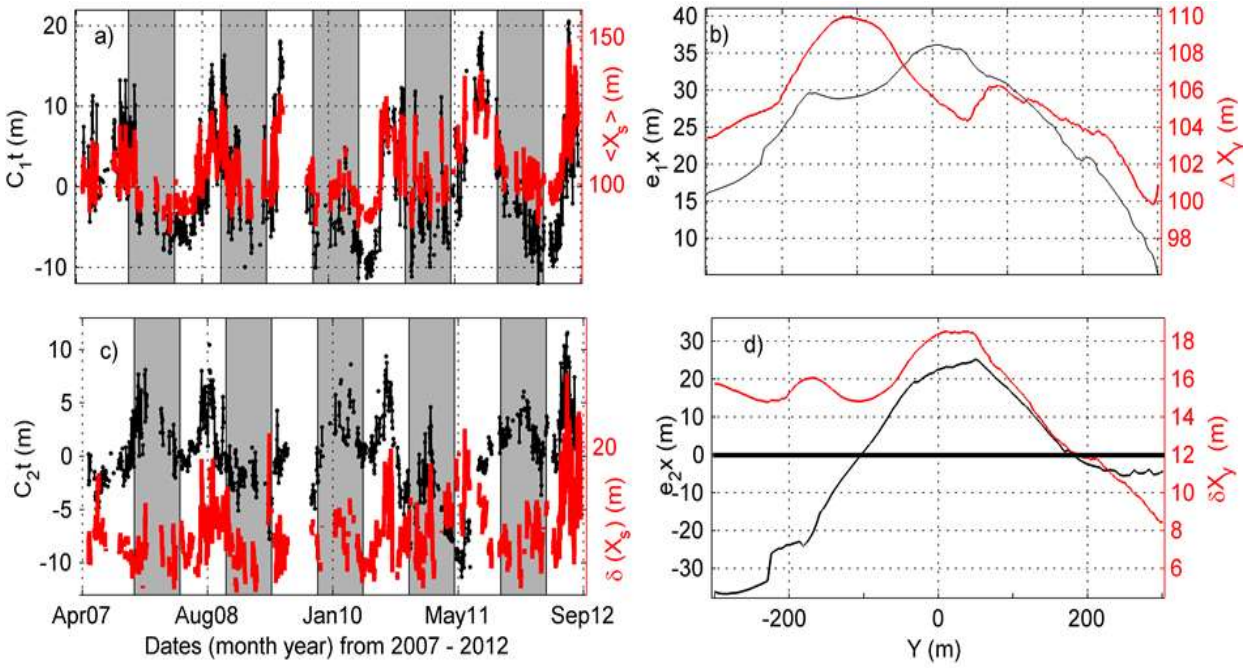

Figure 5.4. EOFs (a) First temporal eigenfunction ($c_1(t)$, *black)* of shoreline variability compared to $<X_s>$ (red line); (b) first spatial functions *($e_1(x)$*, thin black line) compared to ΔX_y (thick red); (c) second temporal eigenfunction ($c_2(t)$, black) compared to $\sigma\ (X_s)$ (red) and, (d) second spatial function ($e_2(x)$, thin black line) compared to cross shore standard deviations (δX_y, thick red). The thick line represents the zero crossing line that will signal deformation or migration. Though only the shoreline location is used, the complex shoreline evolution can be reduced to EOF modes 1 and 2 to describe the $<X_s>$ and $\sigma\ (X_s)$ data.

5.2.3.c Testing the effect of tides and sandbar

Initially, Angnuureng et al. [in revision with Geomorphology], showed that during storms tidal range and sandbar characteristics play a negligible role on shoreline response, but with a more important role on beach recovery. Figure 5.5 represents the relation between daily tide range, daily waves (*Hs*) and shoreline changes for winter, spring, summer, and fall seasons. The colour bar represents the daily tide range. Results suggest that large tide range (red) is associated with more pronounced shoreline change (erosion or accretion) than small tide range.

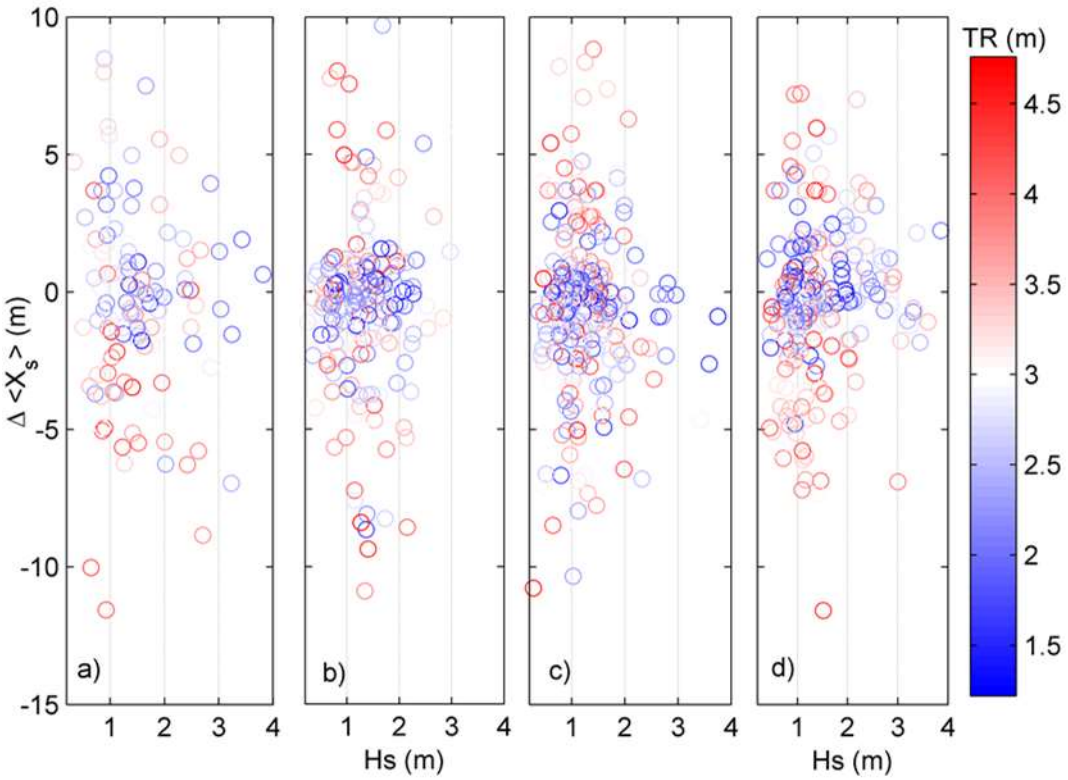

Figure 5.5. Daily changes in shoreline ($\Delta<X_s>$) in relation to wave height and tide (color bar) range during each of the four seasons; a) winter (DJF), b) spring (MAM), c) summer (JJA) and fall (SON).

Coco et al. [2014] stated that the extreme *Hs* coinciding with spring tide (low tide range, *TR*) leads to the largest measured erosive events, which is what we observed here. In contrast, Davidson and Turner [2009] showed that a rise in *TR* can cause the sandbar to decrease in height thus reducing the impact on shoreline erosion. In spring and summer, the data shows that correlations between seasonal daily *TR* and shoreline changes in these seasons were insignificant ($r^2 \sim 0$, $p > 5\%$). However, winter and fall recorded significant correlation between *TR*, *Hs* and shoreline changes ($r^2 \sim 0.2$; $p = 0$). This study supports the idea that tides can modulate the wave power [Davidson et al., 2008] to cause shoreline changes, but also

shows tide may not be efficient all year round. We tested the effect of the wave period *Tp* through the linear cross correlation but it showed no impact.

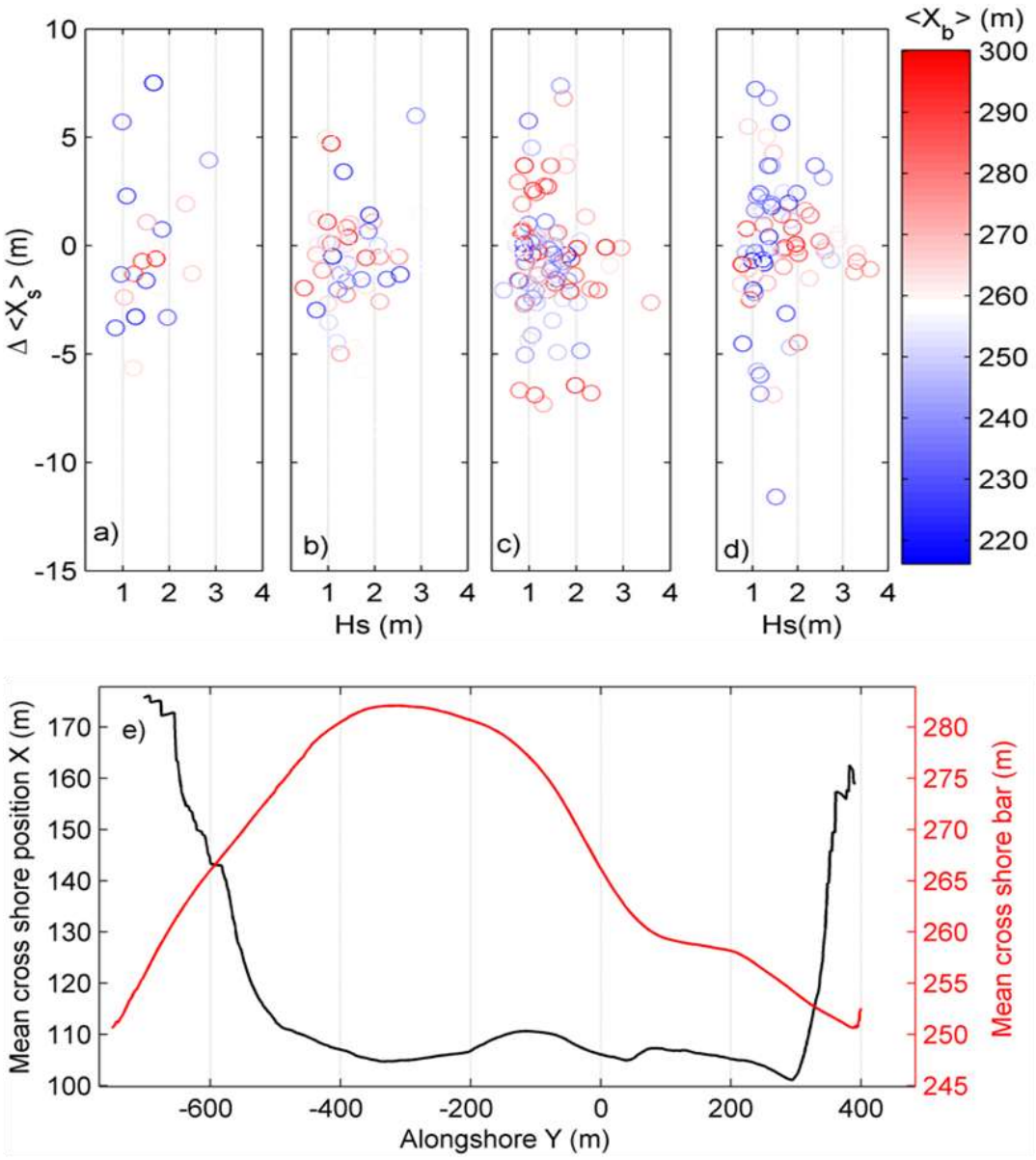

Figure 5.6. Daily changes in shoreline ($\Delta<X_s>$) in relation to wave height and sandbar (color bar: lower values on color bar are much closer to the shoreline) location during each of the four seasons; a) winter (DJF), b) spring (MAM), c) summer (JJA) and fall (SON). e) Schematic of full video covered alongshore sandbar and shoreline: the cross shore average of shoreline locations and sandbar locations.

The same analysis was performed for sandbar location (Figure 5.6). It can be seen on Figure 5.6a that much of shoreline varioability is observed when the sandbar is close to the shoreline (blue colour) while

when the sand bar is far from the shoreline (red color), shoreline change is weaker. Figure 5.6 also shows that summer and fall seasons show the largest variations. This is probably due to the fact that sandbars are closer to the shore during summer and move offshore during winter season. However, we do not have data on the sandbar amplitude and width. By linear correlation of the cross shore average shoreline and sandbar location, to understand further coupling links, data show that on an alongshore distance of 1200 m (full length of study area, Figure 5.6e), sandbar ($<X_b>$) is negatively correlated (r= -0.4, significant at 95% CI, p = 0) with the shoreline, suggesting that erosive shoreline features face more offshore (deeper) sections of the inner bar, in line with Sonu [1973].

5.2.4. Discussion

We showed that Biscarrosse beach is a dynamic beach with varying morphological behaviours evident at a variety of time and space scales. The data shows that seasonal scale is dominant in line with what has been previously reported by Castelle et al. [2014] who showed that the SW France beaches respond predominantly at seasonal timescales to wave modulation. Shoreline change that occurs over a few tens of years or less and that may be in the opposite direction of the long-term trend is difficult to understand and predict. Here, shoreline change due to daily events was observed, with short-term events that account for about 28% of shoreline variability. This percentage also encompasses a large amount of data noisiness because of large errors (~15 m) in the shoreline detection method. Data shows short-term shoreline changes can be quite variable alongshore. For example, the beach is advancing between -100 <Y< 180 m (Figure 5.5 d) while the other portions of the coast are experiencing retreat. It is important, however, for coastal residents to understand that even though a particular beach may have been advancing or stablized over a time, if it has been retreating for the previous decades, then retreat will eventually resume, except if something fundamental, such as an 'unexpected' increase or decrease in the sand supply.

More importantly, we provide new insight into the influence of tide and sandbar distance to the shoreline on shoreline response. Results of the EOF produces well the pattern of alongshore uniform and non-uniform shoreline evolution including 3D deformations presumably enforced by the presence of rip channels. Bruneau et al. [2014] found that rip currents are typically 20 to 45% stronger during falling tide (i.e. increasing TR) than during flood (i.e. decreasing TR). This is inline with the observations in this study provided in Figure 5.5. Bruneau et al. [2014] also found that sediment transport that takes place in rip channels at ebb would thus be up almost one order of magnitude larger compared to flood. This behaviour has the potential to impact the bar/rip system morphodynamics and subsequently the shoreline. As indicated in section 5.2.3.b, though rib channels may migrate (Figure 5.4.b) and affect the shoreline at different longshore locations that could not be addressed properly in this study. Migration of rip channels

and their time-scales are not therefore understood, yet our results have strong implications for tide variation. Obviously at some locations alongshore currents and associated littoral sand transport cause rip currents to migrate, but at the same time they act to destroy the rip channels by filling them [Thornton et al,. 2007].

The primary modes of variability found here have been clearly associated to an alongshore uniform mode and a mode with alongshore varying structure. EOF 1 (Figure 5.4a, top left panel) has been interpreted as seasonal, and its seasonality mimics on-offshore 2D shoreline. To ascertain this we did daily cross correlation (Figure 5.8) of the EOF 1 with the wave conditions (r =0.2; p<5%) which yields a lag of 120 days. This suggests the maximum length of a season in the EOF 1 time series comparable to 2D shoreline time scale of evolution. On the other hand, Figure 5.8 shows the correlation between EOF 2 and the *Hs* (dotted line), with no regular scale of variability which can be explained by the longshore variability. Estimated lag is in 4 years. It describes short-lived morphological events that act to temporarily change the intertidal beach (e.g. bar welding, berm building, scarping etc).

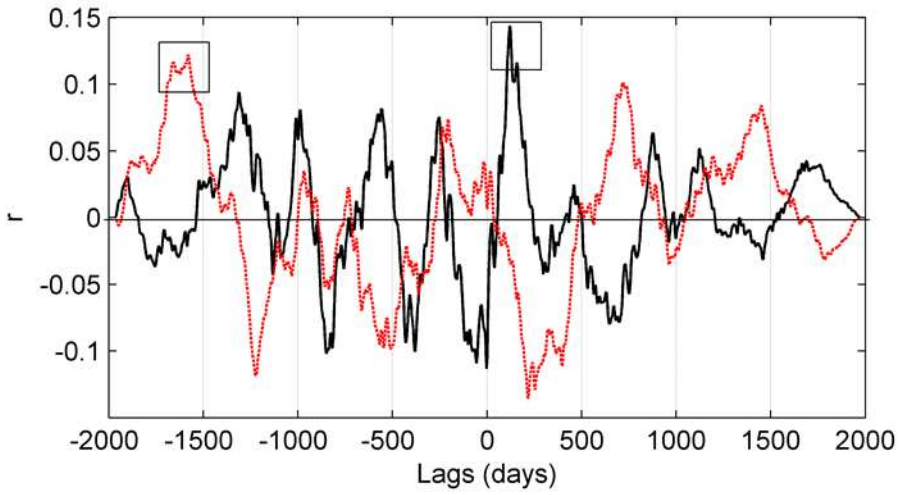

Figure 5.8. Daily running cross correlation between EOF mode 1 and Hs (solid line) and EOF mode 2 and Hs (dash line). Square boxes indicate the maximum correlation and the lag for each cross correlation.

5.2.5. Conclusions

The alongshore-averaged shoreline cross-shore migration (2D) and deformation (3D) at the meso-macrotidal barred Biscarrosse is investigated from a 6-year video monitoring period. As observed in this area [*e.g.* Castelle et al., 2014; Senechal et al., 2015], shoreline variability at seasonal scale is dominant with seasonal scale, short term scale (possibly storm/post-storm recovery) and interannual tendency

contributing to 52, 28, and 20% of the total variability, respectively, even though these percentage encompass data noisiness (mostly in the short-term).

One of the key difficulties with empirical orthogonal function (EOF) lies in interpreting the results in the broader physical context from which they were derived, especially when most of EOF application is on cross-shore variability. The objective here was to relate the individual modes to the local conditions through correlating the derived modes with 2D and 3D alongshore variability. Despite the conditions of data extraction, the EOF method applied on the shoreline is able to separate 2D and 3D behaviours. The first temporal eigenfunction which accounts for 58% of shoreline variability reflects the alongshore-uniform cross-shore variability (2D migration). The second and higher eigenfunctions which contribute around 42% to the shoreline variability depict the longshore non-uniformities (3D deformation). While the 2D variability is dominated by seasonal changes, the 3D shows a larger impact of short term events (non-uniformities developments or alongshore migration).

Our results also show that tidal range and sandbar distance to the shore affects shoreline response to wave regimes with closer sandbar and larger tidal range both enhancing shoreline response (accretion or erosion). These results support previous findings by Angnuureng et al. [in revision with Geomorphology] and Stokes et al. [2015] on the importance of sandbar and tidal modulation of wave impact on beach morphology.

5.3. Equilibrium shoreline dynamics

Predicting the cumulative impact of changing wave conditions on the detailed morphological evolution of wave-dominated coasts requires appropriate wave, current and sediment transport models. For instance, predicting decadal-scale trends in shoreline position along coastlines dominated by drift is most often done using n- line models, such as UNIBEST and GENESIS [e.g. Pelnard-Considere, 1956; Hanson and Kraus, 1989; Ruggiero et al., 2010]. These models, which assume a constant cross-shore profile, do not account for the cross-shore movement therefore rarely capture the short- or seasonal shoreline variability associated with these cross-shroe processes. In contrast, empirical shoreline models addressing cross-shore sand movements can simulate both the short-term impacts of storms as well as the longer term trends related to changing wave conditions [e.g. Frazer et al., 2009; Yates et al., 2009; Anderson et al., 2010; Splinter et al., 2014].

Behavioural models [e.g. Yates et al., 2009; Davidson et al., 2013] provide an attractive alternative to process-based models to address shoreline change. These models are capable of explaining substantial amounts of variance and accurately forecasting beach changes over storm, seasonal and interanual

timescales [e.g. Plant et al., 1999; Yates et al., 2009; Splinter et al., 2011], which is presently unachievable using process-based models. These empirical models have been used to predict two-dimensional, 2D [Yates et al., 2009; Davidson et al., 2013; Castelle et al., 2014; Splinter et al., 2014] behaviour and more recently three- dimensional, 3D shoreline changes [Stokes et al., 2015] under varying waves. Davidson et al. [2013] observed that inclusion of temporally varying equilibrium condition can constrain excessive shoreline variation. They further hypothesised that an observed difference in beach memory (ϕ) related to the differing modal states of beaches. The variation in beach memory dictates the efficiency of sediment exchange between the shoreface and the offshore sandbar, nearshore circulation patterns and the offshore distance of sandbars. In meso-macro tidal environments [large Relative Tide Range index, Masselink and Short, 1993]; the shoreline response to offshore wave variations is important and made complex by the combined effect of sandbar and tide modulation of onshore wave energy [Wright et al., 1987; Banno and Kuriyama, 2012]. In large tidal-range environments, the key role played by the tide in the development of 3D features has been highlighted [Stokes *et al.,* 2015]. Stokes *et al.* [2015] applied the concept of disequilibrium stress to 3D changes at the outer sandbar and the lower beach accounting for the tidal modulation of the response time where the model performance was observed to improve for the outer sandbar due to the inclusion of tide range. In their study, tidal range modulates incoming wave energy. Overall, the effect of sandbar and tide range on the prediction of 3D and 2D shoreline changes still has to be tested in equilibrium shoreline model.

5.3.1. Data requirements to further improve equilibrium-based shoreline models on meso-macrotidal beaches

Both cross-shore and alongshore sediment transport processes drive changes in shoreline position, however, alongshore processes generally act over much longer time frames, and along many exposed coastlines do not dominate the annual shoreline variability [e.g. Davidson and Turner, 2009; Hansen and Barnard, 2010; Yates et al., 2009]. Empirical models therefore assume that shoreline variability due to gradients in alongshore transport is small compared to the variability associated with cross-shore processes and cannot be applied along coastline with prominent longshore processes. These models are sensitive to alongshore variability and fluctuations in data [Miller and Dean, 2004; Yates et al., 2009], data sampling frequency [Splinter et al., 2013], and shoreline proxy [Castelle et al., 2014]. Thus, the empirical nature of these models requires high-quality observational data sets to calibrate model free parameters. Reviewing these models, Splinter et al. [2013] showed that seasonally-dominated sites require longer data sets but less sensitive to sampling interval, while the storm-dominated sites converge on shorter, more frequently sampled data sets. This suggests that monitoring programs of at least two years, with shorelines sampled within the range of 30 days are sufficient to determine initial estimates of

calibration coefficients and hindcast short-term shoreline variability. Model inputs are mainly the characteristics of the time varying offshore waves (Hs, and Tp) and sediment size, with some models even only requiring Hs [Yates et al., 2009].

5.3.2. Modulation of shoreline response time by tide range and sandbar locations

Here the equilibrium model is tested with high-frequency video observations. Additionally, we test the inclusion of tide and sandbar location. For example, Stokes et al. [2015] used the tidal range to address outer sandbar dynamics. Other studies use the relative tide range [Masselink and Short,1993], and hydrodynamic forcing index [Almar et al., 2010]. Below we address the influence of wave energy flux *P*, relative tide range *RTR* and sandbar locations$<X_b>$ on the 2D and 3D shoreline responses. The key priority of this section is to implement and demonstrate the effect of tides and sandbar which is done through the maximum correlations between model predictions and measured data (2D and 3D).

Here we use ShoreFore model [Splinter et al., 2014] based on earlier work [e.g. Davidson et al., 2013]. Davidson and Turner [2009] presented a two-dimensional profile model with considerable skill to hindcast weekly shoreline change. This model was later simplified by Davidson et al. [2010] into a one-dimensional shoreline model that was further modified by Davidson et al. [2013]. Here the concept is extended to both shoreline cross-shore location $<X_s>$ and longshore variability (3D), with higher interest on how tide and sandbar location modulate beach response. Only the key model equations are given below, including those containing the free model parameters, but for more detail see Davidson et al. [2013] and Stokes et al. [2015].

The rate of shoreline change that defines the initial model of Davidson et al. [2013] used here is given by

$$\frac{dX}{dt} = b + c(F^{+} + kF^{-}) \qquad (5.3)$$

k in *Eq.* 5.*3* describes the relative efficiency of positive and negative disequilibria in altering the beach changes, while b and c are the free parameters, with the forcing terms F (Eq. 5.4 and Eq. 5.5) defined as the product of the incident wave power raised to the 0.5 exponent, $P^{0.5}$ and the normalised disequilibrium ($\Delta\Omega$):

$$F^{+} = P^{0.5}\frac{\Delta\Omega}{\sigma_{\Delta\Omega}} \quad when\ \Omega < \Omega_{eq} \qquad (5.4)$$

$$F^{-} = P^{0.5}\frac{\Delta\Omega}{\sigma_{\Delta\Omega}} \quad when\ \Omega > \Omega_{eq} \qquad (5.5)$$

$\Delta\Omega = \Omega_{eq} - \Omega$, and $\Delta\Omega$ is normalised by its standard deviation denoted by $\sigma_{\Delta\Omega}$, so that the rate of change in $<X_s>$ or 3D is predominantly controlled by the rate parameter, c, and the wave power ($P^{0.5}$,*W/m*), rather than the magnitude of $\Delta\Omega$. The disequilibrium term $\Delta\Omega$ incorporates a time-varying equilibrium condition, $\Omega_{eq}(t)$, defined as the weighted average of the antecedent dimensionless fall velocity Ω, and is largely dependent on a memory decay parameter ϕ (Eq. 5.6).

$$\Omega_{eq}(t) = \left[\sum_{i=1}^{D} 10^{-i\Delta t/\phi}\right]^{-1} \sum_{i=1}^{D} \Omega_i 10^{-i\Delta t/\phi} \qquad (5.6)$$

Δt is the time interval of Ω in days, *i* represents the index of data point in the wave forcing time series prior to the calculation point at time t (t=1) on the day and i = D on D days prior to the day of observation which was fixed at 2ϕ in order to reduce the number of free parameters in the model and simplify the optimisation. At each ϕ time, *D* weighted iterations (*i* to *D*) are performed. The value of ϕ is a measure of 'memory decay' of the beach. This is the critical parameter of this section used to evaluate the effect of the tide and sand bar location.

The depth and location of the bar [e.g. Wright et al., 1987] and the associated tidal range, have been recognised as important modulators of wave driven horizontal circulation and therefore the development of nearshore morphology [e.g. Almar et al., 2010; Stokes et al., 2015]. The main effects of the tide consist in limiting the intensity of breaker action at high water. The modulation of both 2D and 3D by the relative tide range (*RTR)* was implemented in place of the wave power given as P_T in Eq. (5.7):

$$P_T = P * RTR \qquad (5.7)$$

Stokes et al. [2015] followed a similar approach when they observed improvement of the model predictions of 3D especially at the outer bar with monthly tidal range.

Storm events typically cause the sandbars to both rapidly deepen and move offshore, whereas calm conditions lead to slow onshore migration and buiding of the bar. To estimate the effect of the wave height limitation due to the breaking over the sanbdbar, a modified version of the wave energy flux was defined P_b (Equation 5.8) that includes the effect of the sand bar location:

$$P_b = P * <X_{bnorm}> \qquad (5.8)$$

This sandbar effect here includes sandbar location normalised by its mean, $< X_{bnorm}>$ and the depth z_c of the bar crest that limits the *Hs.* The crest depth z_c is defined using an approximate link between sandbar

location $<X_b>$ with the commonly used Dean [1991] beach profile equilibrium formula [Dean and Dalrymple, 2002] as;

$$z_c = A(X_b)^{2/3} \quad (5.9)$$

where A is a scale parameter (here was estimated as 0.11, but not shown) which depends primarily on sediment characteristics [Dean and Dalrymple, 2002]. The implementation of the crest depth is similar to the normalised sandbar locations.

Model free parameters ***b*** (m/a) and ***c*** (m/s) in Eq. 5.3 and an offset ***a*** (m) were optimised through least-squares process [see Davidson et al., 2013 for details] after detrending the shoreline and forcing data. The main reason for the least-squares fit procedure is that it approximates the closest nonlinear functions during high-energy conditions, when the fluctuations are also large. Least-squares fit procedures minimize the quadratic error, which biases the results toward the largest changes in the variables.

5.3.3 Sensitivity of the beach memory to tide P_T and crest depth at sandbar location P_b

The model is first calibrated against 60% of the measured data (2007-2010). Figure 5.9 represents ShoreFor callibration and validation (hindcast) results. Figure 5.9a and 5.9b represent the measured and hindcasted evolution of 2D and 3D with the weighted *P(input data)*, P_T (data with *RTR*), and P_b(data with sandbar locations). In Figure 5.9a, model values and input data show dominantly seasonal variation. Overall, the model shows weak agreement with the field data for both erosion and accretion periods but is strongly estimating the cross-shore variability than the longshore variability. Clearly, the shoreline data is noisy short term events and the model therefore has no choice but to try to go in the middle of the scattered data to minimize root mean square error. Hindcast results showed a maximum correlation of approximately, r ~0.54 (Table 5.4) in all three cases.

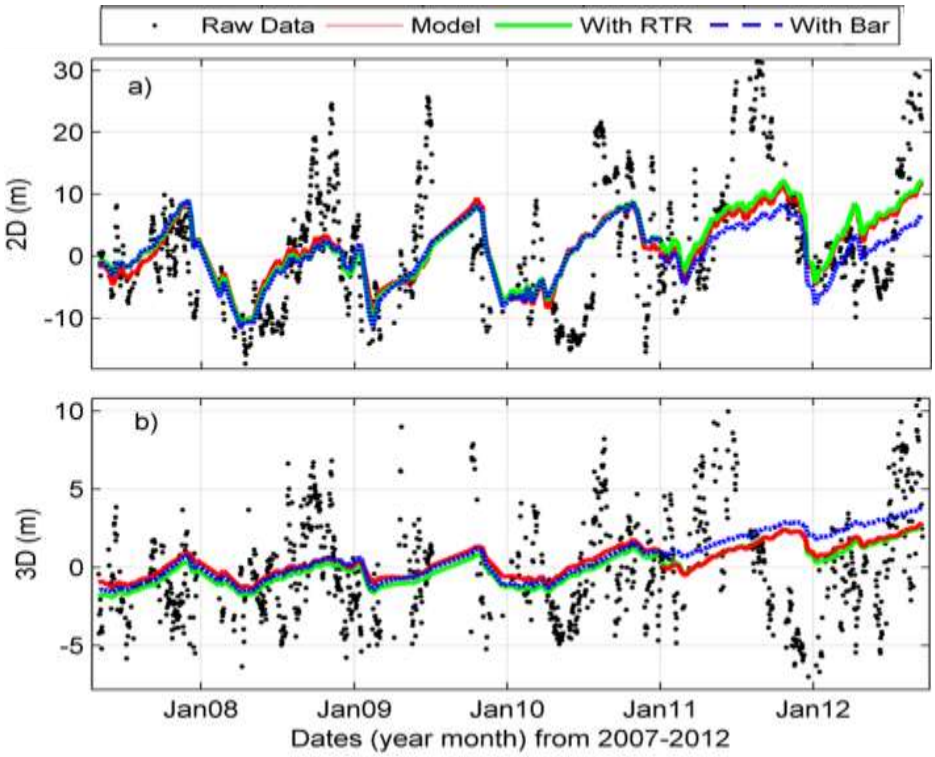

Figure 5.9. Time series of measured a) 2D data and modelled 2D data with the effect of RTR (green line) and sand bar (blue dotted line) b) 3D data and modelled 3D data estimated with data and modelled 3D data with the effect of RTR (green line) and sand bar (blue dotted line).

Table 5.4. Model coefficients and skill assessment results after ShoreFor model and Stokes et al. [2015] for the alongshore-averaged (2D) and non-uniformity (3D) contours. Model skill values are given for calibration and validation; we indicate that the hindcast was only performed with the Davidson et al. [2013] model. *k* ranges from 0.23 to 0.55 for both 3D and 2D shorelines.

2D Data	**Model parameters**			ϕ	**Model r**
	a	**b**	**c (x10^{-8})**		
P flux	102.7	1.24	3.14	360	0.49 (0.54)
P + *RTR*	102.1	0.8	6.8	360	0.49 (0.55)
P + sandbar	102.3	1.1	1.4	360	0.52 (0.52)
3D Data	**Model parameters**			ϕ	**Model r**
	a	**b**	**c(x10^{-8})**		**ShoreFor**
P flux	6.20	0.70	0.30	>1000	0.31 (0.28)
P+*RTR*	6.50	0.57	0.22	270	0.30(0.29)
P+ sandbar	6.20	0.70	0.22	>1000	0.30 (0.29)

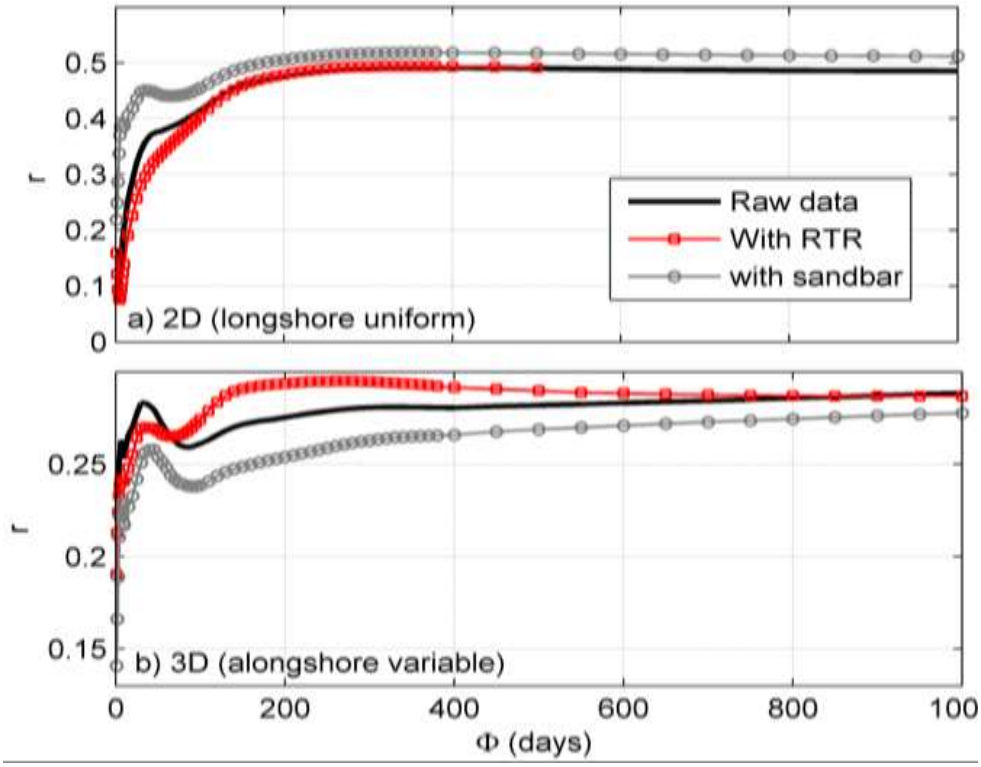

Figure 5.10. Correlation between modelled a) 2D data estimated as well as *RTR* and sandbar locations against measured 2D data b) 3D as well as *RTR* and sandbar locations against measured 3D data. The influence of weighted RTR and sandbar location on beach memory is given by the largest correlations *r* in each of 2D or 3D data.

Data (Table 5.4 and Figure 5.10a) show that the inclusion of *RTR* and sandbar location made very little difference in the prediction of 2D values compared to the use of input data (Figure 5.10a) especially during storms. Similarly, *RTR* poorly improves the model predictions of 3D, as low correlation was observed. However, it proved to be dominated by variations at shorter scale than when the sandbar is included. Results also reveal that the introduction of *RTR* in the model improved the prediction of the 3D data more than the sandbar, shown by the higher correlation (Figure 5.10b), with decrease in the beach memory (ϕ~270 days) decay parameter (Figure 5.10b) compared to that of the sandbar (ϕ>1000 days), suggesting that sandbar effect is not event dependent.

This is consistent to the observations of Stokes et al. [2015] who did not observe any change to the model after inputting *RTR* in the model at the lower beach. Other parameters such as the normalised wave incidence direction were merged with the equilibrium profile depth z_c and tested but these did very little improvement in *r* and *BSS*. This preliminary test indicate that peaked correlations occur at larger values of beach memory (ϕ >100 days), which means that beach changes result from average long term conditions.

The results of this section suggests alongshore shoreline naturally evolves seasonally even with the effect of tides and sandbar location, but the results however reveal the 2D and 3D shorelines may respond at individual storm frequency more to tide effect by the much reduced memory duration.

5.3.4 Conclusions

For the first time we applied an equilibrium shoreline model to the video data at Biscarrosse beach. Previous studies [Stokes et al., 2015] showed that at daily scale, tidal variation does not influence 3D changes at the lower beach. Our study shows that for alongshore-uniform shoreline, sand bar and tide effect do not affect the beach. With an error margin of 9 m on shoreline values, shoreline changes are largely influenced by noise which explains the very low skill of our model R^2<0.30 compared with other sites using beach profiles or video data [Splinter et al. 2014]. Overall, we have recorded very little improvement due to tides or sandbar in the 2D/3D estimation, but these results stand clearly with the importance of considering tide and the presence of the sandbar in predicting rapid shoreline changes. If site characteristics are important, using *HFI* and only *TR* may improve the predictions. Overall, though not evident, these results support previous findings by Angnuureng et al. [in revision with Geomorphology] and Stokes et al. [2015] on the importance of taking into consideration sandbar and tidal modulation of wave impact on morphology. We believe that if more analysis is made with much quality shoreline data (with higher proxy ~1.5 m above MSL), tides and sandbar will significantly improve the model.

CHAPTER SIX

James town beach under video surveillance

6. James town beach evolution under video surveillance

6.1 Introduction

6.2 Background

6.3 Data and methods

6.3.1 Video monitoring system

6.3.1a Camera calibration and installation

6.3.1b Geo-rectification of oblique images to plan view

6.3.2 Hydrodynamic data for James town

6.3.2a Wave and tide data from Era-Interim global reanalysis

6.3.2b Wave characteristics from video images

6.3.3 Morphological data for James town beach: shoreline delineation

6.4 Results

6.4.1 Video observation of waves and shoreline change on the microtidal James town beach in Ghana (*Special Issue of Journal of Coastal Research*).

6.4.1a Validation of vide-derived wave characteristics

6.4.2b Shoreline and morphological evolution: event and overall evolution

6.4.2 Comparing the contribution of H_b, sea level anomaly (*SLA*) and *TR* to shoreline change

6.5 Conclusions

6.1 Introduction

In this thesis a methodology to assess shoreline changes at different time scales (storm events, seasonal and interannual) was proposed for Biscarrosse beach (French Atlantic). A similar proposal was made for James town (Ghana, Gulf of Guinea). At the double barred Biscarrosse beach, wave conditions are dominant and tides are large, while the beach usually experiences numerous storm conditions. At the terrace James town beach, tides are small as well as wave conditions and the dominant forcing condition is unknown. The primary idea of this thesis was to contrast these two sites by following similar methods, to reveal the evolution of each beach. Therefore the analysis that was done for James town beach is given in this chapter.

Analysis of shoreline change trend under the influence of both climatic and anthropogenic forcing is hampered by the availability of archival time series data, especially in developing nations where there is scarcity of data [Boateng, 2006]. However, the novelty/innovation in coupling of archival data with remotely sensed data in data starved locations, to obtain reliable information for developing shoreline management strategies has shown progress. Shoreline studies along the Ghanaian nearshore have been realised through topographic surveys and in-situ measurements using differential GPS as well as satellite images [Appeaning Addo et al., 2008; Angnuureng et al., 2013; Jayson-Quashigah et al., 2013; Wiafe et al., 2013] on irregular basis. These measurements are intermittent both in space and time and the distance covered is often limited. Selecting a particular method for shoreline mapping is influenced largely by several factors including the level of accuracy required, type of output desired, availability of funding and/or equipment, and the method to be adopted to analyse historic rate of change of the shoreline [Moore, 2000]. Although data measured using LIDAR and aerial photographs can cover large spartial widths, they can be expensive and have low time resolution [Li et al., 2002].

Though several portions of the Ghanaian coastline is eroding at varying rates (Figure 6.1), a monitoring scheme using the traditional methods for the Ghana coast does not guarantee the capture of the short term temporal shoreline evolution and other key events. In general, analysing shoreline change in developing countries presents huge challenges (e.g. poor resolution) to coastal scientists and managers due to factors that affect their reliability. Data scarcity prevents studies into the past behaviour of the shoreline position and how it has metamorphosed into the present trend. Where data exist, the inconsistencies in the period of data capture influences systematic change analysis that fails to account for important events (e.g. storm). It is essential for the data gathering strategies to include many approaches to have data spanning a broad ran of times and space. This can be provided by using the video system. Combining shoreline data from two or more sources present a unique opportunity to trace how the shoreline has evolved over the period to its present position. This provides the baseline information to analyse the cyclic behaviour of the

shoreline in the short and long term and how other factors influence the lateral morphological change as well as estimate the shoreline's historic rates of change that enables the prediction of the future position of the shoreline using modelling techniques.

This study therefore focuses on a coastal community where scientific data is scarce, specialised expertise is rare, funding is limited, and local authorities can be unprepared to cooperate. In the wake of these, this chapter presents the application of a video system approach in coastal monitoring along a segment of the James town coastline in Ghana. The main aim was to test the ability of the video system in providing quality and accurate wave data sets in Ghana. First, a background of the study is given and followed by the process of installing the video system. Secondly, the approaches on extraction of wave data and shoreline location from the video system at James town over a 6-month period are discussed. Finally, estimates of wave data from video are compared with hindcast wave data and the main drivers of shoreline changes were identified among waves, water and sea level anomaly.

Figure 6.1. Showing sample coastal erosion along the coastline of Keta-Ghana

6.2 Background study

The coast of Ghana is sub-divided into three major zones (Figure 6.2) namely the Eastern, Central and Western coasts based on geomorphologic characteristics [Boateng, 2006].

The Eastern coast, which is about 149 km long, stretches from Togo Border to Prampram. It is a high-energy beach with wave heights often exceeding 1 m in the surf zone [Ly, 1980]. Wellens-Mensah et al. [2001] explained that the Volta River has a dominant influence on the geomorphology of the Eastern coast. The surface geology of the area is made up of fluvial sediments delivered from the Volta river as well as marine and fluvial-marine sediments and the beaches comprised of medium to coarse sand. Jayson-Quashigah et al. [2013] investigated the potential of medium resolution satellite imagery for mapping shoreline rate of change along the eastern coastline. They showed that the Keta coastline is a highly dynamic feature with average rate of erosion of about 2 m/year. Individual rates along some transect reached 16 m/year, particularly on the east of the Keta Sea Defence site. A related study by Angnuureng et al. [2013] on the impact of the Keta Sea defense structure constructed to control the beach degradation, showed erosion could be so severe (~17 m) at the down drift side of the defense structure.

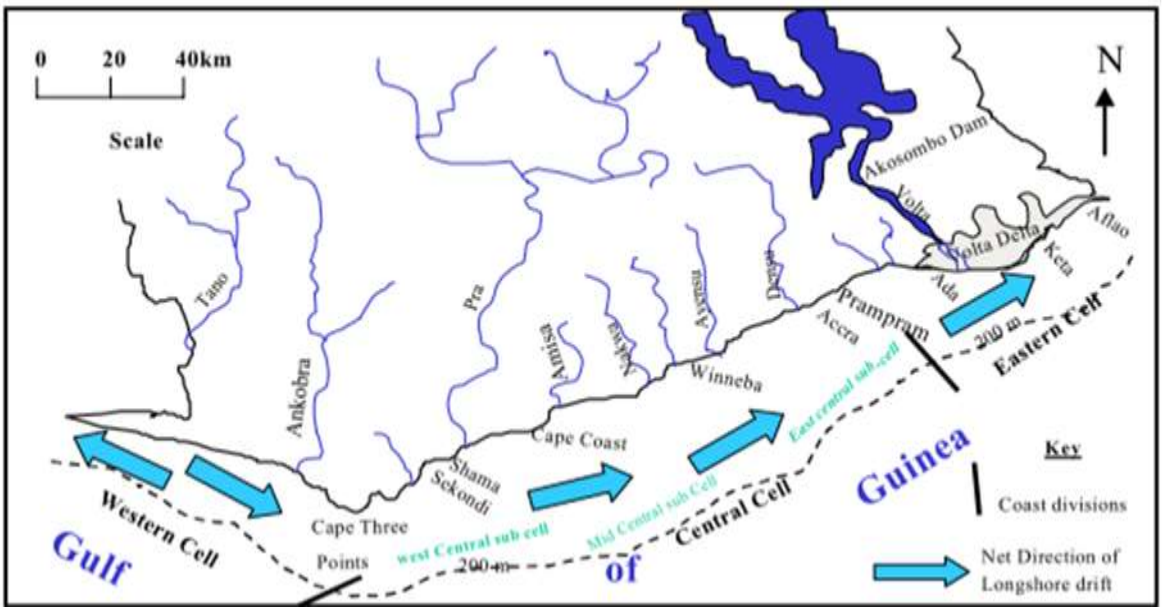

Figure 6.2. Divisions (Western, Central and Eastern) and alongshore transport along the coastline of Ghana (after Boateng, 2006).

Along the Ghanaian coast, erosion has been observed to be increasing over the last decades [Appeaning Addo et al., 2008; Boateng et al., 2009] with about 25 erosion hotspots [erosion higher than 1.5 m/yr, Appeaning-Addo and Lamptey, 2012] identified along the coast of Ghana. Relatively high erosion on the

eastern part the Ghana coast can be attributed to the method of management (e.g. groynes and revetment) which affects the sediment budget [Ly, 1980; Jayson-Quashigah et al., 2013].

The Western coast covers 95 km of shoreline and is a relatively low energy beach. This coast comprises gently sloping, wide and fine sandy beaches backed by coastal lagoons.

The central coast consists of about 321 km of shoreline extending from Laloi Lagoon west of Prampram to the estuary of River Ankobra near Axim. The morphology of this coast is influenced by sediment delivered from a series of north to south draining rivers. It is an embayment coast of sandy beaches, rocky headlands and sandbars with spits enclosing coastal lagoons. The shoreline is almost a straight line and runs in the south-west direction. Wiafe et al. (2013) analysed the risk factors along the entire coastline as summarized in Table 6.1. From Table 6.1, risk factors assigned to various variables show that rocky areas can be highly stable with very low vulnerability while sandy beaches are highly vulnerable. However, along the coastline of Accra including Jamestown, the rate of human encroachment of the coastal lands which influences erosion far exceeds the rate of shoreline change [Appeaning Addo et al., 2013]. Appeaning Addo et al. [2013] found that these large volumes of land lost to human encroachment can result into 1.92 m/yr erosion, which increases the vulnerability.

The Central coast (see Figure 6.2) including Accra, the capital of Ghana and James town represents a medium energy environment. The shoreline position of Accra has changed progressively since 1904 [Appeaning-Addo and Lamptey, 2012]. Accra's shoreline is eroding in the long-term though beaches along certain portions of this coast are fairly stable [Armah and Amlalo, 1998; Boateng, 2006] compared to other zones. Orientation of Accra's shoreline contributes largely to the observed recession trend along the coast [Appeaning-Addo and Lamptey, 2012]. The observed trend is predicted to continue as a result of increasing sea level rise due to global climate change.

Figure 6.3. James town beach. A video camera is located on the lighthouse [40 m above MSL]. Korle Lagoon is open into the sea at the far western site of the beach.

Analysis of bathymetric data indicates that the western and central zones have relatively gentle slopes, while the eastern zone has a considerably steeper slope [Appeaning Addo et al., 2008]. These conditions have significantly influenced the trend of shoreline recession in each of the three geomorphic zones. Coastal erosion intensity therefore varies along the Accra coast. Vulnerability of beaches to forcing and anthropogenic factors has been addressed through both hard [*e.g.* revetments, jetties or breakwaters, and groins reported in Angnuureng et al., 2013] and soft approaches (*e.g.* revegetation and beach nourishment) in attempts to control the changes [*e.g.* Turner and Leatherman, 1997; French, 2001;] yet both methods are debatable. For instance with hard engineering, areas further down the coast can be starved of beach material resulting in more erosion, while soft methods (e.g. beach nourishment) do not last very long as sand will continue to be transported along the coast by longshore drift. The erosion problem becomes worse whenever the countermeasures (i.e. hard or soft structural options) applied is inappropriate, improperly designed, built, or maintained and if the effects on adjacent shores are not carefully evaluated. This is further made complex by the lack of adequate monitoring.

James town is a major fishing community in Ghana (Gulf of Guinea, West Africa) on the eastern part (Figure 6.3) of the Korle lagoon, which is a major ecological site in Accra under the Ghana wetlands management project. The increasing coastal erosion threatens the community, the lighthouse and the old Accra harbor presently being used as a fishing harbor. The nearshore bathymetric profile is relatively gentle and the area experiences periodic high-wave conditions [Sagoe-Addy and Appeaning Addo, 2013]. The mean wave incidence is SSW (Figure 6.4), mean peak period T_p and the mean significant wave height are 10.9 s and 1.4 m, respectively [Appeaning Addo et al., 2008; Angnuureng et al., 2013], but these could periodically rise to 20 s and 3 m. Tide range is micro-tidal with mean value of about 1 m. Oblique waves drive alongshore drift of about $2*10^5$ m^3/yr [Wellens-Mensah et al., 2001] on this gentle beach (slope <0.03). The breaker type is plunging and the longshore current it generates ranges between 0.5 and 2 m/s, which is significantly high and thus responsible for the relatively high rate of sediment transport in the littoral zone.

Table 6.1. Ranking of coastal vulnerability index variables for the Coast of Ghana [cf. Wiafe et al., 2013] due to geomorphology, geology, relative sea level rise (R-SLR), shoreline erosion, tide and significant wave height (*Hs*).

Variable	Very low	Low	Moderate	High	Very high
Geomorphology	Rocky coasts	Medium cliffs	Low cliffs	Estuary lagoon	Deltas, sand, mangroves
Coastal geology	Pegmatite, biotite, tonalite	Amphibolites, Gneiss, quartzite	Lime-,sand- and mudstone, Conglomerate	-	Alluvial sand, silt, clay
Coastal Elevation	>30.0	>20.0 – 30.0	>10.0 – 20.0	>5.0–10.0	0.0 – 5.0
R-SLR (mm/yr)	<1.8	1.8 -2.5	2.5-3.0	3.0-3.4	3.4
Erosion (m/yr)	>2.0	1.0-2.0	-1.0 – 1.0	-2 – (-1)	< -2.0
Tide (m)	>6.0	4.0-6.0	2.0-4.0	1.0-2.0	<1.0
Hs (m)	<0.55	0.5-0.8	0.8-1.0	1.0-1.2	>1.2

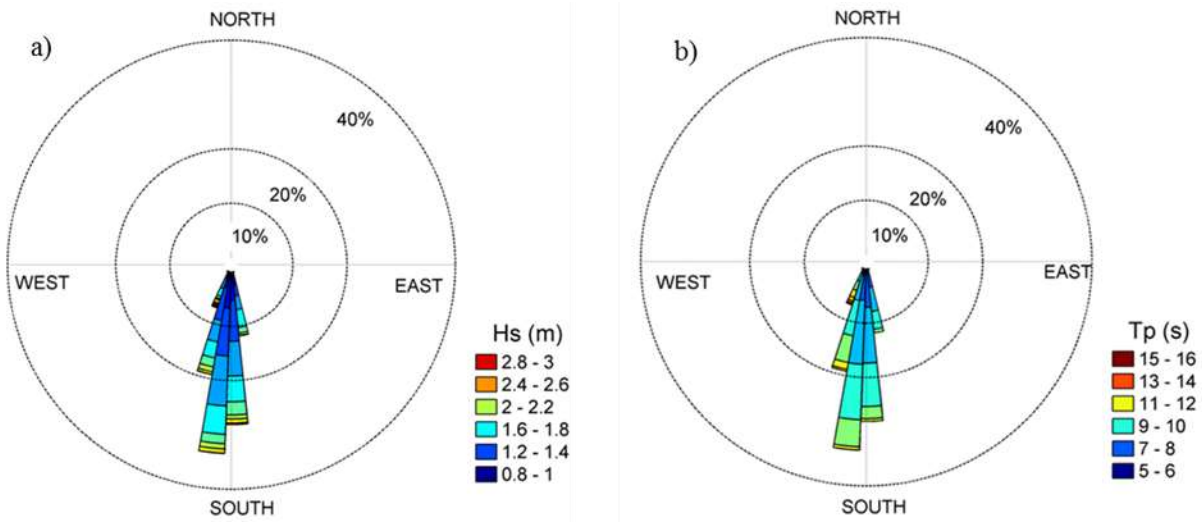

Figure 6.4. James town wave rose diagrams (01/01/2013-30/10/2014) based on data from ERA-Interim reanalysis; a) wave direction and the magnitude of significant wave height, *Hs* (m), b) wave direction and peak period, T_p (s).

6.3 Data and methods

For this study data was retrieved in two ways. Hindcast wave and water level data was obtained from Era-Interim global reanalysis model to be used to validate video observational data. Thus, this section will describe the installation and retrieval of video data and the presentation of the hindcasted data. Morphological data is obtained from video images. Alongshore-average shoreline locations and alongshore variations of shoreline are automatically delineated from timex images.

6.3.1 Video monitoring system

6.3.1a Camera calibration and installation

A 40-m high lighthouse (see, Figure 6.3) was built in the 1930s for navigational purpose. A video camera was mounted on the lighthouse on 14/09/2013, inclined to the beach at an angle of 20°. The camera spatial coverage is about 1.3 km across shore and 2 km along shore and set to record from 6 - 18 hours GMT at 2 Hz. Three types of images are collected every 15 min: snapshot (Figure 6.5a); time exposure (timex) (Figure 6.5b) and time stacks (Figure 6.5c). Timex images are 15 min averaged of snapshot images into a single image [Holland et al., 1997;Almar et al., 2012b], while timestacks are obtained by stack of single cross shore portion [red line Figure 6.5a] within the 15 min to obtain Figure 6.5c. The origin of the camera coordinate system (cross-shore X=720, longshore Y=0) is traced to the lighthouse.

Over six months of 15 min image data was collected including several data gaps due to camera malfunction and times when images were unclear.

6.3.1b Geo-rectification of oblique images to plan view

Seven ground control points on site (Figure 6.5b, red circles) were taken with GPS and converted to Universal Transverse Mercator, UTM (Easting and Northing) coordinates. Including camera location (5.5265, 0.2121) at 30° N UTM zone, images could be geo-rectified from oblique to plan view images by applying the method of direct linear transformation [*e.g.* Argus, Holland et al., 1997], see details in Chapter 3. However, to get the rectified data two approaches were primarily tested and one chosen. First, a zone of interest covering the beach and water (Figure 6.5a, white patch) was selected on the image and rectified at a 1-m resolution before desired information (e.g. shoreline) was extracted.

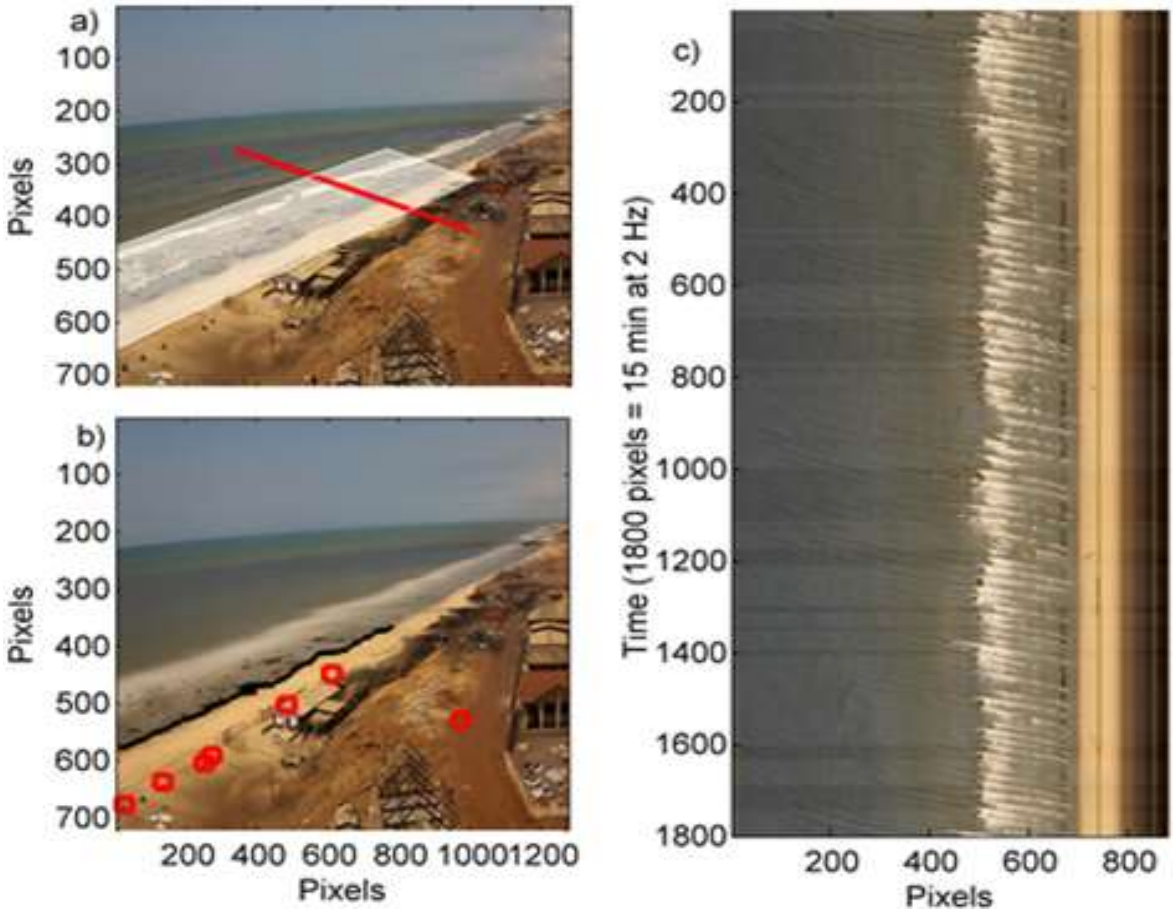

Figure 6.5: Video image types: a) snapshot; selected zone is shaded white while timestack profile is red line b) timex: shoreline is shown black line and GPS points in red circles c) timestack (vertical is time (1800 pixels =15 min at 2 Hz)).

The focal length (4m) based on a least square error minimization method was used for the rectification. For shorter processing time purpose, the shorelines were automatically detected on the oblique images before the rectification. Because of the oblique camera view angle, the pixel resolution at the shoreline for the image lateral edges reaches about 0.5 m, whereas it is about 0.1 m at the lower beach in front of the video system [Almar et al., 2012a], increasing to 1 and 2 m at the lateral edges.

6.3.2 Hydrodynamic data for James town

6.3.2.a Wave and tide data from Era-Interim global reanalysis

To validate video estimates of wave properties, hindcast data of significant wave height *Hs*, direction and peak period T_p have been obtained from Era-Interim global reanalysis [WAM model, The Wamdi Group, 1988] at 0.5° and 6 hr spatial and temporal resolution, respectively [Sterl and Caires, 2005] at the grid point 30°N, 30°W. The wave data stretches from Sep. 2013 to Oct. 2014 while tide was extracted from WXtide model. Because there is no tide gauge at the study site, the tidal subordinate at Accra (0°12' W, 5°32' N), from the nearest tide gauge station, Takoradi (~200 km) was used as the reference point. *Hs* and T_p were transformed into breaker conditions $H_{b(lm)}$ and $T_{p(lm)}$, respectively, following Larson et al. [2010] given in the following equations:

$$H_{b[lm]} = \gamma h_b. \quad (6.1)$$

$$h_b = \lambda C^2/9.81 \quad (6.2)$$

$$\lambda = \Delta (\cos(\pi ø/180)/\alpha)^{2/5} \quad (6.3)$$

$$\Delta = 1 + 0.1649\epsilon + 0.5948\,\epsilon^2 - 1.6787\,\epsilon^3 + 2.86\,\epsilon^4 \quad (6.4)$$

$$\epsilon = (\cos(\pi ø/180)/\alpha)^{2/5} \sin(\pi ø/180)^2 \quad (6.5)$$

$$\alpha = (C\,\gamma^2/Cg)\,(C/\sqrt{9.81\,Hs})^4 \quad (6.6)$$

where γ is an arbitrary constant, C and Cg are phase and group wave velocities, respectively, ø is wave incidence angle, h_b is the depth at breaking and *Hs* is the offshore significant wave height. Beach states were computed using the formulation of Dean parameter [*see* Wright and Short, 1984], $\Omega = H_{b[lm]}/T_{p(lm)}w_s$, where w_s is sediment fall velocity, using the reanalysed wave data. A w_s of 0.05 m/s was used in consistence with similar sandy beaches [*e.g.* Masselink et al., 2009].

Components of storm surge on the Gulf Coast continental shelf include wind setup, inverse barometer effect, wave setup and Coriolis force [Walton and Dean, 2009]. The effect of these parameters on the shoreline may differ from region to region. Wave setup as was given in Chapter 3 can cause an increase in water level elevations on the order of 20–50% of the offshore breaking wave height [Dean and Walton, 2009] and can reach values between 1 m to 12 m of the shoreline location, depending on the site characteristics. However, in a separate study, Walton and Dean [2009] showed that the most important component of storm surge is the wind setup. In this study, the combined effect of wind setup and atmospheric pressure data (the sea level anomaly, SLA) which were also extracted from Era-Interim hindcast reanalysis data is estimated at the shoreline. To assess this, a multiple linear regression was used to estimate the contribution of H_b, SLA and tide range on the shoreline evolution. The procedure of the multiple regression that was described in Chapter 4 is implemented here.

6.3.2.b Wave characteristics from video images

The detection of wave breaker height has been applied and validated at other sites [e.g. Almar et al., 2012b] and therefore only the implementation is given here. Wave breaker height H_b and T_p were obtained from time stack images of James town video station and compared to the model data. T_p was computed from the offshore pixel intensity timeseries following Almar et al. [2008]. The time of propagation Δt between two wave front positions $\Delta x = x2 - x1$ is estimated as the lag of maximum of correlation coefficient between the two wave fronts. The T_p is thus the time lag between two wave fronts (troughs or crests) at the maximum correlation.

The method of detecting wave breaker height relies on the abrupt change of wave optical characteristics at the breakpoint. Following the wave signature induced by breaking, sudden variation in intensity values are identified on the image and an intensity threshold is used to discriminate between breaking and non-breaking pixels. Too high threshold however can affect the roller detection. Pixels above the threshold are grouped by space and time with respect to individual breaking waves. For the evolution of each breaking wave, standard deviation δ of the pixel intensity time series is estimated on a time window about the break point time. Almar et al. [2012b] showed that the width of the peak of δ represents the horizontal projection of wave face covered by the roller (L) which is subsequently projected into vertical H_b, $H_b = L\tan\beta$, where β is the camera viewangle. H_b is obtained as the wave height of the average of all passing breakers over the timestack duration (1800 s or stacking). H_b and T_p were respectively regressed with $H_{b(lm)}$ and $T_{p(lm)}$, propagated from deep water to the breakpoint and a relationship established.

6.3.3 Morphological data for James town beach: shoreline delineation

Following Almar et al. [2012a] who developed the minimum shoreline variability (MSV) approach; a region of interest [ROI] is demarcated on the oblique images to cover both wet (sea) and dry (land) pixels. Beach pixels display high red-channel (R) values and low green (G) values giving high *R* to *G* ratio, whereas water pixels exhibit strong green-channel values and low red values (*i.e.* low *R:G* ratio). Within the ROI (*see* Figure 6.5a), the *R:G* ratios are computed for all pixels. These low and high values of *R: G* mark water and beach respectively based on some bimodal distribution [Almar et al., 2012a]. The local minimum represents the transition between water and beach, that is, the shoreline. In other words the shoreline is represented by the time averaged waterline. Figure 6.5b shows the shoreline *X* delineated automatically. This was repeated for all images, and converted to metric values. To reduce uncertainties, a 1-hr moving average (4 points) was done. The overall error (O (5m)) rises from water level uncertainties due to wave breaking or atmospheric pressure variations or wrong shoreline detection. 2D shoreline migration was estimated via the alongshore averaged cross-shore 2D location $<X>$ (Figure 6.5c). 3D shoreline behaviour (non-uniformities development) was estimated through the standard deviation of cross-shore location along *Y*. Anomaly introduced by the effect of atmospheric pressure and wind was then quantified.

6.4 Results

First, in section 6.4.1, preliminary findings on this West Africa pilot video system that were accepted in the Special Issue (SI) of *Journal of Coastal Research* are presented. They include the validation of video-derived wave parameters (RMSE, correlation with hindcast) and a brief description of the temporal evolution of shoreline and profiles, linked to waves. Secondly, in section 6.4.2, the contributions of H_b, sea level anomaly and tide are compared to identify the dominant influencing parameter.

6.4.1. Video observation of waves and shoreline change on the microtidal James town beach in Ghana (*in the Journal of Coastal Research as a Special Issue*).

Journal of Coastal Research	SI	75	1022 - 1026	Coconut Creek, Florida	2016

Video Oberservation of Waves and Shoreline Change on the Microtidal James Town Beach in Ghana

Donatus B. Angnuureng[†‡*], Rafael Almar[‡], Kwasi Appeaning Addo[§], Bruno Castelle[†], Nadia Senechal[†], Sowah W. Laryea[§], George Wiafe[§]

[†]UMR EPOC, University of Bordeaux / CNRS, Bordeaux, France. [‡]IRD/UMR, LEGOS, Toulouse, France.

[§]MAFS/Remote Sensing Lab., University of Ghana, Accra, Ghana.

www.cerf-jcr.org

www.JCRonline.org

ABSTRACT

Angnuureng, D. B., Almar, R., Appeaning Addo, K., Senechal, N., Castelle, B., Laryea, S. W., Wiafe, G., 2016. Video observation of waves and shoreline change on the microtidal James town Beach in Ghana.. *In:* Vila-Concejo, A.; Bruce, E.; Kennedy, D.M., and McCarroll, R.J. (eds.), *Proceedings of the 14th International Coastal Symposium* (Sydney, Australia). *Journal of Coastal Research*, Special Issue, No. 75, pp. 1022 – 1026, Coconut Creek (Florida), ISSN 0749-0208.

The morphology of sandy beaches is highly dynamic. They are influenced by the geology of the coastal area and external hydrodynamic forcing. On long timescales (years to decades), it is more efficient and convenient to monitor beach evolution through remote sensing technics rather than through direct field measurements. Erosion is a major problem along the coastline of Ghana with over 25 erosion hotspots, including James town. Here, tides, ECMWF EraInterim re-analysis wave data and images covering the beach area have been obtained for the 2013-2014 period. This paper presents preliminary results of the first efforts in processing video-derived observations of waves and shoreline change in Ghana. The pilot application shows a strong potential of the video system in providing fair quality wave data for beach management purposes where video wave characteristics are in good agreement with EraInterim global reanalysis (daily RMSE = 0.8 m and 0.7 m for H_b and T_p, respectively). Shorelines extracted from video suggest large monthly variability driven by wave seasonality while shoreline change shows a subsequent erosion/accretion cycle.

ADDITIONAL INDEX WORDS: *Shoreline location, wave modeling, beach profile changes.*

INTRODUCTION

Understanding coastal processes in the nearshore at different time scales is crucial, especially in the present context of vulnerability to sea level rise (Sagoe-Addy and Appeaning, 2013;Stive *et al.,* 2002). Vulnerability of beaches to natural forcing and anthropogenic factors has been addressed through both hard (*e.g.* revetments, jetties or breakwaters, and groins (Angnuureng *et al.,* 2013)) and soft (*e.g.* revegetation and beach nourishment) approaches in attempts to control the changes (*e.g.* French, 2001;Turner and Leatherman, 1997) yet both methods are debatable. Traditionally, studies in the nearshore have been realised via topographic surveys and in-situ measurements (Stockdon and Holman, 2002). However these measurements are intermittent both in space and time and the distance covered is often limited. The nearshore is a very variable system constantly changing at various timescales (Puleo *et al.,* 2003) and require a high frequency of sampling for adequate characterization. Remote video imagery has been used to measure nearshore processes (*e.g.* Aarninkhof *et al.,* 2003; Armaroli and Ciavola, 2011; Holman and Stanley, 2007; Plant and Holman, 1997) over the past two decades. According to Holman and Stanley (2007), the video system gives good resolutions (cm to m), and is safe and cheap.

From video images, wave height, celerity and period (*e.g.* Almar *et al.,* 2008; Holman and Stanley, 2007); break point and intertidal sandbar locations (Holman and Stanley, 2007; Ruessink *et al.,* 2007), beach profiles, and shoreline position (Almar *et al.,* 2012a; Smith and Bryan, 2007; Plant and Holman, 1997) can be remotely estimated.

Along the Ghanaian coast, erosion has been observed to be increasing over the last decades (Appeaning Addo *et al.,* 2008; Boateng *et al.,* 2009) with over 25 erosion hotspots identified. On the eastern part, this is due to the method of management (*e.g.* groynes and revertment) which affects the sediment budget (Jayson *et al.,* 2013; Ly, 1980). Angnuureng *et al.* (2013) observed that erosion has increased from about 3 to about 17 m/yr. from 2001 to 2011, which has been probably enhanced by sand mining along the coast.

Monitoring of the Ghanaian coastline is mainly done using satellite images albeit rough resolution, aerial photographs and field observation using DGPS on an irregular basis. Though portions of the unmonitored coast remains, a well planned and reliable monitoring scheme with such methods does not guarantee the capture of the short term temporal shoreline evolution. It is then essential for the data gathering strategy to include events in all times and space, that such video system provides.

In the methods section, the James town study area is described and daily nearshore measurements from video imagery presented. The goal is to analyse the shoreline

DOI: 10.2112/SI75-205.1 received 15 October 2015; accepted in revision 15 January 2016.

*Corresponding author: angnuureng@yahoo.com

evolution and the potential of the video system in providing fair quality wave data for beach management purposes.

METHODS

Shoreline and beach profiles were automatically extracted from the timex (or averaged) images and shoreline positions resampled into daily and 15-day values. The shoreline location can be obtained using various definitions (Boak and Turner, 2005) but here the procedure followed minimum shoreline variability (MSV) video technique (Aarninkhof *et al.*, 2003; Almar *et al.*, 2012a). Wave properties (e.g. breaker wave height H_b and peak wave period T_p) at breaking are extracted from video images to compare with hindcast wave data (WAM model, The Wamdi Group, 1988).

Study area

James town is a major fishing community in Ghana (Gulf of Guinea, West Africa) on the eastern part (Figure 1) of the Korle lagoon, which is a major ecological site in Accra under the Ghana wetlands management project. The shoreline erosion in Ghana has risen from 1.13 m/yr. (Appeaning Addo *et al.*, 2008) to a rate of about 2 m/yr. (Wiafe *et al.*, 2013). The increasing coastal erosion threatens the community, the lighthouse and the old Accra harbor presently being used as a fishing harbor.

The nearshore bathymetric profile is relatively gentle (Sagoe-Addy and Appeaning Addo, 2013) and the area experiences periodic high-wave conditions (*e.g.* Sagoe-Addy and Appeaning Addo, 2013). The mean wave incidence is SSW, mean peak period T_p and the mean significant wave height are 10.9 s and 1.4 m (Angnuureng *et al.*, 2013; Appeaning Addo *et al.*, 2008), , respectively, but these could periodically rise to 20 s and 3 m. Tide range is micro-tidal with mean value of 1 m. Oblique waves drive alongshore drift of about $2*10^5$ m^3/yr. (Wellens-Mensah *et al.*, 2002) on this gentle beach (slope <0.03).

The 40-m high lighthouse was built in the for navigation (insert, Figure 1). A video camera was mounted on the lighthouse on 14/09/2013, inclined to the beach at an angle of 20° covering about 1.3 km across shore and 2 km along shore and recording from 6 - 18 hours GMT at 2 Hz. Three kinds of images are collected every 15 min: snapshot (Figure 2a); time exposure (timex) (Figure 2b) and time stacks (Figure 2c). Timex images are 15 min averaged of snapshot images into a single image (Almar *et al.*, 2012b; Holland *et al.*, 1997) while timestacks are obtained by stack of single cross shore section. The origin of the coordinate system (cross-shore X=720, longshore Y=0) is the lighthouse.

Geo-rectification of oblique images to plan view

Seven ground control points on site (Figure 2b, red circles) were taken with GPS and converted to Universal Transverse Mercator, UTM (Easting and Northing) coordinates. Including camera location (5.5265, 0.2121) at 30 N UTM zone, images were geo-rectified from oblique to plan view images by applying the method of direct linear transformation (*e.g.* Argus, Holland *et al.*, 1997). To get the rectified data, two approaches were applied. First, a zone of interest covering the beach and water (Figure 2a, white patch) was selected on the image and rectified at a 1-m resolution before desired information was extracted. We used for the rectification, the focal length (4m) based on a least square error minimization method. For shorter processing time purpose, the shorelines were detected (*see next section*) on the oblique images before the rectification.

Figure 1. James Town Beach. Camera is mounted on lighthouse.

Because of the oblique camera view angle, the pixel resolution at the shoreline for the image lateral edges can be about 0.5 m, whereas it is about 0.1 m at the lower beach in front of the video system (Almar *et al.*, 2012a), increasing to 1 and 2 m at the lateral edges.

Automated shoreline delineation

Following Almar *et al.* (2012a), a region of interest (ROI) is demarcated on the oblique images to cover both wet (sea) and dry (land) pixels. Beach pixels display high red-channel values and low green values giving high $R:G$ ratio, whereas water pixels exhibit strong green-channel values and low red values (*i.e.* low $R:G$). Within the ROI (*see* Figure 2a), the $R:G$ ratios are computed for all pixels. These low and high values of $R:G$ mark water and beach respectively based on some bimodal distribution (Almar *et al.*, 2012a). The local minimum stands for the transition between water and beach, that is, the shoreline. In other words the shoreline is represented by the time averaged waterline. Figure 2b shows the location of the shoreline X delineated automatically. This was repeated for all images, and converted to metric values. To reduce uncertainties, a 1-hr moving average (4 points) was done. The overall error (0.5m) rises from water level uncertainties due to wave breaking or atmospheric pressure variations or wrong shoreline detection. 2D shoreline migration was estimated via the alongshore averaged cross-shore 2D location $<X>$ (Figure 2c). 3D shoreline behaviour (non-uniformities development) was estimated through the standard deviation of cross-shore location along Y.

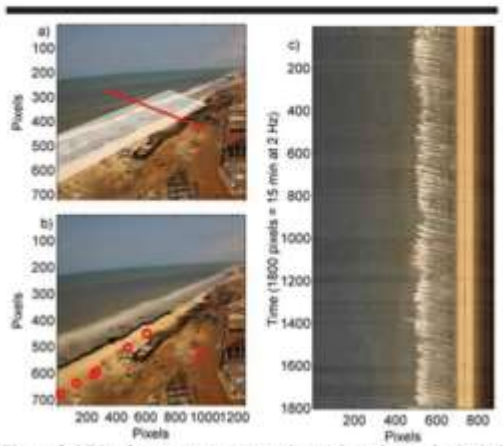

Figure 2. Video image types: a)snapshot; selected zone is shaded white while timestack profile is red line b) timex: shoreline is shown black line and GPS points in red circles c) timestack (vertical is time (1800 pixels =15 min at 2 Hz).

Wave and tide data from models

To validate video estimates of wave properties, hindcast data of significant wave height H_o, direction and peak period T_p have been obtained from EraInterim global reanalysis (WAM model, The Wamdi Group, 1988) at 0.5° and 6 hr spatial and temporal resolution, respectively (Sterl and Caires, 2005) at the grid point 30°N, 30°W. The wave data spans from Sep. 2013 to Oct. 2014. Tide was extracted from WXtide model. Because there is no tide gauge at the study site, the tidal subordinate at Accra (0°12' W, 5°32' N), from the nearest tide gauge station, Takoradi (~200 km) was used as the reference point. H_o and T_p were transformed into breaker conditions $H_{b(lin)}$ and $T_{p(lin)}$, respectively, following Larson *et al.* (2010). Beach states were computed using the formulation of Dean parameter (*see* Wright and Short, 1984), $\Omega = H_{b(lin)}/T_{p(lin)}w_s$, where w_s is sediment fall velocity, using the reanalysed wave data. A w_s of 0.05 m/s was used in consistence with similar sandy beaches (*e.g.* Masselink *et al.*, 2009).

Wave characteristics from video images

Wave breaker height H_b and T_p were obtained from time stack images and compared to the model data. T_p was computed from the offshore pixel intensity timeseries using mean zero-crossing method (Almar *et al.*, 2008). Following the wave signature induced by breaking, sudden variation in intensity values were identified on the image. For each breaker, standard deviation δ of the pixel intensity time series is estimated on a time window about the break point time. Almar *et al.* (2012b) showed that the width of the peak of δ marks the horizontal projection of wave face covered by the roller (L) which is subsequently projected into vertical H_b, $H_b = L\tan\beta$, where β is the camera view angle. H_b is obtained as the wave height of the average of all passing breakers over the timestack duration (1800s or stacking).

H_b and T_p were respectively regressed with $H_{b(lin)}$ and $T_{p(lin)}$, propagated from deep water to the breakpoint and a relationship established. Breaker parameters H_b and T_p from video followed this relationship.

Beach types were assessed from timex images. To estimate the beach profile evolution, 3D data (x, y, z) is needed. The shoreline location constitute 2D (x and y) which means a third axis (z-elevation) is needed. Subsequently profiles (not shown) were inferred from interpolated tide values at the different shoreline times where the profile of the beach at each time follow the tide values. The monthly average profiles were then estimated.

RESULTS

Preliminary findings of this West Africa pilot video system are given in the following subsections. They include the validation of video-derived wave parameters (RMSE, correlation with hindcast) and a brief description of the temporal evolution, extraction of shoreline and slope linked to wave and then tide forcing.

Validation of vide-derived wave characteristics

Figure 3 represents H_b and T_p obtained from regressed video-derived values as a function of hindcasted ones $H_{b(lin)}$ (and modelled $T_{p(lin)}$ from transformation of H_o, *see method section*) following Larson *et al.* (2010). Figure 3a shows that corrected video-derived T_p correlates strongly with hindcast (r = 0.9, daily RMSE = 0.7). Result error is due to variation in image quality. In Figure 3b it is showed that corrected video-derived H_b is in agreement with $H_{b(lin)}$ (r=0.9, daily RMSE=0.8). Overall, these results show the reasonable skills of the video in estimating wave conditions from daily to monthly scale for this beach.

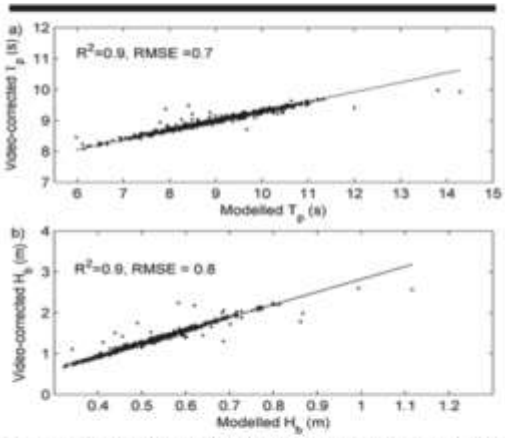

Figure 3. Time series a) corrected T_p from video values against model T_p b) corrected H_b from video values against model H_b. Model values are Larson's model H_b and T_p. Sloping solid lines are the best linear fits.

Shoreline and morphological evolution: event and overall evolution

During the observation period, from Sep. 2013 to Jul. 2014, alongshore averaged shoreline positions $<X>$ ranged from 127 to 211 m with an average at 151 m. Figure 4c gives the daily $<X>$ relative to the initial position $<X_i>$. It shows that shorelines retreat beyond the $<X_i>$ more than they advance. Shoreline alongshore non-uniformity $\Delta(X)$, *i.e*, standard deviation of shoreline X, is 8 m on average due to the presence of cuspate pattern but can fall to 3 m during energetic conditions. H_b ranges from 0.3 to 2.5 m while literature reported between 0 and 2.8 (Angnuureng *et al.*, 2013). T_p ranges from 7 to 14 s at the zero mean crossing shown on the images. Figure 4d shows that H_b decreases from September, 2013 to January, 2014 concomitant to beach advance while after January, 2014, H_b increases progressively corresponding to shoreline recession till June, 2014. In Figure 4c, 15-day averaged shoreline positions are shown; September to early November period recorded beach advance gradually till it peaks in January. Shoreline retreats from January onward (Austral winter) when waves averagely become larger (Figure 4d).

Daily waves (H_b and T_p) did not correlate with shoreline positions as beach morphologies do not respond instantaneously to the changing wave field. Interestingly, similar results were found at a nearby beach (Grand Popo, Bénin) where the short term evolution of the shoreline seems to be more affected by tidal cycles from neap to spring (Bahini, 2015). This is due to the large Relative Tide Index (Masselink and Short, 1993) value which is around 1, even though the environment is microtidal. On the other hand, at the event scale, waves have more influence on $\Delta(X)$ development. $\Delta(X)$ is observed to correlate significantly at 95% ($p = 0.03$) with H_b though with low value ($r \sim 0.16$).

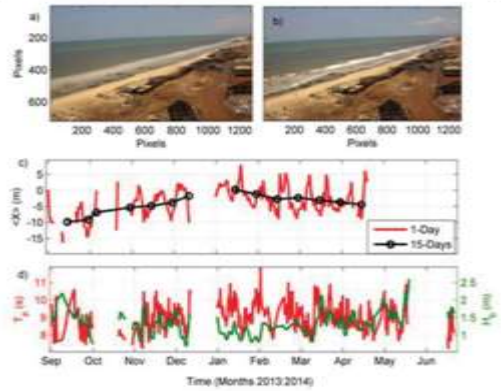

Figure 4. a) Timex b) Snapshot c) Daily (4 point moving average) and 15-Day shoreline locations $<X>$ relative to the initial position $<X_i>$ d) estimated H_b and T_p from video.

At the monthly scale, waves showed large correlation ($r = 0.87$) with $<X>$ and $\Delta(X)$ than tides, TR ($r = -0.57$). This suggests waves have a strong influence on the shoreline location at seasonal scale. $<X>$ correlates with alongshore non-uniformity ($r = 0.3$, significant at 95%) which means errors in $<X>$ decrease with decrease in its values. Though it is too early to conclude, a preliminary recessive change of the beach is envisaged. This is in line with previous studies (Appeaning Addo *et al.*, 2008) who observed an erosion of 1.13 m/yr. along the Accra Coast. Mean beach slope of 0.03 from tides against the horizontal shoreline positions indicates dissipative characteristics based on Wright and Short (1984) classification.

Noteworthy, video-derived beach slopes showed seasonal changes that can be attributed to an adaptation to wave energy modulation: with Ω ranging from 2 (intermediate beach state) in summer to 5 (dissipative) in winter, with steeper and gentle slopes in summer and winter periods

Beach profiles are estimated over a distance of 500 m from camera location and seaward. However, the estimation of topography from video at James town should be further validated using field measurements in order to get more confidence and robust conclusions on beach state evolution and variability.

DISCUSSION AND CONCLUSIONS

On a Ghana coastline of over 550 km presenting a large diversity (embayed and open beaches, sandbarriers, rivermouths) with recurrent shoreline problems, this is the first video system that has been used to continuously collect information on nearshore waves and beach changes.

The predictions of the H_b and T_p from video images and hindcast data are in good agreement, with RMSE of 0.7 and 0.8, respectively. This highlights the accuracy of the video in estimating waves parameters. Shoreline changes at James town show a seasonal response to waves with accretion during the austral summer months (Nov-Jan) and retreat during the winter months. The link between short-term shoreline evolution and waves conditions is less clear, as found at Grand Popo beach, Benin (Bahini, 2015) where short term evolution is attributed to tidal modulation. Overall, beach profile is in more dissipative state than predicted by Wright and Short (1984) classification with the absence of intertidal sandbars as one might expect. Although small, the variability of the beach profile is detectable. The results of the beach profiles show minor features probably due to the presence of small rocks observed around the study area. These rocks are well exposed on the images during low tides.

Beach and shoreline change analysed using video data covering 11 months suggest that breaking wave conditions and intertidal beach morphology can be continuously monitored. The results are consistent with previous findings though we suggest that large number of images be taken to give large seasonal shoreline data and minimise errors. Video deriving wave characteristics and shoreline change from a long-term monitoring perspective proved to be doable along this Ghanaian beach.

ACKNOWLEDGMENTS

The authors give appreciation to the French institute of research for development (IRD), the Office of Naval Research (US-ONR) prioject and Ghana ports and Harbour Authority for their support and also grateful to Benjamin Okyere, Alexander Boateng, Agbemebiase Nunana and Wilson Ako for their

assistance. This research has received support from French grants through French INSU/CNRS EC2CO-LEFE/IRD and ANR (COASTVAR: ANR-14-ASTR-0019).

LITERATURE CITED

Aarninkhof, S.G.J., Turner, I. L., Dronkers, T. D.T. , Caljouw, M., and Nipius, L., 2003. A video-based technique for mapping intertidal beach bathymetry. *Coastal Engineering*, 49, 275–289.

Almar, R, Ranasinghe, R., Catalan, P. A., Senechal, N., Bonneton, P., Roelvink, D., Bryan, K. R., Marieu, V., and Parisot J. P., 2012a. Video-based detection of shorelines at complex meso-macro tidal beaches. *Journal of Coastal Research*, 28(5), 1040-1048.

Almar R, Cienfuegos R, Catalan PA, Michallet H, Castelle B, Bonneton P., and Marieu V., 2012b. A new breaking wave height direct estimation from video. *Coastal Engineering*, 61, 42-48.

Almar, R., Senechal, N., Bonneton, P., 2008. Wave celerity from video imaging: validation with in-situ Pre-ECORS data. *Proc. I. C. C. E.* 1 (5), 661–673.

Angnuureng, D.B., Almar, R., Senechal, N., Castelle, B., Appeaning Addo, K., Marieu, V., and Ranasinghe, R., 2015. Shoreline evolution under sequences of storms from video observation at a meso-macrotidal beach. *Geomorphology with major revision.*

Angnuureng, B. D., Appeaning Addo, K., and Wiafe G., 2013. Impact of sea defense structures on downdrift coasts: The case of Keta in Ghana. *Academia Journal of Environmental Sciences* 1(6), 104-121.

Appeaning Addo, K., Walkden, M., and Mills, J. P., 2008. Detection, Measurement and Prediction of Shoreline Recession in Accra, Ghana. *ISPRS Journal of Photogrammetry and Remote Sensing*, 63(5), 543-558.

Armaroli, C., and Ciavola, P, 2011. Dynamics of a nearshore bar system in the northern Adriatic: A video-based morphological classification. *Geomorphology*, *126*(1), 201-216.

Bahini, A., 2015. Etude par imagerie video de la reponse du Littoral de grand popo benin de 2013 a 2015. Implications pour la stabilite de la plage. CIPMA-Chaire UNESCO, Université d'Abomey-Calavi, M.Sc. Thesis, 21p.

Banno, M., and Kuriyama, Y., 2012. Multiple regression analysis of effects of bar and tide on shoreline change. *The Port and Airport Research Institute,* Kanagawa, 3-1-1, 239-0836.

Boak, E.H., and Turner, I.L., 2005. Shoreline Definition and Detection: A Review. *Journal of Coastal Research,* 21(4), 688–703.

Boateng, I., 2009. Development of Integrated Shoreline Management Planning: A Case Study of Keta, Ghana. *Paper presented at the FIG Working Week 2009.*

French, W. P., 2001. Coastal Defences: Processes, Problems and Solutions. *Psychology Press*, pp 5.

Holman, R.A., and Stanley, J., 2007. The history and technical capabilities of Argus. *Coastal Engineering,* 54, 477 – 491.

Jayson-Quashigah, P. N., Appeaning Addo, K., and Kufogbe, S.K., 2013. Shoreline monitoring using medium resolution satellite imagery, a case study of the eastern coast of Ghana. *Journal of Coastal Research*, 65, 511-516.

Ly, C. K., 1980. The role of the Akosombo Dam on the Volta river in causing coastal erosion in central and eastern Ghana (West Africa). *Marine Geology, 37*(4), 323-332.

Masselink, G., Russell, P., Turner, I., and Blenkinsopp C., 2009. Net sediment transport and morphological change in the swash zone of a high-energy sandy beach from swash event to tidal cycle time scales. *Marine Geology,* 267, 18–35.

Masselink, G., and Short, A., 1993. The Effect of Tide Range on Beach Morphodynamics and Morphology: A Conceptual Beach Model. *Journal of Coastal Research,* 9(3), 785-800.

Plant, N. G., and Holman, R. A., 1997. Intertidal beach profile estimation using video images, *Marine Geology*, 140, 1-24.

Puleo, J.A., Farquharson, G., Fraiser, S.J., and Holland, K.T., 2003. Comparison of optical and radar measurements of surf and swash zone velocity fields. *Journal of Geophysical Research*, *108*(3), 3100-3112.

Ruessink, B. G., Kuriyama, Y., Reniers, A. J. H. M., Roelvink,J. A., and Walstra, D. J. R., 2007. Modeling cross-shore sandbar behavior on the timescale of weeks. *Journalof Geophysical Research,* 112.

Sagoe-Addy, K., and Appeaning Addo, K., 2013. Effect of predicted sea level rise on tourism facilities along Ghana's Accra coast. *Journal of Coastal Conservation and Management.* 17(1), 155-166.

Smith, R. K., and Bryan, K. R., 2007. Monitoring beach face volume with a combination of intermittent profiling and video imagery. *Journal of Coastal Research*, 892-898.

Sterl, A., and Caires, S., 2005. Climatology, variability and extrema of ocean waves- the web-based KNMI/ERA-40 Wave Atlas. *International Journal of Climatology,* 25, 963–977.

Stive, M. J.F.,Aarninkhof, S. G.J., Luc Hamm., Hanson, H., Larson, M., Wijnberg, K. M., Nicholls, R. J., and Capobianco, M., 2002. Variability of shore and shoreline evolution. *Coastal Engineering.* 47, 211–235.

Stockdon, H.F., Sallenger, A.H., List, J.H. and Holman, R.A., 2002. Estimation of shoreline position and change using airborne topographic lidar data. *Journal of Coastal Research,*18(3), 502–513.

Stokes, C, Davidson, M., and Russell P., 2015. Observation and prediction of three-dimensional morphology at a high-energy macrotidal beach. *Geomorphology*, 243,1–13.

The Wamdi Group, 1988. The WAM Model-A Third generation ocean wave prediction model. *Journal of Physical Oceanography,* 18, 1775–1810.

Turner, I.L., and Leatherman,S.P., 1997, Beach Dewatering as a 'Soft' Engineering Solution to Coastal Erosion – History and Critical Review. *Journal of Coastal Research*, 13(4), 1050-1063.

Wiafe G., Boateng I., Addo, A. K., Quashigah, P.N., Ababio S.D. and Laryea S. W., 2013. Handbook of Coastal Processes and Management in Ghana. *The Choir Press*, pp., 274.

Wright, L.D., and Short, A.D., 1984. Morphodynamic variability of surf zones and beaches: A synthesis. *Marine Geology*, 56, 93-118.

6.4.2 Comparing the contribution of H_b, sea level anomaly (*SLA)* and *TR* to shoreline change

James town is a low energy beach coupled with low tide elevations, yet as was seen, shoreline variation can be high. This signifies the interplay of several variables responsible for the variation of the shoreline but the parameters which were investigated here include *SLA*, *TR* and H_b. The *SLA* retrieved from Era-Inerim hindcast ranges from 0.03 to 0.1 m and is dominated by atmospheric pressure variations rather than wind effect as the shelf is narrow and winds are generally weak at this equatorial environment. In percentages, the contribution of these parameters to the variation in shoreline $\Delta(X)$ is provided in table 6.2. Shoreline changes are largely influenced by sea level changes due to atmospheric pressure. The multi-linear regression analyses show that shoreline changes are preferentially explained at daily scale by Sea level Anomaly SLA (derived from wind and inverse barometer, 86%), waves (9%), and tide (5%) but change to 65%, 11 and 24, respectively at monthly scale. Data also shows that at the monthly scale, waves show large cross correlation (r = 0.87) with $\Delta(X)$ than tides, *TR*(r = -0.57). Table 6.2 also suggests waves have a stronger influence on the alongshore non-uniformity than *TR* and SLA on the seasonal scale. The longshore variability is thus influenced by all three at significant levels.

Table 6.2 Contribution of individual parameters (wave height, H_b, tide range, sea level anomaly, SLA due to wind and atmospheric pressure) to the changes in alongshore averaged shoreline and non-unifomity.

	$\langle X \rangle$			$\Delta(X)$		
Parameter / **Different scales**	H_b	*TR*	**SLA**	H_b	*TR*	**SLA**
Monthly scale in %	11	24	65	40	23	37
Daily scale in %	9	5	86	26	6	68

6.5 Conclusions

The predictions of the H_b and T_p from video images and hindcast data are in good agreement. The potential of the video application in estimating wave parameters has been revealed. The variability of the beach profile is detectable from the video images. The profiles that were estimated during this study (in the JCR SI paper) showed the beach might exhibit some dissipative characteristics in contrast to the generally known low-tide terraced state observed at nearby sites (Abessolo et al., 2016), but this has not been validated. Further beach profile evolution analysis is entreated to understand and complement the effect of these parameters. The results show that SLA is dominant at this site. It is recommended that a

long term investigation be done as we hypothesis large influence from the nearby lagoon inlet, wind and pressure induced sea level anomaly which explains over 60 % of observed shoreline changes. Video deriving wave characteristics and shoreline change from a long-term monitoring perspective proved to be possible along the Ghanaian beach and should be applied on other sites.

CHAPTER SEVEN

Conclusions, discussion and perspectives

7.1 General conclusions

7.2 Discussion and perspectives

7.2.1 Scales of variability: linking short event scale to seasonal evolution

7.2.2 Storminess and beach evolution: toward an equilibrium

7.2.3 Role of bathymetry (barred profile and terrace) and tide in modulating wave action

7.2.4 Shoreline change: induced by waves, astronomical or atmospherical tides

7.2.5 Natural and anthropized beach dynamics

7.2.6 Advances in video imagery

Interest of using the full bathymetric/topographic profiles

Toward continuous coastal monitoring in West African

7.2.7 Implications and potential of this thesis for West Africa coastal research and management

7.1 General conclusions

Coastal morphodynamics research faces the current challenge: what are the spatio-temporal scales of shoreline change and the physical processes involved? In this thesis, a methodology to assess shoreline changes at different time scales (storm events, seasonal and interannual) has been developed and applied to Biscarrosse (SW France) and James town (Ghana, Gulf of Guinea), respectively, characteristics of the meso-to-macro tidal high-energy dissipative beaches, typically observed on the French Atlantic coast and the low energy, reflective microtidal beaches, observed on the Gulf of Guinea coast. Video observations of nearshore morphodynamics and hindcasted hydrodynamics (ECMWF EraInterim) from the two sites were analysed. Due to the availability of long video timeseries (6 years of continuous data), Biscarrose was chosen as the main study site and Jamestown (1 year) as a pilot site in West Africa to develop the technique. Following several analysis, the main results indicate that:

- Wave climate is dominated by storms (defined as Hs>5% exceedance threshold) and their seasonal fluctuation of intensity and occurrence, with 75% of storms occurring in winter yielding more than 60 identified storms. Over this period, continuous daily video shoreline monitoring shows that shoreline responds in decreasing order at seasonal, storm event frequency and annual timescales, even though storms are the dominant forcing at Biscarrosse.
- A multi-linear regression on 36 storms shows that whereas current and previous storm intensity play a predominant role on current storm impact, tide and sandbar play a major role in post-storm recovery process rather than on storm impact, by the modulation of the recovery duration.
- An ensemble average on post-storm recovery period shows that Biscarrosse beach recovers rapidly to individual storms (9 days). A clustering of storms also shows that storms in sequence may possibly have a weak cumulative effect.
- The use of EOF method shows good skills in separating uniform and non-uniform shoreline dynamics, even at open beaches, and that they have different temporal variability: first EOF (2D) and second (3D) modes are dominated by seasonal and short term scales, respectively.
- At Jamestown, the water level (astronomical and atmospherical tides) plays a predominant role on shoreline location, compared to a rather continuous wave forcing. Waves and tide estimates from Jamestown video system are in good agreement with hindcasts, which shows that the video technique can be replicated elsewhere in West Africa.

7.2 Discussion and perspectives

7.2.1 Scales of variability: linking short event scale to seasonal evolution

While the shoreline dynamics show variability at several timescales, one major question that is still unanswered is at what timescale a 'modal' beach state should be calculated. While Wright et al. (1985) suggested 30 days of past wave information was sufficient to estimate the current beach state, present results indicate this might be too short and this duration might depend on beach characteristics: dissipative beaches [Davidson et al., 2013; Splinter et al., 2014] are characterised with a long response time, with up to 2000 days of past wave information used to attain the equilibrium state, whereas only 60 days are sufficient at intermediate beaches. The paradox is that most of the shoreline models cannot predict accurately short-term beach response while they perform well at seasonal or longer term. Future work to examine the impact of several model coefficients on timescales of days to weeks using long timeseries data records could improve skills to long-term forecast. This means with the assumption that the modal beach state evolves with the wave conditions, moderating the wave conditions by water levels (modulation breaking by tide morphology) could influence the modal state and certainly improve the short term predictions. This is also supported by the results obtained for Jamestown in this study where short term beach changes are dominated by water level variations rather than waves. To investigate this with further details, the prediction of evolution of alongshore uniform and non-uniform shorelines was tested using equilibrium model [Davidson et al., 2013; Splinter et al., 2014; Stokes et al., 2015], modulating the incident wave power with different tide levels and sandbar locations. Our results show that the inclusion of tides and sandbar in equilibrium beach models could potentially improve understanding and predicting their short-term behaviour. Given that tide and sandbar locations have the potential to dampen the magnitude of wave action, they stand the potential to affect the beach response amplitude and time, and vulnerability to erosion.

7.2.2 Storminess and beach evolution: toward an equilibrium

Our results point out that rather than individual intensity of storms, their recurrence frequency is key: the beach evolves to an energetic equilibrium state under frequent storms. If the interval between two storms is low compared to the recovery period, the beach becomes more resilient to the following storms; the first storm in clusters of storms has larger impact than following ones. In line with previous works [Yates et al., 2009; Castelle et al., 2014], the first winter storms drive the most pronounced erosion because the wave energy disequilibrium and erosion potential are large. During the rest of winter season, even if the beach is often exposed to severe storms, they do not significantly erode the beach as the disequilibrium energy is smaller. However, this is not usually the case as has been observed at other beaches [Ferreira, 2005; Karunarathna et al., 2014] where storm in sequences seem to enhance the impact of storms with a

cumulative effect. Considering variable recurrence frequency, longer storm intervals enhance storm impact. The storm impact will also decrease if the frequency of storms evolves under changing climate, or under regional modes of climate variability [e.g. NAO; Masselink et al., 2015]. As part of the perspectives, the influence of tide variation and sandbars in the cluster study could improve the understanding of storm recurrence effect. The discussion above indicates that the resilience of the beach much depends on the previous state which is related to the interval of storm recurrence and it also stresses the fact that storm studies are still not standardized, but site specific.

7.2.3 Role of bathymetry (barred profile and terrace) and tide in modulating wave action

Tide influence is important for morphodynamics when *RTR* increases due to its control over incoming wave. The presence of double sandbar on the meso-to-macrotidal Biscarrosse beach induces a threshold on wave energy [Senechal et al., 2015] at the shore by height limitation due to breaking over the sandbar which modifies onshore wave energy and frequencies: the magnitude of shoreline change may be highly controlled by the conjugated effect of sandbar and tide [Senechal et al., 2002; Almar et al., 2010; Stokes et al., 2015]. Furthermore, in our study the control of sandbar on the upper beach was observed to increase when migrating toward the shore. The large alongshore non-uniformity of the shoreline could also reflect the signature of the crescentic shape of the sandbar through an intensified coupling [Castelle et et al., 2010; Castelle et al., 2015]. At low-tide terraced micro-tidal beaches such as Jamestown, tide controls wave height limitation by breaking over the terrace [Miles and Russel, 2004; Almeida et al., 2016]. Interestingly, incoming wave energy at the shore is becoming almost independent to offshore wave conditions, making the upper beach morphodynamics to be predominantly controlled by tide (cycle neap to spring tide, [Abessolo et al., 2016]).

7.2.4 Shoreline change: induced by waves, astronomical or atmospherical tides

Shoreline location is also affected at different magnitudes by variations of sea level induced by waves (setup) and other components such as astronomical and atmospherical tides previously given. Wave-induced setup can cause an increase in water level elevations on the order of 20–50% of the offshore breaking wave height [Dean and Walton, 2009]. Results in this thesis indicate that wave-induced setup influences the shoreline extracttion on the range of 2 to 12 m (6 m in the horizontal). Whereas at mid-latitude wave-dominated coasts, wave components have a predominant influence on the location of the shoreline, this might not be the case elsewhere like in tropical environments (e.g. Jamestown) where the sea level at the shore can be predominantly modulated by atmospherical tides (pressure and wind) and long term trends (thermal expansion). This might vary at the scale considered (event, seasonal, interanual), as pointed out recently by Melet et al. [2016] at Cotonou, Bénin. Long term shoreline wave

equilibrium energy models [e.g. Yates et al., 2009] that currently don't account for this slow variation of sea level should be revised in this sense, using a mixture of both waves and sea level variation, to overcome the Brunn rule application [Ranasinghe et al., 2012]. The study further stresses the importance of tides in generating currents that are important in moulding bar-beach topography in macrotidal settings (and not just in modulating water levels that affect bar height and wave dissipation). This is plausible with such a long video data set and requires detail investigation.

7.2.5 Natural and anthropized beach dynamics

Beaches are dynamic but human interests are static. The morphodynamics and influence of anthropogenic factors are not discussed in this thesis. However, the two studied sites are anthropized and this might influence beach behaviour. For example, sand mining is reported in Ghana, which induces sediment loss while beach nourishment is done along Biscarrosse beach. The impact of nourishment or artificial stabilization with geotextiles and dune fixation also affects the evolution [Dean and Dalrymple, 2002; Van den Berg et al., 2010]. In particular, beach nourishment introduces a perturbation to the nearshore system subsequently modified by natural forces in both the cross-shore and longshore directions [Dean and and Dalrymple, 2002]. Van den Berg et al.[2010] found that the nourished shoreline retreats initially due to cross-shore transport because the nourished profile was steeper than the equilibrium profile. It can also cause development of alongshore irregularities and when a dominant littoral drift is present, the nourishment can also migrate. Urbanization/fixation of the dune makes it less potential to mobilize sand to the beach during major storms [Dean and and Dalrymple, 2002; Almar et al., 2009]. For instance, between the natural Truc Vert beach and anthropized Biscarrosse beach, which are only 50 km apart, response to storms is different despite similar forcing conditions. Almar et al., 2009 observe that Biscarrosse beach sandbar is more static compared to the rapid migration at Truc Vert probably because of the upper beach fixation at Biscarrosse. This suggests that when a beach loses its mobility, it might also lose the capacities of resilience to extreme events and adapatation to changing storm regimes.

7.2.6 Advances in video imagery

Interest of using the full bathymetric/topographic profiles

Beach sedimentary system extends from the dune at a point beyond the depth of closure; the shoreline being a small piece of the puzzle. The extraction of full bathymetric/topographic profiles from video [e.g. Lippmann and Holman, 1989; Plant and Holman, 1997; Stockdon and Holman, 2000; Almar et al., 2011] rather than single shoreline could provide useful information on the three dimensional behavior of the

beach. Coastal measured data (bathymetry, time-series of waves, coastal use levels, etc.) have often been difficult for policy-makers to obtain and use, given the high costs involved and difficulties in their application and interpretation. In cases where data are available, it is important that it is sufficiently complete to monitor changes that occur from few days up to several years [Osorio et al., 2012]. Extracting topography from video images allows a better understanding of the overall beach behavior such as the beach state [Peron and Senechal, 2011; Ba and Senechal, 2013] and sediment availability [Stive et al., 2013; Balouin et al., 2016], which is more insightful than shoreline for coastal management and research. Moreover, further investigation on applying bathymetries obtained from video on nearshore modeling is suggested to address the potential and limitation of such an approach. Offshore waves can be substantially different from nearshore waves, in particular for unknown shelf bathymetry or complex irregular coast, like in embayed beaches [Abessolo et al., 2016]. In this sense, using video-derived estimate has major interest. To test this feasibility, in this thesis, we have compared video estimation of wave parameters (height and periods) with local hindcast (Abessolo et al., 2016; Angnuureng et al., 2016). In addition, video has been used to extract water levels (tide and longer components, Abessolo et al., 2016) in order to get climate mode signatures, tide components and more local influences. The importance of water level has been outlined above. Throughout this thesis, from the French Atlantic coast to the Gulf of Guinea, it can be noticed that tide gauge stations are scarce and distant stations are used, which affect the accuracy of the analyses, in particular at Biscarrosse where the Arcachon lagoon tidal gauge is used, inducing phase and amplitude bias.

Toward continuous coastal monitoring in West African

At James town beach, only a single camera was mounted to monitor the beach. Throughout this study, it is shown that video systems can measure numerous hydrodynamic and morphodynamic parameters. This remote sensing technique is cheaper and safer than deploying in-situ instruments. In line with the present work, there is a need to create a network of video stations along the coastline of West Africa. So far, only three stations are established, in Ghana, Senegal and Benin, and important results were obtained at these sites [e.g Almar et al., 2015; Abessolo et al., 2016; Angnuureng et al., 2016]. Further effort is required for the validation of most of the morphodynamic and hydrodynamic parameters that are extracted from the video images. For example, only a field experiment (Almar et al., 2014) was conducted at Grand Popo, Bénin, in order to validate video estimates. At Jamestown, it was possible to extract topographic profiles (Figure 7.1) but the validity of these results could not be tested due to lack of beach survey. An important application with the video system is through structure from motion aerial photography, which is a photogrammetric method for creating three-dimensional models of a feature or topography from

overlapping two-dimensional photographs taken from many locations and orientations to reconstruct the photographed scene [Green, 2012]. This method could enhance the use of the video techniques.

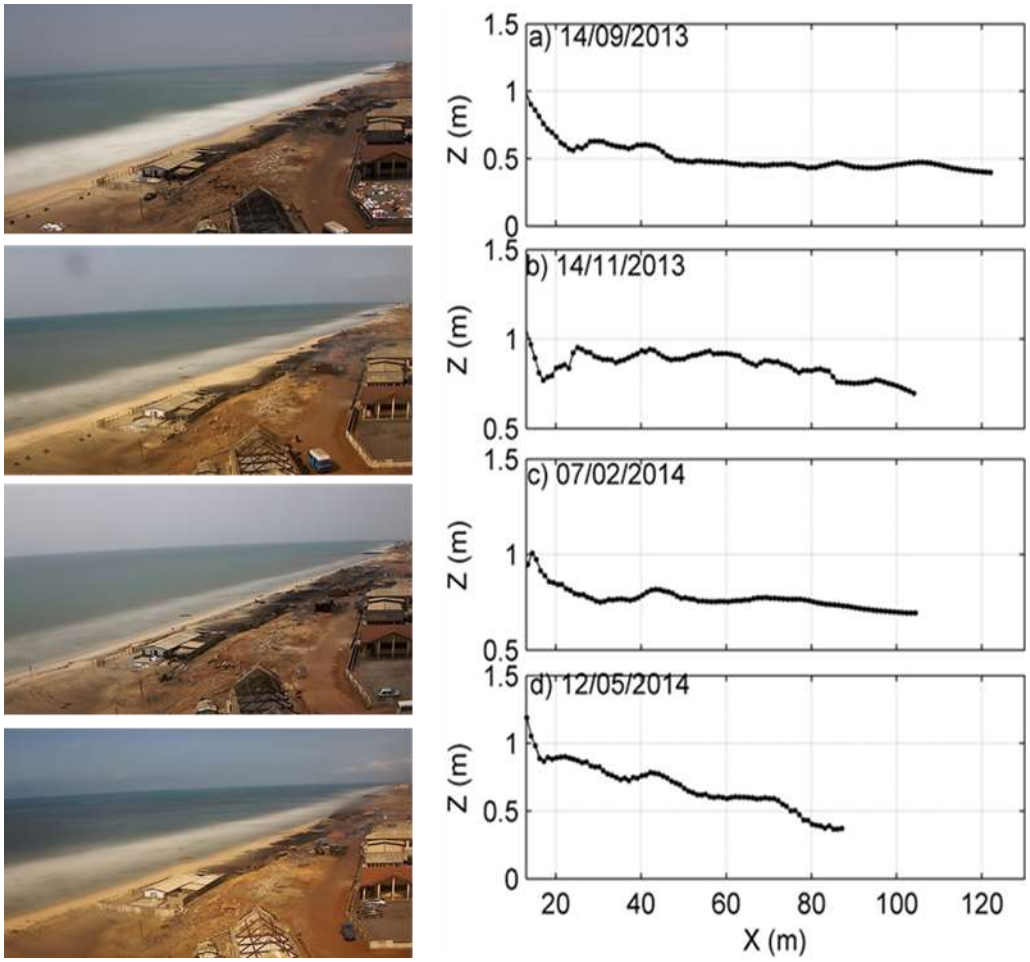

Figure 7.1. Schematic for beach profiles from James tow video images. In a) beach slope is 0.003 with narrow beach b) slope is 0.002 while wide beach is observed c) the slope is 0.0018 with very narrow beach and d) the steepest slope is 0.0081 with a wider beach.

7.2.7 Implications and potential of this thesis for West Africa coastal research and management

As part of the IRD - ARTS (‘Allocations de Rercherche pour une Thèse au Sud’) programmes, and that of the French Embassy in Ghana, designed to strengthen research capacities in West Africa and developing countries, this study is relevant to refining integrated coastal zone management strategies. This work contributes initially to the effort of coastal observation identified as a priority in the coastal scientific community in West Africa. It is anticipated that with some of the tools produced in this study, a video database for coastal management could be mapped as done by other programmes. For instance, WACOM

(MOLOA), in collaboration with IUCN, collects and provides information on coastal evolution and forcing in West Africa: in particular, the vulnerability of these zones to natural hazard and exacerbated anthropization. It is therefore proposed that coastal monitoring programmes provide quality and continuous information for integrated coastal zone management and guidelines for local/regional policy makers in these developing stations. For example, developing early warning systems throughout the coast to inform fishermen and coastal communities on extreme sea state, risk of flooding and erosion. This can be achieved soon with the propagation of the video-derived real time information through the sponsor of MOLOA/Convention d'Abidjan (UEMOA). It is also necessary to build upon a more integrated coastal observation network, maintained over long term, which is a challenge in West Africa, in order to assess the response of this stretch of coast, with all its diversity and regional climate changes.

This low-cost video system intended to complement standard survey tools, although has the additional benefit of enabling the continuous monitoring of beach meso-scale process (spatial temporal scales in the order of km and years) also has the potential to introduce significant amount of errors. The developmnt of the video system is based on terrestrial photogrammetric techniques that involves about three main steps i) camera calibration where the internal camera parameters are determined in the laboratory using open-source software ii) the development of image correction subroutines, which aimed to correct the relatively large image distortions induced by camera optics; this procedure is revealed to be essential as the system is built upon standard non-metric surveillance cameras and iii) the development of image rectification subroutines to transform oblique images into planview images, based on external camera orientation parameters obtained in the field through the surveying of ground control proints. Also, as previously mentioned, the proxies used in the extraction of shoreline also have the potential to be influenced largely due to the video way of extraction. At the moment, to have robust results it is proposed that the video techniques are substantiated with other methods.

BIBLIOGRAPHY

Aagaard, T., J. Nielsen and B. Greenwood. Suspended sediment transport and nearshore bar formation on a shallow intermediate-state beach. *Marine Geology,* 148, 203–225, 1998.

Aarninkhof, S.G. J., I.L. Turner, D.T. Dronkers, M. Caljouw and L. Nipius. A video-base technique for mapping intertidal beach bathymetry. *Coastal Engineering,* 49 (4), 275–289, 2003.

Abessolo Ondoa, G., R. Almar, E. Kestenare, A. Bahini, G-H. Houngue, J. Jouanno, Y. Du Penhoat, B. Castelle, A. Melet, B. Meyssignac, E. Anthony, R. Laibi, G. Alory and R. Ranasinghe. Potential of video cameras in assessing event and seasonal coastline behaviour: a case study at Grand Popo, Benin (Gulf of Guinea). *Journal of Coastal Research,* SI, 75, 442-446, 2016.

Almar, R. E. Kestenare, J. Reyns, J. Jouanno, E.J. Anthony, R. Laibi, M. Hemer, Y. Du Penhoat and R. Ranasinghe. Response of the Bight of Benin (Gulf of Guinea, West Africa) coastline to anthropogenic and natural forcing, Part1: Wave climate variability and impacts on the longshore sediment transport, *Continental Shelf Research*, 110, 48-59,2015.

Almar, R., P. Catalan, R. Ibaceta, C. Blenkinsopp, R. Cienfuegos, M. Villagran, J. C. Aguilera, B. Castelle. Swash zone based reflection during energetic wave conditions at a dissipative beach: toward a wave-by-wave approach. *Coastal Engineering Proceedings, 1*(34), 2014, doi:http://dx.d oi.org/10 .9753/icce.v34.currents.34.

Almar, R., R. Ranasinghe, P. A. Catalan, N. Senechal, P. Bonneton, D. Roelvink, K. R. Bryan, V. Marieu and J. P. Parisot. Video-based detection of shorelines at complex meso-macro tidal beaches. *Journal of Coastal Research*, 28(5), 1040-1048, 2012a. *http://dx.doi.org/10.2112/JCOASTRES-D-10-00149.1*

Almar, R., R. Cienfuegos, P. A. Catalan, H. Michallet, B. Castelle, P. Bonneton and V. Marieu. A new breaking wave height direct estimation from video. *Coastal Engineering*, 61, 42-48, 2012b.

Almar, R., B. Castelle, G. Ruessink, N. Senechal, P. Bonneton and V. Marieu. Two and three-dimensional double-sandbar system behaviour under intense wave forcing and a meso–macro tidal range. *Continental Shelf Res*earch, 30 (7), 781-792, 2010.

Almar, R., B. Castelle, B.G. Ruessink, N. Senechal, P. Bonneton and V. Marieu. High-frequency video observation of two nearby double-barred beaches under high-energy wave forcing. *Journal Coastal Research*, SI 56 (2), 1706–1710, 2009.

Almar, R., N. Senechal and P. Bonneton. Wave celerity from video imaging: validation with in-situ Pre-ECORS data. *Proc. I.C.C.E.* 1 (5), 661–673, 2008.

Anfuso, G., L. Dominguez and F.J. Gracia. Short and medium-term evolution of a coastal sector in Cadiz, SW Spain. *Catena,* 70, 229 – 242, 2007.

Angnuureng, D. B., R. Almar, K. Appeaning Addo, N. Senechal, B. Castelle, S. W. Laryea, G.Wiafe. Video observation of waves and shoreline change on the microtidal James town Beach in Ghana. *Journal of Coastal Research*, S.I, 75, 1022 – 1026, 2016.

Angnuureng, D. B., R. Almar, N. Senechal, B. Castelle, K. Appeaning Addo, V. Marieu and R. Ranasinghe. Shoreline evolution under sequences of storms from video observation at a meso-macrotidal beach, *in revision with Geomorphology*.

Angnuureng, D. B., K. Appeaning Addo and G. Wiafe. Impact of sea defense structures on downdrift coasts: The case of Keta in Ghana. *Academia Journal of Environmental Sciences* 1(6), 104-121, 2013.

Anthony, E. J., N. Marrinerb and C. Morhangea. Human influence and the changing geomorphology of Mediterranean deltas and coasts over the last 6000 years: From progradation to destruction phase? *Earth science reviews*, 139, pp. 336-361, 2014.

Apotsos, A., B. Raubenheimer, S. Elgar and R. T. Guza. Wave-driven setup and alongshore flows observed onshore of a submarine canyon, J. Geophys. Res., 113, 2008, C07025, doi:10.1029/2007JC004514.

Appeaning-Addo, K. Shoreline morphological changes and the human factor: Case study of Accra Ghana. *Journal of coastal conservation,* 17 (1), 85-91, 2013.

Appeaning-Addo, K. and E. Lamptey. Innovative Technique of Predicting Shoreline Change in Developing Countries: Case of Accra Erosion and Causal Factors. *Coastal Hazards*, 1000, 367-402, 2012.

Appeaning Addo, K., M. Walkden and J. P. Mills. Detection, Measurement and Prediction of Shoreline Recession in Accra, Ghana. *ISPRS Journal of Photogrammetry and Remote Sensing*, 63(5), 543-558, 2008, doi:10.1016/j.isprsjprs.2008.04.001.

Armaroli, C. and P. Ciavola. Dynamics of a nearshore bar system in the northern Adriatic: A video-based morphological classification. *Geomorphology*, *126*(1), 201-216, 2011.

Armah, A. K. and D.S. Amlalo. Coastal Zone Profile of Ghana. Accra, Gulf of Guinea Large Marine Ecosystem Project. Ministry of Environment, Science and Technology, 1998.

Ba, A. and N. Senechal. Extreme winter storm versus summer storm: morphological impact on a sandy beach, *Journal Coastal Research,* SI 65, 648-653, 2013.

Bahini, A. Etude par imagerie video de la reponse du Littoral de Grand Popo Benin de 2013 à 2015. Implications pour la stabilité de la plage. CIPMA-Chaire UNESCO, Université d'Abomey-Calavi, M.Sc. Thesis, 21p, 2015.

Balouin, Y., F. Longueville and Y. Colombet. Video assessment of nearshore and beach evolution following the deployment of a geotextile wave breaker. In: Vila-Concejo, A.; Bruce, E.; Kennedy, D.M., and McCarroll, R.J. (eds.), Proceedings of the 14th International Coastal Symposium (Sydney, Australia). *Journal of Coastal Research,* SI 75, 617-621, 2016.

Special Issue, No. 75, pp. 617-621. Coconut Creek (Florida), ISSN 0749-0208. Bauer, E. Interannual changes of the ocean wave variability in the North Atlantic and in the North Sea. *Climate Research*, 18, 63–69, 2001.

Banno, M. and Y. Kuriyama. Multiple regression analysis of effects of bar and tide on shoreline change. *The Port and Airport Research Institute,* Kanagawa, 3-1-1, 239-0836, 2012.

Battjes, J. A. Surf similarity. *Proceedings of the 14th Coastal Engineering Conference,* 466-480, 1974.

Beckley, B. D., F. G. Lemoine, S. B. Luthcke, R. D. Ray and N. P. Zelensky. A reassessment of global and regional mean sea level trends from TOPEX and Jason-1 altimetry based on revised reference frame and orbits, *Geophysical Research Letters,* VOL. 34, L14608, 2007, doi:10.1029/2007GL030002.

Becker, J. M., Y. L. Firing, J. Aucan, R. Holman, M. Merrifield and G. Pawlak. Video-based observations of nearshore sand ripples and ripple migration. VOL. 112, C01007, doi:10.1029/2005JC003451, 2007

Blake, E. S., C. W. Landsea, E. J. Gibney. The Deadliest, costliest and most Intense United States Tropical Cyclones from 1851 to 2010 (And Other Frequently Requested Hurricane Facts) (NOAA Technical Memorandum NWS NHC-6). US-NOAA National Weather Service, National Hurricane Center, 2011.

Birkemeier, W. A. Time scales of nearshore profile changes. *A. M. ASCE*, 1984.

Birrien, F., B. Castelle, D. Dailloux, V. Marieu, D. Rihouey and T.D. Price. Video observation of megacusp evolution along a high-energy engineered sandy beach: Anglet, SW France. *Journal Coastal Research,* SI 65, 1727–1732, 2013.

Blossier, B., K. R. Bryan, and C. Winter. Simple pocket beach rotation model derived from linear analysis, *Proceedings of the Coastal Sediments*, edited by P. Wang, J. D. Rosati, and J. Cheng, San Diego, USA, 1 - 13, 2015.

Boateng, I. Development of Integrated Shoreline Management Planning: A Case Study of Keta, Ghana. *Paper presented at the FIG Working Week 2009.*

Boateng, I. Shoreline Management Planning: Can It Benefit Ghana? A Case Study of UK SMPs and Their Potential Relevance in Ghana, 2006.www.fig.net/resources/proceedings/fig_proceedings/ accra/papers/ts16/ts16_04_boateng.pdf. Accessed on 06/05/2016.

Boak, E. and H I. L. Turner. Shoreline definition and detection: A review. *Journal Coastal Research,* 21(4), 688–703, 2005.

Brooks, H. E. Severe thunderstorms and climate change. Atmospheric Research, 123, 129–138, 2013. doi:10.1016/j.atmosres.2012.04.

Bruneau, N., X. Bertin, B. Castelle and P. Bonneton. Tide-induced flow signature in rip currents on a meso-macrotidal beach. *Ocean Modelling*, 74, 53–59, 2014.

Bruneau, N., B. Castelle, P. Bonneton, R. Pedreros, R. Almar, N. Bonneton, P. Bretel, J. Parisot and N. Senechal. Field observations of an evolving rip current on a meso-macrotidal well-developed inner bar and rip morphology. Cont. Shelf Res. 29, 1650–1662, 2009. http://dx.doi.org/ 10.1016/j.csr.2009. 05.005.

Brunel, C. and F. Sabatier. Potential influence of sea-level rise in controlling shoreline position on the French Mediterranean Coast. *Geomorphology*, 107(1-2), pp.47–57,2009.

Brunn, P. Design and Construction of Mounds for Breakwaters and Coastal Protection, Developments *in Geotechnical Engineering*, 37, pp 802, 1985.

Butel, R., H. Dupuis and P. Bonneton. Spatial variability of wave conditions on the French Aquitanian coast using in-situ data. *Journal of Coastal Research,* SI 36, 96–108, 2002.

Callaghan, D. P., P. Nielsen, A. Short, R. Ranasinghe. Statistical simulation of wave climate and extreme beach erosion. *Coastal Engineering,* 55(5), 375–390, 2008.

Castelle, B., V. Marieu, S. Bujan, K.D. Splinter, A. Robinet, N. Senechal and S. Ferreira. Impact of the winter 2013-2014 series of severe Western Europe storms on a double-barred sandy coast: beach and dune erosion and mega cusp embayments. *Geomorphology* 238, 135-148, 2015.

Castelle, B., V. Marieu, S. Bujan, S. Ferreira, J. P. Parisot, S Capo, N. Senechal, and T. Chouzenoux. Equilibrium shoreline modelling of a high-energy meso-macrotidal multiple-barred beach. *Marine Geology, 347, 85-94,* 2014.

Castelle, B., B.G. Ruessink, P. Bonneton, V. Marieu, N. Bruneau and T.D. Price. Coupling mechanisms in double sandbar systems, part 2: impact on alongshore variability of inner-bar rip channels. *Earth Surface Processes and Landforms,* 35, 771–781,2010.

Castelle, B., P. Bonneton, H. Dupuis, and N. Senechal. Double bar beach dynamics on the high-energy meso-macrotidal French Aquitanian Coast: A review, *Marine Geology*, 245, 141-159, 2007a.

Castelle, B., I.L. Turner, B.G. Ruessink, R.B. Tomlinson. Impact of storms on beach erosion: Broadbeach (Gold Coast, Australia), *Journal Coastal Research*, SI 50, 534 – 539, 2007b.

Castelle, B, Modélisation de l'hydrodynamique sédimentaire au-dessus des barres sableuses soumises à l'action de la houle : application à la côte Aquitaine. PhD thesis, Université de Bordeaux, pp. 35-45, 2004.

Cazenave, A., H. Dieng, B. Meyssignac, K. von Schuckmann, B. Decharme, E. Berthier. The rate of sea-level rise, *Nature Climate Change*, 4, 358–361, 2014, doi: 10.1038/nclimate2159.

Charles, E., D. Idier, J. Thiebot, G. L. Cozannet, R. Pedreros, F. Ardhuin and S. Planton. Present wave climate in the bay of Biscay: spatiotemporal variability and trends from 1958 to 2001. *Journal of Climate,* 25, 2020-2035, 2012. DOI: 10.1175/JCLI-D-11-00086.1

Choowong, M., S. Phantuwongraj, T. Charoentitirat, V. Chutakositkanon, S. Yumuang and P. Charusiri. 2009. Beach recovery after 2004 Indian Ocean tsunami from Phang-nga, Thailand, *Geomorphology*, 104, 134–142

Ciavola, P., C. Armaroli, J. Chiggiato, A. Valentini, M. Deserti, L. Perini, P. Luciani. Impact of storms along the coastline of Emilia-Romagna: the morphological signature on the Ravenna coastline (Italy). *Journal Coastal Research*, SI 50, 540-544, 2007.

Coco, G, N. Senechal, A. Rejas, K.R. Bryan, S. Capo, J.P. Parisot, J.A. Brown, J.H.M. MacMahan. Beach response to a sequence of extreme storms. *Geomorphology* 204, 493–501, 2014.

Coco, G. and A. Brad Murray. Patterns in the sand: From forcing templates to self-organization. *Geomorphology,* 91, 271– 290, 2007.

Coco, G., G. Payne, K.R. Bryan, D. Rickard, D. Ramsay and T. Dolphin. The use of imaging systems to monitor shoreline dynamics. Paper presented at 1st *International Conference on Coastal Zone management and Engineering* in the Middle East, Dubai, United Arab Emirates, 2005.

Cook, D. O. The occurrence and geological work of rip currents off southern California. *Marine Geology*, 9,173-186, 1970.

Cooper, J.A.G. and O.H. Pilkey. Sea-level rise and shoreline retreat: time to abandon the Bruun Rule. *Global Planetal Change*, 43 (3–4), 157–171, 2004a.

Cooper, J.A.G., D.W.T. Jackson, F. Navas, J. McKenna and G. Malvarez. Identifying storm impacts on an embayed, high-energy coastline: examples from western Ireland. Marine Geology 210, 1–4, 261–280, 2004.

Corbella, S. and D. D. Stretch. Shoreline recovery from storms on the east coast of Southern Africa. *Nat. Hazards Earth Syst. Sci.* 12, 11–22, 2012.

Crowell, M., S.P. Leatherman and M.K. Buckley. Historical Shoreline Change: Error Analysis and Mapping Accuracy. *Journal of Coastal Research*, 7,3, pp. 839-852,1991.

Cowell, P.J., M.J.F. Stive, A.W Niedoroda, D.J.P. Swift, H.J. De Vriend, M.C. Buijsman, R.J. Nicholls, P.S. Roy, G.M. Kaminsky, A.J. Clevering, C.W. Reed and P.L. De Boer. The coastal-tract (part 2): applications of aggregated modeling to lower-order coastal change. *Journal of Coastal Research,* 19, (4), 828-848, 2003.

Davidson, M. A., K.D. Splinter and I.L. Turner. A simple equilibrium model for predicting shoreline change. *Coastal Engineering,* 73, 191–202, 2013.

Davidson, M. A. and I. L. Turner. A behavioral template beach profile model for predicting seasonal to interannual shoreline. *Journal of Geophysical Research,* 114, 2009, F01020, doi: 10.1029/2007JF000888.

Davidson, M. A., T. J. O'Hare and K. J. George. Tidal Modulation of Incident Wave Heights: Fact or Fiction? *Journal Coastal Research,* 24 (2), 151 – 159, 2008.

Davidson-Arnott, R. An Introduction to Coastal Processes and Geomorphology, Cambridge University press, pp 52-112, 2010.

Davies, J. L. A morphogenic approach to world shorelines. *Zeitschrift fur Geomorphology,* 8, Mortensen Sonderheft, pp. 127-142,1964.

Davis, R. A. Beach and nearshore zone. In: DAVIS, R.A. (ed.), *Coastal Sedimentary Environments*, New York: Springer-Verlag, 379-444, 1985.

Davis, R. A., W.T. Fox, M.O. Hayes and J.C. Boothroyd. Comparison of ridge and runnel systems in tidal and non-tidal environments. *Journal of Sedimentary Petrology* 42, 413-421, 1972.

Dean, R. G. and T.L. Walton Jr. Wave Setup, Chapter 1, Handbook of Coastal and Ocean Engineering. In: *Kim, Y.C. (Ed.), World Scientific Press, Hackensack, N.J.,* 2009.

Dean, R. G. and R.A. Dalrymple. Coastal Processes with Engineering Applications. Cambridge University Press, United Kingdom, 2002.

Dean, R. G. Equilibrium beach profiles: characteristics and applications. *Journal of Coastal Research* 7(1), 53–84, 1991.

Dissanayake, P., J. Brown and H. Karunarathna. Impacts of storm chronology on the morphological changes of the Formby beach and dune system, UK. *Nat. Hazards Earth Syst. Sci.* 15, 1533–1543, 2015.

Dodet, G., X. Bertin and R. Taborda. Wave climate variability in the North-East Atlantic Ocean over the last six decades. *Ocean Modelling*, 31, 120–131, 2010.

Dolan, R., B.P. Hayden and J. Heywood. A new photogrammetric method for determining shoreline erosion. *Coastal Engineering*, 2(1), 21–39, 1978.

Dolan, R., B.P. Hayden, P. May, S. May. The reliability of shoreline change measurements from aerial photographs. *Shore and Beach*, 48(4), 22-29, 1980.

Dolan, R., B. Hayden and J. Heywood. Analysis of coastal erosion and storm surge hazards. *Coastal Engineering*, 2, 41-53, 1978.

Dolan, R., R. Davis. An intensity scale for Atlantic coast northeast storms. *Journal Coastal Research,* 8(4), 840–853, 1992.

Douglas, B. C., M. Crowell. Long-term shoreline position prediction and error propagation. *Journal of Coastal Research,* 16(1), 145–152, 2000.

Dorsch, W., T. Newland, D. Tassone, S. Tymons and D. Walker. A statistical approach to modeling the temporal patterns of ocean storms. *Journal of Coastal Research*, 24 (6), 1430-1438, 2008.

Dupuis, H., D. Michel, A. Sottolichio. Wave climate evolution in the Bay of Biscay over two decades. *Journal of Marine Systems,* 63, 105–114, 2006.

Fairley, I., M. Davidson, K. Kingston, T. Dolphin, and R. Phillips. Empirical orthogonal function analysis of shoreline changes behind two different designs of detached breakwaters. *Coastal Engineering*, 56, (11–12), 1097-1108, 2009.

Falques, A., G. Coco and D. A. Huntley. A mechanism for the generation of wave-driven rhythmic patterns in the surf zone, *Journal of Geophysical Research*, 105(C10), 24,071–24,088, 2000.

Fenster, M. S., R. Dolan and R.A. Morton. Coastal storms and shoreline change: signal or noise? *Journal Coastal Research*, 17(3), 714–720, 2001.

Ferreira, O. Storm groups versus extreme single storms: predicted erosion and management consequences. *Journal Coastal Research*, SI 42, 221–227, 2005.

Finkl, C. Potential impacts of a federal policy promoting ‘‘No new beach replenishment activities’’ on U.S. shorelines: iterations from SE Florida. In:Proceedings of the 1996 National Conference on Beach Preservation Technology (St. Petersburg, Florida), pp. 281–296.

Fisher, J. and M. Overton. Interpretation of shoreline position from aerial photographs. *Proc. 24th Coastal Engineering Conference (ASCE)*, 1998–2003, 1994.

Flater, D, 2010. *www.wXtide32.com*. Last accessed on 25/01/2016.

Fletcher, C. H., R.A. Mullane, and B.M. Richmond. Beach loss along armored shorelines on Oahu, Hawaiian Islands. *Journal of Coastal Research*, 13(1), 209–215, 1997.

Folorunsho, R. Meteorologically induced storm surge in the gulf of guinea: consequences on coastal resources and infrastructure. *Nigerian Institute for Oceanography and Marine research*, Nigeria, 1995.

Frazer, L. N., T. R. Anderson and C. H. Fletcher. Modeling storms improves estimates of long- term shoreline change. *Geophysical Research Letters* 36, L20404, 2009.

French, W. P. Coastal Defences: Processes, Problems and Solutions. *Psychology Press*, pp 5, 2001.

Gallagher, E. L., S. Elgar, R.T. Guza. Observations of sandbar evolution on a natural beach. *Journal of Geophysical Research*, 103, 3203–3215, 1998.

Galgano, F. A. Shoreline behavior along the atlantic coast of delaware. *Middle States Geographer*, 41:74-81, 2008.

Galgano, F.A. and B.C. Douglas. Shoreline position prediction: methods and errors. *Environmental Geosciences*, 7 (1), 1-10, 2000.

Galvin, C.J. Jr., Breaker Type Classification on Three Laboratory Beaches, Journal of Geophysical Research, 73(12), 3651, 1968.

Geng, Q. and M. Sugi. Possible Change of Extratropical Cyclone Activity due to Enhanced Greenhouse Gases and Sulfate Aerosols-Study with a High-Resolution AGCM. 16, 2262-2274, 2003.

Geng, Q. and M. Sugi. Variability of the North Atlantic cyclone activity in winter analyzed from NCEP–NCAR reanalysis data. *Journal of Climate*, 14, 3863–3873, 2001.

Genz, A. S., C. H. Fletcher, R. A. Dunn, L. N. Frazer and J. J. Rooney. The predictive accuracy of shoreline change rate methods and alongshore beach variation on Maui, Hawaii. *Journal Coastal Research,* 23 (1) 87–105, 2007.

Gilbert, J. and P. Vellinga. Coastal Zone Management. *Climate Change: The IPCC Response Strategies,* pp. 133-158, 1990.

Gourlay, M. Beaches: profiles, processes and permeability. *Coastal Engineering Proceedings*, 1(17), 2011. doi:http://dx.doi.org/10.9753/icce.v17.%

Grasso, F., H. Michallet, E. Barthélemy and R. Certain. Physical modeling of intermediate cross-shore beach morphology: Transients and equilibrium states. *Journal of Geophysical Research,* 114, 2009, C09001.

Green, S. Structure from motion as a tool for arachaeology, MSc thesis, University College London, 128 p., 2012

Grunnet, N. M., and B.G. Ruessink. Morphodynamic response of nearshore bars to a shoreface nourishment. *Coastal Engineering,* 52, 119-137, 2005.

Guannel, G. and H. T. Özkan-Haller. Formulation of the undertow using linear wave theory. *Physics of Fluids*, 26, 056604, 2014. doi: 10.1063/1.4872160.

Guedes, R. M.C., L. J. Calliari, K. T. Holland, N. G. Plant, P.S. Pereira, F. N.A. Alves. Short-term sandbar variability based on video imagery: Comparison between Time–Average and Time–Variance techniques. *Marine Geology,* 289, 122–134, 2011.

Guza, R. T. and F. Feddersen. Effect of wave frequency and directional spread on shoreline runup. *Geophysical Research Letters*, VOL. 39, L11607, 2012. doi:10.1029/2012GL051959.

Hansen, J.E., P.L. Barnard. Sub-weekly to interannual variability of a high-energy shoreline. *Coastal Engineering*, 57, 959–972, 2010.

Hansen, J. E. and P. L. Barnard. The observed relationship between wave conditions and beach response, Ocean beach, San Francisco, CA. *Journal of Coastal Research,* 56,1771-1775, 2009.

Hanson, H. and N. Kraus. Generalized model for simulating shoreline change, Report 1, Technical Reference, Tech. Rep., U. S. Army Engineer Waterways Experiment Station; Coastal Engineering Research Center (U. S.); USACE, 1989.

Hapke, C. J., and M. Christiano. Long-term and Storm-related Shoreline Change Trends in the Florida Gulf Islands National Seashore. *US Geological Survey Open-file Report 2007-1392;* 18, 2007.

Harley, M. D, I. L. Turner, A. D. Short and R. Ranasinghe. A reevaluation of coastal embayment rotation: The dominance of cross-shore versus alongshore sediment transport processes, Collaroy-Narrabeen beach, southeast Australia. *Journal of Geophysical Research,* 116(F4), F04033, 2011.

Hoefel, F. and S. Elgar. Wave-Induced Sediment Transport and Sandbar Migration. *Science,* 299, 1885, 2003; DOI: 10.1126/science.1081448

Holland, K. T., R.A. Holman and T.C. Lippmann. Practical use of video imagery in neareshore oceanographic field studies. *IEEE J. Oceanic Engineering,* 22(1), 81-92, 1997.

Holman, R, and M. Haller. Remote sensing of the nearshore. *Annual Review of Marine Science,* 113, 5-95, 2013.

Holman, R. A. and J. Stanley. The history and technical capabilities of Argus. *Coastal Engineering,* 54, 477 – 491, 2007.

Holman, R. A., A. H. Sallenger, T. C. Lippmann and J. W. Haines, The application of video image processing to the study of nearshore processes. *Oceanography,* 6, 3, 1993.

Horrillo-Caraballo, J.M. and D.E. Reeve. A comparison of the performance of Canonical Correlation Analysis on sand and shingle beaches, Marine Geology, 274, p120-134, 2010.

Iribarren, C.R. and C. Nogales. Protection des Ports, Section II, Comm. 4, XVIIth Int. Nav. Congress, Lisbon, p. 31-80, 1949.

Idier D, B. Castelle, E. Charles and C. Mallet. Longshore sediment flux hindcast: spatio-temporal variability along the SW Atlantic coast of France. *Journal of Coastal Research,* SI 65 1785-1790, 2013.

IPCC, Climate Change. The Physical Science Basis. Contribution of Working Group I to the Fifth Assessment Report of the Intergovernmental Panel on Climate Change, 2013. doi:10.1017/CBO9781107415324.

Jayson-Quashigah, P. N., K. Appeaning Addo and S.K. Kufogbe. Shoreline monitoring using medium resolution satellite imagery, a case study of the eastern coast of Ghana. *Journal of Coastal Research*, 65, 511-516, 2013.

Karunarathna, H., D. Pender, R. Ranasinghe, A. D. Short, D. E. Reeve. The effects of storm clustering on beach profile variability. *Marine Geology,* 348 103–112, 2014.

Karunarathna, H., D.E. Reeve and M. Spivack. Beach profile evolution as an inverse problem. *Continental Shelf Research,* 29, 2234–2239, 2009.

Kaminsky, G. and N. C. Kraus. Evaluation of the depth limited breaker criteria, in Ocean Wave Measurement and Analysis, *Am. Soc. Civ. Eng., Reston, Va,* pp. 180–193, 1994.

Kingston, K.S. Applications of complex adaptive systems, approaches to coastal systems. Plymouth, UK: University of Plymouth, PhD thesis, 106 p, 2003.

Kraus, N.C., M. Larson and D.L. Kriebel. Evaluation of Beach Erosion and Accretion Predictors. *Proc. Coastal Sediments'*91, ASCE, 572-587, 1991.

Kriebel, D.L. and R.G. Dean. Convolution method for time dependent beach-profile response. *Journal of Waterway, Port, Coastal, and Ocean Engineering* (ASCE), 119(2), 204-226, 1993.

Lafon, V, H. Dupuis, H. Howa, J. M. Froidefond,. Determining ridge and runnel longshore migration rate using spot imagery. *Oceanologia Acta,* 25, 149–158, 2002.

Larson, M., L. X. Hoan and H. Hanson. Direct Formula to Compute Wave Height and Angle at Incipient Breaking. *M.ASCE*, 2010. doi: 10.1061/ (ASCE)WW.1943-5460.0000030.

Laugel, A., M. Menendez, M. Benoit, G. Mattarolo, F. Mendez. Wave climate projections along the French coastline: dynamical versus statistical downscaling methods. Ocean Modell. 84, 35–50, 2014. doi:10.1016/j.ocemod.2014.09.002.

Leatherman, S.P. Historical and projected shoreline mapping. Proceedings of the Coastal Zone ’83 (San Diego, California), 2902–2910, 1983.

Lee, G. H., R. J. Nicholls, W. A. Birkemeier. Storm-driven variability of the beach-nearshore profile at Duck, North Carolina, USA, 1981–1991. *Marine Geology,* 148(3):163–177, 1998.

Lee, I. C., B. Wu and R. Li. Shoreline Extractionfrom the Integration of LiDAR Point Cloud Data and Ortophototos Using Mean Shift Segmentation. *ASPRS Conference,* Maryland, 2009.

Leith, C.E. Standard error of time-average estimates of climate means. Journal of Applied Meteorology, 12,1066-1069, 1973.

Lemke, L., J.K. Miller, A. Gorton and E. Livermont. EOF analysis of shoreline changes following an alternative beachfill within a groin field, *Proc. 34th International Conference on Coastal Engineering,* pp. 12, 2014.

Leuliette, E. W., R. S. Nerem and G. T. Mitchum. Results of TOPEX/Poseidon and Jason-1 calibration to construct a continuous record of mean sea level. *Marine Geodesy*, 27, 79–94, 2004.

Li, R., R. Ma and K. Di. Digital Tide-Coordinated Shoreline. *Journal of Marine Geodesy*, 25, 1, 27-36, 2002.

Lippmann, T. C. and R. A. Holman. The spatial and temporal variability of sand bar morphology. *Journal of Geophysical Research,* 95, 11575–11590, 1990.

Lippmann, T. C. and R.A. Holman. Quantification of Sandbar Morphology: A Video Technique Based on Wave Dissipation. *Journal of Geophysical Research,* 94, 995-1011, 1989.

List, J.H. and A.S. Farris . Large-scale shoreline response to storms and fair weather. *Proceedings of the Coastal Sediments ’99* (Long Island, New York), pp. 1324–1337, 1999.

Lotze, H. K., H. S. Lenihan and B. J. Bourque. Depletion, degradation, and recovery potential of estuaries and coastal seas. *Science,* 312: 1806–1809, 2006.

Loureiro, C., O. Ferreira and J.A.G. Cooper. Geologically constrained morphological variability and boundary effects on embayed beaches. *Marine Geology,* 329–331, 1–15, 2012.

Luceno, A., M. Menendez and F. J. Mendez. The effect of temporal dependence on the estimation of the frequency of extreme ocean climate events. Proceedings of the Royal Society A. 462, 1683–1697, 2006.

Ly, C. K. The role of the Akosombo Dam on the Volta River in causing coastal erosion in central and eastern Ghana (West Africa). *Marine Geology, 37*(4), 323-332, 1980.

Komar, P. Beach Processes and Sedimentation, 2nd ed., Prentice Hall, 544 pp., 1998.

Maa, J. P.-Y., C.H. Hobbs III and C.S. Hardaway Jr. A criterion for determining the impact on shorelines caused by altering wave transformation. *Journal of Coastal Research*, 17(1), pp. 107-113, 2001.

Madsen, A. J., N. G. Plant. Intertidal beach slope predictions compared to field data. *Marine Geology*, 173, 121-139, 2001.

Martinez, M.L., A. Intralawan, G. Vazquez, O. Prez-Maqueo, P. Sutton and R. Landgrave. The coasts of our world: Ecological, economic and social importance. *Ecological Economics*, 63(2-3), 254–272,2007.

Maspataud, A., M-H. Ruz and A. Hequette. Spatial variability in post-storm beach recovery along a macrotidal barred beach, southern North Sea. *Journal of Coastal Research*, 56, 88-92, 2009.

Masselink, G., T. Scott, T. Poate, P. Russell, M. Davidson and D. Conley. The extreme 2013/14 winter storms: hydrodynamic forcing and coastal response along the southwest coast of England. *Earth Surface Processes and Landforms*, 10.1002/esp.3836, 1096-9837, 2016.

Masselink, G. and S. van Heteren. Response of wave-dominated and mixed-energy barriers to storms. *Marine Geology***,** 352, pp. 321–347, 2014.

Masselink, G., P. Russell, I. Turner and C. Blenkinsopp. Net sediment transport and morphological change in the swash zone of a high-energy sandy beach from swash event to tidal cycle time scales. *Marine Geology*, 267, 18–35, 2009.

Masselink, G., A. Kroon, R.G.D. Davidson-Arnott. Morphodynamics of intertidal bars in wave-dominated coastal settings- A review. *Geomorphology*, 73, 33–49, 2006.

Masselink, G. and C.B. Pattiaratchi. bSeasonal changes in beach morphology along the sheltered coastline of Perth, Western Australia. *Marine Geology*, 172, 243–263,2001.

Masselink, G., A.D. Short. The effect of tide range on beach morphodynamics and morphology: a conceptual beach model. *Journal Coastal Research*, 9(3), 785–800, 1993.

May, S. K., W.H. Kimball, N. Grady and R. Dolan. CEIS: The Coastal Erosion Information System. *Shore and Beach*, 50, 19-26, 1982.

McKenzie, P. Rip-current systems. *Journal of Geology*, 66, 103-113, 1958.

Meade, R. H. and J.A. Moody. Causes for the decline of suspended-sediment discharge in the Mississippi River system, 1940–2007. *Hydrological Processes*, 24, pp. 35–49, 2010.

Melet, A., R. Almar, B. Meyssignac. What dominates sea level at the coast: a case study for the Gulf of Guinea . *Ocean Dynamics*, 66:623–636, 2016.

Mendoza, E. T., J. A. Jimenez, J. Mateo. A coastal storms intensity scale for the Catalan sea (NW Mediterranean). *Natural Hazards Earth System Science*, 11, 2453–2462, 2011.

Miller, J. K., R.G. Dean. Shoreline variability via empirical orthogonal function analysis: Part I temporal and spatial characteristics. *Coastal Engineering*, 54, 111 – 131, 2007a.

Miller, J. K., and R. G. Dean. Shoreline variability via empirical orthogonal function analysis: Part II relationship to nearshore conditions, *Coastal Engineering*, 54(2), 133-150, 2007b.

Miller, J. K. and R. G. Dean. A simple new shoreline change model. *Coastal Engineering,* 51, 531–556, 2004.

Moore, L.J., P. Ruggiero, J.H. List. Comparing mean high water and high water line shorelines: should proxy-datum offsets be incorporated in shoreline change analysis? *Journal Coastal Research,* 22 (4), 894–905, 2006.

Moore, L.J. Shoreline Mapping Techniques. *Journal of Coastal Research,* 16, 1, 111-124, 2000.

Morton, R. A., J. C. Gibeaut and J. G. Paine. Meso-scale transfer of sand during and after storms: implications for prediction of shoreline movement, Marine Geology, 126, 161–179, 1995.

Morton, R. A., J. G. Paine, and J. G. Gibeaut. Stages and durations of post-storm beach recovery, southeastern Texas coast, USA. J. Coast. Res. 10:884–908, 1994.

Morton, R. A., M.P. Leacht, J.G. Painet and M.A. Cardozat. Monitoring beach changes using GPS surveying techniques. *Journal Coastal Research*, 9 (3), 702-720, 1993.

National Research Council. Managing Coastal Erosion. Washington, D.C.: *National Academy Press*, 182p, 1990a.

North, G. R., T. L. Bell, R. F. Cahalan and F. J. Moeng. Sampling errors in the estimation of empirical orthogonal functions. *Monthly Weather Review*, 110(7), 699-7606, 1982.

Osorio, A.F., R. Medina and M. Gonzalez. An algorithm for the measurement of shoreline and intertidal beach profiles using video imagery: PSDM. *Computers and Geosciences*, 2012, doi:10.1016/j.cageo.2011.12.008

Pajak, M.J. and S.P. Leatherman. The high water line as shoreline indicator. Journal of Coastal Research, 18(2), 329–337, 2002.

Pape, L. Predictability of nearshore sandbar behavior. Thesis, Netherlands Geographical Studies, Utrecht University, The Netherlands, 2010.

Pape, L. and B. G. Ruessink. Multivariate analysis of nonlinearity in sandbar behavior. *Nonlinear Processes Geophysics,* 15, 145–158, 2008.

Pearre, N. S. and J. A. Puleo. Quantifying Seasonal Shoreline Variability at Rehoboth Beach, Delaware, Using Automated Imaging, *Journal of Coastal Research*, 25 (4), 900 – 914, 2009.

Peron, C. and N. Senechal. Dynamic of a meso to macro-tidal double barred beach: inner bar response. *Journal of Coastal Research,* SI 64, 120-124, 2011.

Pianca, C., R. Holman and E. Siegle. Shoreline variability from days to decades: Results of long-term video imaging. *Journal of Geophysical Research, Oceans* 120, 2159–2178, 2015. doi: 10.1002/2014JC010329.

Pinto, J. G., T. Spangehl, U. Ulbrich and P. Speth. Assessment of winter cyclone activity in a transient ECHAM4-OPYC3 GHG experiment. *Meteor,* Z., 15, 279–291, 2006.

Plant, N. G., S. G. J. Aarninkhof, I. L. Turner and K. S. Kingston. The performance of shoreline detection models applied to video imagery, *Journal Coastal Research*, 23(3), 658-670, 2007.

Plant, N. G., M. H. Freilich and R. A. Holman The role of morphologic feedback in surf zone sand bar response, *J. Geophys. Res.*, 106, 973–990, 2001.

Plant, N. G, R. A. Holman, M. H. Freilich and W. A. Birkemeier. A simple model for interannual sandbar behavior. *Journal of Geophysical Research,* 104(C7), 15755-15776, 1999.

Plant, N. and R. Holman. Extracting morphologic information from field data. *Coastal Engineering Proceedings* 1(26), 1998. doi:http://dx.doi.org/10.9753/icce.v26.

Plant, N. G. and R. A. Holman. Intertidal beach profile estimation using video images. *Marine Geology,* 140, 1-24, 1997.

Pradjoko, E. and H. Tanaka. Aerial photograph of Sendai Coast for shoreline behavior analysis. *Coastal Engineering Proceedings, 1*(32), 2010, doi:http://dx.doi.org/10.9753/icce.v32.sediment.92

Pruszak, Z., R. Ostrowski and J. Schönhofer. Variability and correlations of shoreline and dunes on the southern Baltic coast (CRS Lubiatowo, Poland), Oceanologia 53, 1, Pages 97–120, 2011.

Price, T. D. and B.G. Ruessink. Observations and conceptual modelling of morphological coupling in a double sandbar system. *Earth Surface Processes and Landforms,* 38, 477-489, 2013.

Price, T. D. and B.G. Ruessink. State dynamics of a double sandbar system. *Continental Shelf Research,* 31, 659–674, 2011.

Puleo, J. A., G. Farquharson, S.J. Fraiser and K. T. Holland. Comparison of optical and radar measurements of surf and swash zone velocity fields. *Journal of Geophysical Research*, *108*(3), 3100-3112, 2003.

Ranasinghe, R., T.M. Duong, S. Uhlenbrook, D. Roelvink and M.J.F. Stive. Climate change impact assessment for inlet-interrupted coastlines. *Nature Climate Change*, 3. 1, pp. 83–87, 2013.

Ranasinghe, R., D. Callaghan and J.A. Roelvink. "Does a more sophisticated storm erosion model improve probabilistic erosion estimates?" *In: Proceedings of 7th International Conference on Coastal Dynamics. Bordeaux, France*, pp. 1277 – 1286, 2013.

Ranasinghe, R., R. A. Holman, M. A. de Schipper, T. C. Lippmann, J. Wehof, T. Minh Duong, D. Roelvink and M.J.F. Stive. Quantification of nearshore morphological recovery time scales using Argus video imaging: Palm Beach, Sydney and Duck, NC. *Coastal Engineering Proceedings*, 1(33), 24, 2012.

Ranasinghe, R., D. Callaghan and M.J.F. Stive. Estimating coastal recession due to sea level rise: beyond the Bruun rule. *Climatic Change,* 110 (3–4), 561–574, 2012.

Ranasinghe, R. and M. J. F. Stive. Rising seas and retreating coastlines. *Climatic Change*, 97, 465–468, 2009.

Ranasinghe, R., G. Symonds, K. Black and R. Holman. Morphodynamics of Intermediate Beaches: A Video Imaging and Numerical Modelling Study. *Coastal Engineering,* 51, 629-655, 2004.

Rangel-Buitrago, N. and G. Anfuso. An application of Dolan and Davis (1992) classification to coastal storms in SW Spanish littoral. *Journal of Coastal Research*, SI64 (*Proceedings of the 11th International Coastal Symposium*), Szczecin, Poland, 0749-0208, 2011.

Reeve, D. E., A. Pedrozo-Acuña and M. Spivack. Beach memory and ensemble prediction of shoreline evolution near a groyne. *Coastal Engineering,* 86, 77–87, 2014.

Rihouey, D. and Ph. Maron. Empirical eigenfunction analysis of long-term bathymetric data along the beaches of Anglet. *Transactions on the Built Environment,* vol. 70, 1743-3509, 2003.

Rosen, P. S. Increasing Shoreline Erosion Rates with Decreasing Tidal Range in the Virginia Chesapeake Bay. *Chesapeake Science* 18(4), 383-386, 1977.

Ruessink, B. G., Y. Kuriyama, A. J. H. M. Reniers, J. A. Roelvink and D. J. R. Walstra. Modeling cross-shore sandbar behavior on the timescale of weeks. *Journal of Geophysical Research,* 112, 2007.

Ruessink, B. G., K. M. Wijnberg, R. A. Holman, Y. Kuriyama and I. M. J. van Enckevort. Intersite comparison of interannual nearshore bar behavior. *Journal of Geophysical Research* 108, 3249, 2003.

Ruessink, B.G. and A. Kroon. The behaviour of a multiple bar system in the nearshore zone of Terschelling: 1965–1993. *Marine Geology,* 121, 187–197, 1994.

Ruggiero, P. Is the Intensifying Wave Climate of the U.S. Pacific Northwest Increasing Flooding and Erosion Risk Faster Than Sea-Level Rise? *Journal of Waterway, Port, Coastal, and Ocean Engineering,* 139(2), pp.88–97, 2013.

Ruggiero, P., G. M. Kaminsky, G. Gelfenbaum and B. Voigt. Seasonal to interannual morphodynamics along a high-energy dissipative littoral cell. *Journal of Coastal Research*, 21, 553–578, 2005.

Ruggiero, P., J. Cote, G. Kaminsky and G. Gelfenbaum. Scales of variability along the Columbia River littoral cell. *Coastal Sediments '99* (Long Island, New York, ASCE), pp. 1692-1707, 1999.

Sallenger, A. H. Storm impact scale for barrier islands. *Journal of Coastal Research,* 16, 890-895, 2000.

Saffir, H. Design and construction requirements for hurricane resistant construction. *American Society of Civil Engineers, ASCE Preprint* No. 2830, New York, 20 pp., 1977.

Sagoe-Addy, K. and K. Appeaning Addo. Effect of predicted sea level rise on tourism facilities along Ghana's Accra coast. *Journal of Coastal Conservation and Management*. 17(1), 155-166, 2013.

Scavia, D., J. C. Field, D. F. Boesch, R. W. Buddemeier, V. Burkett, D. R. Cayan, M. Fogarty, M. A. Harwell, R. W. Howart, C. Mason and others. Climate change impacts on U.S. coastal and marine ecosystems. *Estuaries,* 25(2):149-64, 2002.

Svendson, I.B. Introduction to nearshore hydrodynamics. *World Scientific*, pp. 229-263, 2006.

Senechal, N., G. Coco, B. Castelle and V. Marieu. Storm impact on the seasonal shoreline dynamics of a meso- to macrotidal open sandy beach (Biscarrosse, France), *Geomorphology*, 228, 448–4, 2015.

Senechal, N., T. Gouriou, B. Castelle, J.-P. Parisot, S. Capo, S. Bujan and H. Howa. Morphodynamic response of a meso- to macro-tidal intermediate beach based on a long-term data set. *Geomorphology*, 107, 263–274, 2009.

Senechal, N., P. Bonneton and H. Dupuis. Field experiment on secondary wave generation on a barred beach and the consequent evolution of energy dissipation on the beach face. *Coastal Engineering*, 46, 233–247, 2002.

Shepard, F. P. Beach cycles in Southern California. U.S. Army Corps of Engineers, Beach erosion board technical memorandum, 20, 26 pp, 1950.

Shepard, F. P. and D. L. Inman. Nearshore circulation. *Proc. 1st Conf. Coast. Eng.* ASCE, 50-59, 1951.

Shi, F., F. Cai, J. T. Kirby, J. Zheng. Morphological modeling of a nourished bayside beach with a low tide terrace. *Coastal Engineering, 78, 23–34,* 2013.

Short, A. D. and G. Masselink. Embayed and structurally controlled embayed beaches, in Handbook of Beach and Shoreface Morphodynamics, edited by A. D. Short, *Wiley Chichester*, pp. 230–250, 1999.

Small, C. and R.J. Nicholls. A global analysis of human settlement in coastal zones. Journal of Coastal Research, 19 (3), 584–599, 2003.

Smith, R. K. and K. R. Bryan. Monitoring beach face volume with a combination of intermittent profiling and video imagery. *Journal of Coastal Research*, 892-898, 2007.

Smit, M. W. J., S.G.J. Aarnikhof, K.M. Wijberg, M. Gozalez, K.S. Kingston, H.N. Southgate, G. Ruessink, R.A. Holman, E. Siegle, M. Davidson, R. Medina. The role of video imagery in predicting daily to monthly coastal evolution. *Coastal Engineering*, 54, 539–553, 2007.

Sonu, C. J. Three-dimensional beach changes. *Journal of Geology*, 81, 42 – 64,1973.

Sonu, C. J. Collective movement of sediment in littoral environment. *Journal of Coastal Engineering*, 24, 373 – 400, 1968.

Spencer, T., M. Schuerch, R. J. Nicholls, J. Hinkel, D. Lincke, A.T. Vafeidis, R. Reef, L. McFadden and S. Brown. Global coastal wetland change under sea-level rise and related stresses: The DIVA Wetland Change Model, *Global and Planetary Change*, 139, 15–30, 2016.

Splinter, K. D., J.T. Carley, A. Golshani and R. Tomlinson. A relationship to describe the cumulative impact of storm clusters on beach erosion. *Coastal Engineering*, 83, 49–55, 2014a.

Splinter, K. D., I. L. Turner, D. A. Davidson, P. Barnard, B. Castelle and J. Oltman-Shay. A generalized equilibrium model for predicting daily to inter-annual shoreline response. *Journal of Geophysical Research- Earth Surface*, 119, 1936-1958, 2014b.

Splinter, K. D., I. L. Turner and M. A. Davisdson. How much data is enough? The importance of morphological sampling and duration for calibration of empirical shoreline models. *Coastal Engineering*, 77, 14-27, 2013.

Sterl, A. and S. Caires. Climatology, variability and extrema of ocean waves- the web-based KNMI/ERA-40 Wave Atlas. *International Journal of Climatology*, 25, 963–977, 2005.

Stive, M.J.F., M. de Schipper, A. Luijendijk, R. Ranasinghe, J. van Thiel de Vries, S. Aarninkhof, C. van Gelder-Maas, S. de Vries, M. Henriquez and S. Marx. The Sand Engine: A Solution For Vulnerable Deltas In The 21st Century? , 2013, *uuid:3d2037f0-001b-4426-8c0e-463df9dd78ed*

Stive, M. J.F., S. Aarninkhof, G.J. Luc Hamm., H. Hanson, M. Larson, K. M. Wijnberg, R. J. Nicholls and M. Capobianco. Variability of shore and shoreline evolution. *Coastal Engineering.* 47, 211–235, 2002.

Stive, M.J.F., J.A. Roelvink and H.J. De Vriend. Large-scale coastal evolution concept. The Dutch Coast. *Proc. 22nd Int. Conf. on Coastal Engineering*, ASCE, New York, vol. 9, pp. 1962–1974,1990.

Stockdon, H.F., A. H. Sallenger Jr., R.A. Holman and P.A. Howd. A simple model for the spatially-variable coastal response to hurricanes. *Marine Geology*, 238, 1–20, 2007.

Stockdon, H. F., R.A. Holman, P.A. Howd and A.H. Sallenger Jr. Empirical parameterization of setup, swash and runup. *Coastal Engineering*, 53, 573-588, 2006.

Stockdon, H.F, A.H. Sallenger Jr., J.H. List and R.A. Holman. Estimation of shoreline position and change using airborne topographic lidar data. *Journal Coastal Research*, 18(3), 502–513, 2002.

Stockdon, H.F. and R.A. Holman. Estimation of wave phase speed and nearshore bathymetry from video imagery. Journal of Geophysical Research C9 (105), 22,015–22,033, 2000..

Stokes, C., M. Davidson and P. Russell. Observation and prediction of three-dimensional morphology at a high-energy macrotidal beach. *Geomorphology* 243, 1–13, 2015.

Stokes, C.H., P. Russell, D. Conley, E. Beaumont and D. Greaves. Exploring Monthly To Seasonal Beach Morphodynamics Using Empirical Orthogonal Functions. In: Conley, D.C., Masselink, G., Russell, P.E. and O'Hare, T.J.(eds.), Proceedings 12thInternational Coastal Symposium(Plymouth, England), *Journal of Coastal Research*, S.I. 65, pp.1868-1873, 2013.

Svendsen, I. A. and V. Putrevu. Surf-zone hydrodynamics. *In Adv. Coastal Ocean Engineering, 2*, 1-72, 1996.

Takeda, I. and T. Sunamura. Conditions for beach erosion on a barred beach. *Geomorphology*, 36, pp. 453–464, 1992.

Thieler, E.R. and W.W. Danforth. Historical shoreline mapping (I): improving techniques and reducing positioning errors. Journal of Coastal Research, 10(3), 549–563, 1994.

The Wamdi Group. The WAM Model-A Third generation ocean wave prediction model. *Journal of Physical Oceanography*, 18, 1775–1810, 1988.

Thornton, E.B., J.H. MacMahan and A.H. Sallenger Jr. Rip currents, mega-cusps, and eroding dunes. *Marine Geology,* 240, 151-167, 2007.

Tolman, H.L. A third generation model for wind waves on slowly varying, unsteady and inhomogeneous depths and currents. *Journal of Physical Oceanography* 21, 782–797, 1991.

Turki, I., R. Medina and M. Gonzalez. Beach memory. In: *McKee Smith, Jane (Ed.), Proceedings of the 33rd International Conference*, *World Scientific,* Santander, Spain, 2012.

Turner, I., V. Leyden, G. Symonds, J. McGrath, A. Jackson, T. Jancar, S. Aarninkhof and I. Elshoff. Comparison of observed and predicted coastline changes at the Gold Coast artificial (surfing) reef, Sydney, Australia. In: *Proceedings of the International Conference on Coastal Engineering*, Sydney, 2001.

Turner, I. L. and S.P. Leatherman. Beach Dewatering as a 'Soft' Engineering Solution to Coastal Erosion – History and Critical Review. *Journal of Coastal Research*, 13(4), 1050-1063, 1997.

United Nations (UN) Atlas of the Oceans. Human Settlements on the Coast, 2010. URL: http://www.oceansatlas.org (Uses Human Settlements on the Coast) (accessed August 9th, 2015).

Verhagen, H.J. Sand waves along the Dutch coast. Coastal Eng., 13, 129–147, 1989.

van de Lageweg, W.I., K.R. Bryan, G. Coco and B.G. Ruessink. Observation of shoreline–sandbar coupling on an embayed beach. *Marine Geology*, 344, 101–114, 2013.

van Gent, M.R.A., J.S.M. van Thiel de Vries, E.M. Coeveld, J.H. de Vroeg and J. Van de Graaff. Large-scale dune erosion tests to study the influence of wave periods. *Coastal Engineering*, 55, 1041–1051, 2008.

van Enckevort, I.M.J. and B.G. Ruessink. Video observations of nearshore bar behaviour. Part 1: alongshore uniform variability. *Continental Shelf Research* 23, 501–512, 2003.

van Enckevort, I.M.J. and B.G. Ruessink. Effect of hydrodynamics and bathymetry on video estimates of nearshore sandbar position. *J Journal of Geophysical Research*, 106 (C8), 16969–16979, 2001.

Vousdoukas, M. I, L., P. M. Almeida and Ó. Ferreira. Beach erosion and recovery during consecutive storms at a steep-sloping, meso-tidal beach. Earth Surface Processes Landforms, 37, 583 – 593, 2012.

Walstra, D.J.R., A.J.H.M. Reniers, R. Ranasinghe, J.A. Roelvink and B.G. Ruessink. On bar growth and decay during interannual net offshore migration. *Coastal Engineering*, 60, 190-200, 2012. doi:10.1016/j.coastaleng.2011.10.00

Walton, T. L. J. and R. G. Dean. Landward limit of wind setup on beaches. *Ocean Engineering*, 36 (9-10), 763-766, 2009.

Watanabe, A. and M. Dibajnia. A numerical model of wave deformation in surf zone, Proc. 21st Int. Conf. on CoastalEng., ASCE, pp. 578-587, 1988.

Watanabe, A. and K. Maruyama. Numerical modeling of nearshore wave field under combined refraction, diffraction and breaking, Coastal Engineering in Japan, JSCE, Vol. 29, pp. 19-39,1986.

Wang, P., B.A. Ebersole and E. R. Smith. Longshore Sand Transport – Initial Results from Large-Scale Sediment Transport Facility. *USACE, ERDC/CHL CHETN-II-46*, 2002.

Wang, X. and V. Swail. Trends of atlantic wave extremes as simulated in a 40-yr wave hindcast using kinematically reanalyzed wind fields. *Journal of Climate,* 15, 1020–1035, 2001.

Wang, X., W. Wang and C. Tong. A review on impact of typhoons and hurricanes on coastal wetland ecosystems, *Acta Ecologica Sinica*, 36, 1, pp 23–29, 2016.

Weaver, R. and D. Slinn. Influence of bathymetric fluctuations on coastal storm surge. Coastal Engineering, 57 (1):62–70, 2010, doi:10.1016/j.coastaleng.2009.09.012.

Wellens-Mensah, J., A.K. Armah, D.S. Amlalo, and R.K. TettehCoastal zone profile of Ghana: unpublished report on Ghana to global international water (giwa) association, oceanography department, University of Ghana, 2001.

Wiafe, G, I. Boateng, K. Appeaning Addo, P.N. Quashigah, S.D. Ababio and S. W. Laryea. Handbook of Coastal Processes and Management in Ghana. *The Choir Press*, pp., 274, 2013.

Winant, C.D. and D.G. Aubrey. Stability and Impulse Response of Empirical Eigenfunctions. Proceedings of the 15th International Conference on Coastal Engineering. ASCE Publishing, New York, NY, pp. 1312 – 1325, 1976.

Winant, C.D., D.L. Inman and C.E. Nordstron. Description of seasonal beach changes using empirical eigenfunctions, *Journal of Geophysical Research,* 80 (15), 1979 – 1986, 1975

Woolf, D. K., P.G. Challenor and P.D. Cotton, The variability and predictability of North Atlantic wave climate. *Journal of Geophysical Research*, 107 (C10), 3145, 2002.

Wright, L.D., P. Nielsen, A.D. Short and O. Greenm. Morphodynamics of a macrotidal beach: *Marine Geology*, 50, 97-128, 1982b.

Wright, L.D., A.D. Short, J.D. Boon III, B. Hayden, S. Kimball and J.H. List. The morphodynamic effects of incident wave Groupiness and tide range on an energetic beach, *Marine Geology*, 74, 1-20, 1987.

Wright, L.D., A.D. Short and M.O. Green. Short-term changes in the morphodynamic states of beaches and surf zones: an empirical predictive model. *Marine Geology,* 62, 339-364, 1985.

Wright, L.D. and A.D. Short. Morphodynamic variability of surf zones and beaches: A synthesis. *Marine Geology*, 56, 93-118, 1984.

Yates, M. L., R. T. Guza and W. C. O'Reilly. Equilibrium shoreline response: Observations and modeling. *Journal of Geophysical Research*, 114, 2009.

Zhang, K., B. Douglas and S. Leatherman. Do storms cause long-term beach erosion along the U.S. East Barrier Coast? *The Journal of Geology,* 110(4), 493–502, 2002.

APPENDIX A

Shoreline Evolution under Sequences of Storms From 6-year Video Observation at a Meso-Macrotidal Beach (Wang Ping, Rosati Julie and D Cheng Jun. Proceedings of the Coastal Sediments, 35, 2015. *World Scientific*)

SHORELINE EVOLUTION UNDER SEQUENCES OF STORMS FROM 6-YEAR VIDEO OBSERVATION AT A MESO-MACROTIDAL BEACH

DONATUS BAPENTIRE ANGNUURENG[1], RAFAEL ALMAR[2], NADIA SENECHAL[1], BRUNO CASTELLE[1], KWASI APPEANING ADDO[3], VINCENT MARIEU[1]

1. *UMR EPOC, University of Bordeaux 1/CNRS, Bordeaux, France. donatus.angnuureng@u-bordeaux.fr, b.castelle@epoc.u-bordeaux1.fr, and n.senechal@epoc.u-bordeaux1.fr.*
2. *IRD/UMR, LEGOS, Toulouse, France. rafael.almar@ird.fr*
3. *MAFS/Remote Sensing Laboratory, University of Ghana, P. O. Box LG 99, Accra, Ghana. kappeaning-addo@ug.edu.gh*

Abstract: This paper addresses the impact of individual and sequence of storms on the macro-tidal Biscarrosse beach, SW France, using 6-year video observation, including the influence of tides and sandbar location. Following 5% exceedance of wave heights (*Hs* >3.68 m), over 60 individual storms (>15 a year) are observed. On average, the beach shows 9 days of recovery from post-storm beach state to prior-to-storm state. Results suggest that the most pronounced erosion is caused by first and second storms in clusters while following storms show less impact. Clusters show relatively higher impact (1.12) as encountered for individual storms. Shoreline change is influenced by waves with major erosion occurring mainly at spring tide range and when inner sandbars are distant/far from shore.

Introduction

In the context of climate change and increasing population along the coasts, understanding coastal processes is extremely important for public safety, protection of landowners and resources, and for natural environment conservation. Of primary concern to coastal management is the beach stability as well as its safety. For this reason, it is important to know and understand the beach changes at various spatio-temporal scales.

The alternating occurrence of storms and calm periods cause significant profile changes that vary from severe erosion to post-storm slower recovery. The impact of storms on beaches is complex simply due to the non-linear response of the morphology to the forcing. Indeed, beach response to storms also depends on the previous beach configuration (e.g. Yates et al., 2009; Grasso et al., 2009) and wave history (e.g. Splinter et al., 2014; Senechal et al., 2015; Wright and Short, 1984). Beach vulnerability to the influence of storms found in literature follow diverse ways (e.g. Callaghan et al., 2008; Corbella and Stretch 2012; Splinter, et al., 2014) through conceptual models (Stive et al., 2002), equilibrium models (Yates et al., 2009) and long term versus intensive but short-time data

set (e.g. Plant and Holman 1997; Ranasinghe et al., 2012; Senechal et al., 2015). However, the study of storm impacts on shoreline change has shown different conclusions from cumulative storm analyses (e.g. Karunarathna et al., 2014; Coco et al., 2014; Splinter et al., 2014; Ferreira 2005) that suggest that sequence of storms enhance erosion, to non-cumulative analyses (e.g. Frazer et al., 2009; Davidson et al., 2013) which show that shoreline change is influence by storms of varied magnitudes. Besides, it should be noted that the time interval between successive storms in a storm cluster and the post-storm recovery ability of the beach, which are site-specific characteristics play a significant role in determining the level of beach erosion. The beach recovery period thus varies for different beaches. For instance at the microtidal Palm and Duck beaches, Ranasinghe et al. (2012) observed diverse beach recovery in the order of 5-10 days, enough for the beaches to evolve from their post-storm state to their modal states.

Shoreline and nearshore sandbars are part of the complex nearshore interactive system. Previous studies at Biscarrosse (e.g., Almar et al., 2009; Ba and Sénéchal 2013) primarily focused on sandbar response on the timescales of a cluster of storms down to individual storm, and at Truc Vert focused on shoreline response from days to years (e.g. Castelle et al., 2014; Coco et al., 2014). Although the variability of these coastal features and their connection to environmental factors have been the focus of numerous analyses, the direct interactions between them are yet weakly identified, especially at macrotidal coasts. For example, tides are key to nearshore morphodynamics as they disturb the residence time of wave breaking and swash changes. Also, the duration that certain wave processes take on the sandbar is mainly a function of the tide range (Masselink et al., 2006) which is a matter of tidal ranges. Tide range variation leads to inner bar changes (Almar et al., 2010) which can subsequently influence shorelines.

The present work builds on by estimating the connection among sandbars, tides and shoreline change at this macrotidal barred beach. In this paper, first, beach post-storm recovery duration is estimated; secondly the relative impact of storms and storm clusters (sequence of storms) are compared; and finally the modulation of tides and sandbar on storm impact is explored.

Method

The field site

Biscarosse beach in the southern part of the French Atlantic coast (Figure 1) is exposed to long and relatively energetic swells originating mainly from the W-NW (yearly-averaged significant wave height, Hs = 1.7 m, peak period T_p= 10.3 s). Waves show a seasonal variability with longer and more energetic waves

during winter and less energetic waves during summer. The tidal range with average value of 2.9 m can increase up to 5 m under spring tide conditions. Biscarrosse is an open double-barred beach; the outer bar often exhibits crescentic patterns, while the inner-bar in the intertidal domain commonly exhibits a TBR morphology that can sustain energetic events (e.g. Peron and Senechal 2011). Detailed description of the site is given in literature (Castelle et al., 2007; Senechal et al., 2015; Ba and Senechal 2013).

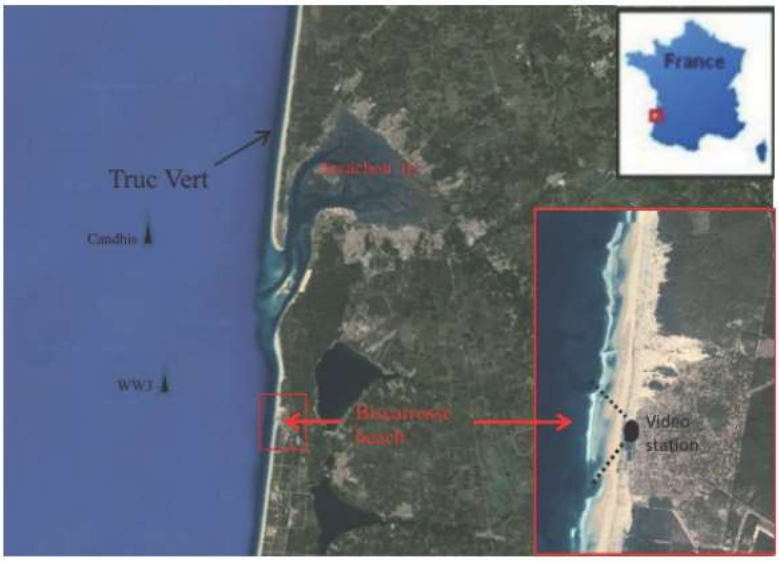

Figure 1. This is a schematic of Biscarrosse beach site showing buoys, video station and Arcachon (tide gauge location).

Storm characterisation

Wave data have been gathered from WW3 model at every 3 hours at the grid point -1°30' W, 44°30' N facing the beach (details are given in Castelle et al., 2014). To further correct this dataset, in-situ measurements collected by the Candhis (National In Situ Swell Records Center) directional wave buoy moored at 50 m water depth (1°26.8'W, 44°39.15' N, Figure 1) is used. The wave energy density (E) is estimated as Hs^2 at each wave event.

In this work, the 5% exceedance probability of wave heights ($Hs_{5\%}$ =3.68 m) is used as a threshold to define storm conditions (see for instance Splinter et al., 2014). A storm is defined as continuous period when wave heights exceed this threshold and lasting at least a tide cycle (12 hrs.) following Dolan and Davis (1992) approach. The analysis is based commonly on local Hs thresholds, the

energy *(I)* and duration of storm waves. The data was used to compute *I* as in equation (1) which takes into consideration only the duration and the maximum storm wave height Hs_{max} that are greater than 3.68 m.

$$I = \int_{t1}^{t2} Hs^2{}_{\max}\, dt \qquad (1)$$

where *t1* and *t2* define the beginning and the end of the storm respectively.

Tidal elevation is extracted from WXtide model. Due to the absence of tide gauge at Biscarrosse, the data are extracted with reference to the closest point which is Arcachon substation at 1°10 W, 44°40 N (Figure 1), 30 km distant from Biscarrosse, pending a phase-lag correction. Tides are extracted at fifteen minute step to correspond with video shoreline data.

Extraction of shoreline location

A shore-based video system has been installed at Biscarrosse beach in April, 2007 by EPOC in collaboration with the New Zealand National Institute of Water and Atmosphere (NIWA). The video station is composed of five color cameras fixed on the top of the foredune at 26 m above the mean sea level (MSL) (Almar et al., 2009). The system provides every 15 min three types of images: instant, cross-shore time stacks and time exposure (timex) images.

10-min timex images are used for the shoreline detection. As done in previous works (e.g. Ba and Senechal 2013; Seneschal et al., 2015) in the same area, 0.45 m above MSL is used as the shoreline proxy to select video images. The images are merged (Figure 2a) and rectified on a 1x1 m grid using conventional photogrametry method (Holland et al., 1997). Shoreline delineation (thick line, Figure 2a) is then performed visually by a human operator to insure a good quality dataset for each image at the specific tidal level (0.45 m +- 0.1 cm). This also ensures that errors due to the selected tidal level (0.45 m) are minimized compared to automated detection. In all, the fifteen-minute shoreline positions used here are obtained by alongshore-averaged cross-shore shoreline locations $<X_s>$ over a length-scale appropriate to the camera coverage to minimize the influence of more localized alongshore variability (e.g. beach cusps). The dataset covers 1038 days in 6 years which is 54.2% of the measurement period (~1 shoreline data every 2 days on average) excluding days when images are of bad quality (e.g. sun glint, fog) and discarded. On the whole, accuracy on alongshore-averaged cross-shore shoreline location $<X_s>$ is about 6 m.

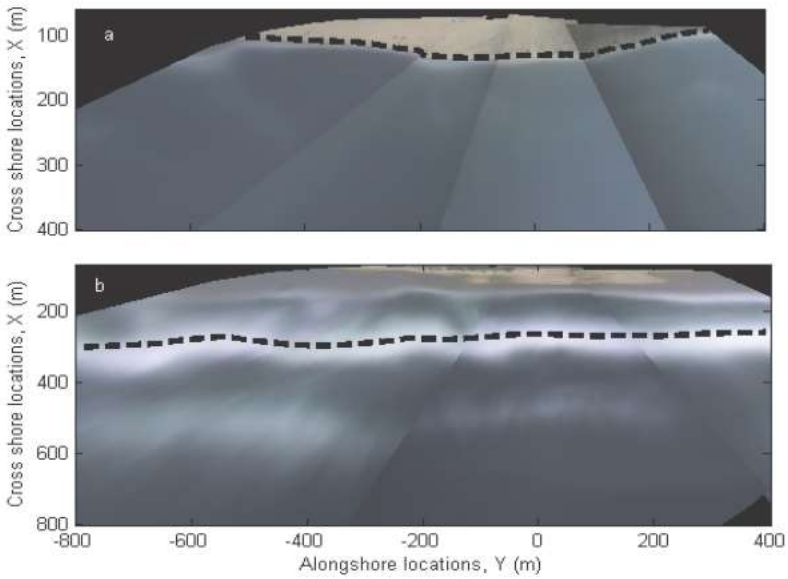

Figure 2. Merged 10-averaged image with manual detection of a) shoreline (29 Sept. 2008) and (b) sandbar crest (15 June, 2007) as green lines.

Extraction of inner sandbar locations

Timex images are also used to manually track the inner bar locations. The high-intensity bands associated to breaking in the plan view images (see Figure 2b) make a good proxy for bar crest location (Lippmann and Holman 1989; Pape and Ruessink 2008). Inner-bar extraction is performed at the same water level (0.55 m below MSL). Following similar criteria by Senechal et al., (2015) and Van de Lageweg et al., (2013), images at Hs > 2.5 m are excluded because under such conditions wave breaking occurs continuously from the outer bar to the shore and inner bar is not visible. 411 daily alongshore-averaged cross-shore sandbar positions $<X_b>$ are obtained which is 20% of the entire period. Average accuracy on $<X_b>$ can reach 7 m. Masselink and Short (1993) show that tides play a passive role in sediment transport and beach morphology as they alternately expose and submerge a large portion of the beach and the inner surf zone. To analyse the impacts of tides, neap tidal range (Tr<2.75) are separated from spring tide range (Tr>2.75 m). This limit is the highest value of all minima in the tide range signal. Consequently the correlation coefficients at neap and spring tide range are estimated between $<X_s>$ and Hs. The correlation between $<X_s>$ and Hs is estimated at points of short distance $<X_b>$ (<266 m) where the threshold marks the mean $<X_b>$ position as well as the distance (spatial) when the sandbar positions transit from summer to winter. This was repeated for the

distant $<X_b>$ (> 266 m) to understand the impacts of far and near sandbars on shoreline changes.

Results and discussions

Time series data are initially presented on Figure 3 including *Hs*, $<X_s>$ and $<X_b>$. Figure 3a and 3d show that the evolutions of hydrodynamic forcing of tides and waves respectively have large seasonal variations. Observations on Figure 3b indicate $<X_s>$ as well follows a seasonal pattern with wave variation where $<X_s>$ values are low during winter (80 m) and larger in summer (160 m). Analysis shows that the alongshore variability is rather low in winter and increase in summer. $<X_b>$ in Figure 3c reveal a wide range of variations from 202 m to 326 m than $<X_s>$ with outermost location in winter. On average, the distance $<X_b>$ - $<X_s>$ is 162 m but can be larger (227 m) during high wave conditions (winter) and small during low wave conditions (102 m in summer).

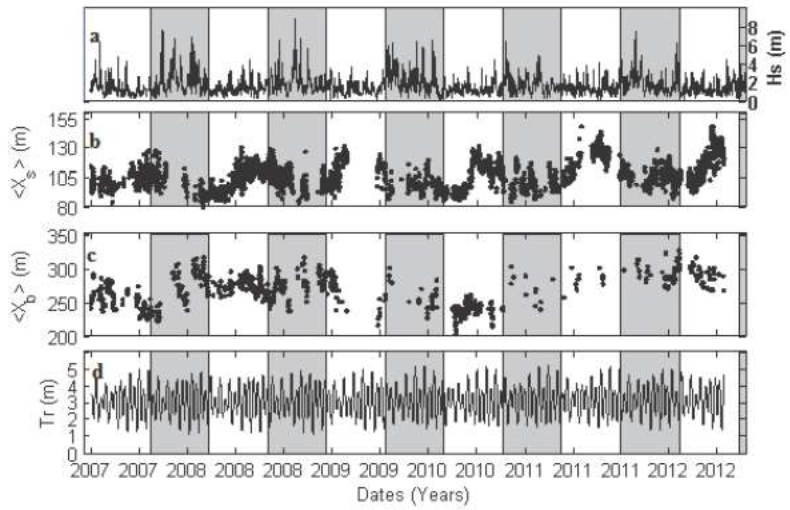

Figure 3. Time series data sets a) *Hs* (b) $<X_b>$ and (c) $<X_s>$. For (b) and (c) the camera is located on the land and shorter distances are closer to the camera.

Characteristics of individual storms

On average, energy *I* values are 1047 m^2hr though can reach 16540 m^2hr. Storms average duration and Hs_{max} are 30 hours and 4.8 m respectively. In extreme cases, storms are observed to last as long as 10 days and have *Hs* above 8 m. Storms of similar energy record vast difference in beach changes (summarized in table 1). Table 1 shows that storms occurred more in 2008

(~23%) and 2009 (~23%) than any other year. The average return period is about 21 days though 60% of these intervals between storms are less than 10 days. Figure 4 shows that severe storms (6 m) occur preferably during winter (76% Nov-Mar: patched rectangles) and have low occurrence in summer (24% Apr-Oct). In 2011, despite the storms, accretion is observed as a consequence of less severe stormy waves.

Table 1. The storm characteristics from 2007-2012

	Num. of Storms	Hs_{max} (m)	I_{max} (10^3 m^2hr)	% severe storms (> 6 m)	Av. ΔX (m)	Max Duration hr
2007	7	7.6	7.1	14	-0.7	123
2008	20	6.8	3.3	21	-0.7	78
2009	19	8.7	16.5	28	-3.8	219
2010	15	6.5	2.1	21	-4.2	51
2011	10	7.3	1.2	7	2.2	111
2012	12	6.2	2.4	7	-0.9	84

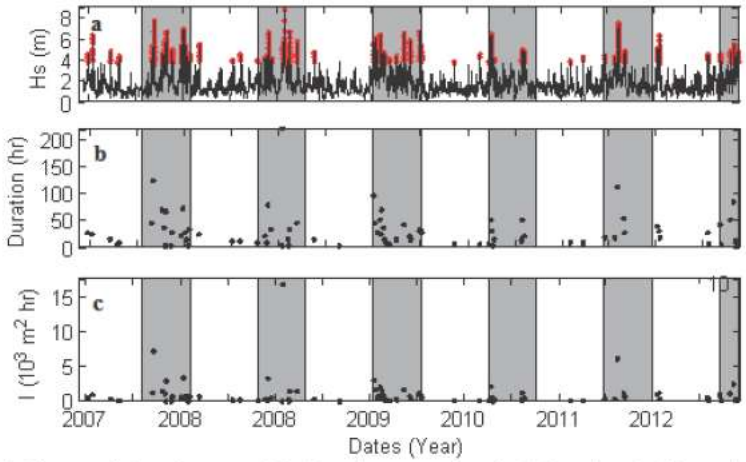

Figure 4. Characteristics of storms: a) *Hs* (showing storms in red) (b) Durations (c) Energy intensity due to each storm (I_s).

In Figure 5, post-storm recovery shoreline location is shown for the first 20 days following the end of the storms. Shoreline evolution show continuous recovery as expected during calm periods. A continuous accretion (3.7 m/day) is observed during the first 9 days and after, reaches stabilization. These post-storm evolutions therefore suggest an average 9-day recovery period at Biscarrosse beach. This result falls in line with results found at other sites as reported in the literature (e.g. Ranasinghe et al., 2012).

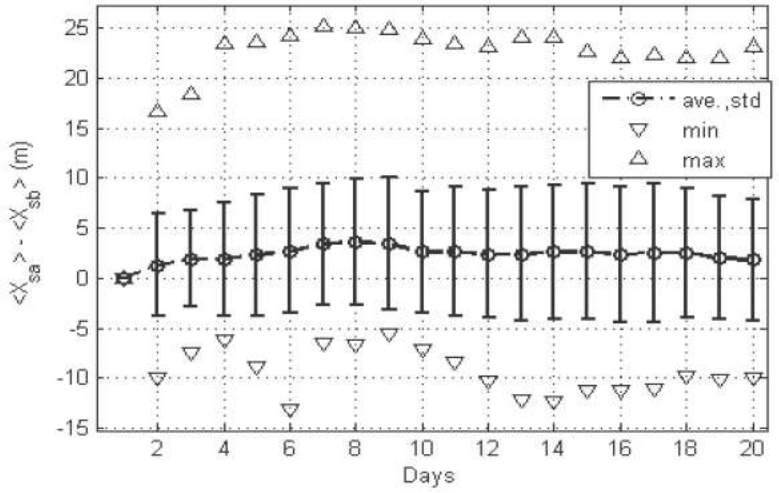

Figure 5. Average post-storm shoreline profile, shows maximum and minimum shoreline changes in a day. $<X_{sa}>$ -$<X_{sb}>$ is $<X_s>$ at the end of recovery minus that at start of recovery period.

Relative impact of individual storms and clusters

Based on recovery period obtained from the previous section of this paper, a storm cluster is defined as a group of storms which has the time interval between the successive storms to be less than 10 days. 16 clusters are obtained with 2 to 11 groups of single storms. The cluster with 11 storms observed from Nov-Dec, 2009 with a total energy of 10374 m^2hr results in 5 m shoreline retreat. However a smaller cluster (4 storms) with energy of 16935 m^2hr results in 11.8 m shoreline retreat. This relates erosion more to the energy of clusters than the number of storms in the cluster. As indicated on Figure 6, these results given by the ratio of slopes in regression lines for cluster of storms (cl = -0.84*Ic-6) and individual storms (sl = -0.75*I-0.6) confirm that cluster of storms have relatively larger (1.12 times) impact than single storms where Ic are the total cluster energy. The ΔX with respect to each storm in each cluster as shown in Figure 7 reveals that beach erosion is due to first and second rank storms in each cluster while higher rank storms show less erosive trend. The ΔX due to energetic storms and cluster of storms as described above influence only 16% the total shoreline variability notwithstanding the extreme wave events. Almar et al., 2010 showed that tide range variations have a large influence on the inner-bar dynamics, which will be discussed in the next subsection.

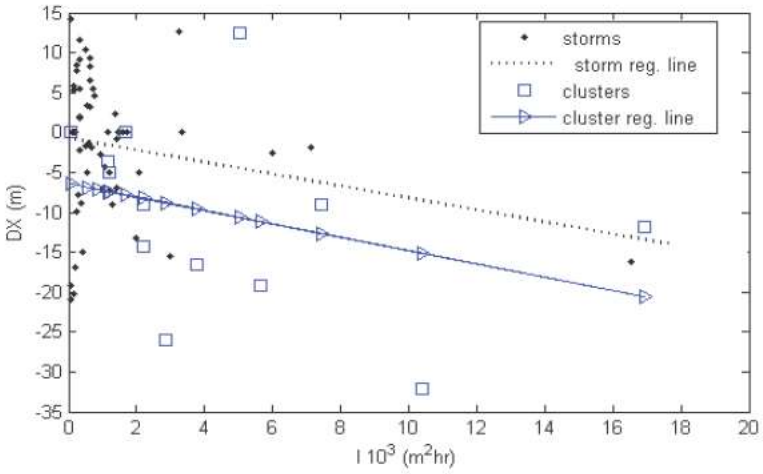

Figure 6. The Impacts of storms (dots) and clusters (square).

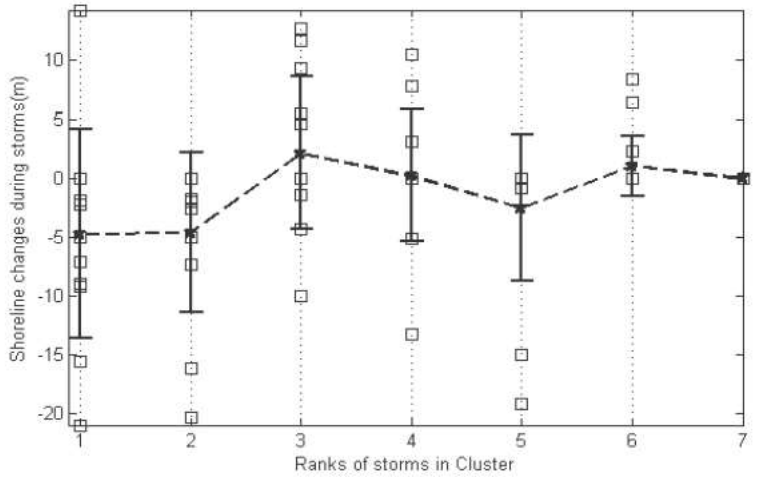

Figure 7. This shows the ranks of storms against the shoreline changes of each cluster.

Tidal range and sandbar distance modulation of wave-driven shoreline change

The effect of tides on shoreline change is estimated through correlation analysis between *Hs* and $<X_s>$ at different tidal ranges in table 2, with a significant correlation (0.3, significant at 95%) at neap tides and no correlation at spring tide (not significant at 95%) at spring tide. Spring tides largely influence $<X_b>$

and $<X_s>$ changes (~16 %) with rather weak effect of waves. Using the same analysis for distance, the influence of $<X_b>$-$<X_s>$, a correlation is peformed between *Hs* and $<X_s>$. A significant correlation between *Hs* and $<X_s>$ is found for short distances (0.3, significant at 95 %) which shows that waves have predominant effect on shoreline changes. For distant sandbars, correlation between *Hs* and $<X_s>$ is not significant at 95% , indicating weaker influence of waves on shoreline changes. Evident in table 2 is the difference in sign for the correlation between *Hs* with $<X_b>$ and $<X_s>$, indicating that for increasing wave energy, inner bar and shorleine move offshore and inland, respectively.

Table 2. Results of correlation between waves and $<X_s>$ at different $<X_b>$ and *Tr*. Correlation is not significant considering the 95% level .

Correlating	***Hs* vs $<X_b>$**	***Hs* vs $<X_s>$**
	r	**r**
Neap Tides	0.50	-0.30
Spring Tides	0.20	Not significant
Short distance $<X_b>$	-	0.30
Distant $<X_b>$	-	Not significant

Conclusions

6 years of 10-minute average video images were collected at the double-barred beach of Biscarrosse, SW France. The effects of storms, storm clusters, tides, and inner bar location on the shoreline dynamics have been addressed. With 5% exceedance probability of *Hs* ($Hs_{5\%}$ = 3.68 m) as storm threshold, over 60 individual storms (~15 storms per year) were identified. An ensemble average analysis shows that shoreline recovers (accretes) in 9 days after storms. In storm clusters, the first two storms lead to higher erosion than following storms in the cluster. This is in line with equilibrium-based approach where storms are less and less effective in eroding the beach as the beach progressively reaches a new equilibrium with the prevailing wave conditions. It is observed that clusters have relatively larger impact than individual storms.

Moreso, correlation analysis at different tidal ranges reveal that tidal range has a substantial influence on shoreline changes in particular for spring tide. The distance between shoreline and sandbar might be of importance, larger distances leading to less storm-induced erosion. These results argue in favor of integrating sandbar and tide effects in shoreline equilibrium models which could substantially enhance their effectiveness.

Acknowledgement

The first author's PhD is co-funded by SCAC (French embassy in Ghana) and ARTS-IRD programs. Authors acknowledge the Region Aquitaine for financially supporting the installation of the video system at Biscarrosse.

References

Almar, R., Castelle, B., Ruessink, G., Sénéchal, N., Bonneton, P., Marieu, V. (2010). Two and three-dimensional double-sandbar system behaviour under intense wave forcing and a meso–macro tidal range, *Continental Shelf Res*earch, 30 (7), 781-792.

Almar, R., Castelle, B., Ruessink, B.G., Sénéchal, N., Bonneton, P., Marieu, V., 2009. High-frequency video observation of two nearby double-barred beaches under high-energy wave forcing, *Journal of Coastal Research,* SI 56 (2), 1706–1710.

Ba, A. and Sénéchal, N. (2013). Extreme winter storm versus summer storm: morphological impact on a sandy beach, *Journal of Coastal Research*, SI 65, 648-653.

Callaghan, D.P., Nielsen, P., Short, A. and Ranasinghe, R. (2008). Statistical simulation of wave climate and extreme beach erosion, *Coastal Engineering* 55, 375 – 390.

Castelle, B., Marieu, V., Bujan, S., Ferreira, S., Parisot, J. P., S Capo, Sénéchal, N. and Chouzenoux, T. (2014). Equilibrium shoreline modelling of a high energy meso macrotidal multiple-barred beach, *Marine Geo.*347, 85-94

Castelle, B., Bonneton, P., Dupuis, H. and Senechal, N. (2007). Double bar beach dynamics on the high-energy meso-macrotidal French Aquitanian Coast: A review, *Marine Geology*, 245, 141-159.

Coco, G., Senechal, N., Rejas, A., Bryan, K.R., Capo, S., Parisot, J.P., Brown, J.A. and MacMahan, J.H.M. (2014). Beach response to a sequence of extreme storms, *Geomorphology*, 204, 493–501.

Corbella, S. and Stretch, D. D., 2012. Shoreline recovery from storms on the east coast of Southern Africa, *Nat. Hazards Earth Syst. Sci.,* 12, 11–22.

Davidson, M. A., Turner, I. L., and Splinter, K. D. (2013). Predicting shoreline response to cross-shore processes in a changing wave climate, *Coastal Dynamics*, pp.431-442

Dolan, R. and Davis, R., 1992. An intensity scale for Atlantic coast northeast storms, *Journal of Coastal Research*, 8(4), 840–853.

Frazer, L. N., Anderson, T. R. and Fletcher, C. H. (2009b). Modeling storms improves estimates of long- term shoreline change, *Geophys. Res. Lett*., 36, L20404, doi: 10.1029/2009GL040061.

Ferreira, O., 2005. Storm groups versus extreme single storms: predicted erosion and management consequences, *Journal of Coastal Research,* 42, 221–227.

Grasso, F., Michallet, H., Barthélemy, E. and Certain, R. (2009). Physical modeling of intermediate cross-shore beach morphology : Transients and equilibrium states, *Journal of Geophysical Research*, Vol. 114, C09001, doi: 10.1029/2009JC005308.

Holland, K.T., Holman, R.A. and Lippmann, T.C. (1997). Practical use of video imagery in neareshore oceanographic field studies, *IEEE Journal of Oceanic Engineering,* 22(1), 81-92.

Karunarathna, H., Pender, D., Ranasinghe, R., Short, A. D. and Reeve D. E. (2014). The effects of storm clustering on beach profile variability. *Marine Geology* 348 103–112.

Lippmann, T. C. and Holman, R. A. (1989). Quantification of Sand Bar Morphology: A Video Technique Based on Wave Dissipation, *Journal of Geophysical Research,* 94, 995-1011.

Masselink, G., Kroon, A. and Davidson-Arnott, R.G.D. (2006). Morphodynamics of intertidal bars in wave-dominated coastal settings- A review, *Geomorphology* 73, 33–49.

Masselink, G. and Short, A. D. (1993). The Effect of Tide Range on Beach Morphodynamics and Morphology: A Conceptual Beach Model, *Journal of Coastal Research*, 9(3) 785-800.

Pape, L. and Ruessink, B. G. (2008). Multivariate analysis of nonlinearity in sandbar behavior, *Nonlinear Processes Geophysics*, 15, 145–158

Plant, N. G and Holman, R. A. (1997). Intertidal beach profile estimation using video images, *Marine Geology*, 140, 1-24

Péron, C and Sénéchal, N., 2011. Dynamic of a meso to macro-tidal double barred beach: inner bar response, *Journal of Coastal Research,* SI 64, 120-124.

Ranasinghe, R., Holman, R., de Schipper, M.A., Lippmann, T., Wehof, J., Minh Duong, T., Roelvink, D., Stive, M.J.F. (2012). Quantification of nearshore morphological recovery time scales using Argus video imaging: Palm Beach, Sydney and Duck, NC, *Coastal Eng. Proceedings, 1(33), sediment.24.*

Senechal, N., Coco, G., Castelle, B., and Marieu, V. (2015). Storm impact on the seasonal shoreline dynamics of a meso- to macrotidal open sandy beach (Biscarrosse, France), *Geomorphology,* 228,448–461

Splinter, K.D., Carley, J.T., Golshani, A., Tomlinson, R. (2014). A relationship to describe the cumulative impact of storm clusters on beach erosion, *Coastal Engineering* 83, 49–55.

Stive, M. J., Aarninkhof, S.G.J., Hamm, L., Hanson, H., Larson, M., Wijnberg, K.M., Nicholls, R.J., Capobianco, M. (2002). Variability of shore and shoreline evolution, *Coastal Engineering* 47, 211–235.

Stockdon, H. F., Holman, R.A., Howd, P.A., and Sallenger, A.H. (2006). Empirical parameterisation of setup, swash and run up, *Coastal engineering*, 53, 573-588.

Van de Lageweg, W.I., Bryan, K.R., Coco, G., Ruessink, B.G., 2013. Observations of shoreline–sandbar coupling on an embayed beach. *Marine Geology*, 344, 101–114.

Wright, L.D., Short, A.D., Boon III, J.D., Hayden, B., Kimball, S. and List, J.H., (1987). The morphodynamic effects of incident wave Groupiness and tide range on an energetic beach, *Marine Geology*, 74, 1-20.

Wright, L.D. and Short, A.D. (1984). Morphodynamic variability of surf zones and beaches: A synthesis, *Marine Geology*, 56, 93-118.

Yates, M. L., Guza, R. T. and O'Reilly W. C. (2009). Equilibrium shoreline response: Observations and modeling, *Journal of Geo. Research*, 114.

APPENDIX B

Noise reduction and removal of outliers

Noise Reduction

Signal averaging in signal processing technique applied in time domain, increases the strength of a signal relative to noise that is obscuring it. By averaging a set of replicate measurements, the signal-to-noise ratio, *S/N*, will be increased, ideally in proportion to the square root of the number of measurements. Assuming there is noise Z in a shoreline data signal, the per-sample variance of the noise is given by

Var (Z) = σ^2

Averaging a random variable in definite number,

$$\text{Var}\left(\frac{1}{n}\sum_{i=1}^{n} z_i\right) = \frac{1}{n^2} Var\left(\sum_{i=1}^{n} z_i\right) = \frac{1}{n^2}\sum_{i=1}^{n} Var\ (z_i)$$

Provided the noise is uncorrelated, the mean of the noise is zero and the variance is constant. Thus assuming the noise variance is constant,

$$\text{Var}\left(\frac{1}{n}\sum_{i=1}^{n} z_i\right) = \frac{1}{n^2} n\sigma^2 = \frac{1}{n}\sigma^2 = N_{avg}$$

This suggests that averaging n realizations of the same, uncorrelated noise reduces noise power by a factor of n.

Removing outliers

In statistics, the standard score is the signed number of standard deviations an observation or datum is above the mean. A positive standard score indicates a datum above the mean, while a negative standard score indicates a datum below the mean. Standard score z is also called z-score or normal scores. The standard scorer of a raw data x is given by

$$z = \frac{x-\mu}{\sigma}$$

Where μ is the mean and σ is the standard deviation. In this study, about 99% of shoreline data have a z-score between -3 and 3. This means if a data point is outside this range, it is considered an outlier or false data.